Title
Development of Chemical Probes for Studying Formaldehyde Biology

Author
Brewer, Thomas Francis

Publication Date
2017

Peer reviewed|Thesis/dissertation

Development of Chemical Probes for Studying Formaldehyde Biology

By

Thomas Francis Brewer

A dissertation submitted in partial satisfaction of the

requirements for the degree of

Doctor of Philosophy

in

Chemistry

in the

Graduate Division

of the

University of California, Berkeley

Committee in charge:

Professor Christopher J. Chang, Chair

Professor Matthew B. Francis

Professor Ming C. Hammond

Professor Niren Murthy

Spring 2017

Development of Chemical Probes for Studying Formaldehyde Biology

by Thomas Francis Brewer

Abstract

Development of Chemical Probes for Studying Formaldehyde Biology

By Thomas Francis Brewer

Doctor of Philosophy in Chemistry

University of California, Berkeley

Professor Christopher J. Chang, Chair

Formaldehyde (FA) is a reactive carbonyl species (RCS) produced in living systems through a diverse set of cellular pathways that span epigenetic regulation to metabolic processing of endogenous metabolites. At the same time, however, aberrant elevations in FA contribute to pathologies ranging from cancer and diabetes to heart, liver, and neurodegenerative diseases. Traditional methods for the detection of biological FA rely on sample destruction and/or extensive processing, resulting in a loss of spatiotemporal information. Disentangling the complex interplay between FA physiology and pathology motivates the development of chemical tools that can enable selective detection of this RCS in biological environments with spatial and temporal fidelity. This dissertation describes the design and applications of a FA-responsive homoallylamine trigger which undergoes imine condensation with FA, followed by 2-aza-Cope rearrangement and hydrolysis, irreversibly forming a diagnostic product. Importantly, this 2-aza-Cope reactivity-based trigger was found to discriminate FA from other RCS such as methylglyoxal, 4-hydroxynonenal, and glucosone as well as from simple carbonyl-containing species such as acetaldehyde and pyruvate.

Throughout this body of work, emphasis was placed on the design of FA probes whose responsiveness and readout could be applied to interrogate FA biology in a number of biological systems. To this end, the FA-reactive trigger was appended to a variety of useful diagnostic readouts, including intensity-based fluorescence (FA Probe-1), excitation-ratiometric fluorescence (Ratiometric FA Probe-1 and Ratiometric FA Probe-2), bioluminescence (FA Luciferin-1), and immunohistochemistry (Puromycin FA Probe-1). All of these probes were shown to be responsive and selective toward FA *in vitro* and subsequently characterized in various cell culture model systems. This work established the utility of the 2-aza-Cope reaction as a FA detection platform and demonstrated its versatility for generating many functional imaging probes, paving the way for future interrogation of FA biology in living, intact systems.

Dedication

To my parents,
for unfaltering love and support.

Table of Contents

Acknowledgments

I would like to thank my family for supporting me, particularly my brother Kevin and my sister Fallon, as well as my parents Kevin and Bridget. Their love and guidance has cheered me on throughout my life, and I have always counted on their support as a foundation for all my efforts.

Thank you to Professor Chris Chang for mentoring me throughout my graduate career, allowing me to rise to the challenges of synthetic chemistry and chemical biology and guiding me in my growth as a scientist. All of the members of the Chang Lab have helped to make my time in graduate school enjoyable and fruitful. Their friendship and support has been invaluable to me. I would like to thank Lakshmi Krishnamoorthy, Carl Onak, Mark Vander Wal, Marie Heffern, Joey Cotruvo, Brian Michel, Eva Nichols, Cheri Ackerman, and Ryan Walvoord for their guidance and training to me.

Thank you to Ben Thuronyi, Vivian Lin, Dan Finley, Stephen Wilson, Professor Michelle Chang, Professor Matt Francis, and Professor Ming Hammond for providing me with training as an organic chemist and chemical biologist during my first year of graduate school.

I thank Allegra Aron and Cameron Baker for their camaraderie and constant support throughout our time in graduate school together. I can always lean on them when times are rough, and they are the first people I turn to when I have good news to celebrate. Their friendship is dear to me and continues to brighten my life.

I thank Brooke Bullock and Professor Bobby Arora for their advice and training to me as an undergraduate. They helped to shape my passion as a young scientist and their encouragement is what brought me to graduate school.

Finally, I would like to thank Jesse Koehler for his unconditional love and support.

Chapter 1

Detection of small molecule analytes in living systems

Portions of this work were published in the following scientific journals:

Brewer, T. F.;* Garcia, F. J.;* Onak, C. S.;* Carroll, K. S.; Chang, C. J. "Chemical Approaches to Discovery and Study of Sources and Targets of Hydrogen Peroxide Redox Signaling Through NADPH Oxidase Proteins." *Annu. Rev. Biochem.* **2015**, *84*, 765–790.

Bruemmer, K. J.;* Brewer, T. F.;* Chang, C. J. "Fluorescent probes for imaging formaldehyde in biological systems." *Curr. Opin. Chem. Biol.* **2017**, *39*, DOI: 10.1016/j.cbpa.2017.04.010.

* denotes equal contribution

1.1. Background and Motivation

Reactive species such as hydrogen peroxide (H_2O_2) and formaldehyde (FA) have well-established toxicity in living systems and participate in the pathophysiology of various disease states. At the same time, however, these reactive species are produced endogenously and play diverse roles in maintaining normal physiology. Better understanding of how, when, and why these small molecules are produced in living systems will help to elucidate how cells maintain the delicate balance between signal and stress, potentially leading to new insights in human health and disease.

Owing to the transient nature of reactive species, fluorescence-based probes, which generally display high sensitivity and can be used to determine spatial and temporal distributions in live specimens, are particularly appealing tools for the detection of H_2O_2, FA, and related species. Novel probes must meet a high bar in terms of their selectivity, kinetics, and photophysical properties. An ideal chemical probe must be inert to the conditions present in the cell and should not require the addition of other reagents. Furthermore, the probe must be selective against similar analytes, and it should exhibit a turn-on, rather than turn-off, response in order to minimize background. Ideally, a family of probes with varying wavelengths should be available so that their use can be tailored to the specific application and made compatible with probes for different species. To introduce the reader to this area of research, an overview of relevant FA and H_2O_2 probes is presented.

1.2. Formaldehyde (FA)

Formaldehyde (FA) is an endogenously-produced reactive carbonyl species (RCS) released in biological processes ranging from epigenetics to one carbon metabolism (Figure 1.1).[1-2] Although more widely known as an environmental toxin and carcinogen,[3] FA is found at relatively high concentrations intracellularly under normal physiological conditions, reaching up to 500 μM in certain organelles.[4-5] FA is a one-carbon fuel involved in maintenance of cell homeostasis, and its abundance and high reactivity suggest a potential role as a physiological signaling molecule.[6-8] FA is the product of demethylation events of *N*-methylated amino acid residues (e.g. lysine, arginine, histidine) mediated by demethylase enzymes,[9] such as lysine specific demethylase 1 (KDM1)[10-11] and Jumonji domain-containing proteins (Figure 1).[12-14] FA is also produced through *N*-demethylation of DNA and RNA bases, such as m^6A, by AlkB homologues (ALKBH).[15] Methylation and demethylation events signal transcription factors to promote or repress transcription, and disruption of normal methylation markers could have wide ranging effects in disease states, particularly cancer progression.[16-17] Similarly, metabolism of methylated amines, including the abundant endogenous metabolite methylamine, by semicarbazide-sensitive amine oxidases (SSAO) release FA.[18-19] Several demethylase enzymes utilize tetrahydrofolate (THF) as a cofactor to bind FA, yielding 5,10-methylene-THF, known as "active formaldehyde."[20-21] Folate derivatives are essential for mitochondrial one-carbon metabolism, in which demethylation events release FA, which is further incorporated into important cellular building blocks such as amino acids, purines, and phospholipids.[22] A canonical example is the sarcosine pathway, where dimethylglycine dehydrogenase (DMGDH) and sarcosine dehydrogenase (SARDH) demethylate dimethylglycine sequentially, yielding two equivalents of FA and glycine.[23] Owing to the toxic nature of FA, it is efficiently metabolized by the enzyme alcohol dehydrogenase 5 (ADH5, also known as formaldehyde dehydrogenase, *S*-nitrosogluthathione reductase, and alcohol dehydrogenase 3) as its glutathione adduct, *S*-(hydroxymethyl)glutathione.[24-27]

The aforementioned examples provide motivation for developing new FA detection technologies. Owing to the prevalence of FA in industrial settings as well as in household items, several sensitive FA detection methods have been devised,[28] including methods utilizing high-performance liquid chromatography (HPLC),[29-30] gas chromatography (GC),[31] mass spectrometry (MS),[32] as well as preconcentration/chemical ionization MS.[33] However, the study of FA and its roles in physiology and pathology is still limited by the lack of detection methods that can provide spatiotemporal resolution in living cells and more complex biological specimens. One emerging approach utilizes fluorescence-based probes, which offer high selectivity and sensitivity and can be used *in situ*. Reactivity-based fluorescent probes have been successfully employed to image a variety of biological analytes,[34-36] including the carbonyl species carbon monoxide[37-41] and methylglyoxal,[42] and recent efforts have focused on the development of reactivity-based probes for FA. The following discussion aims to summarize the current progress toward creating responsive and selective fluorescent reporters for FA, along with an outlook toward improvements in the field.

1.2.1. Design considerations for fluorescent formaldehyde probes

Effective fluorescent probes for imaging FA in living cells and higher specimens must meet several criteria. Key considerations are fast reactivity with FA and selectivity of the reaction against other biological analytes, especially other biologically-relevant RCS which possess similar electrophilic carbonyl groups. These competing RCS, including acrolein, 4-hydroxynonenal, and methylglyoxal, as well as other aldehyde-containing metabolites such as acetaldehyde, are generated primarily during metabolism and oxidative stress conditions, such as ethanol metabolism and lipid peroxidation.[43-44] Compared to the high micromolar endogenous concentration of FA, steady-state concentrations of other RCS range from high nanomolar to low micromolar[45] and are estimated to be higher in various disease states.[46] Thus, the large variety of continually-generated RCS and their similar electrophilic reactivity makes selectivity the most important hurdle to overcome for developing reliable FA detection methods.

Several different but complementary mechanisms for FA detection have been reported, including 2-aza-Cope-, formimine-, and aminal-based detection methods (Figure 1.2), all offering unique advantages and disadvantages that are summarized below and in Table 1.1. In addition, such probes rely on a number of fluorescent scaffolds suitable for biological imaging with excitation wavelengths that span the visible to near-infrared spectrum and/or possess reasonable two-photon cross-sections;[47] ultraviolet excitation is less desirable owing to interference from native autofluorescence from chromophores in the cell such as NADH and flavins as well as the potential for photodamage and oxidative stress induced by irradiation with high-energy light. FA detection can be realized by attaching various reactivity switches to fluorophore platforms, utilizing well-developed fluorescent response mechanisms ranging from spirocyclization, photoinduced electron transfer (PeT), internal charge transfer (ICT), fluorophore uncaging, and ratiometric detection.[48]

1.2.2. Formaldehyde probes utilizing the aza-Cope reaction

We[49] and Chan's laboratory[50] independently and simultaneously developed the 2-aza-Cope-based strategy utilizing a homoallylic amine as a selective trigger for FA reactivity. In this scheme, the homoallylamine condenses with FA, undergoes the 2-aza-Cope rearrangement, and subsequent hydrolysis yields an aldehyde or ketone product (Figure 1.2). The 2-aza-Cope reaction exhibits high selectivity for FA over other RCS and carbonyl species, such as acetaldehyde, methylglyoxal, and 4-hydroxynonenal. The change in nucleophilicity and electronic properties on

conversion of a homoallylamine to a carbonyl can be harnessed to provide a fluorescence turn-on or ratio change. Initial probes utilized near-infrared-emitting silicon rhodamine/rhodol scaffolds as the fluorophore with different sensing mechanisms to elicit a fluorogenic response. We reported Formaldehyde Probe 1 (FAP-1), whose homoallylamine favors an initial spirocyclized, weakly emissive state (see Chapter 2).[49] After FA reaction, the product aldehyde is incapable of spirocyclization, leading to an open, fluorescent product with an 8-fold turn-on response to 100 μM FA after 1 h. High sensitivity and selectivity allowed FAP-1 to respond to exogenously-added FA in living cells within 30 min, and was also able to detect a decrease in endogenous FA levels in cells upon LSD1 inhibition. Concurrent work by the Chan group reported FP-1, which utilizes a PeT mechanism to elicit a fluorescent response.[50] Specifically, a nitrobenzene moiety was appended to the homoallylamine, which quenches the rhodamine through donor-excited PeT. After the 2-aza-Cope reaction, hydrolysis liberates the fluorophore from the nitrobenzene moiety, resulting in 7-fold fluorescence turn-on response to 250 μM FA after 3 h. In cells, FP-1 displayed a 1.2-fold turn-on to 1 mM FA after 3 h. These reports demonstrated the feasibility of utilizing fluorescence-based probes to detect FA in living cells, and specifically the utility of the 2-aza-Cope reaction as a detection platform.

The 2-aza-Cope strategy has subsequently been extended to other fluorophore scaffolds, establishing the generality of this reactive trigger for FA detection. Indeed, several groups have reported 2-aza-Cope probes for FA based on an ICT mechanism using an unfunctionalized homoallylamine switch. A homoallylamine appended to a naphthalene fluorophore furnished a UV-excitable ratiometric probe (reported by different groups as RFFP and AENO).[51-52] These first-generation probes are highly selective for FA and exhibit good ratiometric responses, but are limited by relatively slow reaction kinetics, taking hours to display a statistically significant turn-on signal to millimolar levels of exogenously-added FA, thus limiting their applicability to image endogenous FA pathways. The first examples of two-photon FA probes FATP-1[53] and TPNF[54] were applied to image FA in tissue and zebrafish, respectively. Both FATP-1 and TPNF report a 3-hour incubation in cells to show a statistically significant turn-on response but illustrate the compatibility of the 2-aza-Cope reaction with tissue and whole organism settings.

While highly selective, the use of a parent homoallylamine for the 2-aza-Cope reaction leaves room for improvement owing to its relatively slow reaction kinetics. Indeed, in organic synthesis, 2-aza-Cope reactions are often performed at higher temperatures to promote reactivity; however, biological constraints preclude altering temperature above physiological levels, and as such improving reactivity must be addressed through structural modifications of the homoallylamine trigger. Recent efforts from our lab led to the development of a 2-aza-Cope-based trigger for FA with improved kinetics through structural modification of the homoallylamine moiety.[55] In particular, appending *gem*-dimethyl substituents accelerated the 2-aza-Cope reaction about 10-fold through the Thorpe-Ingold effect,[56] allowing for a responsive and selective series of FA probes. One such probe, FAP573, was capable of visualizing increased endogenous FA levels in ADH5 knockout cells compared to the wildtype counterpart. Furthermore, we extended this strategy to develop an excitation-ratiometric FA detection platform capable of detecting changes in endogenous FA with internal calibration (see Chapter 3).[57] Overall, this aforementioned collection of fluorescent probes demonstrates the broad applicability of the 2-aza-Cope reaction for detection of biological FA, and further extensions of this strategy will allow for tuning of excitation/emission wavelengths and subcellular localization, as well as expansion to other imaging modalities.

1.2.3. Formimine- and aminal-based formaldehyde probes

Alternative reactivity-based approaches for FA detection exploit the formimine- or aminal-forming properties between FA and amines. Both approaches display fast reaction kinetics but are more challenging to tune for FA selectivity over other aldehydes, thus offering distinct advantages and disadvantages over the 2-aza-Cope strategy. Lin and colleagues have elegantly employed a hydrazine moiety to create a series of probes using the 1,8-naphthalimide fluorophore (Na-FA).[58] The free amine on the hydrazine initially quenches fluorescence through a PeT mechanism, which is blocked after formimine formation. By modifying the fluorescent scaffold, lysosome-targeting (Na-FA-Lyso)[59] and biotin-guided (1)[60] FA probes were created. Na-FA displays an *in vitro* 900-fold increase in fluorescence to 100 μM FA in 30 min, but *in cellulo* reactivity appears to be more sluggish and comparable to 2-aza-Cope congeners. A key set of tissue imaging experiments include endogenous changes in FA from the addition of sodium bisulfite, a FA scavenger which lowers levels of free FA by sequestration as the bisulfite adduct. Bisulfite addition shows a decrease in fluorescence compared to basal conditions, suggesting the probes are capable of imaging changes in endogenous FA *in cellulo*. An important consideration in performing such FA sequestration experiments is to verify the in vitro response of FA probes toward bisulfite alone does not display fluorescence quenching. Formimine-based probes can also respond to simple aldehydes such as acetaldehyde, albeit with much less of a response compared to FA, and this promiscuity provides a promising starting point to create probes for acetaldehyde and other RCS in addition to FA.

Aminal formation-based probes exploit slightly different reactivity to detect FA. The Lin group reported R6-FA, which utilizes a spirocyclization method, similar to FAP-1, to induce a fluorescence turn-on.[61] The spirocyclized amine moiety is linked to a free, FA-reactive amine. The Schiff base resulting from reaction with FA is more electrophilic than the xanthone fluorophore, resulting in aminal heterocycle formation and concurrent fluorescent turn-on. While highly reactive (FA-induced turn-on occurs within 10 seconds), this method displays relatively poor selectivity for FA over other carbonyl-containing species. Along similar lines, the Zeng group utilized aminal heterocycle formation to create a dual methylglyoxal/FA probe (L).[62] However, fluorescence turn-on by FA and turn-off by methylglyoxal makes *in cellulo* experiments difficult to interpret, as both analytes are present in the micromolar concentration range, limiting its application.

1.2.4. Conclusion and outlook

Development of a variety of fluorescent probes for FA has greatly expanded the capabilities to image FA in living biological systems. All three strategies show promise for further interrogation of the roles FA plays in biology. However, probe sensitivity remains hindered by either reaction kinetics for the 2-aza-Cope strategy or selectivity for the formimine- and aminal-based detection methods. Further investigation into the mechanisms of previously unstudied FA biological pathways will benefit from a method able to combine the advantages of the two approaches to create a responsive and selective modality. The tunability of the homoallylamine moiety for the 2-aza-Cope strategy, as demonstrated in FAP573 and the RFAP platform,[55, 57] presages the potential for increased reactivity while conserving selectivity. Due to its generality, as showcased by the various probes discussed above, the 2-aza-Cope strategy shows promise for extension into alternate imaging modalities. Indeed, we recently reported a positron emission tomography-based probe, [^{18}F]FAC-FDG, for *in vivo* FA imaging.[63] Likewise, the fast kinetics of formimine formation offer a large advantage which could be harnessed through further tuning to inhibit reactivity toward competing carbonyl species. In particular, increased steric encumbrance

could afford enhanced selectivity over larger aldehydes. Future experiments with improved FA probes will help elucidate the roles FA may play in physiology and disease related to demethylation events, one-carbon metabolism, and downstream effects of FA metabolism.

1.3. Hydrogen Peroxide (H_2O_2)

Hydrogen peroxide (H_2O_2) is widely perceived as a reactive and toxic chemical inimical to the processes of life. It was discovered by Thenard in 1818,[64] after which it was used as a bleaching agent and disinfectant. In 1900, Loew's discovery of catalase[65] which serves to efficiently decompose and thus eliminate this molecule reinforced its perception as an unwanted toxin. The realization in 1971 by Chance that the body itself generated H_2O_2 in the mitochondria[66] was interpreted as an inefficiency of aerobic metabolism, wherein H_2O_2 was an accidental byproduct.[67] Even Babior's discovery of the phagocytic oxidase in 1973[68] which deliberately produces superoxide ($O_2^{\bullet-}$) and its dismutation product H_2O_2, did not shake this view. The enzyme seemed to be confined to specialized immune cells, where it produced H_2O_2 in the interior of the phagosome specifically for its toxic properties in order to destroy engulfed pathogens.[68-69] Indeed, subsequent documentation by Habermehl of the production of H_2O_2 in response to the pro-inflammatory cytokines interleukin-1 and TNF-α[70] reinforced the notion that the biological role of H_2O_2 was restricted to the immune system. More recently, however, H_2O_2 has become widely appreciated as a beneficial molecule with functions more subtle than bacterial killing. Finkel's 1995 discovery of deliberate H_2O_2 production by vascular smooth muscle cells,[71] followed by the detection of widespread enzymatic production of reactive oxygen species (ROS) in 1999 by Lambeth,[72] has supported the notion of H_2O_2 as a cellular signaling agent and challenged the idea that its presence is indicative solely of oxidative stress. From this point forward, its perceived role in biology has thus progressed from that of a toxin, to an agent of the immune system, to a key component of such diverse biological phenomena as the circadian rhythm,[73-74] cell migration,[75-77] and stem cell proliferation (Figure 1.3).[78]

Elucidating the signalling roles of H_2O_2 in normal physiology and disease has been hampered by the difficulty in detecting H_2O_2 itself, as well as H_2O_2-induced modifications, with chemical specificity in complex biological systems. After a brief introduction reprising the major ROS produced by cells and mechanisms of thiol oxidation, this discussion focuses on recent progress in chemical approaches for specific detection of hydrogen peroxide and different oxidative post-translational modifications (oxPTMs) of protein cysteine thiols, with particular emphasis on those chemical properties that differentiate one ROS or cysteine modification from another. In keeping with this general theme, attention is restricted to reagents that have enabled the discovery and understanding of new redox biology within native cellular environments. Along the way, examples from the literature are included that highlight ways in which redox signalling via cysteine oxidation can be used to control protein function and signal transduction pathways. This discussion serves to introduce the reader to reaction-based probes in the context of ROS, an approach described in Appendix 1 and Appendix 2 to detect superoxide, the primary product of NADPH oxidase-mediated reduction of dioxygen.

1.3.1. H_2O_2 and reactive oxygen species (ROS)

Among the diverse collection of cellular ROS, hydrogen peroxide stands out as a molecule with ideal signaling properties. It possesses sufficient reactivity to modify potential signaling targets, yet it is also stable enough to diffuse appreciable distances within the cell, reacting with select targets.[79] Furthermore, it can be rapidly produced and quickly eliminated, making it ideal

for rapid, short-lived signaling bursts. Average hydrogen peroxide concentrations in healthy mammalian cells can range from 1 to 700 nM, with higher levels being associated with oxidative stress and cell death.[80] However, local H_2O_2 concentrations can be considerably higher than the average value. The floodgate model of oxidative signaling proposes rapid increases in local H_2O_2 can temporarily overwhelm antioxidant defenses, allowing reaction with targets for signaling purposes.[81] Thus, while high global concentrations of H_2O_2 cause oxidative stress, brief bursts can be beneficial to cellular physiology. Cellular sources of H_2O_2 include primarily the mitochondria and the endoplasmic reticulum (ER),[82] as well as various oxidases, including the NADPH oxidase (Nox) proteins,[67] amine oxidases,[83] acyl-CoA oxidases,[84] and cytochrome P450 enzymes.[85] Among these sources, the Nox family of proteins appear to be critical for the production of H_2O_2 for signaling purposes. Unlike other oxidases, the Nox proteins generate superoxide ($O_2^{\bullet-}$) as their primary product, which can then disproportionate to H_2O_2. The founding member of the Nox family is the phagocytic oxidase, which was characterized in the context of immune defense before the discovery of H_2O_2 as a signaling agent. This enzyme generates ROS within phagocytes in order to damage and eliminate engulfed pathogens. More recently, however, Nox family members have been found to be ubiquitously expressed in mammalian tissue types.[72] Thus, the widespread expression and deliberate H_2O_2 production of these enzymes is incompatible with the notion of H_2O_2 as solely a toxic byproduct. Indeed, these facts suggest that H_2O_2 serves a beneficial function. Combined with the ideal chemical properties of H_2O_2 as a messenger molecule, the aforementioned observations have motivated the study of Nox-derived H_2O_2 signaling.

1.3.2. Chemical tools for detection of H_2O_2 sources

1.3.2a. Criteria for H_2O_2 probes. To gain a complete understanding of the function of H_2O_2, it is important to have the ability to detect its production at the source, the effects on its immediate target, and the downstream consequences (Figure 1.4). Novel probes must meet a high bar in terms of their selectivity, kinetics, and photophysical properties. An ideal chemical probe for H_2O_2 must be inert to the conditions present in the cell and should not require the addition of other reagents. Furthermore, the probe must be selective against similar analytes, and it should exhibit a turn-on, rather than turn-off, response in order to minimize background. Ideally, a family of probes with varying wavelengths should be available so that their use can be tailored to the specific application and made compatible with probes for different species.

1.3.2b. Classes of H_2O_2 detection strategies. Numerous strategies have been implemented to address the issue of detecting H_2O_2, including strategies based on proteins,[86-88] nanotubes,[89] hyperpolarization,[90] ultrasound,[91] mass spectrometry,[92] and chemiluminescence.[93] The potential of the chemiluminescent modality is best demonstrated by the firefly-luciferin based boronate probe PCL1 (Figure 1.5b), which can be used in a luciferase-expressing mouse to measure H_2O_2 bursts in whole living mice (Figure 1.6a).[94] The next-generation probe PCL2 contains a second reactive trigger to report on simultaneous H_2O_2 generation and caspase activity in a model of acute inflammation.[95] The most promising class of probes is small-molecule fluorescent sensors. These sensors do not require additives or particular enzymes, and a wide variety of analogs are accessible to synthetic chemists, permitting the development of a flexible array of tools with differing optical, photophysical, and chemical properties.

1.3.2c. Early small molecule fluorescent probes. The fluorescent probes dihydrodichlorofluorescein (H_2DCF) and dihydrodichlorofluorescein diacetate (H_2DCFDA) have been used extensively to detect ROS.[96] These probes have been fruitfully employed in biological studies, but their lack of ROS specificity and photoactivation of the unoxidized molecule can confound results.[97] Another ROS detection technology of historical interest is the Amplex Red

assay.[98] This assay is sensitive, but the requirement of the enzyme additive makes it infeasible for use within living cells. In this context, our laboratory introduced a useful class of biocompatible small molecule fluorescent probes that rely on the oxidation of an arylboronate by hydrogen peroxide to produce a phenol (Figure 1.5a).[99-102] The boronate moiety masks a phenol, with the result that the unactivated probe exhibits significantly lower fluorescence than the oxidized molecule. By appending this chemical modification to various fluorescent scaffolds, a variety of probe molecules can be produced. The boronate oxidation takes advantage of the chemical characteristics of H_2O_2; specifically, its enhanced, α-effect nucleophilicity and weak O─O bond.[103] The electrophilic boronate undergoes a nucleophilic addition by H_2O_2, forming a charged tetrahedral boronate complex. The complex then undergoes a 1,2-insertion where the C─B bond migrates onto a peroxide oxygen, breaking the weak O─O bond and releasing water. Hydrolysis of this intermediate produces boric acid, concomitantly freeing the activated probe.

This oxidation has been shown to be highly selective for H_2O_2 over other biologically relevant species, including superoxide, hypochlorite, hydroxyl radical, alkyl hydroperoxides, and nitric oxide.[104] Although more recent findings show that certain boronates also react toward highly reactive species such as peroxynitrite, these molecules are generally produced in much lower quantities and exhibit short biological half-lives compared to H_2O_2.[105-107] In experimental settings where peroxynitrite or similar highly reactive species are a concern, boronate-based probes must be used with caution in concert with appropriate controls, generally either reducing H_2O_2 levels with antioxidants or inhibiting its enzymatic production. The first-generation probe Peroxyfluor 1 (PF1) featured dual arylboronates, which produced a large turn-on response. However, the turn-on kinetics were relatively slow, since the probe required two equivalents of H_2O_2 to produce the maximal turn-on.[101] Nevertheless, this probe marked the innovation of a water- and cell-compatible chemistry that has been subsequently improved and allowed the discovery of novel H_2O_2 signaling processes relating to neuronal, stem, and immune cells.[102] In this context, it is worth noting that this H_2O_2-sensitive aryl boronate chemistry has been applied toward other goals, such as masked metal chelators[108-109] and enzyme inhibitors[110] as prodrugs.

1.3.2d. Monoboronate probes for detecting endogenous H_2O_2 production. The monoboronate probe PG1 (Figure 1.5c) marks a key advance over the first-generation PF1. This asymmetric probe based on a Tokyo Green platform[111] features a single reactive boronate handle, allowing for much more rapid signal accumulation.[112] This probe has been used to directly image the endogenous H_2O_2 burst of A431 cells upon epidermal growth factor (EGF) stimulation. Excitingly, PG1 has also been validated in primary neuronal culture, a more technically challenging model system, enabling the first direct fluorescence imaging of the neuronal H_2O_2 burst in response to EGF (Figure 1.6b). PG1 demonstrates the usefulness of real-time fluorescence imaging in mapping out cellular signaling pathways. Specifically, owing to the rapid and reliable response of this probe, it was possible to determine that the neuronal H_2O_2 burst in response to EGF is dependent on the EGF receptor (EGFR) kinase domain, phosphatidylinositol-3-OH kinase (PI3K), Rac1, and Nox. Furthermore, H_2O_2 production is independent of NO synthase, and by extension, peroxynitrite, as shown by inhibitor controls. These conclusions were established by sequentially applying pharmacological inhibitors of these various enzymes and monitoring the response of the probe to the H_2O_2 produced, if any. It is thus evident that the boronate probe platform opens up a host of possibilities for elucidating fundamental biological processes, particularly in the realm of cellular signal propagation.

Further derivatives exploit the modularity of the monoboronate platform to expand the available color palette. Access to probes with sensitivity to varying wavelengths of light allows

users to monitor two or more analytes concurrently, taking advantage of the power of multi-channel imaging experiments. Additional green monoboronate probes include Peroxyfluor 2 (PF2) and Peroxyfluor 3 (PF3), based on the fluorescein scaffold, and the slightly red-shifted Peroxy Emerald 1 (PE1), a rhodol derivative. Peroxy Yellow 1 (PY1) is an additional rhodol-based probe with an excitation maximum at 514 nm, and Peroxy Orange 1 (PO1), a rhodol constructed from a julolidine building block (Figure 1.5d), can be excited at 540 nm.[104] This latter probe was used successfully in a dual-channel imaging experiment in RAW264.7 macrophages in combination with aminophenyl fluorescein (APF), a green probe which reacts with highly reactive oxygen species (hROS), which include a subset of ROS such as peroxynitrite, hypochlorite, and hydroxyl radical that are more oxidizing relative to hydrogen peroxide.[113] PO1 exhibits sufficient spectral separation from APF to allow simultaneous imaging of both H_2O_2 and hROS. With the ability to visualize these two ROS fluxes in the same space at the same time, it was discovered that RAW264.7 macrophages contain three types of phagosomes when activated: phagosomes which produce primarily H_2O_2, those which primarily produce hROS, and those which produce both (Figure 4c).[104] Perhaps more importantly, direct treatment with HOCl did not generate a fluorescence response from the PO1 boronate, showing that these types of probes show selectivity for H_2O_2 over this ROS in cellular contexts.

1.3.2e. Trappable H_2O_2 probes. The boronate-based scaffold is also flexible enough to accommodate trapping and targeting groups, allowing for the modulation of the spatial localization of these chemical tools. A trappable probe is one which can freely diffuse across the cellular membrane to enter the cell but then tends to remain inside the cell, enhancing the sensitivity of the probe by increasing its intracellular concentration.[114] In practice, this goal can be achieved by masking a carboxylic acid or phenol as an ester. Trappable probes can be removed from the extracellular media, allowing confirmation that observed signal corresponds to an increase in H_2O_2 flux within the cell rather than a result of extracellular oxidation.

A first-generation trappable yellow H_2O_2 probe, Peroxy Yellow Methyl Ester (PY1ME) (Figure 1.5e) has been used to address an apparent paradox in Nox-derived H_2O_2 signaling. Nox proteins produce extracellular H_2O_2; therefore, to play an intracellular signaling role, this Nox-derived H_2O_2 must cross the plasma membrane. PY1ME was used to test the hypothesis that H_2O_2 can travel through mammalian cell aquaporins.[115] PY1ME features good cellular retention upon washing, and importantly, washing guarantees that probe signal originates only from within the cells. H_2O_2 treatment of probe-loaded HEK293T cells overexpressing Aquaporin-1 (AQP1), AQP3, AQP8, or a control plasmid demonstrates that H_2O_2 flux into the cell is enhanced over control by AQP3 and AQP8, but not AQP1 (Figure 1.6d).[116] This result is reasonable given that AQP1 is a classical aquaporin known to only transport water, while AQP3 and AQP8 are exemplars of aquaglyceroporins and unorthodox aquaporins, which are known to transport small solutes in addition to water.

The green boronate probe PF6AM features two acetoxymethyl (AM) groups, one masking a carboxylic acid and the other masking a phenol (Figure 1.5f), which are well-known trapping groups.[114] These greatly enhance its accumulation in cells as well as its sensitivity. This probe has been used to elucidate a beneficial role of H_2O_2 in the brain. Specifically, exposing adult hippocampal progenitor cells to the fibroblast growth factor FGF-2, which is known to regulate proliferation, results in H_2O_2 production that is detectable by PF6AM (Figure 1.6e).[78] The H_2O_2 produced oxidizes the active site Cys124 of protein phosphatase PTEN, converting it into a disulfide with Cys71. This oxidized PTEN is unable to catalyze dephosphorylation,[117] most importantly of the kinase Akt, which propagates the FGF-2 signal.[118] This H_2O_2-dependent

cascade ultimately results in the maintenance of normal neuronal stem cell growth and proliferation. Use of PF6AM has also demonstrated that the H_2O_2 burst in neural stem cells is Nox-dependent, as the Nox inhibitor diphenyleneiodonium chloride (DPI) abrogates both the probe's fluorescence turn-on and the downstream dephosphorylation of Akt. Furthermore, RNAi knockdown of the specific isoform Nox2 also abolishes the signaling phenotype, which conclusively implicates this protein in the pathway.[78] PF6AM has also been fruitfully employed to detect endogenously-generated H_2O_2 in the developing chick lens,[119] Nox-dependent H_2O_2 in stimulated neutrophils,[120] and H-RAS^{V12}-induced H_2O_2 production in human fibroblasts.[121]

1.3.2f. Targetable H_2O_2 probes. In addition to trapping strategies, targeting H_2O_2 probes to specific subcellular regions can enhance their sensitivity and spatial resolution. The mitochondrion is a natural organelle to target with such a strategy, owing to its known $O_2^{\bullet-}$ and H_2O_2 production profile. The boronate-based probe MitoPY1 features a triphenylphosphonium moiety for mitochondrial targeting.[122] This lipophilic, cationic group allows MitoPY1 to travel down the cellular charge gradient into the mitochondrion.[123] MitoPY1 is a yellow probe, and it is sensitive enough to detect paraquat-induced H_2O_2 in the mitochondria, which presages its utility in elucidating oxidative stress in models of neurodegeneration, such as in Parkinson's disease. MitoPY1, in conjunction with PF6AM, has also been used to detect Na^+-dependent H_2O_2 increases in mitochondria-rich epithelial cells of the renal medullary thick ascending limb.[124] The nucleus is another chemically targetable organelle of interest with respect to H_2O_2 signaling, and the H_2O_2-responsive probe NucPE1 (Figure 1.5g) was identified as nuclearly-localized. This probe has been used to demonstrate a decrease in nuclear H_2O_2 flux in *C. elegans* overexpressing the Sir-2.1 gene, which is implicated in extending the lifespan of model organisms (Figure 1.6f).[125] Further subcellular locales can be targeted with H_2O_2-selective probes by taking advantage of SNAP labeling technology.[126] In this paradigm, the enzyme O6-alkylguanine-DNA alkyltransferase (AGT) is fused to a protein of interest or a localizing sequence and expressed in a relevant biological system. The fluorescent probes SPG1 and SPG2 can then be introduced into the cells to tag the arbitrarily localized AGT protein. This strategy has been demonstrated for localization to the plasma membrane, nucleus, mitochondria, and endoplasmic reticulum.[127]

1.3.3. Chemical tools for elucidating H_2O_2 oxidative post-translational modification (oxPTM) targets

1.3.3a. Introduction to cysteine oxPTMs. Cysteine is the most sensitive protein side chain to H_2O_2-mediated oxidation. Cysteine is oxidized *via* a two-electron nucleophilic substitution that yields a sulfenic acid ("sulfenylation"), and this oxidation is implicated in a number of important biochemical transformations (Figure 1.7). The propensity of cysteine residues toward oxidation is influenced mainly by three general factors: 1) thiol nucleophilicity, 2) protein microenvironment, and 3) proximity to reactive oxygen species.[128] Second-order rate constants for cysteine oxidation can vary dramatically within proteins, ranging from 20 M^{-1} s^{-1} as observed with protein tyrosine phosphatases (PTPs) to 10^7 M^{-1} s^{-1} for peroxiredoxin (Prx) and suggest that proximity to their Nox oxidant source may be an important determinant of protein oxidation.[129] Oxidized cysteine residues can exist as stable sulfenic acids if they are inaccessible to low-molecular-weight thiols, such as glutathione (GSH), and such stable modifications have been observed in more than 40 proteins.[130-132] Depending on the surrounding protein microenvironment and redox conditions, the sulfenic acid may also undergo secondary reactions to yield more stable cysteine oxoforms, such as disulfides, cyclic sulfonamides,[133-136] sulfinic acids (RSO_2H), and sulfonic (RSO_3H) acids.[137-139] The condensation of a sulfenic acid to a disulfide or sulfenamide protects against irreversible overoxidation,[134-135] as S-S and S-N bonds can be reduced through the activity of

thioredoxin/thioredoxin reductase (Trx/TR) or glutaredoxin/glutaredoxin reductase (Grx/GR) systems.[129, 140]

Cysteine sulfenylation has emerged as an important oxPTM in the spatial and temporal regulation of protein activity during redox signaling events.[141] Sulfenic acids have been identified in the catalytic cycle of multiple enzymes, and the formation of sulfenic acids has also been linked to oxidative stress-induced transcriptional changes in bacteria.[142-143] Less is known about the mechanisms that underlie sulfenic acid-mediated regulation of mammalian protein function and signaling pathways; however, the oxidation of cysteine residues has been associated with an expanding range of biological activities and has been implicated in the regulation of metabolism, immune responses, stem cell biology, pathogenesis of cancers, neurodegeneration, and growth factor signaling pathways.[128, 144-145]

1.3.3b. Indirect methods to detect sulfenic acids. Indirect approaches monitor the reactivity of unoxidized cysteines as a proxy for changes in redox homeostasis. Oxidized cysteines are identified by either the loss of labeling by thiol-modifying reagents or the restoration of labeling after reduction. These indirect approaches block all free thiols with alkylating agents and therefore are typically restricted to analysis of cell lysates or purified proteins. The main indirect chemical method is derived from the biotin-switch assay and involves 1) alkylation of free thiols, 2) reduction of sulfenylated cysteines with arsenite, and 3) labeling of nascent thiols with biotinylated N-ethylmaleimide (NEM) or other tagged alkylating agents (Figure 1.8a). The biotinylated proteins can be enriched and digested for proteomic analysis or imaged by Western blot analysis to assess changes in cysteine oxidation.[146-147] Alternatively, unoxidized cysteines can be alkylated using biotinylated iodoacetamide (BIAM), where loss of labeling correlates with sulfenylation (Figure 1.8b). A variation of this approach led to the development of an acid-cleavable BIAM-based isotope-coded affinity tag (ICAT) that allows for the simultaneous identification and quantification of redox-sensitive cysteine thiols (Figure 1.8c).[148-149]

1.3.3c. Nucleophilic approaches to directly detect sulfenic acids. Several methods that take advantage of the electrophilic nature of sulfenic acids have been developed for their direct detection. The selective reaction between dimedone and protein sulfenic acids was first reported by Benitez and Allison in 1974 (Figure 1.9a).[150] Under aqueous conditions, cyclic 1,3-diketones do not react with thiols, sulfinic acids, or other functional groups commonly found in biomolecules.[151] Indeed, dimedone itself can be a powerful tool to identify sulfenic acid modifications through whole-proteome shotgun proteomics[152] and the chemically selective reaction of dimedone has been exploited to detect sulfenylated proteins by MS, fluorescence, and avidin blotting approaches.[153]

Dimedone itself lacks spectral or affinity tags to aid in subsequent analysis of sulfenylated proteins. The first dimedone-based probes consisted of 1,3-cyclohexadione nucleophiles directly conjugated to fluorophores such as isatoic acid and 7-methoxycoumarin (DCP-MCC) (Figure 1.9b).[151] A stable protein sulfenic acid derived from H_2O_2 treatment of a mutant form of the bacterial peroxidase AhpC (C165S) was shown to selectively react with the fluorophore-functionalized 1,3-cyclohexadione derivatives. Additionally, the compounds were unreactive toward protein thiols, disulfides, nitrosothiols, sulfinic acids, and sulfonic acids. Probes that incorporate biotin handles (Biotin-Dimedone & DCP-Bio1) for affinity tag isolation or fluorophore tags, such as fluorescein (DCP-FL1) and rhodamine (DCP-Rho1) for visualization, have also been synthesized (Figure 1.9b).[154-155] These probes were used to study sulfenylated proteins in cells and in cell lysates, including proteomic analysis of isolated H_2O_2-perfused rat hearts to understand oxidative stress in cardiac tissues;[155] detection of vascular endothelial growth factor (VEGF)-

stimulated oxidation of proteins to elucidate VEGF receptor signaling and angiogenesis;[156-157] and detection of sulfenylated PTPs and protein tyrosine kinases (PTKs) during cell signaling.[158-160] Furthermore, 1,3-diketone nucleophiles that deviate from the quintessential dimedone scaffold, such as 4-(ethylthio)cylopentane-1,3-dione (BP1)[161] and β-ketoesters,[162] have also been reported to act as chemoselective nucleophiles toward sulfenylated proteins (Figure 1.9b).

Direct conjugation of a probe to biotin or a fluorophore can have detrimental effects on the efficiency of labeling. Commonly, tagged derivatives suffer from diminished cell uptake and trafficking properties.[163-166] As a consequence, sulfenylated proteins often need to be labeled from cell lysate. However, the redox balance of the cell is disrupted by lysis,[167] leading to artificial oxidation, which can both increase the probability of observing false-positives and over-oxidize sulfenylated proteins. Additionally, biotin- or fluorophore-tagged probes display decreased binding efficiency and biased protein labeling due to the increased steric bulk of the probe.[165, 168] An alternative approach for detection of sulfenylated proteins within cells utilizes small, membrane-permeable dimedone derivatives bearing either an alkyne or azide handle (Figure 1.9c). These smaller probes alleviate issues surrounding diffusion across the cell membrane. DAz-1 consists of a 1,3-cyclohexanedione nucleophile functionalized with an azide handle through an amide bond at the 5-position.[169] Following covalent modification of sulfenylated proteins, biotin or fluorophore tags can be conjugated onto the azide via Staudinger ligation (Figure 1.9e) or Huisgen [3 + 2] Cycloaddition (click chemistry) (Figure 1.9f).[170-171] DAz-1 was shown to be selective for sulfenylated proteins in their purified form and in living cells.[132] Initial studies with DAz-1 revealed differences in protein labeling patterns between cell lysates and live cells, highlighting the importance of probing intact cells to investigate the redox regulation of proteins. DAz-1 was also used to study the importance of sulfenylation of a resolving cysteine in the thiol peroxidase (Gpx3), which senses oxidative stress in yeast,[172] and to identify a unique reducing system in the bacterial periplasm that protects single cysteine residues from oxidation.[173]

Subsequent dimedone-based probes, DAz-2 and DYn-2, directly incorporate an azide or alkyne handle at the 4-position of the warhead and show enhanced nucleophilicity over DAz-1 (Figure 1.9c).[174] DAz-2 was used to profile the global sulfenome in human tumor cell lines and uncovered more than 175 new sulfenylated proteins, which are distributed throughout the cell and function in a diverse array of biological processes.[175] DYn-2 incorporates an alkyne handle since several studies have emerged which indicate that alkynyl-chemical reporters, in combination with azido-detection tags, offer superior sensitivity relative to the reverse combination.[166, 176] Recently, DYn-2 was used in global profiling studies to reveal dynamic protein sulfenylation during EGF signaling in human epidermal A431 cells and identified a key residue (Cys797) of the EGF receptor kinase to be susceptible to sulfenylation and a regulator of receptor kinase activity.[177] Additionally, several PTPs were found to be sulfenylated in response to EGF stimulation and the sensitivity of each protein towards oxidation correlated with their proximity to the oxidant source (Nox). EGFR was shown to be most sensitive to oxidation since it forms a complex with Nox2.[177] Therefore, it is surmised that the extent of sulfenylation of redox-senstive proteins is dependent on their proximity to the Nox oxidant source and is likely to be distinct for varying cell signaling pathways and cell type-specific phenomena

1.3.3d. Immunological approaches to detect sulfenic acids. Immunological methodologies may offer enhanced selectivity and sensitivity for detecting sulfenylated proteins from a complex proteome. To this end, an antibody that is specific for the dimedone-cysteine thioether adduct epitope has been developed and applied to a protein microarray to monitor differences in sulfenic acid modification across various cancer cell lines.[169] Additionally, the

dimedone antibody was used to demonstrate cysteine sulfenylation during EGF signaling and colocalization of the oxidized proteins with Nox2.[177] A similar antibody was reported for the detection of dimedone-modified GAPDH and used to study GAPDH sulfenylation in cardiac myocytes exposed to exogenous H_2O_2.[178]

1.3.3e. Approaches to quantify sulfenic acids. In addition to detection, identification, and mapping of sulfenylated proteins, dimedone-based probes can be used to quantify redox-dependent changes associated with physiological and pathological processes. The isotope-coded d_6-dimedone and 2-iododimedone (ICDID) strategy was developed for this purpose. The key feature of the ICDID strategy is that the pair of probes generate nearly chemically identical proteins which differ only in a 6-deuterium label. The ICDID method consists of the following workflow: 1) sulfenylated proteins are derivatized with d_6-dimedone, 2) excess reagent is removed and free thiols are labeled with iododimedone, 3) protein samples are digested, and 4) the resulting peptides are separated and analyzed by LC-MS (Figure 1.10b). The extent of sulfenylation of a particular cysteine residue can be determined by dividing the heavy-isotope labeled peak by the sum of the heavy- and light-isotope labeled peaks.[179]

Alternatively, a set of isotopically light and heavy versions of DAz-2 have been developed to monitor relative changes in protein sulfenylation.[180] A key feature of the isotopically labeled DAz-2 is that it facilitates mapping and quantifying the specific site of cysteine oxidation. The use of biotin tags for enrichment and purification of tagged protein sulfenic acids can give rise to complicated MS/MS spectra due to fragmentation of the biotin handle, making database searching challenging. It would therefore be ideal to remove the biotin tag after enrichment of the labeled proteins or peptides, and a variety of cleavable linkers have been reported for this purpose. The isotopically-labeled DAz-2 derivatives can be used in combination with an TFA-cleavable linker to facilitate enrichment, elution, detection, and quantification of sulfenylated proteins (Figure 1.10c).[180] Additionally, β-ketoesters functionalized with an alkyne handle were reported and evaluated as NH_2OH-cleavable probes for the detection of sulfenylated proteins,[162] though it should be noted that linear diketones have been reported to cross-react with amines such as lysine.[181] Recently, a highly efficient chemoproteomics workflow that utilizes isotopically light and heavy versions of DYn-2 (Figure 1.9c) was used to identify ~1000 sulfenylated sites on more than 700 different proteins in cells.[182] Moreover, the workflow allowed for quantification of dynamic changes in cellular sulfenylation during growth factor stimulation and identified a novel site of oxidation on SIRT6, a histone deacetylase, revealing an unexpected role of this protein as a redox sensor and transducer.

1.3.3f. Protein-specific methods to detect sulfenic acids. Though the dimedone-based probes have shown wide utility for the investigation of protein cysteine oxidation, the low abundance of specific signaling proteins have hindered their detection using traditional dimedone-based approaches. Reversible PTP oxidation has emerged as an important cellular regulatory mechanism,[183] and, due to the lack of sensitive and robust methods for detecting oxidized PTPs,[184] a direct method to detect oxidized phosphatases in cells to facilitate investigations of PTP redox cycling during cell signaling events has been developed. These redox-based probes (RBPs) consist of three components: 1) a cyclic 1,3-diketone nucleophile to react with oxidized active-site cysteine, 2) a module that directs binding to the PTP target, and 3) a reporter tag used for the identification, purification, or direct visualization of the probe-labeled proteins (Figure 1.9d).[168] The RBPs exhibited enhanced binding and detection of the sulfenylated PTPs compared to the parent compounds lacking the binding module. More recently, RBPs bearing an alkyne handle were used to investigate insulin-induced H_2O_2 production and ROS-mediated oxidative

inactivation of PTP1B,[185] outlining a physiological role of redox regulation during insulin signaling. It seems likely that the RBP methodology can be applied to other phosphatases to better understand their role in redox biology.

Immunochemical approaches have also been developed for the detection of specific proteins prone to oxidation. One approach utilizes an antibody that recognizes the conserved catalytic motif that is found in all PTPs in conjunction with an antibody that recognizes the terminally hyperoxidized catalytic cysteine.[186] This indirect method was used for the global proteomic assessment of the PTP "redoxome."[187] Importantly, this relies on an alkylate-reduce-oxidize approach similar to the alkylate-reduce-alkylate modified biotin switch approach mentioned above (Figure 1.8a), and so cannot differentiate phosphatases regulated by reversible oxidation from those that are inherently hyperoxidized. Another approach utilizes an antibody consisting of a single-chain variable fragment (ScFv) that has been generated to directly and selectively detect the unique structural conformation adopted by the oxidized PTP1B once the oxidized active site cysteine condenses to the cyclic sulfonamide.[188] These conformation-sensing antibodies were able to trap PTP1B in the inactive conformation permitting sustained insulin signaling in human embryonic kidney (HEK) cells.

As phosphatases are viable therapeutic targets, in the broader sense, the development of protein-targeted probes has unveiled the possibility of developing a new class of lead compounds for the development of alternative therapeutics to ameliorate diseases associated with aberrant phosphatase activity. Trapping of the oxidized phosphatase by way of small molecules bearing a nucleophilic center may be a practical means to inhibit further catalytic activity and offers an out-of-the-box approach for the design and development of a new class of therapeutics. This concept can be further adapted to other classes of proteins that contain a redox-sensitive cysteine, such as EGFR.[189-191]

1.3.3g. Electrophilic probes to detect sulfenic acids. The sulfur atom of the sulfenic acid has been shown to act as both an electrophile and as a weak nucleophile. Due to this duality of cysteine sulfenic acids, electrophilic compounds can react with the oxidized cysteine residue. 7-Chloro-4-nitrobenz-2-oxa-1,3-dizole (NBD-Cl)[192] has been used to detect sulfenylation of several proteins including AhpC peroxidase, NADH peroxidase, OhrR repressor, PTPs, recombinant human α1-antitrypsin, and human serum albumin (HSA).[131, 192-195] Strained cycloalkynes such as Bicyclo[6.1.0]nonyne (BCN) have been shown to detect sulfenylated proteins *in vitro* and may be applied to detect sulfenylated proteins *in vivo*, although alternative reaction pathways may interfere since cysteine thiols are highly susceptible to thiol-yne addition and, in the presence of ROS, may lead to formation of a doubly-conjugated byproduct.[196-200] Additionally, arylboronic acids and cyclic benzoxaboroles have been implemented for the reversible detection of sulfenylated proteins.[201] Since boronic acids are susceptible to oxidation and can react with H_2O_2, these probes may not be apt for detection of sulfenylated proteins during redox signaling events.

1.3.3h. Direct methods to detect sulfinic and sulfonic acids. Sulfenic acids can be oxidized to sulfinic acids in the presence of high concentrations of ROS, a process termed sulfinylation. Recent studies have implicated sulfinylation as a regulator of biological function. The formation and function of the cysteine sulfinic acid has been extensively characterized in Prx and has been proposed to regulate signaling events.[81] The discovery of the sulfinic acid reductase sulphiredoxin (Srx), an ATP-dependent protein that specifically reduces the sulfinic acid in Prx, led to a paradigm shift in the understanding of protein regulation by H_2O_2 whereby sulfinic acids can serve a regulatory function analogous to a disulfide or sulfenic acid.[202] The sulfinic acid has also been observed in several other proteins including nitrile hydratase, matrilysin, and the

Parkinson's disease protein DJ-1.[203-205] Current methods to detect protein sulfinic acids are relatively few, but include: a mass increase of 32 Da, acidic electrophoretic gel shifts, and antibodies that recognize a sulfinic/sulfonic acid peptide from a specific protein.[206-208] Such approaches facilitate study of sulfinic acids in individual proteins, but have limited utility in global analysis. An alternative approach is to design a probe in which the product of the reaction with the sulfinic acid is uniquely stable. Along these lines, aryl-nitroso compounds have been investigated for their unique reaction with sulfinic acids.[209] The initial reaction to form a sulfinic acid-derived *N*-sulfonyl hydroxylamine product is reversible, but the intermediate can be trapped by ester-functionalized aryl-nitroso compounds to give an irreversible *N*-sulfonylbenziosoxazolone adduct with excellent first-order reaction rates (7.86 min^{-1}) in the formation of cyclic product (Figure 1.11a). The aryl-nitroso compounds are chemoselective since reaction with a thiol yields a sulfonamide species that can be cleaved with nucleophiles. Additionally, the aryl-nitroso compounds do not cross-react with other sulfur and non-sulfur containing biological functional groups. This novel selective ligation reaction may have utility for detection of protein sulfinylation in biological systems.[210]

In the presence of strong oxidizing reagents, sulfinic acids can be further oxidized to the sulfonic acid, which represents the highest oxidation state of the cysteine sulfur atom. The sulfonic acid modification has been characterized in a small group of proteins, including mammalian copper/zinc superoxide dismutase where it has been speculated that damage resulting from hyperoxidation plays a role in diseases like familial amyotrophic lateral sclerosis.[211] It has also been speculated that the sulfonic acid modification may be used to target proteins for degradation.[212] Additionally, it has been proposed that sulfonic acid modification of Prx could enhance its proposed chaperone activity.[213] Elucidation of the sulfonic acid modification in biological and pathological states has been hindered by a lack of tools that can trap and tag the sulfonic acid modification on proteins. The use of antibodies for detection of the sulfonic acid is the most common technique for detection in specific proteins (Figure 1.11b).[207] However, the antibodies cannot be applied to detect sulfonic acids in a whole proteome and have issues differentiating between the sulfinic and sulfonic acids. Poly arginine (PA)-coated nanodiamonds have been utilized for the selective enrichment of sulfonic acid modified peptides. BSA, used as a model system in this study, was oxidized with performic acid, digested, and sulfonic acid-containing peptides were enriched and eluted from PA-coated nanodiamonds with phosphoric acid, with subsequent identification of oxidized peptides by MALDI-MS analysis.[214]

1.3.4. Outlook and summary points

As the perceived role of H_2O_2 in biology has evolved from that of toxin to immune agent to signaling agent, so too has the chemical toolbox for studying reactive oxygen species expanded in breadth and depth. Fluorescence and bioluminescence imaging offer attractive modalities for visualizing the sources and generation of H_2O_2 and exploring the role of this potentially harmful molecule in both pathology and physiology. Dimedone-based probes have shown great utility in the identification of the cysteine targets of H_2O_2-derived oxPTMs. However, the understanding of the importance of cysteine oxidation and the roles it plays in redox biology continues to expand, and so must the chemical toolbox for elucidation of oxidative modifications in biological settings. The cellular lifetime of sulfenic acids has been hypothesized to be relatively short, and recent studies have shown that the reaction between dimedone and a sulfenic acid is relatively slow. It is thus likely that many sulfenylated proteins remain undetected due to incomplete trapping of this oxPTM by dimedone-based probes. We need to expand our search toward novel nucleophiles that show enhanced reactivity and selectivity toward the sulfenic acid. Moreover, the emergence of

protein sulfinylation as a cell signaling mechanism motivates the development of robust tools and new approaches that can identify protein targets that are susceptible to sulfinylation. The widespread ability of different tissues to produce H_2O_2 and its relevance to numerous biological pathways and systems presages the discovery of further integration of this enigmatic ROS in the processes of life.

Summary Points:

1. Nox-derived H_2O_2 is an important signaling agent in biological systems, and H_2O_2-mediated oxidation of cysteines to cysteine sulfenic acids appears to play a key role in many signaling pathways.
2. The selective reaction between H_2O_2 and aryl boronates has allowed the design of many aryl boronate–based probes, which offer a means to visualize H_2O_2 fluxes with high spatial and temporal resolution in living systems when used with appropriate controls.
3. Based on the specific application, aryl boronate probes with differing excitation/emission wavelengths and subcellular localization can be selected for H_2O_2 visualization.
4. Dimedone-based probes offer a way to visualize and identify the cysteine targets of H_2O_2 oxidation. Many variants allow cysteine sulfenic acid detection by fluorescence or Western blot.
5. Dimedone-based probes have been developed for proteomics applications, in which sulfenic acid–containing proteins can be identified and the extent of sulfenylation can be quantified.

1.4. Dissertation Overview

An understanding of the principles of chemical reactivity has enabled the design of probes with properties tailored for varied biological applications, with a particular emphasis on *in cellulo* detection of reactive species via fluorescence microscopy which can shed light on the spatial and temporal distribution of RCS and ROS in cells. This dissertation focuses on the design, synthesis, and application of varied probes for the detection of biological FA, with appendices detailing efforts to detect superoxide, an important ROS.

Chapter 2 presents the development of a first-generation fluorescence intensity-based probe for FA detection utilizing a highly selective 2-aza-Cope rearrangement as a reactive trigger. After establishing sensitivity and selectivity *in vitro*, FA Probe-1 (FAP-1) is applied to detect both exogenous and endogenously-produced FA in cell culture model systems.

Chapter 3 describes the extension of the 2-aza-Cope-based reactive trigger to an excitation-ratiometric detection platform. The Ratiometric FA Probe (RFAP) platform is shown to retain the high selectivity and sensitivity of FAP-1 with increased sensitivity *in cellulo* and is additionally employed to show an increase in endogenously-produced FA in an ADH5 knockout model.

Chapter 4 details efforts toward *in vivo* FA detection modalities utilizing the 2-aza-Cope platform; specifically, the design, synthesis, and characterization of FA Luciferin-1 (FA-Luc-1) and Puromycin-FA-1 (Puro-FA-1), probes which enable bioluminescence- and immunohistochemistry-based readouts.

Figures

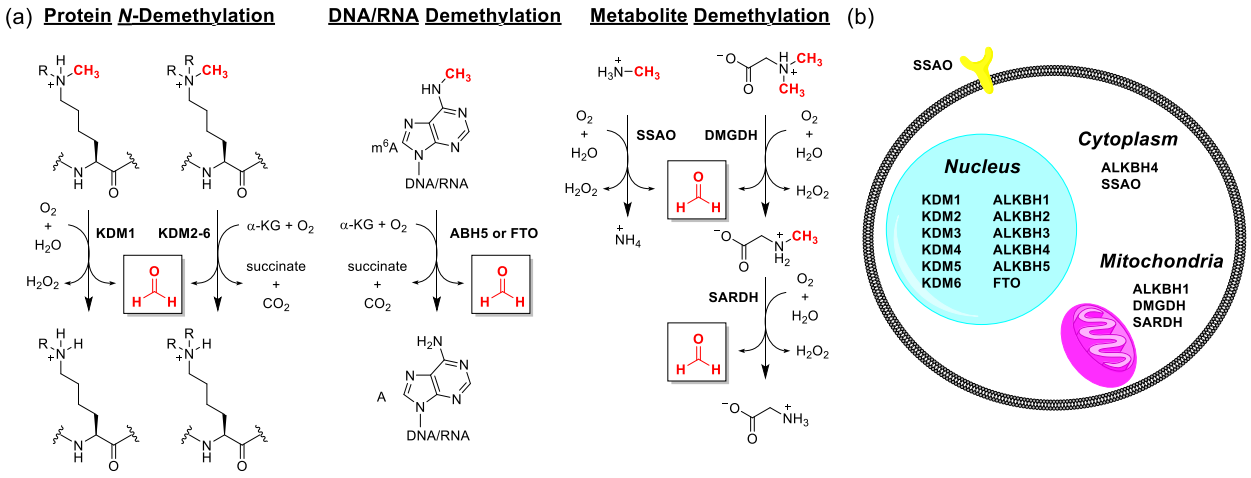

Figure 1.1. (a) Selected enzymatic pathways that generate FA in biological systems. (b) Subcellular localization of FA-generating enzymes. Abbreviations: α-KG, α-ketoglutarate; KDM, lysine demethylase; ALKBH, AlkB homologues; SSAO, semicarbazide-sensitive amine oxidases; DMGDH, dimethylglycine dehydrogenase; SARDH, sarcosine dehydrogenase; FTO, fat mass and obesity-associated protein.

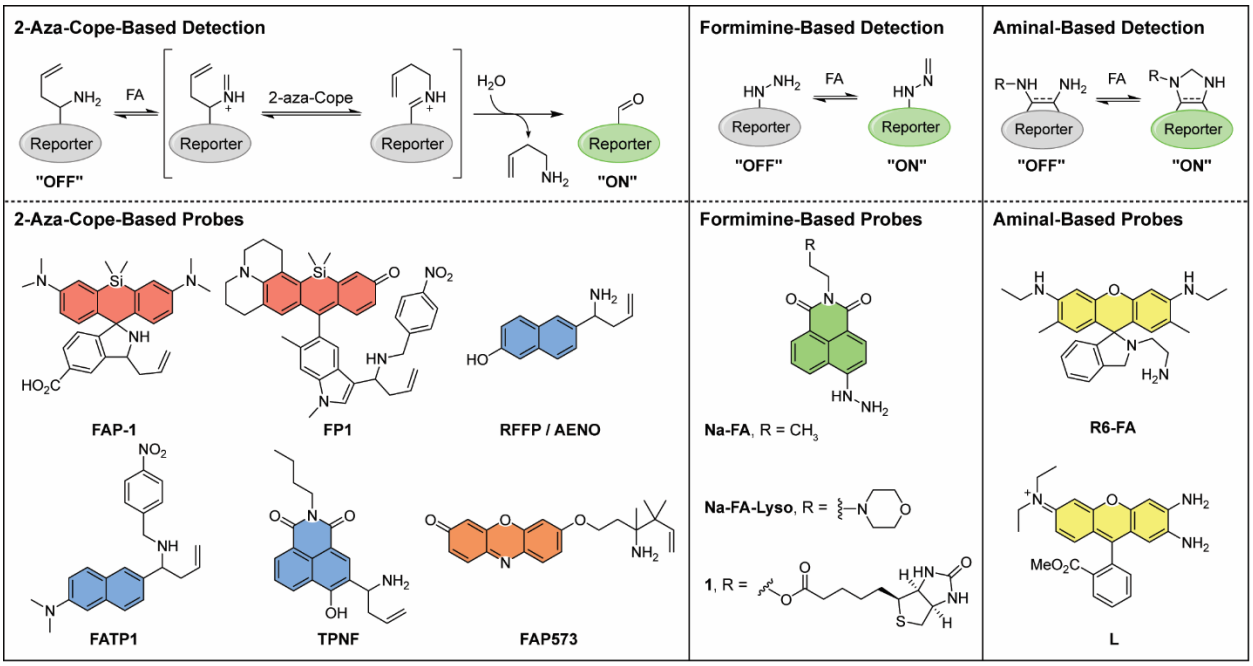

Figure 1.2. Molecular probes for the detection of FA. Three general detection strategies have been taken: 2-aza-Cope-based, formimine-based, and aminal-based. Coloring reflects excitation wavelengths.

Table 1.1. Summary of fluorescent FA probes.

	λ_{ex} (nm)	λ_{em} (nm)	Response to FA *in vitro*
aza-Cope-based probes			
FAP-1[49]	645	662	8-fold turn-on to 0.1 mM FA (1 h, 20 mM PBS)
FP1[50]	620	649	7-fold turn-on to 0.5 mM FA (3 h, PBS)
RFFP[51] /	318	359 (pre-FA) 451 (post-FA)	53-fold ratio change to 3 mM FA (4 h, 25 mM PBS/1% acetone)
AENO[52]	319	513	ca. 110-fold turn-on to 5 mM FA (3 h, 10 mM PBS/ 20% DMF)
FATP1[53]	390	526	25-fold turn-on to 0.2 mM FA (3 h, 20 mM PBS/5% DMSO)
TPNF[54]	350	510	20-fold turn-on to 5 mM FA (3 h, 10 mM PBS/0.5% DMSO)
FAP573[55]	573	585	4.2-fold turn-on to 0.1 mM FA (2 h, 20 mM PBS/0.1% DMSO)
Formimine-based probes			
Na-FA[58]	440	543	900-fold turn-on to 0.1 mM FA (30 min, 10 mM PBS/1% DMSO)
Na-FA-Lyso[59]	440	543	350-fold turn-on to 0.2 mM FA (30 min, 10 mM PBS/1% DMSO)
1[60]	428	541	140-fold turn-on to 0.5 mM FA (8 min, 10 mM PBS/1% DMSO)
Aminal-based probes			
R6-FA[61]	530	560	7.4-fold turn-on to 0.01 mM FA (10 sec, 25 mM PBS/50% DMF)
L[62]	520	620	ca. 7-fold turn-on to 10 mM FA (10 mM Tris/30% EtOH)

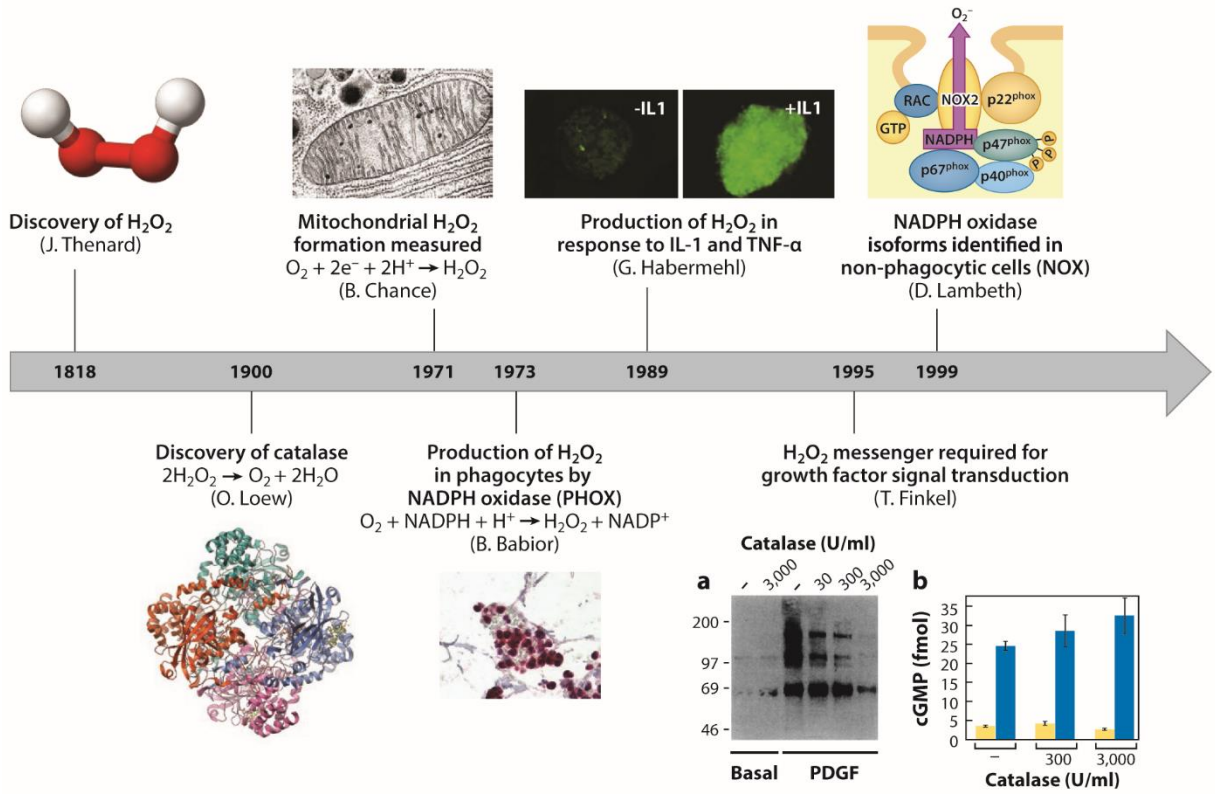

Figure 1.3. The perceived role of H_2O_2 in biology has evolved from toxin to agent of the immune system to a key component of signaling pathways. Abbreviations: cGMP, cyclic guanosine monophosphate; IL, interleukin; PDGF, platelet-derived growth factor; TNF, tumor necrosis factor.

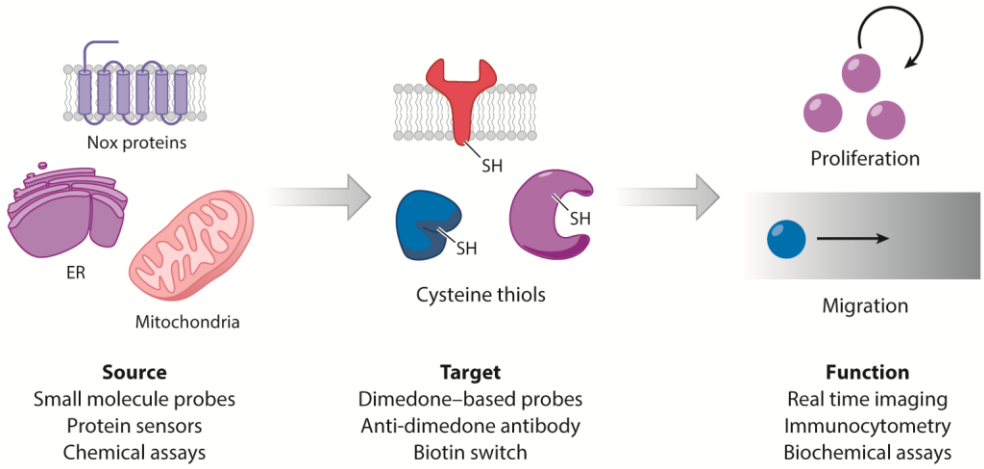

Figure 1.4. Strategies for detection of the sources, targets, and downstream consequences of H_2O_2 signaling. Abbreviations: ER, endoplasmic reticulum; Nox, NADPH oxidase.

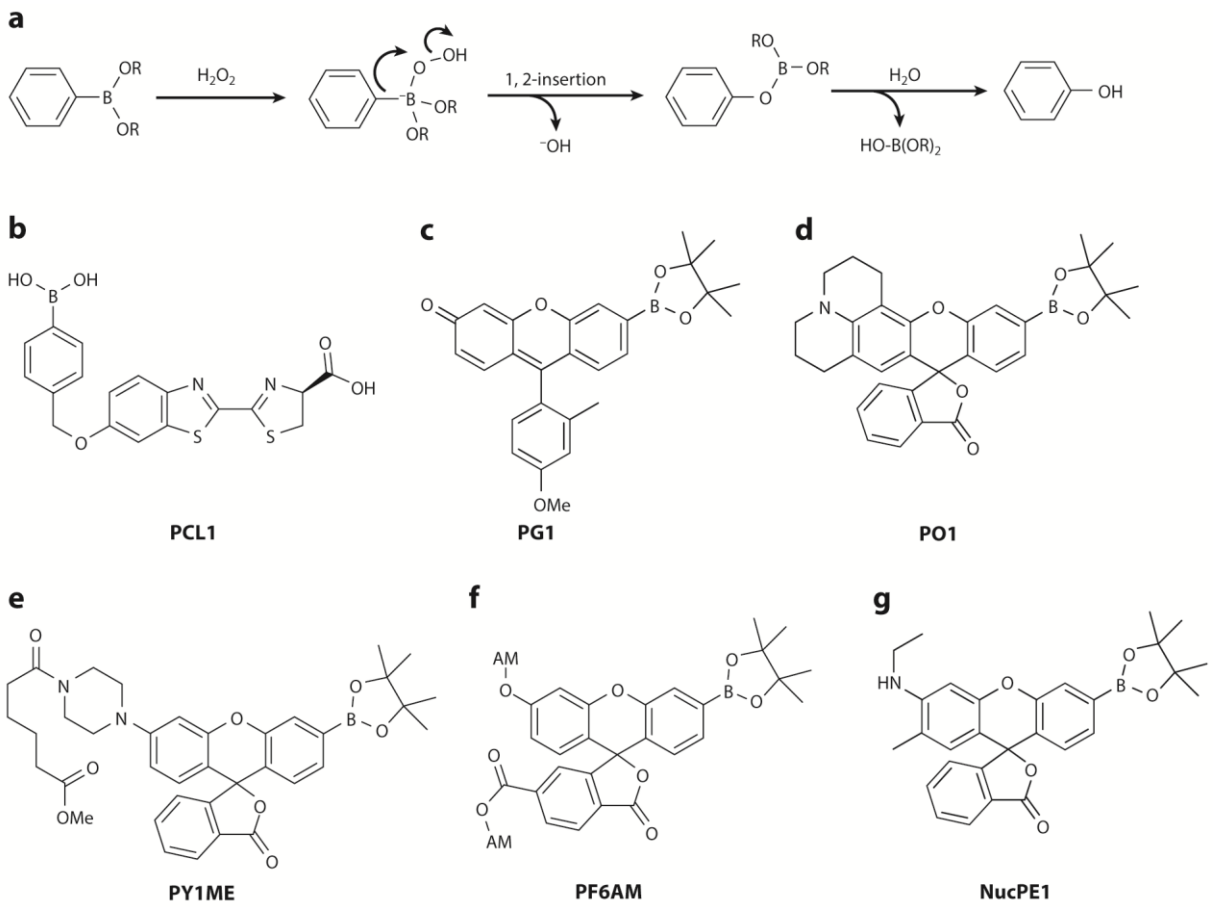

Figure 1.5. Arylboronates are a selective platform for H_2O_2 detection. (a) General oxidation of an arylboronate by H_2O_2. (b–g) Selected small-molecule boronate-based probes for H_2O_2. Abbreviations: PG1, Peroxy Green 1; PO1, Peroxy Orange 1; NucPE1, Nuclear Peroxy Emerald 1; PF6AM; Peroxyfluor-6 acetoxymethyl ester; PY1ME, Peroxy Yellow 1 Methyl Ester.

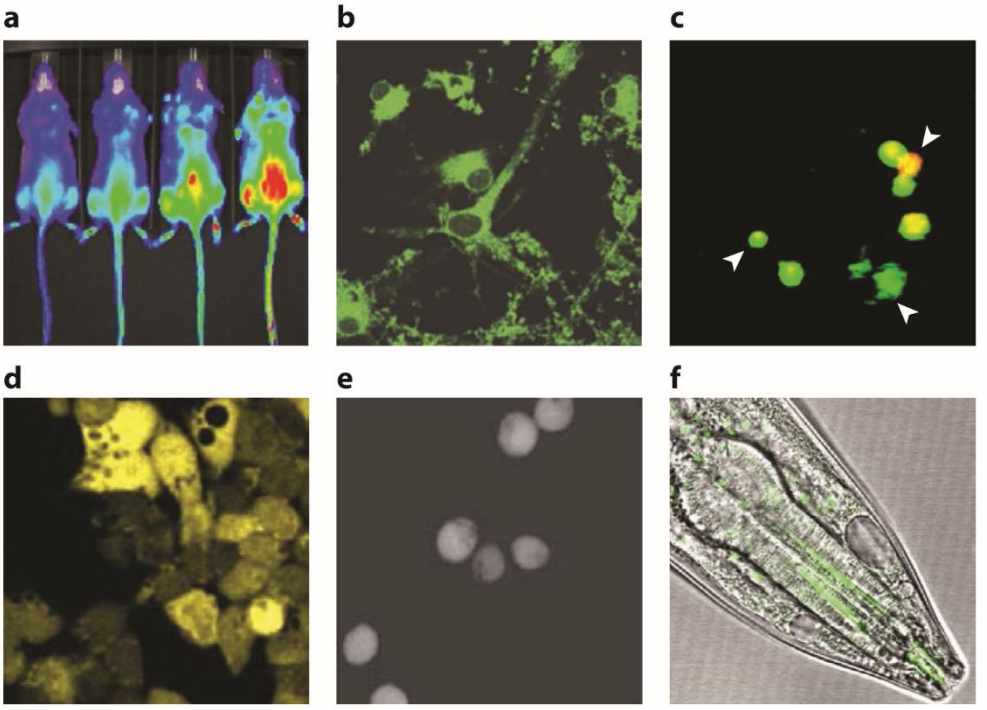

Figure 1.6. Applications of small-molecule boronate probes. (a) Response of PCL1 to increasing amounts of H_2O_2 in live mice. (b) PG1 detects H_2O_2 production by neurons stimulated with epidermal growth factor. (c) PO1 and APF detect three distinct types of phagosomes, which produce primarily H_2O_2 (orange), primarily hROS (green), and both (yellow). (d) PF6AM detects H_2O_2 production by adult hippocampal progenitor cells stimulated with fibroblast growth factor 2. (e) PY1ME detects increased H_2O_2 uptake by cells expressing aquaporin-3. (f) NucPE1 detects nuclear H_2O_2 fluxes in Caenorhabditis elegans. Abbreviations: APF, aminophenyl fluorescein; hROS, highly reactive oxygen species; NucPE1, Nuclear Peroxy Emerald 1; PF6AM, Peroxyfluor-6 Acetoxymethyl Ester; PG1, Peroxy Green 1; PO1, Peroxy Orange 1; PY1ME, Peroxy Yellow 1 Methyl Ester.

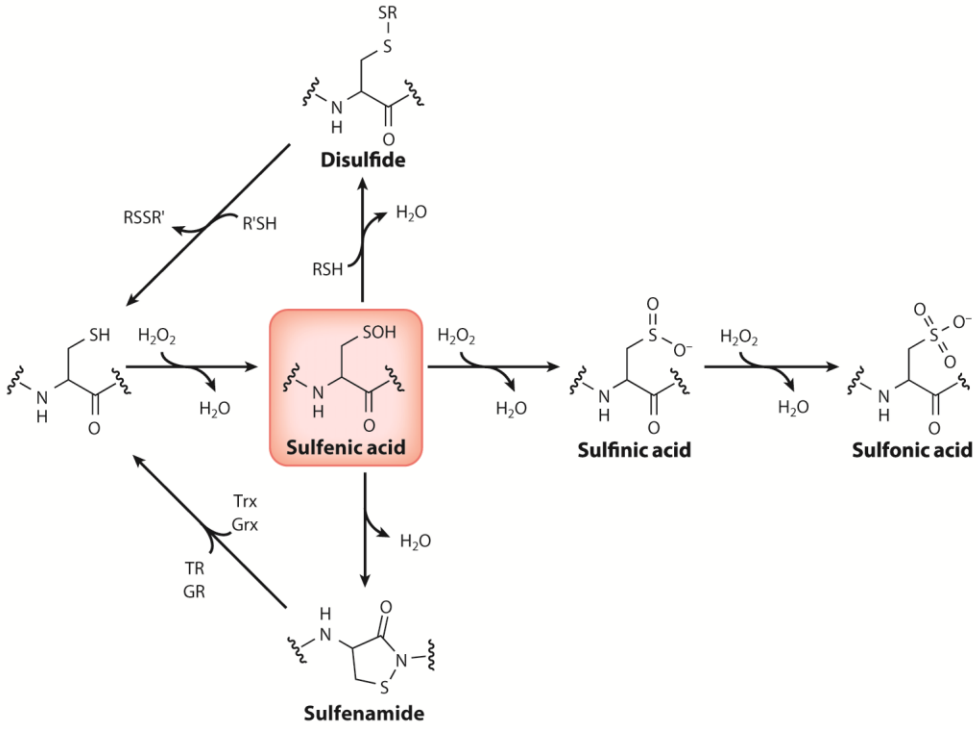

Figure 1.7. Oxidative modifications of cysteine residues by H_2O_2.

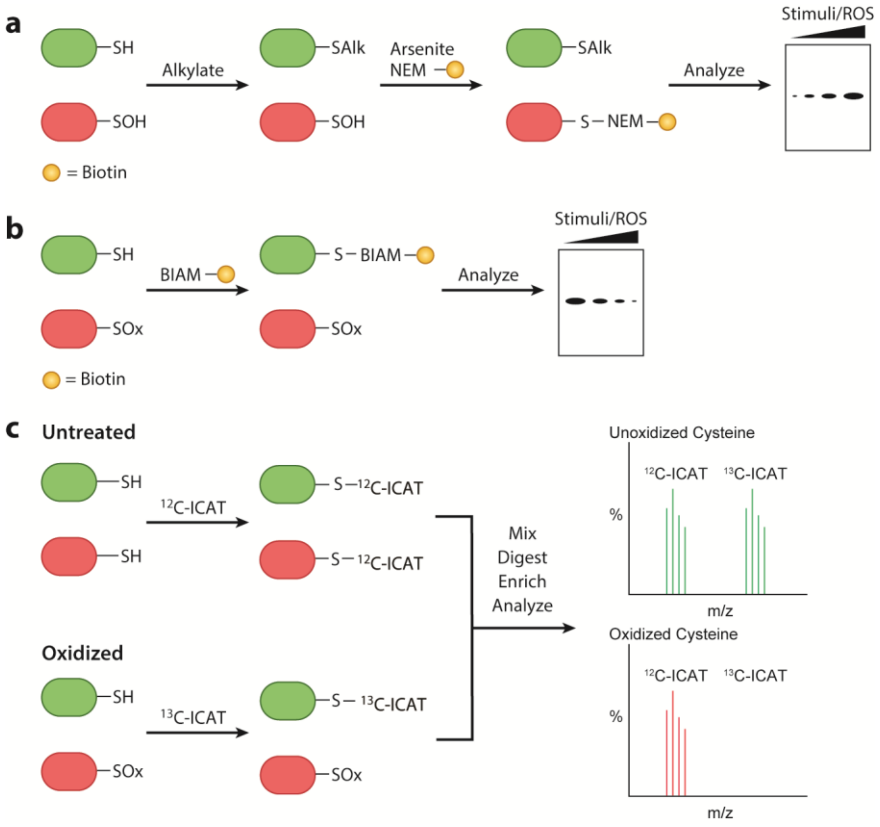

Figure 1.8. Indirect approaches to detect protein sulfenic acids. (a) Modified biotin switch technique adapted to indirectly detect sulfenic acid–modified proteins. (b) Loss of reactivity with thiol-modifying reagents, such as BIAM, indirectly monitors cysteine oxidation. (c) ICAT reagents determine the ratio of oxidized cysteine residues.

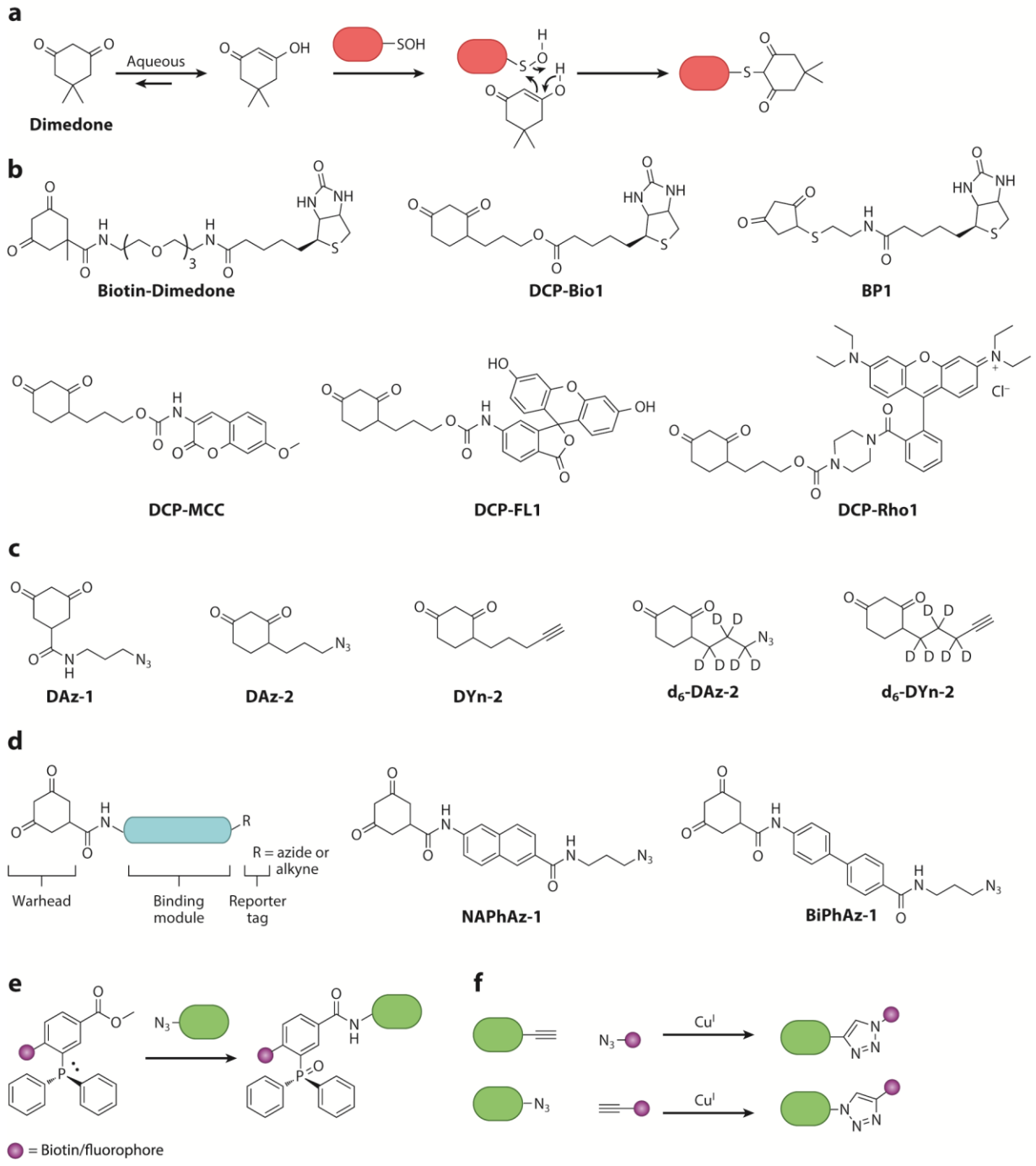

Figure 1.9. Dimedone-based probes for chemoselective detection of protein sulfenic acids. (a) Chemoselective reaction to yield a stable thioether adduct. (b) Dimedone-based probes directly conjugated with biotin or fluorescent tags. (c) Dimedone-based probes with bioorthogonal handles for subsequent enrichment or detection of sulfenic acid–modified proteins. (d) Redox-based probes that target the redox-sensitive catalytic cysteine in protein tyrosine phosphatases through incorporation of a chemical scaffold with high affinity for the enzyme's active site. (e,f) Bioorthogonal reactions for appending tags to dimedone-based probes with handles. Abbreviations: BP1, 4-(ethylthio)cylopentane-1,3-dione; DCP-FL1, fluoresceinamine-5′-N-[3-(2,4-

dioxocyclohexyl)propyl)]carbamate; DCP-MCC, 3-(2,4-dioxocyclohexyl)propyl 7-methoxy-2-oxo-2H-chromen-3-ylcarbamate; DCP-Rho1, rhodamine B [4-[3-(2,4-dioxocyclohexyl)propyl]carbamate]piperazine amide.

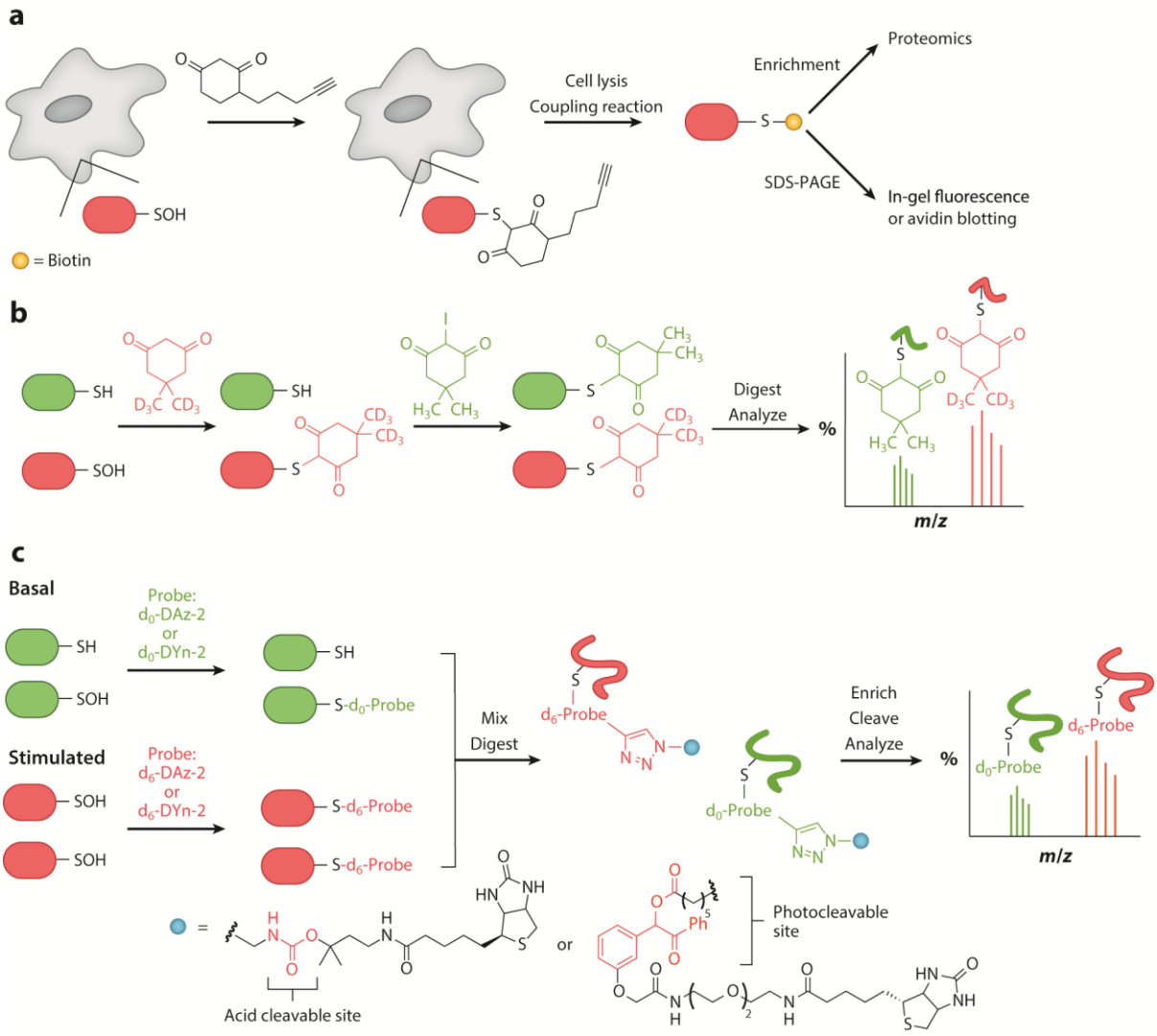

Figure 1.10. Methods to directly detect protein sulfenic acids. (a) Direct in situ labeling of sulfenylated proteins using cell-permeable chemoselective reagents. (b) Isotope-coded dimedone 2-iododimedone allows for quantification of sulfenylated proteins. (c) Use of acid-cleavable linkers and isotopically labeled DAz-2 to facilitate enrichment and quantification of sulfenylated proteins. Abbreviations: ACL, acid-cleavable linker; SDS-PAGE, sodium dodecyl sulfate polyacrylamide gel electrophoresis.

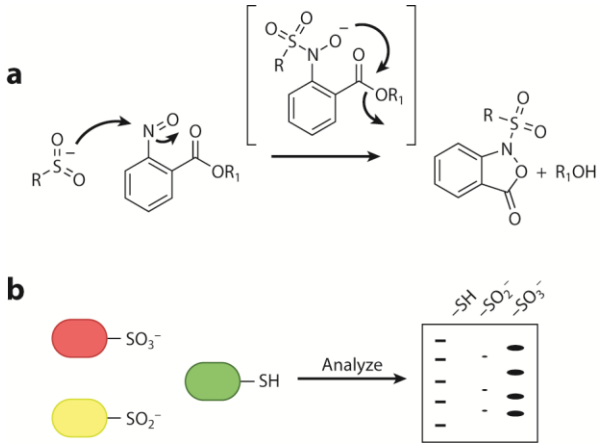

Figure 1.11. Detection of sulfinic and sulfonic acid–modified proteins. (a) Reaction of a sulfinic acid with an aryl-nitroso compound to yield a stable cyclic sulfonamide analog. (b) Antibodies that recognize the sulfonic acid–modified proteins.

1.5. References

1. He, R. Q.; Lu, J.; Miao, J. Y. *Sci. China Life Sci.* **2010,** *53*, 1399-1404.
2. Tibbetts, A. S.; Appling, D. R. *Annu. Rev. Nutr.* **2010,** *30*, 57-81.
3. Liteplo, R. G.; Beauchamp, R.; Meek, M. E.; Chénier, R., *Formaldehyde: Concise International Chemical Assessment Document*. WHO: Geneva, 2002.
4. Tong, Z.; Han, C.; Luo, W.; Wang, X.; Li, H.; Luo, H.; Zhou, J.; Qi, J.; He, R. *Age* **2013,** *35*, 583-596.
5. Heck, H. D.; Casanova-Schmitz, M.; Dodd, P. B.; Schachter, E. N.; Witek, T. J.; Tosun, T. *AIHA J.* **1985,** *46*, 1-3.
6. Thompson, C. M.; Ceder, R.; Grafström, R. C. *Toxicol. Lett.* **2010,** *193*, 1-3.
7. Tulpule, K.; Dringen, R. *J. Neurochem.* **2013,** *127*, 7-21.
8. Fox, J. T.; Stover, P. J. *Vitam. Horm.* **2008,** *79*, 1-44.
9. Walport, L. J.; Hopkinson, R. J.; Schofield, C. J. *Curr. Opin. Chem. Biol.* **2012,** *16*, 525-534.
10. Luka, Z.; Pakhomova, S.; Loukachevitch, L. V.; Calcutt, M. W.; Newcomer, M. E.; Wagner, C. *Protein Sci.* **2014,** *23*, 993-998.
11. Hancock, R. L.; Dunne, K.; Walport, L. J.; Flashman, E.; Kawamura, A. *Epigenomics* **2015,** *7*, 1-21.
12. Tsukada, Y.; Fang, J.; Erdjument-Bromage, H.; Warren, M. E.; Borchers, C. H.; Tempst, P.; Zhang, Y. *Nature* **2006,** *439*, 811-816.
13. Yamane, K.; Toumazou, C.; Tsukada, Y.; Erdjument-Bromage, H.; Tempst, P.; Wong, J.; Zhang, Y. *Cell* **2006,** *125*, 483-495.
14. Walport, L. J.; Hopkinson, R. J.; Chowdhury, R.; Schiller, R.; Ge, W.; Kawamura, A.; Schofield, C. J. *Nat. Commun.* **2016,** *7*, 11974.
15. Tsujikawa, K.; Koike, K.; Kitae, K.; Shinkawa, A.; Arima, H.; Suzuki, T.; Tsuchiya, M.; Makino, Y.; Furukawa, T.; Konishi, N.; Yamamoto, H. *J. Cell. Mol. Med.* **2007,** *11*, 1105-1116.
16. Wissmann, M.; Yin, N.; Müller, J. M.; Greschik, H.; Fodor, B. D.; Jenuwein, T.; Vogler, C.; Schneider, R.; Günther, T.; Buettner, R.; Metzger, E.; Schüle, R. *Nat. Cell Biol.* **2007,** *9*, 347-353.
17. Pontel, L. B.; Rosado, I. V.; Burgos-Barragan, G.; Garaycoechea, J. I.; Yu, R.; Arends, M. J.; Chandrasekaran, G.; Broecker, V.; Wei, W.; Liu, L.; Swenberg, J. A.; Crossan, G. P.; Patel, K. J. *Mol. Cell* **2015,** *60*, 177-188.
18. O'Sullivan, J.; Unzeta, M.; Healy, J.; O'Sullivan, M. I.; Davey, G.; Tipton, K. F. *NeuroToxicology* **2004,** *25*, 303-315.
19. Andrés, N.; Lizcano, J. M.; Rodriguez, M. J.; Unzeta, M.; Mahy, N. *J. Histochem. Cytochem.* **2001,** *49*, 209-217.
20. Steenkamp, D. J.; Husain, M. *Biochem. J.* **1982,** *203*, 707-715.
21. Leys, D.; Basran, J.; Scrutton, N. S. *EMBO J.* **2003,** *22*, 4038-4048.
22. Scotti, M.; Stella, L.; Shearer, E. J.; Stover, P. J. *Wiley Interdiscip. Rev. Syst. Biol. Med.* **2013,** *5*, 343-365.
23. Tralau, T.; Lafite, P.; Levy, C.; Combe, J. P.; Scrutton, N. S.; Leys, D. *J. Biol. Chem.* **2009,** *284*, 17826-17834.
24. Staab, C. A.; Hellgren, M.; Höög, J. O. *Cell Mol. Life Sci.* **2008,** *65*, 3950-3960.

25. Staab, C. A.; Alander, J.; Brandt, M.; Lengqvist, J.; Morgenstern, R.; Grafström, R. C.; Höög, J. O. *Biochem. J.* **2008,** *413*, 493-504.
26. Teng, S.; Beard, K.; Pourahmad, J.; Moridani, M.; Easson, E.; Poon, R.; O'Brien, P. J. *Chemico-biological interactions* **2001,** *130-132*, 285-296.
27. MacAllister, S. L.; Choi, J.; Dedina, L.; O'Brien, P. J. *Chemico-biological interactions* **2011,** *191*, 308-314.
28. Salthammer, T.; Mentese, S.; Marutzky, R. *Chem. Rev.* **2010,** *110*, 2536-2572.
29. Gubisne-Haberle, D.; Hill, W.; Kazachkov, M.; Richardson, J. S.; Yu, P. H. *J. Pharmacol. Exp. Ther.* **2004,** *310*, 1125-1132.
30. Soman, A.; Qiu, Y.; Chan Li, Q. *J. Chromatogr. Sci.* **2008,** *46*, 461-465.
31. Takeuchi, A.; Takigawa, T.; Abe, M.; Kawai, T.; Endo, Y.; Yasugi, T.; Endo, G.; Ogino, K. *Bull. Environ. Contam. Toxicol.* **2007,** *79*, 1-4.
32. Li, Q.; Sritharathikhun, P.; Motomizu, S. *Anal. Sci.* **2007,** *23*, 413-417.
33. Kato, S.; Burke, P. J.; Koch, T. H.; Bierbaum, V. M. *Anal. Chem.* **2001,** *73*, 2992-2997.
34. Chan, J.; Dodani, S. C.; Chang, C. J. *Nat. Chem.* **2012,** *4*, 973-984.
35. Lee, M. H.; Kim, J. S.; Sessler, J. L. *Chem. Soc. Rev.* **2015,** *44*, 4185-4191.
36. Yang, Y.; Zhao, Q.; Feng, W.; Li, F. *Chem. Rev.* **2013,** *113*, 192-270.
37. Wang, J.; Karpus, J.; Zhao, B. S.; Luo, Z.; Chen, P. R.; He, C. *Angew. Chem. Int. Ed.* **2012,** *51*, 9652-9656.
38. Michel, B. W.; Lippert, A. R.; Chang, C. J. *J. Am. Chem. Soc.* **2012,** *134*, 15668-15671.
39. Zheng, K.; Lin, W.; Tan, L.; Chen, H.; Cui, H. *Chem. Sci.* **2014,** *5*, 3439-3448.
40. Chaves-Ferreira, M.; Albuquerque, I. S.; Matak-Vinkovic, D.; Coelho, A. C.; Carvalho, S. M.; Saraiva, L. M.; Romão, C. C.; Bernardes, G. J. L. *Angew. Chem. Int. Ed.* **2015,** *54*, 1172-1175.
41. Wilson, J. L.; Kobeissi, S. F.; Oudir, S.; Haas, B.; Michel, B.; Randé, J.-L. D.; Ollivier, A.; Martens, T.; Rivard, M.; Motterlini, R.; Foresti, R. *Chem. Eur. J.* **2014,** *20*, 14698-14704.
42. Wang, T.; Douglass, E. F.; Fitzgerald, K. J.; Spiegel, D. A. *J. Am. Chem. Soc.* **2013,** *135*, 12429-12433.
43. Seitz, H. K.; Stickel, F. *Genes Nutr.* **2010,** *5*, 121-128.
44. Ellis, E. M. *Pharmacol. Ther.* **2007,** *115*, 13-24.
45. Siegel, D.; Meinema, A. C.; Permentier, H.; Hopfgartner, G.; Bischoff, R. *Anal. Chem.* **2014,** *86*, 5089-5100.
46. Aldini, G.; Dalle-Donne, I.; Colombo, R.; Facino, R. M.; Milzani, A.; Carini, M. *ChemMedChem* **2006,** *1*, 1045-1058.
47. Lavis, L. D.; Raines, R. T. *ACS Chem. Biol.* **2008,** *3*, 142-155.
48. Lakowicz, J. R., *Principles of Fluorescence Spectroscopy*. 3rd ed.; Springer: New York, 2006.
49. Brewer, T. F.; Chang, C. J. *J. Am. Chem. Soc.* **2015,** *137*, 10886-10889.
50. Roth, A.; Li, H.; Anorma, C.; Chan, J. *J. Am. Chem. Soc.* **2015,** *137*, 10890-10893.
51. He, L.; Yang, X.; Liu, Y.; Kong, X.; Lin, W. *Chem. Commun.* **2016,** *52*, 4029-4032.
52. Xu, J.; Zhang, Y.; Zeng, L.; Liu, J.; Kinsella, J. M.; Sheng, R. *Talanta* **2016,** *160*, 645-652.
53. Li, J.-B.; Wang, Q.-Q.; Yuan, L.; Wu, Y.-X.; Hu, X.-X.; Zhang, X.-B.; Tan, W. *Analyst* **2016,** *141*, 3395-3402.
54. Xie, Z.; Ge, J.; Zhang, H.; Bai, T.; He, S.; Ling, J.; Sun, H.; Zhu, Q. *Sens. Actuators B Chem.* **2017,** *241*, 1050-1056.

55. Bruemmer, K. J.; Walvoord, R. R.; Brewer, T. F.; Burgos-Barragan, G.; Wit, N.; Pontel, L. B.; Patel, K. J.; Chang, C. J. *J. Am. Chem. Soc.* **2017**, DOI: 10.1021/jacs.6b12460.
56. Jung, M. E.; Piizzi, G. *Chem. Rev.* **2005,** *105*, 1735-1766.
57. Brewer, T. F.; Burgos-Barragan, G.; Wit, N.; Patel, K. J.; Chang, C. J. *Chem. Sci.* **2017**, DOI: 10.1039/C7SC00748E.
58. Tang, Y.; Kong, X.; Xu, A.; Dong, B.; Lin, W. *Angew. Chem. Int. Ed.* **2016,** *55*, 3356-3359.
59. Tang, Y.; Kong, X.; Liu, Z.; Xu, A.; Lin, W. *Anal. Chem.* **2016,** *88*, 9359-9363.
60. Lee, Y. H.; Tang, Y.; Verwilst, P.; Lin, W.; Kim, J. S. *Chem. Commun.* **2016,** *52*, 11247-11250.
61. He, L.; Yang, X.; Ren, M.; Kong, X.; Liu, Y.; Lin, W. *Chem. Commun.* **2016,** *52*, 9582-9585.
62. Liu, C.; Jiao, X.; He, S.; Zhao, L.; Zeng, X. *Dyes Pigm.* **2017,** *138*, 23-29.
63. Liu, W.; Truillet, C.; Flavell, R. R.; Brewer, T. F.; Evans, M. J.; Wilson, D. M.; Chang, C. J. *Chem. Sci.* **2016,** *7*, 5503-5507.
64. Thenard, L. J. *Ann. Chim. Phys.* **1818,** *8*, 306-313.
65. Loew, O. *Science* **1900,** *11*, 701-702.
66. Chance, B.; Oshino, N. *Biochem. J.* **1971,** *122*, 225-233.
67. Chance, B.; Sies, H.; Boveris, A. *Physiol. Rev.* **1979,** *59*, 527-605.
68. Babior, B. M.; Kipnes, R. S.; Curnutte, J. T. *J. Clin. Investig.* **1973,** *52*, 741–744.
69. Rossi, F.; Zatti, M. *Cell. Mol. Life Sci.* **1964,** *20*, 21–23.
70. Radeke, H. H.; Meier, B.; Topley, N.; Flöge, J.; Habermehl, G. G.; Resch, K. *Kidney Int.* **1990,** *37*, 767-775.
71. Sundaresan, M.; Yu, Z.-X.; Ferrans, V. J.; Irani, K.; Finkel, T. *Science* **1995,** *270*, 296–299.
72. Bedard, K.; Krause, K.-H. *Physiol. Rev.* **2007,** *87*, 245–313.
73. O'Neill, J. S.; Reddy, A. B. *Nature* **2011,** *469*, 498-503.
74. O'Neill, J. S.; van Ooijen, G.; Dixon, L. E.; Troein, C.; Corellou, F.; Bouget, F.-Y.; Reddy, A. B.; Millar, A. J. *Nature* **2011,** *469*, 554-558.
75. Kim, J.-S.; Huang, T. Y.; Bokoch, G. M. *Mol. Biol. Cell* **2009,** *20*, 2650-2660.
76. Gianni, D.; Taulet, N.; DerMardirossian, C.; Bokoch, G. M. *Mol. Biol. Cell* **2010,** *21*, 4287-4298.
77. Niethammer, P.; Grabher, C.; Look, A. T.; Mitchison, T. J. *Nature* **2009,** *459*, 996-999.
78. Dickinson, B. C.; Peltier, J.; Stone, D.; Schaffer, D. V.; Chang, C. J. *Nat. Chem. Biol.* **2011,** *7*, 106–112.
79. D'Autreaux, B.; Toledano, M. B. *Nat. Rev. Mol. Cell Biol.* **2007,** *8*, 813–824.
80. Stone, J. R.; Yang, S. *Antioxid. Redox Signal.* **2006,** *8*, 243–270.
81. Wood, Z. A.; Poole, L. B.; Karplus, P. A. *Science* **2003,** *300*, 650-653.
82. Araki, K.; Inaba, K. *Antioxid. Redox Signal.* **2012,** *16*, 790-799.
83. Dawkes, H. C.; Phillips, S. E. V. *Curr. Opin. Struct. Biol.* **2001,** *11*, 666–673.
84. Kim, J.-J. P.; Miura, R. *Eur. J. Biochem.* **2004,** *271*, 483–493.
85. Halliwell, B.; Gutteridge, J. M. C., *Free Radicals in Biology and Medicine*. Oxford University Press: Oxford, 1999.
86. Belousov, V. V.; Fradkov, A. F.; Lukyanov, K. A.; Staroverov, D. B.; Shakhbazov, K. S.; Terskikh, A. V.; Lukyanov, S. *Nat. Methods* **2006,** *3*, 281-286.
87. Markvicheva, K. N.; Bilan, D. S.; Mishina, N. M.; Gorokhovatsky, A. Y.; Vinokurov, L. M.; Lukyanov, S.; Belousov, V. V. *Bioorg. Med. Chem.* **2011,** *19*, 1079-1084.

88. Bilan, D. S.; Pase, L.; Joosen, L.; Gorokhovatsky, A. Y.; Ermakova, Y. G.; Gadella, T. W. J.; Grabher, C.; Schultz, C.; Lukyanov, S.; Belousov, V. V. *ACS Chem. Biol.* **2012,** *8*, 535-542.
89. Zhang, X.; Huang, Y.; Gu, A.; Wang, G.; Fang, B.; Wu, H. *Chin. J. Chem.* **2012,** *30*, 501-506.
90. Lippert, A. R.; Keshari, K. R.; Kurhanewicz, J.; Chang, C. J. *J. Am. Chem. Soc.* **2011,** *133*, 3776-3779.
91. Olson, E. S.; Orozco, J.; Wu, Z.; Malone, C. D.; Yi, B.; Gao, W.; Eghtedari, M.; Wang, J.; Mattrey, R. F. *Biomaterials* **2013,** *34*, 8918-8924.
92. Cochemé, Helena M.; Quin, C.; McQuaker, Stephen J.; Cabreiro, F.; Logan, A.; Prime, Tracy A.; Abakumova, I.; Patel, Jigna V.; Fearnley, Ian M.; James, Andrew M.; Porteous, Carolyn M.; Smith, Robin A. J.; Saeed, S.; Carré, Jane E.; Singer, M.; Gems, D.; Hartley, Richard C.; Partridge, L.; Murphy, Michael P. *Cell Metab.* **2011,** *13*, 340-350.
93. Lee, D.; Khaja, S.; Velasquez-Castano, J. C.; Dasari, M.; Sun, C.; Petros, J.; Taylor, W. R.; Murthy, N. *Nat. Mater.* **2007,** *6*, 765-769.
94. Van de Bittner, G. C.; Dubikovskaya, E. A.; Bertozzi, C. R.; Chang, C. J. *Proc. Natl. Acad. Sci. USA* **2010,** *107*, 21316-21321.
95. Van de Bittner, G. C.; Bertozzi, C. R.; Chang, C. J. *J. Am. Chem. Soc.* **2013,** *135*, 1783-1795.
96. Cathcart, R.; Schwiers, E.; Ames, B. N. *Anal. Biochem.* **1983,** *134*, 111-116.
97. Chen, X.; Zhong, Z.; Xu, Z.; Chen, L.; Wang, Y. *Free Radic. Res.* **2010,** *44*, 587-604.
98. Zhou, M.; Diwu, Z.; Panchuk-Voloshina, N.; Haugland, R. P. *Anal. Biochem.* **1997,** *253*, 162-168.
99. Kuivila, H. G.; Wiles, R. A. *J. Am. Chem. Soc.* **1955,** *77*, 4830-4834.
100. Kuivila, H. G.; Armour, A. G. *J. Am. Chem. Soc.* **1957,** *79*, 5659-5662.
101. Chang, M. C.; Pralle, A.; Isacoff, E. Y.; Chang, C. J. *J. Am. Chem. Soc.* **2004,** *126*, 15392-3.
102. Lippert, A. R.; Van de Bittner, G. C.; Chang, C. J. *Acc. Chem. Res.* **2011,** *44*, 793-804.
103. Jencks, W. P.; Carriuolo, J. *J. Am. Chem. Soc.* **1960,** *82*, 1778-1786.
104. Dickinson, B. C.; Huynh, C.; Chang, C. J. *J. Am. Chem. Soc.* **2010,** *132*, 5906-5915.
105. Sikora, A.; Zielonka, J.; Lopez, M.; Joseph, J.; Kalyanaraman, B. *Free Radic. Biol. Med.* **2009,** *47*, 1401-1407.
106. Zielonka, J.; Sikora, A.; Hardy, M.; Joseph, J.; Dranka, B. P.; Kalyanaraman, B. *Chem. Res. Toxicol.* **2012,** *25*, 1793-1799.
107. Sun, X.; Xu, Q.; Kim, G.; Flower, S. E.; Lowe, J. P.; Yoon, J.; Fossey, J. S.; Qian, X.; Bull, S. D.; James, T. D. *Chem. Sci.* **2014,** *5*, 3368-3373.
108. Charkoudian, L. K.; Pham, D. M.; Franz, K. J. *J. Am. Chem. Soc.* **2006,** *128*, 12424-12425.
109. Wei, Y.; Guo, M. *Angew. Chem. Int. Ed.* **2007,** *46*, 4722-4725.
110. Major Jourden, J. L.; Cohen, S. M. *Angew. Chem. Int. Ed.* **2010,** *49*, 6795-6797.
111. Urano, Y.; Kamiya, M.; Kanda, K.; Ueno, T.; Hirose, K.; Nagano, T. *J. Am. Chem. Soc.* **2005,** *127*, 4888-4894.
112. Miller, E. W.; Tulyathan, O.; Isacoff, E. Y.; Chang, C. J. *Nat. Chem. Biol.* **2007,** *3*, 263-267.
113. Setsukinai, K.-i.; Urano, Y.; Kakinuma, K.; Majima, H. J.; Nagano, T. *J. Biol. Chem.* **2003,** *278*, 3170-3175.
114. Tsien, R. Y. *Nature* **1981,** *290*, 527-528.

115. Rojek, A.; Praetorius, J.; Frøkiaer, J.; Nielsen, S.; Fenton, R. A. *Annu. Rev. Physiol.* **2008,** *70*, 301-327.
116. Miller, E. W.; Dickinson, B. C.; Chang, C. J. *Proc. Natl. Acad. Sci. USA* **2010,** *107*, 15681–15686.
117. Kwon, J.; Lee, S.-R.; Yang, K.-S.; Ahn, Y.; Kim, Y. J.; Stadtman, E. R.; Rhee, S. G. *Proc. Natl. Acad. Sci. USA* **2004,** *101*, 16419-16424.
118. Peltier, J.; O'Neill, A.; Schaffer, D. V. *Dev. Neurobiol.* **2007,** *67*, 1348-1361.
119. Basu, S.; Rajakaruna, S.; Dickinson, B. C.; Chang, C. J.; Menko, A. S. *Mol. Vis.* **2014,** *20*, 458-467.
120. Sakai, J.; Li, J.; Subramanian, Kulandayan K.; Mondal, S.; Bajrami, B.; Hattori, H.; Jia, Y.; Dickinson, Bryan C.; Zhong, J.; Ye, K.; Chang, Christopher J.; Ho, Y.-S.; Zhou, J.; Luo, Hongbo R. *Immunity* **2012,** *37*, 1037-1049.
121. Yang, M.; Haase, A. D.; Huang, F.-K.; Coulis, G.; Rivera, K. D.; Dickinson, B. C.; Chang, C. J.; Pappin, D.; Neubert, T. A.; Hannon, G. J.; Boivin, B.; Tonks, N. K. *Mol. Cell* **2014,** *55*, 782-790.
122. Dickinson, B. C.; Chang, C. J. *J. Am. Chem. Soc.* **2008,** *130*, 9638-9639.
123. Ross, M. F.; Kelso, G. F.; Blaikie, F. H.; James, A. M.; Cochemé, H. M.; Filipovska, A.; Ros, T.; Hurd, T. R.; Smith, R. A. J.; Murphy, M. P. *Biochemistry* **2005,** *70*, 222-230.
124. Ohsaki, Y.; O'Connor, P.; Mori, T.; Ryan, R. P.; Dickinson, B. C.; Chang, C. J.; Lu, Y.; Ito, S.; Cowley, A. W. *Am. J. Physiol. Ren. Physiol.* **2011,** *302*, F95-F102.
125. Dickinson, Bryan C.; Tang, Y.; Chang, Z.; Chang, Christopher J. *Chem. Biol.* **2011,** *18*, 943-948.
126. Juillerat, A.; Gronemeyer, T.; Keppler, A.; Gendreizig, S.; Pick, H.; Vogel, H.; Johnsson, K. *Chem. Biol.* **2003,** *10*, 313-317.
127. Srikun, D.; Albers, A. E.; Nam, C. I.; Iavarone, A. T.; Chang, C. J. *J. Am. Chem. Soc.* **2010,** *132*, 4455-4465.
128. Lo Conte, M.; Carroll, K. S. *J. Biol. Chem.* **2013,** *288*, 26480-26488.
129. Winterbourn, C. C.; Hampton, M. B. *Free Radic. Biol. Med.* **2008,** *45*, 549-561.
130. Salsbury, F. R., Jr.; Knutson, S. T.; Poole, L. B.; Fetrow, J. S. *Protein Sci.* **2008,** *17*, 299-312.
131. Carballal, S.; Alvarez, B.; Turell, L.; Botti, H.; Freeman, B. A.; Radi, R. *Amino acids* **2007,** *32*, 543-551.
132. Reddie, K. G.; Seo, Y. H.; Muse Iii, W. B.; Leonard, S. E.; Carroll, K. S. *Mol. Biosyst.* **2008,** *4*, 521-531.
133. Lee, J. W.; Soonsanga, S.; Helmann, J. D. *Proc. Natl. Acad. Sci. USA* **2007,** *104*, 8743-8748.
134. Salmeen, A.; Andersen, J. N.; Myers, M. P.; Meng, T. C.; Hinks, J. A.; Tonks, N. K.; Barford, D. *Nature* **2003,** *423*, 769-773.
135. van Montfort, R. L.; Congreve, M.; Tisi, D.; Carr, R.; Jhoti, H. *Nature* **2003,** *423*, 773-777.
136. Yang, J.; Groen, A.; Lemeer, S.; Jans, A.; Slijper, M.; Roe, S. M.; den Hertog, J.; Barford, D. *Biochemistry* **2007,** *46*, 709-719.
137. Hugo, M.; Turell, L.; Manta, B.; Botti, H.; Monteiro, G.; Netto, L. E.; Alvarez, B.; Radi, R.; Trujillo, M. *Biochemistry* **2009,** *48*, 9416-9426.
138. Sohn, J.; Rudolph, J. *Biochemistry* **2003,** *42*, 10060-10070.
139. Turell, L.; Botti, H.; Carballal, S.; Ferrer-Sueta, G.; Souza, J. M.; Duran, R.; Freeman, B. A.; Radi, R.; Alvarez, B. *Biochemistry* **2008,** *47*, 358-367.

140. Berndt, C.; Lillig, C. H.; Holmgren, A. *Am. J. Physiol. Heart Circ. Physiol.* **2007,** *292*, H1227-H1236.
141. Finkel, T. *J. Cell Biol.* **2011,** *194*, 7-15.
142. Paulsen, C. E.; Carroll, K. S. *Chem. Rev.* **2013,** *113*, 4633-4679.
143. Paulsen, C. E.; Carroll, K. S. *ACS Chem. Biol.* **2010,** *5*, 47-62.
144. Holmstrom, K. M.; Finkel, T. *Nat. Rev. Mol. Cell Biol.* **2014,** *15*, 411-421.
145. Schieber, M.; Chandel, N. S. *Curr. Biol.* **2014,** *24*, R453-R462.
146. Marino, S. M.; Li, Y.; Fomenko, D. E.; Agisheva, N.; Cerny, R. L.; Gladyshev, V. N. *Biochemistry* **2010,** *49*, 7709-7721.
147. Boivin, B.; Tonks, N. K. *Methods Enzymol.* **2010,** *474*, 35-50.
148. Sethuraman, M.; McComb, M. E.; Huang, H.; Huang, S.; Heibeck, T.; Costello, C. E.; Cohen, R. A. *J. Proteome Res.* **2004,** *3*, 1228-1233.
149. Sethuraman, M.; Clavreul, N.; Huang, H.; McComb, M. E.; Costello, C. E.; Cohen, R. A. *Free Radic. Biol. Med.* **2007,** *42*, 823-829.
150. Benitez, L. V.; Allison, W. S. *J. Biol. Chem.* **1974,** *249*, 6234-6243.
151. Poole, L. B.; Zeng, B. B.; Knaggs, S. A.; Yakubu, M.; King, S. B. *Bioconjug. Chem.* **2005,** *16*, 1624-1628.
152. Martinez-Acedo, P.; Gupta, V.; Carroll, K. S. *J. Mass Spectrom.* **2014,** *49*, 257-265.
153. Leonard, S. E.; Carroll, K. S. *Curr. Opin. Chem. Biol.* **2011,** *15*, 88-102.
154. Poole, L. B.; Klomsiri, C.; Knaggs, S. A.; Furdui, C. M.; Nelson, K. J.; Thomas, M. J.; Fetrow, J. S.; Daniel, L. W.; King, S. B. *Bioconjug. Chem.* **2007,** *18*, 2004-2017.
155. Charles, R. L.; Schroder, E.; May, G.; Free, P.; Gaffney, P. R.; Wait, R.; Begum, S.; Heads, R. J.; Eaton, P. *Mol. Cell. Proteomics* **2007,** *6*, 1473-1484.
156. Oshikawa, J.; Urao, N.; Kim, H. W.; Kaplan, N.; Razvi, M.; McKinney, R.; Poole, L. B.; Fukai, T.; Ushio-Fukai, M. *PLoS One* **2010,** *5*, e10189.
157. Kaplan, N.; Urao, N.; Furuta, E.; Kim, S. J.; Razvi, M.; Nakamura, Y.; McKinney, R. D.; Poole, L. B.; Fukai, T.; Ushio-Fukai, M. *Free Radic. Res.* **2011,** *45*, 1124-1135.
158. Michalek, R. D.; Nelson, K. J.; Holbrook, B. C.; Yi, J. S.; Stridiron, D.; Daniel, L. W.; Fetrow, J. S.; King, S. B.; Poole, L. B.; Grayson, J. M. *J. Immunol.* **2007,** *179*, 6456-6467.
159. Wani, R.; Qian, J.; Yin, L.; Bechtold, E.; King, S. B.; Poole, L. B.; Paek, E.; Tsang, A. W.; Furdui, C. M. *Proc. Natl. Acad. Sci. USA* **2011,** *108*, 10550-10555.
160. Klomsiri, C.; Rogers, L. C.; Soito, L.; McCauley, A. K.; King, S. B.; Nelson, K. J.; Poole, L. B.; Daniel, L. W. *Free Radic. Biol. Med.* **2014,** *71*, 49-60.
161. Qian, J.; Klomsiri, C.; Wright, M. W.; King, S. B.; Tsang, A. W.; Poole, L. B.; Furdui, C. M. *Chem. Commun.* **2011,** *47*, 9203-9205.
162. Qian, J.; Wani, R.; Klomsiri, C.; Poole, L. B.; Tsang, A. W.; Furdui, C. M. *Chem. Commun.* **2012,** *48*, 4091-4093.
163. Cohen, M. S.; Hadjivassiliou, H.; Taunton, J. *Nat. Chem. Biol.* **2007,** *3*, 156-160.
164. Seo, Y. H.; Carroll, K. S. *Proc. Natl. Acad. Sci. USA* **2009,** *106*, 16163-16168.
165. Hang, H. C.; Loureiro, J.; Spooner, E.; van der Velden, A. W.; Kim, Y. M.; Pollington, A. M.; Maehr, R.; Starnbach, M. N.; Ploegh, H. L. *ACS Chem. Biol.* **2006,** *1*, 713-723.
166. Speers, A. E.; Cravatt, B. F. *Chem. Biol.* **2004,** *11*, 535-546.
167. Go, Y. M.; Jones, D. P. *Biochim. Biophys. Acta* **2008,** *1780*, 1273-1290.
168. Leonard, S. E.; Garcia, F. J.; Goodsell, D. S.; Carroll, K. S. *Angew. Chem. Int. Ed.* **2011,** *50*, 4423-4427.
169. Seo, Y. H.; Carroll, K. S. *Bioorg. Med. Chem. Lett.* **2009,** *19*, 356-359.

170. Patterson, D. M.; Nazarova, L. A.; Prescher, J. A. *ACS Chem. Biol.* **2014,** *9*, 592-605.
171. Truong, T. H.; Carroll, K. S. *Curr. Protoc. Chem. Biol.* **2012,** *4*, 101-122.
172. Paulsen, C. E.; Carroll, K. S. *Chem. Biol.* **2009,** *16*, 217-225.
173. Depuydt, M.; Leonard, S. E.; Vertommen, D.; Denoncin, K.; Morsomme, P.; Wahni, K.; Messens, J.; Carroll, K. S.; Collet, J. F. *Science* **2009,** *326*, 1109-1111.
174. Gupta, V.; Carroll, K. S. *Biochim. Biophys. Acta* **2014,** *1840*, 847-875.
175. Leonard, S. E.; Reddie, K. G.; Carroll, K. S. *ACS Chem. Biol.* **2009,** *4*, 783-799.
176. Charron, G.; Zhang, M. M.; Yount, J. S.; Wilson, J.; Raghavan, A. S.; Shamir, E.; Hang, H. C. *J. Am. Chem. Soc.* **2009,** *131*, 4967-4975.
177. Paulsen, C. E.; Truong, T. H.; Garcia, F. J.; Homann, A.; Gupta, V.; Leonard, S. E.; Carroll, K. S. *Nat. Chem. Biol.* **2012,** *8*, 57-64.
178. Maller, C.; Schroder, E.; Eaton, P. *Antioxid. Redox Signal.* **2011,** *14*, 49-60.
179. Seo, Y. H.; Carroll, K. S. *Angew. Chem. Int. Ed.* **2011,** *50*, 1342-1345.
180. Truong, T. H.; Garcia, F. J.; Seo, Y. H.; Carroll, K. S. *Bioorg. Med. Chem. Lett.* **2011,** *21*, 5015-5020.
181. Zhu, X.; Tanaka, F.; Lerner, R. A.; Barbas, C. F. r.; WIlson, I. A. *J. Am. Chem. Soc.* **2009,** *131*, 18206-18207.
182. Yang, J.; Gupta, V.; Carroll, K. S.; Liebler, D. C. *Nat. Commun.* **2014,** *5*, 4776.
183. Tanner, J. J.; Parsons, Z. D.; Cummings, A. H.; Zhou, H.; Gates, K. S. *Antioxid. Redox Signal.* **2011,** *15*, 77-97.
184. Karisch, R.; Neel, B. G. *FEBS J.* **2013,** *280*, 459-475.
185. Garcia, F. J.; Carroll, K. S. *Eur. J. Med. Chem.* **2014,** *88*, 28-33.
186. Persson, C.; Sjoblom, T.; Groen, A.; Kappert, K.; Engstrom, U.; Hellman, U.; Heldin, C. H.; den Hertog, J.; Ostman, A. *Proc. Natl. Acad. Sci. USA* **2004,** *101*, 1886-1891.
187. Karisch, R.; Fernandez, M.; Taylor, P.; Virtanen, C.; St-Germain, J. R.; Jin, L. L.; Harris, I. S.; Mori, J.; Mak, T. W.; Senis, Y. A.; Ostman, A.; Moran, M. F.; Neel, B. G. *Cell* **2011,** *146*, 826-840.
188. Haque, A.; Andersen, J. N.; Salmeen, A.; Barford, D.; Tonks, N. K. *Cell* **2011,** *147*, 185-198.
189. Truong, T. H.; Carroll, K. S. *Biochemistry* **2012,** *51*, 9954-9965.
190. Truong, T. H.; Carroll, K. S. *Crit. Rev. Biochem. Mol. Biol.* **2013,** *48*, 332-356.
191. Schwartz, P. A.; Kuzmic, P.; Solowiej, J.; Bergqvist, S.; Bolanos, B.; Almaden, C.; Nagata, A.; Ryan, K.; Feng, J.; Dalvie, D.; Kath, J. C.; Xu, M.; Wani, R.; Murray, B. W. *Proc. Natl. Acad. Sci. USA* **2014,** *111*, 173-178.
192. Ellis, H. R.; Poole, L. B. *Biochemistry* **1997,** *36*, 15013-15018.
193. Denu, J. M.; Tanner, K. G. *Biochemistry* **1998,** *37*, 5633-5642.
194. Fuangthong, M.; Helmann, J. D. *Proc. Natl. Acad. Sci. USA* **2002,** *99*, 6690-6695.
195. Griffiths, S. W.; King, J.; Cooney, C. L. *J. Biol. Chem.* **2002,** *277*, 25486-25492.
196. Poole, T. H.; Reisz, J. A.; Zhao, W.; Poole, L. B.; Furdui, C. M.; King, S. B. *J. Am. Chem. Soc.* **2014,** *136*, 6167-6170.
197. van Geel, R.; Pruijn, G. J.; van Delft, F. L.; Boelens, W. C. *Bioconjug. Chem.* **2012,** *23*, 392-398.
198. Beatty, K. E.; Fisk, J. D.; Smart, B. P.; Lu, Y. Y.; Szychowski, J.; Hangauer, M. J.; Baskin, J. M.; Bertozzi, C. R.; Tirrell, D. A. *ChemBioChem* **2010,** *11*, 2092-2095.
199. Lo Conte, M.; Staderini, S.; Marra, A.; Sanchez-Navarro, M.; Davis, B. G.; Dondoni, A. *Chem. Commun.* **2011,** *47*, 11086-11088.

200. Kim, E. J.; Kang, D. W.; Leucke, H. F.; Bond, M. R.; Ghosh, S.; Love, D. C.; Ahn, J. S.; Kang, D. O.; Hanover, J. A. *Carbohydr. Res.* **2013,** *377*, 18-27.
201. Liu, C. T.; Benkovic, S. J. *J. Am. Chem. Soc.* **2013,** *135*, 14544-14547.
202. Jonsson, T. J.; Johnson, L. C.; Lowther, W. T. *Nature* **2008,** *451*, 98-101.
203. Murakami, T.; Nojiri, M.; Nakayama, H.; Odaka, M.; Yohda, M.; Dohmae, N.; Takio, K.; Nagamune, T.; Endo, I. *Protein Sci.* **2000,** *9*, 1024-1030.
204. Fu, X.; Kassim, S. Y.; Parks, W. C.; Heinecke, J. W. *J. Biol. Chem.* **2001,** *276*, 41279-41287.
205. Blackinton, J.; Lakshminarasimhan, M.; Thomas, K. J.; Ahmad, R.; Greggio, E.; Raza, A. S.; Cookson, M. R.; Wilson, M. A. *J. Biol. Chem.* **2009,** *284*, 6476-6485.
206. Witze, E. S.; Old, W. M.; Resing, K. A.; Ahn, N. G. *Nat. Methods* **2007,** *4*, 798-806.
207. Woo, H. A.; Kang, S. W.; Kim, H. K.; Yang, K. S.; Chae, H. Z.; Rhee, S. G. *J. Biol. Chem.* **2003,** *278*, 47361-47364.
208. Hamann, M.; Zhang, T.; Hendrich, S.; Thomas, J. A. *Methods Enzymol.* **2002,** *348*, 146-156.
209. Lo Conte, M.; Carroll, K. S. *Angew. Chem. Int. Ed.* **2012,** *51*, 6502-6505.
210. Lo Conte, M.; Lin, J.; Wilson, M. A.; Carroll, K. S. *ACS Chem. Biol.* **2015,** *10*, 1825-1830.
211. Fujiwara, N.; Nakano, M.; Kato, S.; Yoshihara, D.; Ookawara, T.; Eguchi, H.; Taniguchi, N.; Suzuki, K. *J. Biol. Chem.* **2007,** *282*, 35933-35944.
212. Tasaki, T.; Kwon, Y. T. *Trends Biochem. Sci.* **2007,** *32*, 520-528.
213. Lim, J. C.; Choi, H. I.; Park, Y. S.; Nam, H. W.; Woo, H. A.; Kwon, K. S.; Kim, Y. S.; Rhee, S. G.; Kim, K.; Chae, H. Z. *J. Biol. Chem.* **2008,** *283*, 28873-28880.
214. Chang, Y. C.; Huang, C. N.; Lin, C. H.; Chang, H. C.; Wu, C. C. *Proteomics* **2010,** *10*, 2961-2971.

Chapter 2

Design, synthesis, and application of a first-generation 2-aza-Cope-based probe for detection of formaldehyde in living cells

Portions of this work were published in the following scientific journal:

Brewer, T. F.; Chang, C. J. "An Aza-Cope Reactivity-Based Fluorescent Probe for Imaging Formaldehyde in Living Cells." *J. Am. Chem. Soc.* **2015**, *37*, 10886–10889.

Abstract

Formaldehyde (FA) is a reactive carbonyl species (RCS) produced in living systems that has been implicated in epigenetics as well as in the pathologies of various cancers, diabetes, and heart, liver, and neurodegenerative diseases. Traditional methods for biological FA detection rely on sample destruction and/or extensive processing, resulting in a loss of spatiotemporal information. To help address this technological gap, we present the design, synthesis, and biological evaluation of a fluorescent probe for live-cell FA imaging that relies on a FA-induced aza-Cope rearrangement. Formaldehyde Probe-1 (FAP-1) is capable of detecting physiologically-relevant concentrations of FA in aqueous buffer and in live cells with high selectivity over potentially competing biological analytes. Moreover, FAP-1 can visualize endogenous FA produced by lysine-specific demethylase 1 (LSD1) in a breast cancer cell model, presaging the potential utility of this chemical approach to probe RCS biology.

2.1. Introduction

Formaldehyde (FA), the simplest aldehyde, is a reactive carbonyl species (RCS) that has long been known as a human toxin and carcinogen that is released into the environment from natural (e.g., biomass combustion, solar degradation of humic substances, vegetation and microbe emissions) as well as anthropogenic (e.g., FA production and fumigation, vehicle exhaust, etc.) sources.[1] At the same time, FA is also produced endogenously in the body by demethylase and oxidase enzymes that regulate epigenetics[2-3] and metabolism[4-5] such as lysine-specific demethylase 1 (LSD1),[6] JmjC domain-containing proteins,[7-10] and semicarbazide-sensitive amine oxidase (SSAO).[11] Active degradation by formaldehyde dehydrogenase/*S*-nitrosoglutathione reductase (GSNOR) and aldehyde dehydrogenase 2 (ALDH2)[12] enzymes gives physiological FA levels ranging from 100 μM in blood to 400 μM intracellularly.[13-15] Elevations of FA and related RCS are implicated in a variety of disease pathologies, including various cancers,[16] neurodegenerative diseases,[15, 17-18] diabetes, and chronic liver and heart disorders.[19] The rapidly growing list of modified DNA[20-22] and RNA[23] bases, particularly *N*-methylated bases whose demethylation pathways may involve FA production,[24-26] presage a diverse array of important contributions for FA chemistry to biology.

Despite its significance, methods for monitoring FA within intact, living biological specimens remain underdeveloped. Current methods for FA analysis rely on radiometry,[27] gas chromatography (GC/GC-MS),[28-29] selected ion flow tube mass spectrometry (SIFT-MS),[30-31] and high performance liquid chromatography (HPLC),[32-33] which offer high sensitivity and selectivity but are limited by the need for sample processing and/or destruction of the intact specimens. As such, we sought to develop FA-responsive fluorescence-based probes that would give the potential to track this RCS in living samples. We now report the design, synthesis, and application of Formaldehyde Probe-1 (FAP-1), a first-generation reactivity-based fluorescent indicator for selective imaging of FA in solution and in living cells at physiological levels, including endogenous FA production in a cancer cell model.

2.2. Methods

2.2.1. General synthetic methods

All reactions utilizing air- or moisture-sensitive reagents were performed in dried glassware under an atmosphere of dry N_2. When dry solvent was used the solvent was passed over activated alumina. Other reagents were used without further purification. Silica gel P60 (SiliCycle) was used for column chromatography and SiliCycle 60 F254 silica gel (precoated sheets, 0.25 mm

thick) was used for analytical thin layer chromatography and visualized by fluorescence quenching under UV light. 3,7-Bis(*N*,*N*-dimethylamino)-5,5-dimethyldibenzo[*b*,*e*]silin-10(5*H*)-one (**7**) was synthesized according to literature procedures.[34] 4-bromo-3-methylbenzoic acid was purchased from AK Scientific (Union City, CA); 4-hydroxynonenal solution was purchased from Cayman Chemical (Ann Arbor, MI); glucosone and tranylcypromine were purchased from Santa Cruz Biotech (Dallas, TX); and all other reagents were purchased from Sigma-Aldrich (St. Louis, MO). ^{1}H NMR and ^{13}C NMR spectra were collected in $CDCl_3$ or CD_3OD (Cambridge Isotope Laboratories, Cambridge, MA) at 25 °C on Bruker AVB-400 and AV-600 with ^{13}C operating frequencies of 101 MHz and 150 MHz, respectively, at the College of Chemistry NMR Facility at the University of California, Berkeley. All chemical shifts are reported in the standard δ notation of parts per million relative to residual solvent peak at 7.26 ($CDCl_3$) or 3.31 (CD_3OD) for ^{1}H and 77.16 ($CDCl_3$) or 49.00 (CD_3OD) for ^{13}C as an internal reference. Splitting patterns are indicated as follows: br, broad; s, singlet; d, doublet; t, triplet; m, multiplet; dd, doublet of doublets. Low-resolution electrospray mass spectral analyses were carried out using a LC-MS (Agilent Technology 6130, Quadrupole LC/MS). High resolution mass spectral analyses (ESI-MS) and low-resolution electron-impact mass spectral analyses were carried out at the College of Chemistry Mass Spectrometry Facility at the University of California, Berkeley.

2.2.2. Probe synthesis and new compound characterization

***tert*-Butyl 4-bromo-3-methylbenzoate (3)**

To a stirred suspension of 4-bromo-3-methylbenzoic acid (20 g, 93 mmol) and DMAP (17 g, 140 mmol) in 200 mL of ^{t}BuOH:THF, 1:1, was carefully added Boc_2O (40.6 g, 186 mmol) with evolution of gas. Once gas evolution had ceased, the reaction mixture was warmed to 70 °C. TLC (5% EtOAc/hexanes) showed complete consumption of starting material after 12 h. The solvent was removed under reduced pressure. To remove residual Boc_2O,[35] the crude reaction mixture was re-dissolved in 150 mL EtOH, imidazole (15 g, 220 mmol) was added, and the solution was stirred at ambient temperature for 3 h. EtOH was removed under reduced pressure, and the residual solid was re-suspended in 200 mL EtOAc and washed sequentially with 10% aq K_2CO_3 (1 x 200 mL), H_2O (1 x 200 mL), 1 M HCl (2 x 200 mL), and brine (1 x 200 mL). The organic layer was dried over anhydrous $MgSO_4$ and concentrated under reduced pressure. Purification by silica column chromatography (4% EtOAc/hexanes) afforded **3** as a colorless liquid (17.7 g, 70% yield). ^{1}H NMR (400 MHz, $CDCl_3$) δ 7.82 (d, J = 2.0 Hz, 1H), 7.63 (dd, J = 8.3, 2.1 Hz, 1H), 7.55 (d, J = 8.3 Hz, 1H), 2.42 (s, 3H), 1.58 (s, 9H); ^{13}C NMR (151 MHz, $CDCl_3$) δ 165.2, 137.9, 132.2, 131.5, 131.1, 129.8, 128.1, 81.3, 28.1, 22.8; LRMS calcd. for $C_{12}H_{15}BrO_2$ (M^+) 270.03, found 270.

***tert*-Butyl 4-bromo-3-(dibromomethyl)benzoate (4)**

To a stirred solution of **3** (7.7 g, 28.4 mmol) in 200 mL $PhCF_3$ in a 2-neck round-bottom flask fitted with a reflux condenser were added portions of NBS (5.05 g, 28.4 mmol) and AIBN (0.07 g, 0.42 mmol) at ambient temperature followed by heating at 115 °C for 2 hours for a total of three iterations. AIBN (0.07 g, 0.42 mmol) was added a final time, and the reaction mixture was heated at 115 °C for 2 hours, then cooled to ambient temperature. The reaction mixture was filtered through a sintered funnel, and the residual solid was washed with DCM (ca. 100 mL). The combined filtrate was washed sequentially with 1 M aq. NaOH (2 x 200 mL), H_2O (1 x 200 mL), and brine (1 x 200 mL). The organic layer was dried over anhydrous $MgSO_4$, and the

solvent was removed under reduced pressure to afford **4** as a pale yellow liquid that crystallized on standing (11.7 g , 96% yield). ^{1}H NMR (400 MHz, $CDCl_3$) δ 8.58 (d, *J* = 2.1 Hz, 1H), 7.72 (dd, *J* = 8.4, 2.1 Hz, 1H), 7.51 (d, *J* = 8.3 Hz, 1H), 7.03 (s, 1H), 1.59 (s, 9H); ^{13}C NMR (101 MHz, $CDCl_3$) δ 164.0, 140.5, 132.7, 132.6, 132.0, 131.6, 124.3, 82.1, 39.1, 28.2. LRMS calcd. for $C_{12}H_{13}Br_3O_2$ (M^+) 425.85, found 426.

***tert*-Butyl 4-bromo-3-formylbenzoate (5)**

To a stirred solution of **4** (5.5 g, 12.8 mmol) in 150 mL MeCN was added a solution of $AgNO_3$ (5.45 g, 32 mmol) in 35 mL H_2O. The reaction mixture was heated to 70 °C for 24 h, whereupon TLC (5% EtOAc in hexanes) indicated complete consumption of starting material. The reaction mixture was cooled to 0 °C, filtered through celite, and concentrated under reduced pressure. The resulting residue was diluted with H_2O (50 mL) and extracted with EtOAc (2 x 100 mL). The combined organic layers were washed with H_2O (2 x 150 mL) and brine (1 x 200 mL), then dried over anhydrous $MgSO_4$. The solvent was removed under reduced pressure, and purification by silica column chromatography (3% EtOAc/hexanes) afforded **5** as a colorless liquid that crystallized on standing (1.32 g, 36% yield). ^{1}H NMR (400 MHz, $CDCl_3$) δ 10.28 (s, 1H), 8.36 (d, *J* = 2.2 Hz, 1H), 7.96 (dd, *J* = 8.3, 2.2 Hz, 1H), 7.63 (d, *J* = 8.3 Hz, 1H), 1.53 (s, 9H); ^{13}C NMR (101 MHz, $CDCl_3$) δ 190.8, 163.86, 135.4, 134.0, 133.3, 132.1, 131.0, 130.7, 82.2, 28.1. LRMS calcd. for $C_{12}H_{13}BrO_3$ (M^+) 284.00, found 284.

***tert*-Butyl 4-bromo-3-(1-((*tert*-butoxycarbonyl)amino)but-3-en-1-yl)benzoate (6)**

To a solution of compound **5** (1.2 g, 4.2 mmol) in 40 mL MeOH at 0 °C was added 6 mL of NH_3 solution (7 N in MeOH, 42 mmol). The reaction mixture was stirred at 0 °C for 30 min, then allylboronic acid pinacol ester (0.95 mL, 5 mmol) was added, and the reaction mixture was warmed to ambient temperature and stirred for 10 h. The solvent was removed under reduced pressure, and purification by silica column chromatography (0→ 5% MeOH /DCM) afforded 0.98 g of a mixture of **S1** and pinacol as a colorless liquid which was used directly without further purification. ^{1}H NMR (asterisks denote pinacol peaks, 400 MHz, $CDCl_3$) δ 8.09 (d, *J* = 2.1 Hz, 1H), 7.67 (dd, *J* = 8.3, 2.2 Hz, 1H), 7.56 (d, 1H, *J* = 8.3 Hz), 5.85-5.73 (m, 1H), 5.20-5.07 (m, 2H), 4.41 (dd, *J* = 8.4, 4.5 Hz, 1H), 2.54 (m, 1H), 2.36-2.22 (m, 1H), 1.58 (s, 9H), 1.22* (s, 19H). ^{13}C NMR (asterisks denote pinacol peaks, 101 MHz, $CDCl_3$) δ 165.3, 144.8, 134.9, 132.9, 131.7, 129.1, 128.4, 128.2, 118.3, 81.6, 75.1*, 53.7, 42.1, 28.3, 25.0*. LRMS calcd. for $C_{15}H_{21}BrNO_2$ (M+H) 326.08, found 326.0.

To a solution of crude amine **S1** in 100 mL THF was added Boc_2O (0.50 g, 2.2 mmol, 1.2 eq as determined by ^{1}H NMR of crude **S1**) and the reaction was stirred for 14h, whereupon TLC (10% EtOAc/hexanes) indicated complete consumption of **S1**. The solvent was removed under reduced pressure, and purification by silica column chromatography (5% EtOAc/hexanes) afforded **6** as a colorless oil which crystallized on standing (630 mg, 35% yield over 2 steps). ^{1}H NMR (3:1 rotamer ratio, asterisks denote minor rotamer peaks, 400 MHz, $CDCl_3$) δ 7.89 (s, 1H), 7.64 (dd, *J* = 8.3, 2.1 Hz, 1H), 7.51 (d, *J* = 8.3 Hz, 1H), 5.78-5.57 (m, 1H), 5.45* (br. s., 1H), 5.33-5.16 (m, 1H), 5.17-4.99 (m, 2H), 2.62-2.40 (m, 1H), 2.40-2.25 (m, 1H), 1.52 (s, 9H), 1.35 (s, 9H), 1.21* (br. s., 9H). ^{13}C NMR (101 MHz, $CDCl_3$) δ 165.0, 155.0, 142.0, 133.4, 133.0, 131.4, 129.1, 128.0, 127.5, 118.7, 81.4, 79.5, 53.3, 39.5, 28.3, 28.1. LRMS calcd. for $C_{20}H_{27}BrNO_4$ (M-H) 424.11, found 424.0.

Formaldehyde Probe-1 (FAP-1)

To a flame-dried 2-neck round-bottomed flask was added compound **6** (0.315 g, 0.74 mmol) and 10 mL of anhydrous THF. The resultant solution was cooled to -78 °C and a solution of PhLi (1.9 M in dibutyl ether, 0.39 mL, 0.74 mmol) was added dropwise. After 1 hour of reaction at -78 °C, a solution of *t*-BuLi (1.7 M in pentane, 0.87 mL, 1.5 mmol) was added dropwise to the reaction mixture. After 10 min at -78 °C, a solution of compound **7** (0.048 g, 0.15 mmol) in anhydrous THF (7 mL) was added dropwise, and the reaction mixture was allowed to warm to ambient temperature and stirred for 3 h, during which time the solution changed from pale yellow to dark red in color. The reaction was quenched with 1 M HCl (5 mL), causing a change to dark blue in color. The crude reaction mixture was diluted with saturated aq. $NaHCO_3$ (100 mL) and extracted with EtOAc (4 x 50 mL). The combined organic layers were washed with brine (200 mL) and dried over anhydrous $MgSO_4$. The solvent was removed under reduced pressure, and the crude material was dissolved in TFA:DCM, 1:1 (50 mL) and stirred at ambient temperature for 12 hours. The solvent was removed under reduced pressure, and purification by preparative reverse-phase HPLC (linear gradient from 30% MeCN / 70% H_2O / 0.05% formic acid to 100% MeCN / 0.05% formic acid over 60 minutes) afforded **FAP-1** as a pale blue powder (25.0 mg, 34% yield). ^{1}H NMR (400 MHz, CD_3OD) δ 8.16 (s, 1H), 8.04 (d, 1H, *J* = 8.1 Hz), 7.07 (dd, *J* = 9.4, 2.9 Hz, 2H), 6.96 (d, *J* = 7.9 Hz, 1H), 6.80 (d, *J* = 9.0 Hz, 1H), 6.74 (dd, *J* = 9.0, 2.8 Hz, 1H), 6.63 (dd, *J* = 9.0, 2.9 Hz, 1H), 6.44 (d, *J* = 9.0 Hz, 1H), 5.97-5.82 (m, 1H), 5.32-5.18 (m, 2H), 2.98 (d, *J* = 15.1 Hz, 12H), 2.93-2.73 (m, 2H), 2.65 (s, 1H), 0.64 (s, 3H), 0.54 (s, 3H). ^{13}C NMR (101 MHz, CD_3OD) δ 151.3, 151.2, 149.0, 140.7, 138.8, 138.1, 133.5, 133.0, 132.6, 132.1, 132.0, 131.0, 126.5, 125.0, 120.5, 118.2, 117.4, 115.1, 115.1, 80.0, 62.9, 40.4, 40.3, 38.2, 0.6, -1.9. Note: carboxylic acid carbon not observed. HRMS calcd. for $C_{30}H_{36}O_2N_3Si$ (M+H) 498.2571, found 498.2563.

2.2.3. Spectroscopic materials and methods

Milli-Q water was used to prepare all aqueous solutions. All spectroscopic measurements were performed in 20 mM PBS, pH 7.4. Absorption spectra were recorded using a Varian Cary 50 spectrophotometer, and fluorescence spectra were recorded using a Photon Technology International Quanta Master 4 L-format scan spectrofluorometer equipped with an LPS-220B 75-W xenon lamp and power supply, A-1010B lamp housing with integrated igniter, switchable 814 photocounting/analog photomultiplier detection unit, and MD5020 motor driver. Samples for absorption and emission measurements were contained in 1-cm × 1-cm quartz cuvettes (1.4-mL volume, Starna).

2.2.4. Quantum yield determination

Quantum yield was determined using zinc phthalocyanine (ZnPc) as a standard according to a published method.[36] For FAP-1 and ZnPc, the absorbance spectra were measured within an absorbance range below 0.1. The quantum yield was calculated according to the equation: $\phi_{sample} = \phi_{standard} (Grad_{sample}/Grad_{standard})(\eta_{sample}^2/\eta_{standard}^2)$; where ϕ is the quantum yield, $\phi_{standard} = 0.34$ in 1% pyridine/toluene,[37] Grad is the slope of the plot of absorbance versus integrated emission intensity, and η is the refractive index of the solvent.

2.2.5. Measurement of partition coefficient

A modified version of the shake method was used to determine the partition coefficient or log $D_{oct/wat}$ value for FAP-1.[38] Briefly, 1-octanol-saturated PBS (248 μL), PBS-saturated 1-octanol (248 μL), and 1 mM solution of FAP-1 in DMSO (5 μL) were added to a 0.6-mL microcentrifuge

tube. The dye was partitioned between the layers via vortexing for 30 s. The microcentrifuge tube was centrifuged on a bench-top minifuge at 4k rpm for 4 minutes to separate the layers. A portion of the 1-octanol layer (200 μL) was transferred to a 96-well plate, and the fluorescence emission from 665−700 nm was measured (excitation at 645 nm) using a Synergy Mx multimode microplate reader (BioTek Instruments, Inc.) equipped with fluorescence module. The concentration of dye in the 1-octanol layer was determined by comparison with a standard curve constructed from six data points. Measurements were performed in triplicate to give log $D_{oct/wat}$ = 0.53 ± 0.01 (mean ± standard deviation).

2.2.6. FAP-1 fluorescence response to FA

999 μL of a 10.01 μM solution of FAP-1 in 20 mM PBS (pH 7.4) was prepared by diluting a 10 mM DMSO stock solution of FAP-1 into pre-warmed PBS (37 °C) in a 1-cm × 1-cm quartz cuvette. 1 μL of 100 mM stock solution of FA (freshly prepared by diluting commercial 37 wt. % in H_2O FA solution) was added (for a final concentration of 100 μM), and the mixture was mixed by vigorous pipetting for 5 s, followed by acquisition of the t = 0 spectrum. Emission spectra (λ_{ex} = 645 nm, λ_{em} = 655–750 nm) were collected at 0, 20, 45, 60, 90, and 120 min (see Figure 2.1). Temperature was maintained at 37 °C throughout the experiment by immersing the cuvette in a heated water bath between measurements.

2.2.7. FAP-1 in vitro *detection limit*

999 μL of a 10.01 μM solution of FAP-1 in 20 mM PBS (pH 7.4) was prepared by diluting a 10 mM DMSO stock solution of FAP-1 into pre-warmed PBS (37 °C) in a 1-cm × 1-cm quartz cuvette. 1 μL of a FA stock solution (either 5 mM or 1 mM, freshly prepared by diluting commercial 37 wt. % FA solution with Milli-Q water) or 1 μL of PBS was added (for a final concentration of 5 μM, 1 μM, or 0 μM FA), and the mixture was mixed by vigorous pipetting for 5 s and placed in a 37 °C water bath. Emission spectra were obtained after 120 min. Statistical analyses for multiple comparisons were performed using one-way ANOVA with the Bonferroni correction in the statistical analysis software, R.

2.2.8. Selectivity tests

999 μL of a 10.01 μM solution of FAP-1 (for 4-hydroxynonenal cuvette: 998.4 μL of a 10.016 μM solution of FAP-1) in 20 mM PBS (pH 7.4) was prepared by diluting a 10 mM DMSO stock solution of FAP-1 into pre-warmed PBS (37 °C) in a 1-cm × 1-cm quartz cuvette. The analyte of interest was added to the cuvette to bring the concentration of analyte to 100 μM (unless otherwise specified) and the concentration of FAP-1 to 10 μM, followed by mixing by vigorous pipetting for 5 seconds, and a t = 0 spectrum was acquired. The cuvette was placed in a 37 °C water bath. Emission spectra were recorded by quickly removing the cuvette from the water bath, obtaining the spectrum, and returning the cuvette to the bath. Spectra were taken at t = 0, 20, 45, 60, 90, and 120 min (see Figure 2.2). see Appendix 3 for detailed protocols on RCS stock preparation.

FA: 1 μL of 100 mM stock solution of FA in Milli-Q water (freshly prepared by diluting 3.76 μL commercial 37 wt. % FA solution to 500 μL with Milli-Q water) was added to 999 μL of a 10.01 μM solution of FAP-1 in PBS.

Acetaldehyde: 1 μL of 100 mM stock solution of acetaldehyde in Milli-Q water (freshly prepared by diluting 2.8 μL neat acetaldehyde to 500 μL with Milli-Q water) was added to 999 μL of a 10.01 μM solution of FAP-1 in PBS.

Glucose: 1 μL of 1 M stock solution of glucose in Milli-Q water (freshly prepared by dissolving 180 mg of glucose in 1 mL Milli-Q water) was added to 999 μL of a 10.01 μM solution of FAP-1 in PBS.

4-hydroxynonenal (4-HNE): 1.56 μL of 64 mM stock solution of 4-HNE in EtOH (commerical stock) was added to 998.4 μL of a 10.016 μM solution of FAP-1 in PBS.

Dehydroascorbate: 1 μL of 100 mM stock solution of dehydroascorbic acid in Milli-Q water (freshly prepared by dissolving 0.87 mg of dehydroascorbic acid in 50 μL Milli-Q water) was added to 999 μL of a 10.01 μM solution of FAP-1 in PBS.

Glucosone: 1 μL of 100 mM stock solution of glucosone in Milli-Q water (freshly prepared by dissolving 0.9 mg of gluocosone in 50 μL Milli-Q water) was added to 999 μL of a 10.01 μM solution of FAP-1 in PBS.

Sodium pyruvate: 1 μL of 100 mM stock solution of sodium pyruvate in Milli-Q water (freshly prepared by dissolving 11 mg of sodium pyruvate in 1 mL Milli-Q water) was added to 999 μL of a 10.01 μM solution of FAP-1 in PBS.

Oxaloacetate: 1 μL of 100 mM stock solution of oxaloacetate in Milli-Q water (freshly prepared by dissolving 15 mg of oxaloacetic acid in 1.135 mL Milli-Q water) was added to 999 μL of a 10.01 μM solution of FAP-1 in PBS.

H_2O_2: 1 μL of 100 mM stock solution of H_2O_2 in Milli-Q water (freshly prepared by diluting 10.2 μL of commercial 9.8 M H_2O_2 to 1 mL with Milli-Q water) was added to 999 μL of a 10.01 μM solution of FAP-1 in PBS.

Glutathione: All buffers and stocks were deoxygenated by bubbling a stream of nitrogen gas for 30 minutes. 50 μL of a 100 mM stock solution of glutathione in PBS (freshly prepared by dissolving 615 mg of glutathione in deoxygenated PBS; pH was brought to 7.4 with deoxygenated 1 M NaOH for a final volume of 20 mL) was added to 950 μL of a 10.53 μM solution of FAP-1 in deoxygenated PBS. The screw-top cuvette was capped for the duration of the timecourse.

Methylglyoxal: 1 μL of 100 mM stock solution of methylglyoxal in Milli-Q water (freshly prepared by diluting 7.7 μL of neat methylglyoxal to 500 μL with Milli-Q water) was added to 999 μL of a 10.01 μM solution of FAP-1 in PBS.

2.2.9. Cell culture

HEK293T cells were maintained in exponential growth as a monolayer in Dulbecco's Modified Eagle Medium, high glucose, (DMEM, Invitrogen) supplemented with glutamax (Gibco), 10% fetal bovine serum (FBS, Hyclone) and 1% non-essential amino acids (NEAA, Gibco), and incubated at 37 °C in 5% CO_2. One day before imaging, the cells were passaged and plated in DMEM with glutamax (phenol red-free) supplemented with 10% FBS on poly-d-lysine-coated 4-well Lab Tek borosilicate chambered coverglass slides (Nunc) at 1.8×10^5 per well and allowed to grow to 65% confluence before imaging experiments. MCF7 cells were maintained in exponential growth as a monolayer in DMEM, high glucose, supplemented with glutamax and sodium pyruvate (Gibco), 10% FBS, and 1% NEAA. Two days before imaging, the cells were passaged and plated in DMEM with glutamax (phenol red-free) supplemented with 10% FBS on poly-d-lysine-coated 4-well Lab Tek borosilicate chambered coverglass slides at 8×10^4 per well and allowed to grow to 50% confluence before imaging experiments. Inhibitor treatments were begun after one day of growth.

2.2.10. Confocal fluorescence imaging experiments

Confocal fluorescence imaging studies were performed with a Zeiss laser scanning microscope 710 with a 20x objective lens using Zen 2009 software (Carl Zeiss). FAP-1 was excited using a 633 nm HeNe laser, and emission was collected using a META detector between 638 to 747 nm. Hoechst 33342 was excited with a 405 nm diode laser, and emission was collected using a META detector between 450 and 500 nm. BSS (136.9 mM NaCl, 5.37 mM KCl, 1.26 mM $CaCl_2$, 0.81 mM $MgSO_4$, 0.44 mM KH_2PO_4, 0.335 mM Na_2HPO_4, 10 mM PIPES; pH to 7.2 with NaOH) was used as the imaging buffer for all confocal experiments. The cells were imaged at 37 °C throughout the course of the experiment. Image analysis and quantification was performed using ImageJ (National Institutes of Health). For quantification of fluorescence intensity, four fields of cells within the same well were imaged. A region of interest (ROI) was created around each cell in each image. The mean fluorescence intensity of each cell was measured (using "Measure" function) and averaged across the four fields imaged. For each condition, multiple wells were analyzed using this process, and the values were averaged across independent experiments for statistical analysis. Statistical analyses for multiple comparisons were performed using one-way ANOVA with the Bonferroni correction in the statistical analysis software, R.

2.2.11. Exogenous FA addition in HEK293T cells

The DMEM media was aspirated from the chambers containing cells and replaced with 500 μL BSS containing 10 μM FAP-1 (diluted from 10 mM stock in DMSO) and incubated at 37 °C for 30 minutes. The buffer was then replaced with 500 μL fresh BSS containing no probe, and the cells were imaged to provide the t = 0 timepoint. 200 μL of the buffer was removed from each well and mixed with vehicle control (5 μL H_2O) or FA (5 μL of 20.2 mM FA for 200 μM final concentration upon re-addition to well, 5 μL 50.5 mM FA for 500 μM final concentration upon re-addition to well, 5 μL 101 mM FA for 1 mM final concentration upon re-addition to well; all FA stocks freshly prepared by diluting 37 wt. % commercial FA). The cells were then incubated at 37 °C for 30 min prior to imaging for the t = 30 timepoint. For nuclear staining studies, cells were incubated with 1 μM Hoechst 33342 at 37 °C for 15 min prior to imaging.

2.2.12. LSD1 inhibitor experiments in MCF-7 cells

Vehicle (10 μL Milli-Q water), tranylcypromine (TCP; 0.5 μL of a 20.2 mM stock in Milli-Q water, 20 μM final concentration), or GSK-LSD1 (10 μL of a 51 μM stock in Milli-Q water, 1 μM final concentration) were added to wells containing MCF7 cells in DMEM supplemented with 10% FBS and incubated at 37 °C in 5% CO_2 for 20 hours. The DMEM media was removed from the chambers containing cells and replaced with 500 μL BSS containing 10 μM FAP-1 (diluted from 10 mM stock in DMSO) and the same concentration of inhibitor as the 20-hour treatment (no inhibitor, 20 μM TCP, or 1 μM GSK-LSD1) and incubated at 37 °C for 60 minutes, then imaged. For nuclear staining studies, cells were incubated with 1 μM Hoechst 33342 at 37 °C for 15 min prior to imaging

2.2.13. Colocalization experiments

Colocalization experiments were performed in live HEK293T cells. HEK293T cells were labeled with ER-Tracker Green, BODIPY FL C_5-Ceramide, LysoTracker Green DND-26, MitoTracker Green FM, and Hoechst 33342 (Life Technologies) according to the manufacturer's instructions. Labeled HEK293T cells were then loaded with FAP-1 by incubating with 10 μM FAP-1 in BSS (diluted from 10 mM stock in DMSO) for 30 minutes at 37 °C. The buffer was then replaced with 500 μL fresh BSS containing no probe (for FA addition experiment, the buffer was

instead replaced with 500 μL BSS containing 1 mM FA followed by 30 min incubation), and the cells were imaged using a Zeiss laser scanning microscope 710 with a 63x oil-immersion objective lens using Zen 2009 software (Carl Zeiss). FAP-1 was excited using a 633 nm HeNe laser, and emission was collected using a META detector between 638 to 747 nm. ER-Tracker Green, BODIPY FL C_5-Ceramide, LysoTracker Green DND-26, and MitoTracker Green FM were excited using a 488 nm Ar laser, and emission was collected using a META detector between 500 and 600 nm. Hoechst 33342 was excited with a 405 nm diode laser, and emission was collected using a META detector between 450 and 500 nm.

2.3. Results

2.3.1. Design, synthesis, and evaluation of Formaldehyde Probe-1 (FAP-1)

We[39] and others[40-42] have exploited reactivity-based fluorescence detection for transient small-molecule analytes, including carbonyl species such as CO[43-47] and methylglyoxal,[48] and we sought to employ this general approach to FA detection. Our present design exploits an FA-induced 2-aza-Cope reaction to transform a homoallylic amine into an aldehyde coupled to a fluorogenic turn-on response.[49] Indeed, previous attempts to monitor FA have relied on formimine formation;[50-51] however, this condensation tends to have an unfavorable equilibrium constant in water, leading to difficulty in detecting low concentrations of the RCS. We reasoned that an aza-Cope rearrangement could trap the imine and lead to accumulation of a fluorescent product after hydrolysis (Scheme 2.1). Inspired by the work of Urano, Nagano, and co-workers that aminomethyl silicon rhodamine dyes are weakly emissive at physiologically-relevant pH due to spirocyclization,[52-53] we designed FAP-1 with a homoallylamine that would favor ring closure and low fluorescence. Upon reaction with FA, imine formation and subsequent 2-aza-Cope rearrangement and hydrolysis would yield an aldehyde product that is incapable of spirocyclization would give a fluorescence turn-on. Spirocyclization-based strategies have been employed fruitfully to detect a wide variety of biological analytes.[54-55] FAP-1 was synthesized in 7 steps, utilizing a key boronate-mediated aminoallylation to install the reactive trigger (Scheme 2.2).

With FAP-1 in hand, we tested its fluorescence turn-on response to FA in aqueous solution buffered to pH 7.4, in which it shows good solubility (log $D_{oct/wat} = 0.53 \pm 0.01$). FAP-1 is weakly fluorescent (ε_{650} = 190 M^{-1} cm^{-1}, ϕ_{fl} = 0.36; Figure 2.3, Figure 2.4) and exhibits a ca. 8-fold fluorescence turn-on response (λ_{max} = 645 nm, λ_{em} = 662 nm) upon treatment with 100 μM FA, a physiological concentration of this RCS, within 1 h (Figure 2.1).[13-14] This fluorescence enhancement is likely due to the increase in absorptivity observed during FA treatment (Figure 2.3b). At extended incubation times, the turn-on response saturates at ca. 45-fold (Figure 2.5). At a 10 μM FAP-1 concentration and a 2-hour cutoff, the *in vitro* detection limit for FA was found to be 5 μM (Figure 2.6). To verify that the observed fluorescence turn-on response was the result of the proposed 2-aza-Cope reaction, the reaction between FAP-1 and FA was monitored by LC-MS, which shows clean conversion from FAP-1 to a product with the expected mass of aldehyde **2** (Figure 2.7).

FAP-1 shows good selectivity for FA over potentially competing biological RCS, including 4-hydroxynonenal, dehydroascorbate, glucosone, oxaloacetate, and methylglyoxal, as well as over simple carbonyl-containing molecules including acetaldehyde, pyruvate, and glucose (Figure 2.2). FAP-1 is not responsive to 10 μM methylglyoxal, which is above its single-digit micromolar physiological range,[56] but does show a small response to super-physiological levels (100 μM) of this RCS. In addition, we exposed FAP-1 to oxidizing and reducing conditions that could be

encountered in the cell—specifically, 100 μM H_2O_2 and 5 mM glutathione—and observed no change in fluorescence (Figure 2.2).

2.3.2. Validation of FAP-1 for molecular imaging of FA in live cells

Having established that the 2-aza-Cope-based trigger of FAP-1 can selectively detect FA in solution at physiological levels, we next evaluated its ability to visualize changes in FA in living cells using confocal microscopy (Figure 2.8). Treatment of HEK293T cells with 10 μM FAP-1 for 30 min followed by washing to remove excess probe and addition of various concentrations of FA (200 μM to 1 mM) showed a significant and dose-dependent fluorescence turn-on in FA-treated cells over control cells (Figure 2.8a-d, 2.8f), demonstrating the ability of FAP-1 to detect FA in a cellular context. Notably, these FA concentrations fall well within a physiological concentration range, which is estimated at ca. 100 μM in blood,[13] 400 μM intracellularly,[14] and up to 700-800 μM in several cancer tissues.[57] To rule out the possibility of photoactivation and/or photobleaching interfering with fluorescence intensity measurements, we conducted photostability studies in HEK293T cells. FAP-1 exhibits consistent fluorescence intensity during 100 scans with 6% laser power (used for all imaging experiments), but exhibits slight photobleaching at 50% laser power (Figure 2.9). Moreover, cell viability was verified using Hoechst 33342 staining, which clearly showed intact and viable nuclei (Figure 2.8e), as well as a propidium iodide exclusion assay, which indicated no significant difference between FA-treated and untreated cells (Figure 2.10a). To further probe the cellular distribution of FAP-1, we performed colocalization studies using commercial organelle-targeted dyes. FAP-1 was found to be excluded from the nucleus (Figure 2.11m-r, Table 2.1), but showed overlap with endoplasmic reticulum-, Golgi apparatus-, lysosome-, and mitochondria-targeted dyes (Figure 2.11a-l, Table 2.1). In addition, the distribution of FAP-1 was not appreciably affected by the addition of 1 mM FA (Figure 2.11p-r).

2.3.3. FAP-1 enables imaging of endogenous FA production by LSD1 in MCF-7 cells

We next moved on to show that FAP-1 could be applied to image endogenous FA levels in a disease model. Specifically, elevated FA levels in certain cancers have been attributed to overexpression of LSD1, where pharmacological inhibition of LSD1 can lead to an observable decrease in FA.[58] To determine whether FAP-1 was able to visualize changes in endogenously-produced FA, we employed the MCF7 human breast cancer cell line that is known to overexpress LSD1.[59] Upon treatment of MCF7 cells with 20 μM tranylcypromine (TCP), an LSD1 inhibitor with an IC50 of 2 μM,[60] a ca. 20% decrease in FAP-1 fluorescence signal compared to control cells was observed. Additionally, treatment with 1 μM GSK-LSD1, a more potent LSD-1 inhibitor (IC50 of 42 nM),[61] also attenuated FAP-1 fluorescence (Figure 2.12). Taken together, the data show that FAP-1 is capable of detecting endogenously-produced FA in a disease model.

2.4. Conclusion

To close, we have presented the design, synthesis, and properties of FAP-1, a new type of fluorescent indicator for selective and sensitive detection of formaldehyde via a 2-aza-Cope reaction. FAP-1 features a robust fluorescence turn-on response to biologically-relevant concentrations of FA, as well as selectivity over potentially competing analytes. Furthermore, FAP-1 is capable of detecting exogenous and endogenous FA in live cells. Current efforts are underway to utilize FAP-1 and develop next-generation versions to probe the biology of reactive carbonyl species, specifically in the context of epigenetics, aging, and disease.

2.5. Acknowledgments

We thank the NIH (GM 79465) for support of this work. C.J.C. is an Investigator of the Howard Hughes Medical Institute. T.F.B. was partially supported by a Chemical Biology Training Grant from the NIH (T32 GM066698). We thank Ann Fischer (UC Berkeley Tissue Culture Facility) for expert technical assistance.

Figures

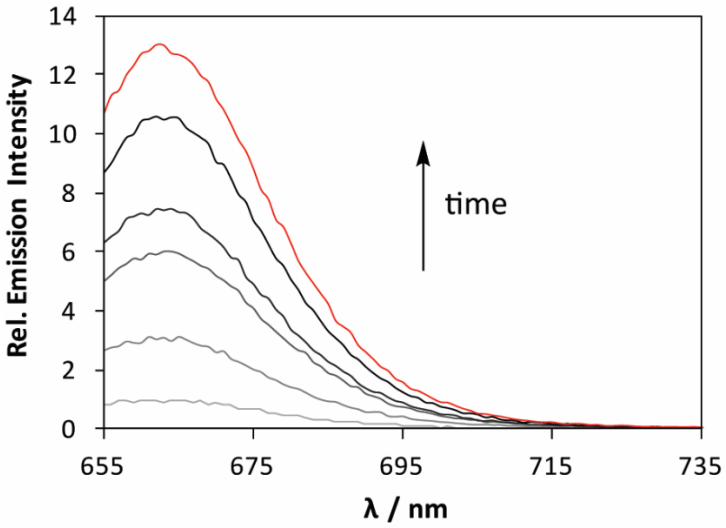

Figure 2.1. Fluorescence response of 10 μM FAP-1 to 100 μM FA. Data were acquired at 37 °C in 20 mM PBS (pH 7.4) with excitation at λ_{ex} = 645 nm. Emission was collected between 655 and 750 nm. Time points represent 0, 20, 45, 60, 90, and 120 (red trace) min after addition of 100 μM FA.

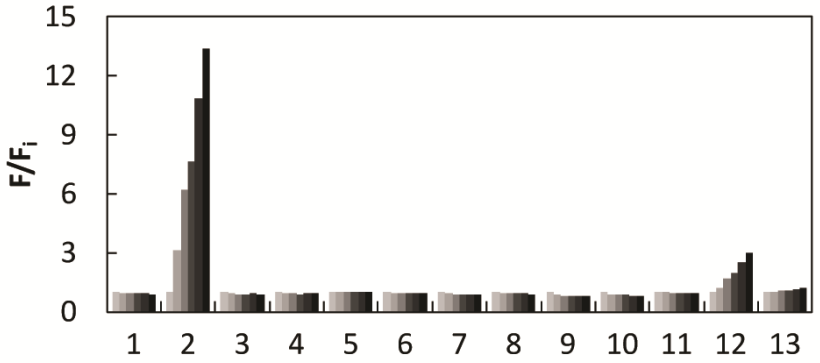

Figure 2.2. Fluorescence response of 10 μM FAP-1 to biologically relevant RCS and carbonyl-containing molecules. Bars represent relative emission from 655-700 nm at 0, 20, 45, 60, 90, and 120 (black) min after addition. Data shown are for 100 μM of all species unless otherwise denoted. Data were acquired in 20 mM PBS (pH 7.4) at 37 °C with excitation at λ_{ex} = 645 nm. Legend: (1) PBS; (2) FA; (3) acetaldehyde; (4) 4-hydroxynonenal; (5) dehydroascorbate; (6) glucose, 1 mM; (7) glucosone; (8) oxaloacetate; (9) pyruvate; (10) H_2O_2; (11) glutathione, 5 mM; (12) methylglyoxal; (13) methylglyoxal, 10 μM.

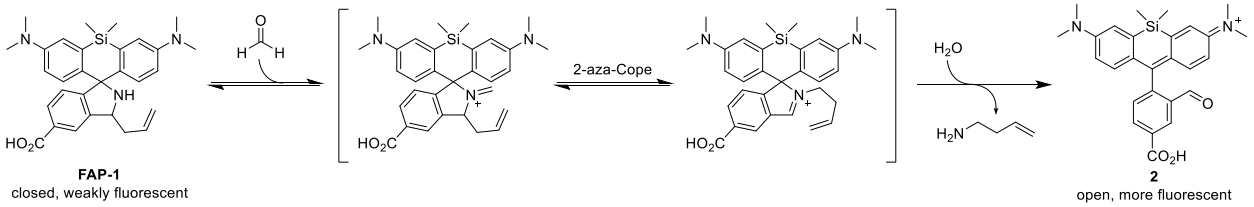

Scheme 2.1. Design of formaldehyde probe FAP-1.

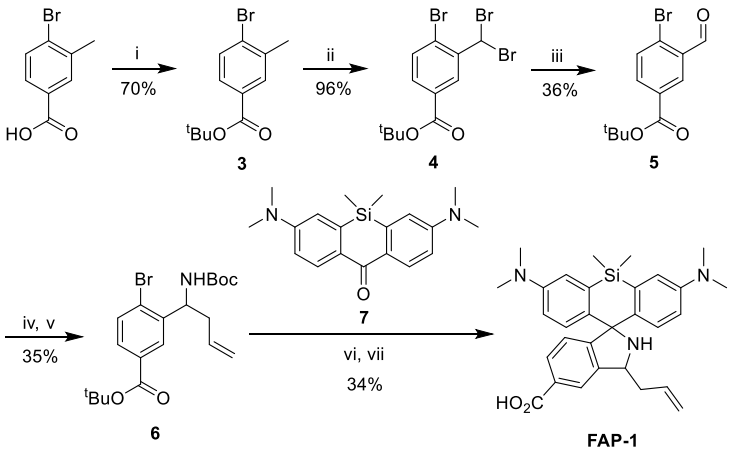

Scheme 2.2. Synthesis of FAP-1. Reagents and conditions: (i) Boc_2O, DMAP, THF, ^tBuOH, 70 °C, 12 h; (ii) NBS, AIBN, $PhCF_3$, 115 °C, 8 h; (iii) $AgNO_3$, H_2O, MeCN, 70 °C, 24 h; (iv) NH_3, MeOH, 0 °C, then allylboronic acid pinacol ester, rt, 10 h; (v) Boc_2O, THF, rt, 14 h; (vi) PhLi, THF, -78 °C, then ^tBuLi, THF, -78 °C, then **7**, -78 °C to rt, 3 h; (vii) TFA:DCM, 1:1, rt, 12 h.

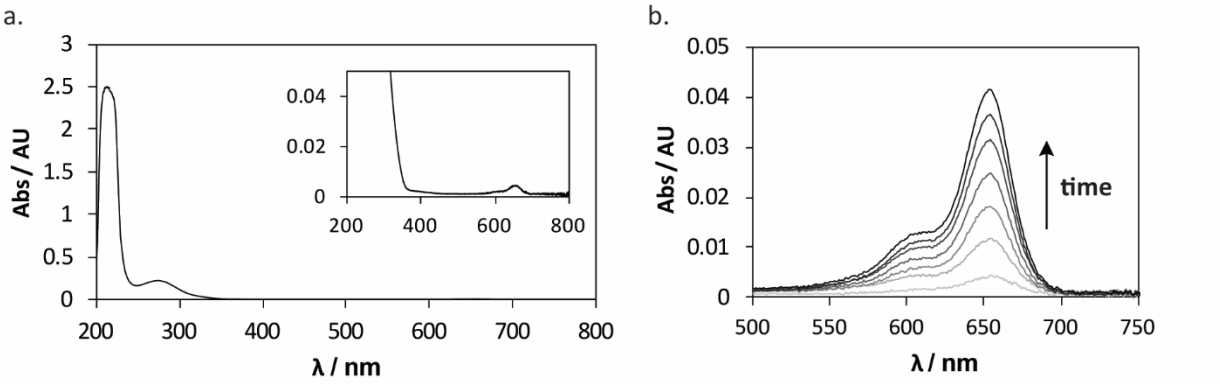

Figure 2.3. UV-visible spectra of FAP-1. Data were acquired in 20 mM PBS (pH 7.4) with 10 μM FAP-1. (a) UV-visible spectrum of FAP-1 with magnified inset. (b) UV-visible response of 10 μM FAP-1 to 100 μM FA. Time points represent 0, 20, 40, 60, 80, 100, and 120 (black trace) minutes after addition of 100 μM FA; saturation was not reached during this time.

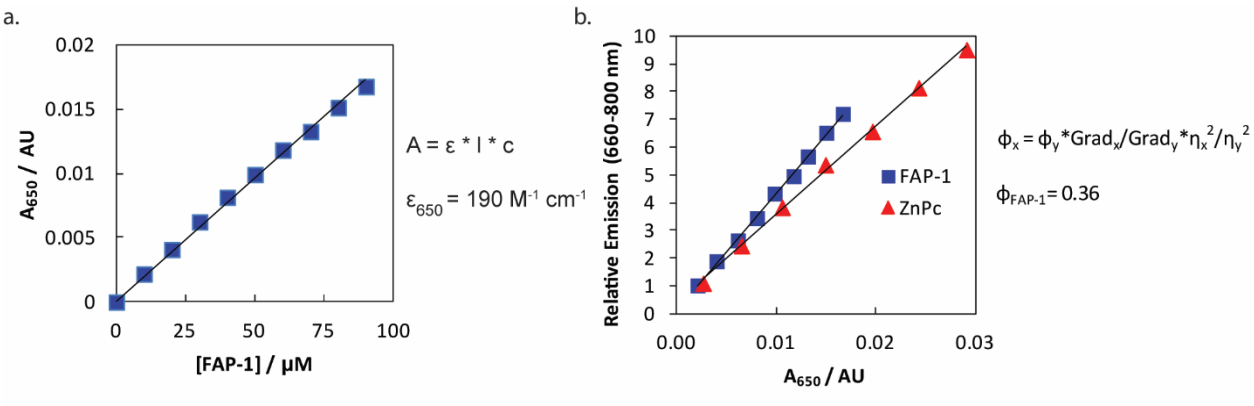

Figure 2.4. Determination of (a) molar attenuation coefficient and (b) ϕ_{fl} for FAP-1. Data for FAP-1 were acquired in 20 mM PBS (pH 7.4) with λ_{ex} = 650 nm, while data for zinc phthalocyanine (ZnPc) were acquired in 1% pyridine/toluene with λ_{ex} = 650 nm.

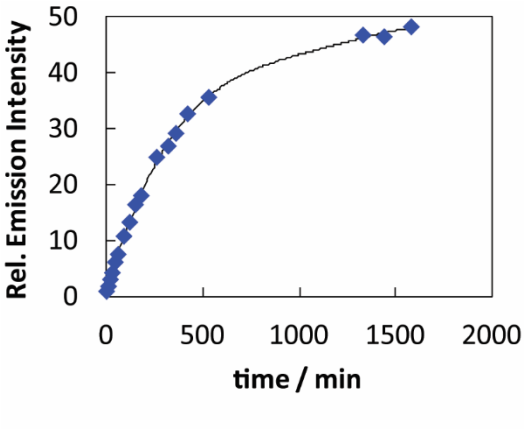

Figure 2.5. Turn-on saturation of 10 μM FAP-1 to 100 μM FA. Data were acquired at 37 °C in 20 mM PBS (pH 7.4) with excitation at λ_{ex} = 645 nm. Emission was collected between 655 and 750 nm.

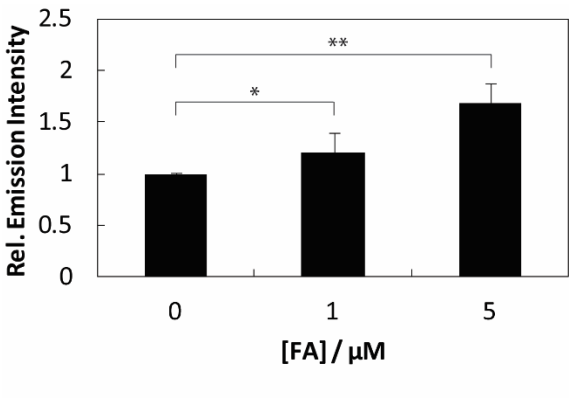

Figure 2.6. Fluorescence response of 10 µM FAP-1 to low concentrations of FA. Data were acquired in 20 mM PBS (pH 7.4) at 37 °C with excitation at λ_{ex} = 645 nm. Bars represent relative emission from 655-700 nm 2 hours after addition. Statistical analyses for multiple comparisons were performed using one-way ANOVA with the Bonferroni correction in the statistical analysis software, R. Values are shown as mean ± standard deviation (n=3). * P > 0.01, ** P < 0.01.

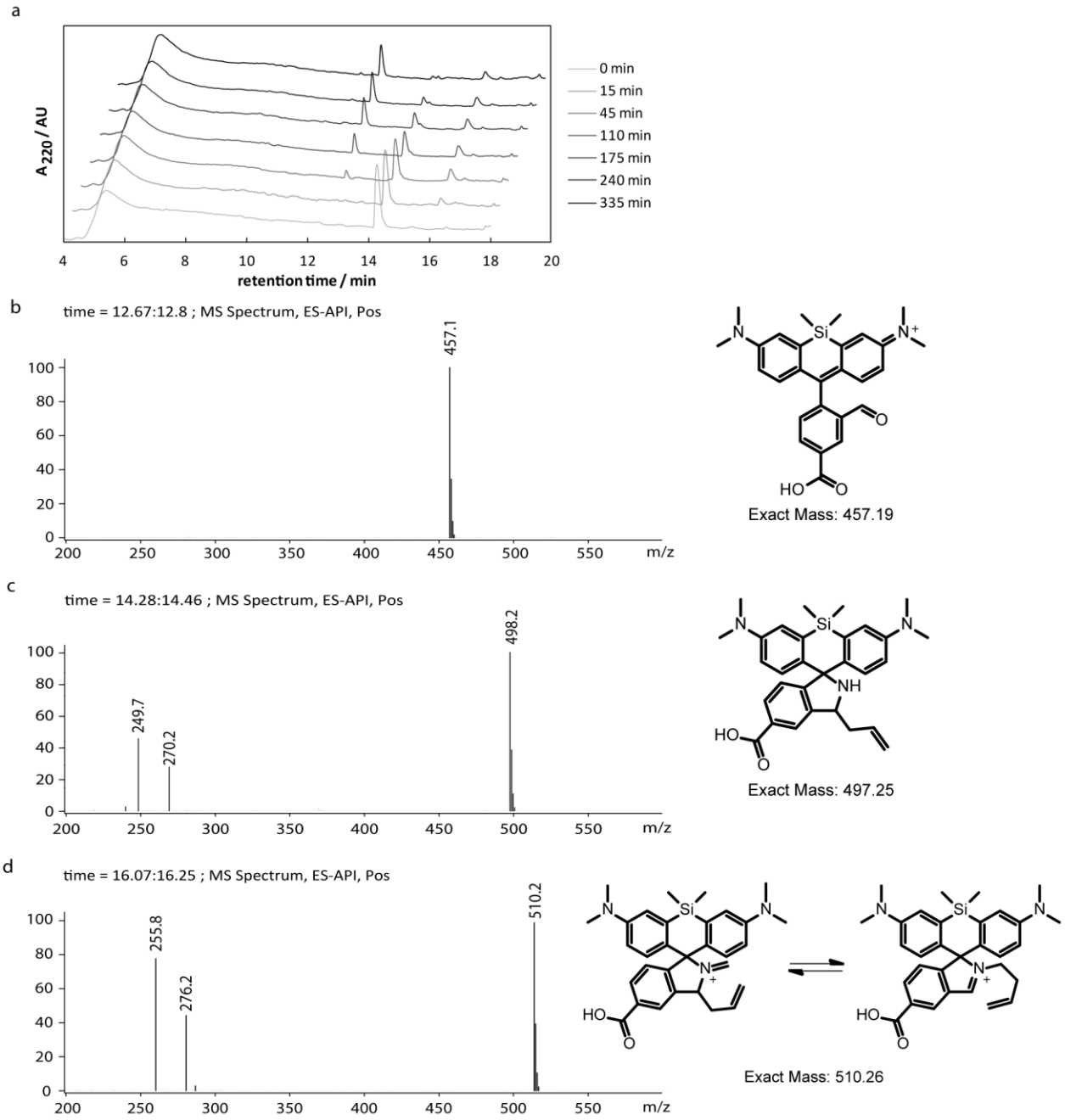

Figure 2.7. LC-MS timecourse of reaction between 100 μM FAP-1 and 1 mM FA at 25 °C in 20 mM PBS (pH 7.4). HPLC runs used a linear gradient from 5 % MeCN / 95 % H_2O / 0.05 % formic acid to 95 % MeCN / 5 % H_2O / 0.05 % formic acid over 16 min using an Agilent 300extend-C18, 3.5 μm, 4.6 × 100mm column. (a) Reverse-phase HPLC profile at 220 nm at different timepoints during reaction. Mass spectra of peaks eluting at (b) 12.7 min, (c) 14.3 min, and (d) 16.1 min during gradient.

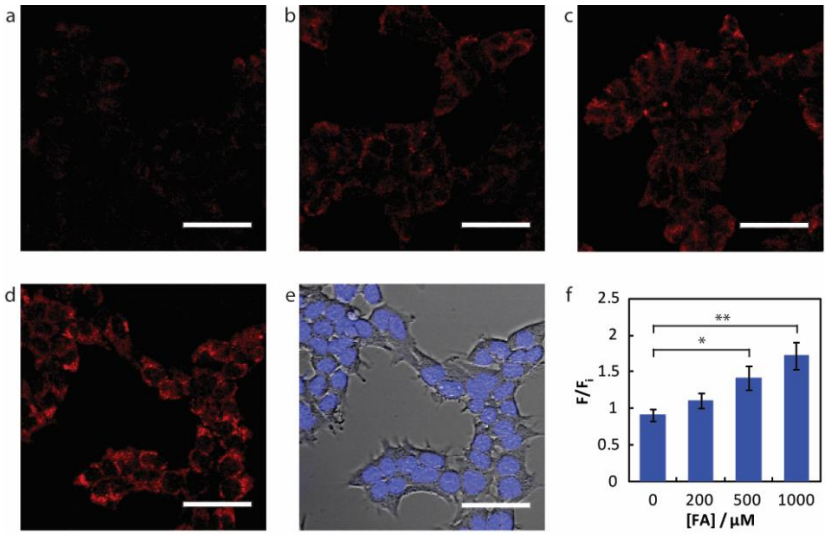

Figure 2.8. Confocal microscopy of FA detection in live HEK293T cells using FAP-1. Cells were treated with 10 µM FAP-1 in BSS for 30 min at 37 °C, followed by an exchange into fresh BSS and addition of varying FA concentrations. Images are taken 30 min after addition of (a) vehicle, (b) 200 µM FA, (c) 500 µM FA, and (d) 1 mM FA. (e) Bright-field image of cells in (d) overlaid with image of 1 µM Hoechst 33342. Scale bar represents 50 µm in all images. (f) Mean fluorescence intensities of HEK293T cells treated with varying concentrations of FA for 30 min relative to mean fluorescence intensity before FA addition; error bars denote SEM, n=3. * $P < 0.005$, ** $P < 0.0005$.

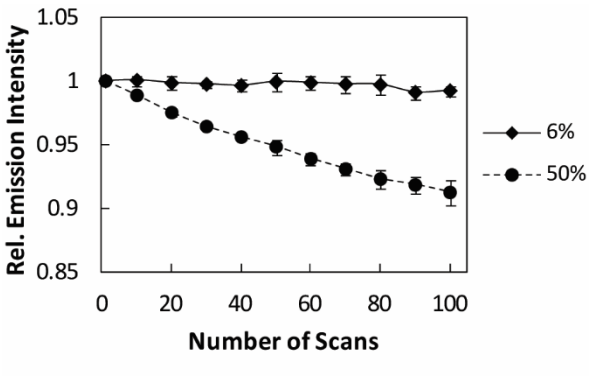

Figure 2.9. Photostability study with FAP1. A field of HEK293T cells loaded with 10 μM FAP-1 in BSS at 37 °C was irradiated using 50% laser power (dashed line) or 6% laser power (solid line) with a pinhole of 1 airy unit for 100 scans. Emission was normalized to the first scan for each field. Error bars represent standard deviation, n = 5.

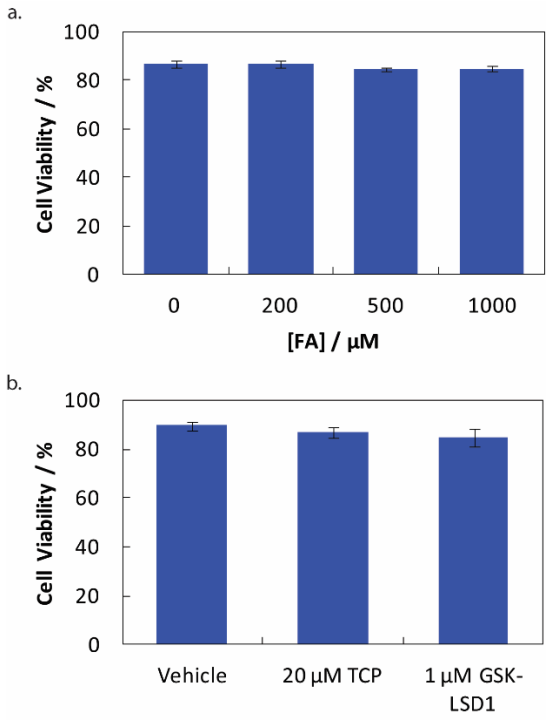

Figure 2.10. Flow cytometric analysis of cell viability using propidium iodide (PI) exclusion. Cells were plated in 12-well polystyrene culture plates (Corning). After the designated treatments below, cells were dislodged from wells by gentle agitation and filtered through 35 µm nylon mesh cap into a 12 x 75 mm polystyrene tube (Corning) for flow cytometry. Cell viability was calculated as the percentage of PI-negative cells. a) HEK293T cells were incubated with indicated concentrations of FA in BSS at 37 °C for 30 min, then exchanged into PBS containing 3 µM PI and incubated for 10 min before flow cytometry. b) MCF7 cells were treated with indicated concentrations of inhibitor in DMEM supplemented with 10% FBS for 20h at 37 °C in 5% CO_2, then exchanged into PBS containing 3 µM PI and incubated for 10 min before flow cytometry. Error bars denote SEM, n=3.

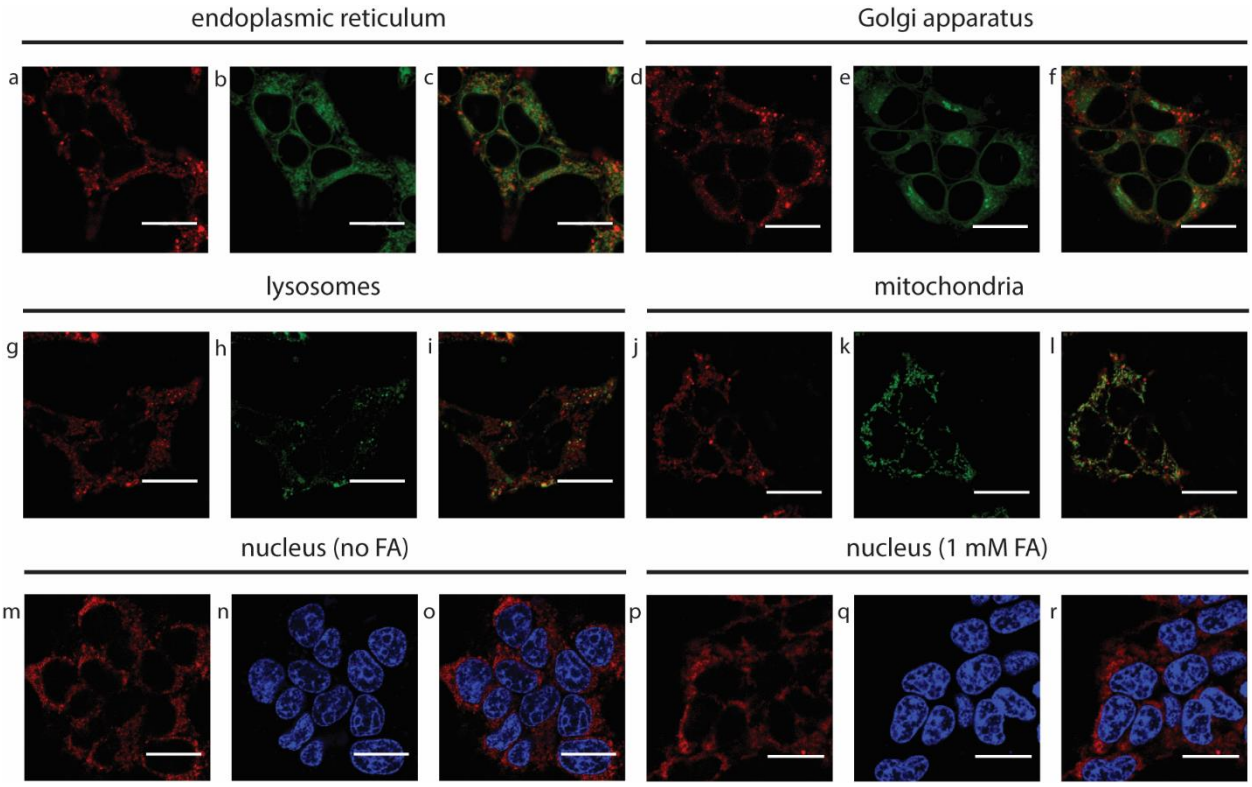

Figure 2.11. Colocalization studies with FAP1 in HEK293T cells. Endoplasmic reticulum: (a) FAP-1 (red), (b) ER-Tracker Green (green), (c) merge of (a) and (b). Golgi apparatus: (d) FAP-1 (red), (e) BODIPY FL C_5-Ceramide (green), (f) merge of (d) and (e). Lysosomes: (g) FAP-1 (red), (h) LysoTracker Green DND-26 (green), (i) merge of (g) and (h). Mitochondria: (j) FAP-1 (red), (k) MitoTracker Green FM (green), (l) merge of (j) and (k). Nuclei: (m) FAP-1 (red), (n) Hoechst 33342 (blue), (o) merge of (m) and (n). Nuclei after treatment of HEK293T cells with 1 mM FA for 30 min: (p) FAP-1 (red), (q) Hoechst 33342 (blue), (r) merge of (p) and (q). Scale bar represents 20 μm in all images.

	Pearson's Coefficient
ER-Tracker Green	0.51 ± 0.02
BODIPY Fl C_5-Ceramide	0.60 ± 0.05
LysoTracker Green DND-26	0.56 ± 0.06
MitoTracker Green	0.59 ± 0.04
Hoechst 33342	0.09 ± 0.04

Table 2.1. Quantification of colocalization studies. Pearson's coefficients were calculated using the JACoP plugin for ImageJ and averaged across 4 separate fields of cells. Error represents the standard deviation between different fields of cells.

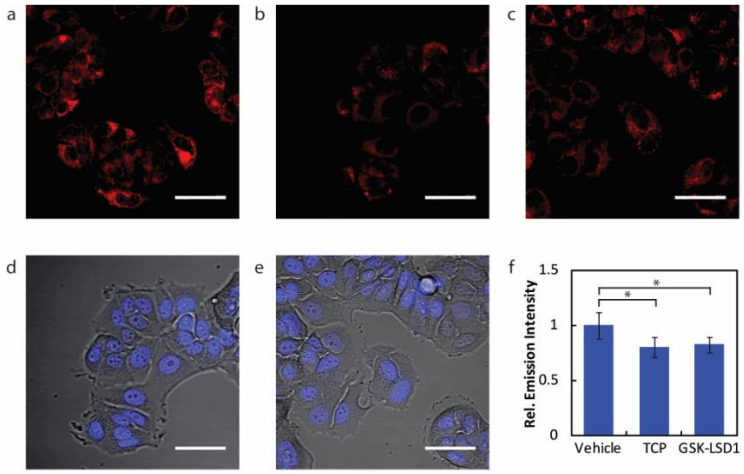

Figure 2.12. Confocal microscopy of FAP-1 in TCP- and GSK-LSD1-treated MCF-7 cells. Cells were pretreated with inhibitor (TCP or GSK-LSD1) for 20 h, followed by exchange into fresh BSS with 10 μM FAP-1 and incubation for 60 min at 37 °C. Images are of cells treated with (a) vehicle, (b) 20 μM TCP, (c) 1 μM GSK-LSD1. (d) and (e) Bright-field images of cells in (b) and (c), respectively, overlaid with images of 1 μM Hoechst 33342. Scale bar represents 50 μm in all images. (f) Mean fluorescence intensities of MCF-7 cells treated with, vehicle, 20 μM TCP, or 1 μM GSK-LSD1. Error bars denote SEM, n=6. * $P < 0.005$.

2.6. References

1. Liteplo, R. G.; Beauchamp, R.; Meek, M. E.; Chénier, R., *Formaldehyde: Concise International Chemical Assessment Document*. WHO: Geneva, 2002.
2. Kooistra, S. M.; Helin, K. *Nat. Rev. Mol. Cell Biol.* **2012,** *13*, 297-311.
3. Tong, Z.; Han, C.; Luo, W.; Li, H.; Luo, H.; Qiang, M.; Su, T.; Wu, B.; Liu, Y.; Yang, X.; Wan, Y.; Cui, D.; He, R. *Sci. Rep.* **2013,** *3*, Article 1807.
4. Fitzpatrick, P. F. *Arch. Biochem. Biophys.* **2010,** *493*, 13-25.
5. Klinman, J. P. *Biochim. Biophys. Acta* **2003,** *1647*, 131-137.
6. Shi, Y.; Lan, F.; Matson, C.; Mulligan, P.; Whetstine, J. R.; Cole, P. A.; Casero, R. A.; Shi, Y. *Cell* **2004,** *119*, 941-953.
7. Tsukada, Y.; Fang, J.; Erdjument-Bromage, H.; Warren, M. E.; Borchers, C. H.; Tempst, P.; Zhang, Y. *Nature* **2006,** *439*, 811-816.
8. Shi, Y.; Whetsine, J. R. *Mol. Cell* **2007,** *25*, 1-14.
9. Klose, R. J.; Yamane, K.; Bae, Y.; Zhang, D.; Erdjument-Bromage, H.; Tempst, P.; Wong, J.; Zhang, Y. *Nature* **2006,** *442*, 312-316.
10. Cloos, P. A. C.; Christensen, J.; Agger, K.; Maiolica, A.; Rappsilber, J.; Antal, T.; Hansen, K. H.; Helin, K. *Nature* **2006,** *442*, 307-311.
11. Yu, P. H.; Wright, S.; Fan, E. H.; Lun, Z. R.; Gubisne-Harberle, D. *Biochim. Biophys. Acta* **2003,** *1647*, 193-199.
12. Teng, S.; Beard, K.; Pourahmad, J.; Moridani, M.; Easson, E.; Poon, R.; O'Brien, P. J. *Chemico-biological interactions* **2001,** *130-132*, 285-296.
13. Heck, H. D.; Casanova-Schmitz, M.; Dodd, P. B.; Schachter, E. N.; Witek, T. J.; Tosun, T. *AIHA J.* **1985,** *46*, 1-3.
14. Andersen, M. E.; Clewell, H. J.; Bermudez, E.; Dodd, D. E.; Willson, G. A.; Campbell, J. L.; Thomas, R. S. *Toxicol. Sci.* **2010,** *118*, 716-731.
15. Tong, Z.; Han, C.; Luo, W.; Wang, X.; Li, H.; Luo, H.; Zhou, J.; Qi, J.; He, R. *Age* **2013,** *35*, 583-596.
16. Baan, R.; Grosse, Y.; Straif, K.; Secretan, B.; El Ghissassi, F.; Bouvard, V.; Benbrahim-Tallaa, L.; Guha, N.; Freeman, C.; Galichet, L.; Cogliano, V. *Lancet Oncol.* **2009,** *10*, 1143-1144.
17. Tong, Z.; Zhang, J.; Luo, W.; Wang, W.; Li, F.; Li, H.; Luo, H.; Lu, J.; Zhou, J.; Wan, Y.; He, R. *Neurobiol. Aging* **2011,** *32*, 31-41.
18. Miao, J.; He, R., *Chronic Formaldehyde-Mediated Impairments and Age-Related Dementia*. InTech: Shanghai, 2012.
19. Tulpule, K.; Dringen, R. *J. Neurochem.* **2013,** *127*, 7-21.
20. Kohli, R. M.; Zhang, Y. *Nature* **2013,** *502*, 472-479.
21. Jones, P. A. *Nat. Rev. Genet.* **2012,** *13*, 484-492.
22. Shen, L.; Song, C.-X.; He, C.; Zhang, Y. *Annu. Rev. Biochem.* **2014,** *83*, 585-614.
23. Jia, G.; Fu, Y.; Zhao, X.; Dai, Q.; Zheng, G.; Yang, Y.; Yi, C.; Lindahl, T.; Pan, T.; Yang, Y.-G.; He, C. *Nat. Chem. Biol.* **2011,** *7*, 885-887.
24. Greer, Eric L.; Blanco, Mario A.; Gu, L.; Sendinc, E.; Liu, J.; Aristizábal-Corrales, D.; Hsu, C.-H.; Aravind, L.; He, C.; Shi, Y. *Cell* **2015,** *161*, 868-878.
25. Fu, Y.; Luo, G.-Z.; Chen, K.; Deng, X.; Yu, M.; Han, D.; Hao, Z.; Liu, J.; Lu, X.; Doré, Louis C.; Weng, X.; Ji, Q.; Mets, L.; He, C. *Cell* **2015,** *161*, 879-892.

26. Zhang, G.; Huang, H.; Liu, D.; Cheng, Y.; Liu, X.; Zhang, W.; Yin, R.; Zhang, D.; Zhang, P.; Liu, J.; Li, C.; Liu, B.; Luo, Y.; Zhu, Y.; Zhang, N.; He, S.; He, C.; Wang, H.; Chen, D. *Cell* **2015,** *161*, 893-906.
27. Szarvas, T.; Szatloczky, E.; Volford, J.; Trezl, L.; Tyihak, E.; Rusznak, I. *J. Radioanal. Nucl. Chem.* **1986,** *106*, 357-367.
28. Ebeler, S. E.; Clifford, A. J.; Shibamoto, T. *J. Chromatogr. B.* **1997,** *702*, 211-215.
29. Takeuchi, A.; Takigawa, T.; Abe, M.; Kawai, T.; Endo, Y.; Yasugi, T.; Endo, G.; Ogino, K. *Bull. Environ. Contam. Toxicol.* **2007,** *79*, 1-4.
30. Spanel, P.; Smith, D.; Holland, T. A.; Al Singary, W.; Elder, J. B. *Rapid Commun. Mass Spectrom.* **1999,** *13*, 1354-1359.
31. Kato, S.; Burke, P. J.; Koch, T. H.; Bierbaum, V. M. *Anal. Chem.* **2001,** *73*, 2992-2997.
32. Yu, P. H.; Cauglin, C.; Wempe, K. L.; Gubisne-Harberle, D. *Anal. Biochem.* **2003,** *318*, 285-290.
33. Luo, W. H.; Li, H.; Zhang, Y.; Ang, C. Y. W. *J. Chromatogr. B.* **2001,** *753*, 253-257.
34. Pastierik, T.; Šebej, P.; Medalová, J.; Štacko, P.; Klán, P. *J. Org. Chem.* **2014,** *79*, 3374-3382.
35. Basel, Y.; Hassner, A. *Synthesis* **2001,** *2001*, 0550-0552.
36. Williams, A. T. R.; Winfield, S. A.; Miller, J. N. *Analyst* **1983,** *108*, 1067-1071.
37. Bishop, S. M.; Beeby, A.; Parker, A. W.; Foley, M. S. C.; Phillips, D. *J. Photochem. Photobiol., A* **1995,** *90*, 39-44.
38. Rothbard, J. B.; Jessop, T. C.; Lewis, R. S.; Murray, B. A.; Wender, P. A. *J. Am. Chem. Soc.* **2004,** *126*, 9506-9507.
39. Chan, J.; Dodani, S. C.; Chang, C. J. *Nat. Chem.* **2012,** *4*, 973-984.
40. Chen, X.; Tian, X.; Shin, I.; Yoon, J. *Chem. Soc. Rev.* **2011,** *40*, 4783-4804.
41. Yang, Y.; Zhao, Q.; Feng, W.; Li, F. *Chem. Rev.* **2013,** *113*, 192-270.
42. Cho, D.-G.; Sessler, J. L. *Chem. Soc. Rev.* **2009,** *38*, 1647-1662.
43. Wang, J.; Karpus, J.; Zhao, B. S.; Luo, Z.; Chen, P. R.; He, C. *Angew. Chem. Int. Ed.* **2012,** *51*, 9652-9656.
44. Michel, B. W.; Lippert, A. R.; Chang, C. J. *J. Am. Chem. Soc.* **2012,** *134*, 15668-15671.
45. Zheng, K.; Lin, W.; Tan, L.; Chen, H.; Cui, H. *Chem. Sci.* **2014,** *5*, 3439-3448.
46. Chaves-Ferreira, M.; Albuquerque, I. S.; Matak-Vinkovic, D.; Coelho, A. C.; Carvalho, S. M.; Saraiva, L. M.; Romão, C. C.; Bernardes, G. J. L. *Angew. Chem. Int. Ed.* **2015,** *54*, 1172-1175.
47. Wilson, J. L.; Kobeissi, S. F.; Oudir, S.; Haas, B.; Michel, B.; Randé, J.-L. D.; Ollivier, A.; Martens, T.; Rivard, M.; Motterlini, R.; Foresti, R. *Chem. Eur. J.* **2014,** *20*, 14698-14704.
48. Wang, T.; Douglass, E. F.; Fitzgerald, K. J.; Spiegel, D. A. *J. Am. Chem. Soc.* **2013,** *135*, 12429-12433.
49. Roth, A.; Li, H.; Anorma, C.; Chan, J. *J. Am. Chem. Soc.* **2015,** *137*, 10890-10893.
50. Song, H.; Rajendiran, S.; Kim, N.; Jeong, S. K.; Koo, E.; Park, G.; Thangadurai, T. D.; Yoon, S. *Tetrahedron Lett.* **2012,** *53*, 4913-4916.
51. Zhou, W.; Dong, H.; Yan, H.; Shi, C.; Yu, M.; Wei, L.; Li, Z. *Sens. Actuators B Chem.* **2015,** *209*, 664-669.
52. Uno, S.-n.; Kamiya, M.; Yoshihara, T.; Sugawara, K.; Okabe, K.; Tarhan, M. C.; Fujita, H.; Funatsu, T.; Okada, Y.; Tobita, S.; Urano, Y. *Nat. Chem.* **2014,** *6*, 681-689.
53. Lukinavičius, G.; Johnsson, K. *Nat. Chem.* **2014,** *6*, 663-664.
54. Chen, X.; Pradhan, T.; Wang, F.; Kim, J. S.; Yoon, J. *Chem. Rev.* **2012,** *112*, 1910-1956.

55. Grimm, J. B.; Sung, A. J.; Legant, W. R.; Hulamm, P.; Matlosz, S. M.; Betzig, E.; Lavis, L. D. *ACS Chem. Biol.* **2013,** *8*, 1303-1310.
56. Kalapos, M. P. *Diabetes Res. Clin. Pract.* **2013,** *99*, 260-271.
57. Tong, Z.; Luo, W.; Wang, Y.; Yang, F.; Han, Y.; Li, H.; Luo, H.; Duan, B.; Xu, T.; Maoying, Q.; Tan, H.; Wang, J.; Zhao, H.; Liu, F.; Wan, Y. *PLoS One* **2010,** *5*, e10234.
58. Mei, L.; Liu, J.; Liu, F.-Y.; Tong, Z.-Q.; Li, Z.-H.; Chen, W.; Luo, W.-H.; Li, H.; Luo, H.-J.; Tang, Y.; Tang, J.-M.; Cai, J.; Liao, F.-F.; Wan, Y. *PLoS ONE* **2013,** *8*, e58957.
59. Lim, S.; Janzer, A.; Becker, A.; Zimmer, A.; Schule, R.; Buettner, R.; Kirfel, J. *Carcinogenesis* **2009,** *31*, 512-520.
60. Lee, M. G.; Wynder, C.; Schmidt, D. M.; McCafferty, D. G.; Shiekhattar, R. *Chem. BIol.* **2006,** *13*, 563-567.
61. Ortega Muñoz, A.; Fyfe, M. C. T.; Martinell Pedemonte, M.; Estirate Martínez, M. D. L. A.; Valls Vidal, N.; Kurz, G.; Castro Palomino, L. J. C. (Hetero)aryl Cyclopropylamine Compounds as LSD1 Inhibitors. US 20150025054, 2015.

Chapter 3

Development of an excitation-ratiometric formaldehyde imaging platform and its application in living cells

Portions of this work were published in the following scientific journal:

Brewer, T. F.; Burgos-Barragan, G.; Wit, N.; Patel, K. J.; Chang, C. J. "A 2-aza-Cope reactivity-based platform for ratiometric fluorescence imaging of formaldehyde in living cells." *Chem. Sci.* **2017**, *8*, 4073-4081.

Abstract

Formaldehyde (FA) is a major reactive carbonyl species (RCS) that is naturally produced in living systems through a diverse array of cellular pathways that span epigenetic regulation to metabolic processing of endogenous metabolites. At the same time, however, aberrant elevations in FA contribute to pathologies ranging from cancer and diabetes to heart, liver, and neurodegenerative diseases. Disentangling the complex interplay between FA physiology and pathology motivates the development of chemical tools that can enable selective detection of this RCS in biological environments with spatial and temporal fidelity. We report the design, synthesis, and biological evaluation of Ratiometric Formaldehyde Probe (RFAP) indicators for excitation-ratiometric fluorescence imaging of formaldehyde production in living systems. RFAP-1 and RFAP-2 utilize FA-dependent aza-Cope reactivity to convert an alkylamine-functionalized coumarin platform into its aldehyde congener with a ca. 50-nm shift in excitation wavelength. The probes feature visible excitation and emission profiles, high selectivity for FA over a variety of RCS and related reactive biological analytes, including acetaldehyde, with up to a 6-fold change in fluorescence ratio. The RFAP indicators can be used to monitor changes in FA levels in biological samples by live-cell imaging and/or flow cytometry. Moreover, RFAP-2 is capable of visualizing differences in resting FA levels between wild-type cells and models with genetic knockout of ADH5, a major FA-metabolizing enzyme, establishing the utility of this ratiometric detection platform for identifying and probing sources of FA fluxes in biology.

3.1. Introduction

Formaldehyde (FA) is a reactive carbonyl species (RCS) that plays diverse roles in human health and disease. FA is a common environmental toxin, where it is produced by a broad range of natural (e.g., forest fires, solar degradation of humic substances, and emissions from vegetation and microbes) and anthropogenic (e.g., industrial FA production, plywood manufacturing, and vehicle exhaust) sources.[1] Indeed, FA is classified as a human carcinogen by the EPA, as environmental exposure to FA has long been associated with initiation and progression of several types of cancer.[2] Moreover, elevated levels of FA and other RCS have also been implicated in other disease states including neurodegenerative diseases, diabetes, and chronic liver and heart disorders.[3-5] As such, environmental FA presents a significant risk to human health, and the permissible exposure level is set to 0.75 ppm by OSHA.

Despite its toxicity, FA is also a ubiquitous and essential metabolite in biological systems, where it is produced through diverse pathways including one-carbon metabolism,[6-7] epigenetic N-demethylation of DNA, RNA, and histones,[8-10] and small molecule metabolism.[11] Indeed, FA production in the human body has been estimated to be as high as 1.4 mmol/min.[12] Compensatory FA metabolism by ADH5 (also known as FA dehydrogenase or ADH3) and ALDH2[13] leads to steady-state FA concentrations ranging from 50-100 μM in blood to 200-500 μM intracellularly, though concentrations can reach as high as 800 μM in certain disease states.[3, 14-16]

The signal/stress dichotomy of FA and its small, transient nature motivates the development of new chemical methods to enable its detection in living systems. However, traditional methods for FA analysis in biological samples[17-22] typically involve extensive sample processing and/or destruction, leading to a loss of spatiotemporal resolution and an inability to follow FA fluxes *in situ*. Recent efforts by our laboratory[23] and others[24-33] have produced fluorescence-based probes for selective FA bioimaging using reactivity approaches,[34-37] based largely on either 2-aza-Cope rearrangement or formimine formation as an FA-responsive reaction. These reagents have found utility for FA detection in living cells,[23-27] tissues,[28-31] and food samples.[32]

Despite this notable progress in FA detection, several key challenges remain unsolved. In particular, the vast majority of the above-mentioned chemical tools for FA imaging rely on a turn-on response, which is useful for preserving spatial resolution for qualitative comparative studies but can limit quantitative measurements due to potential variations in sample illumination and/or collection as well as non-homogeneous probe loading, particularly when experimental conditions may alter probe localization.[38] An additional concern is the pH sensitivity of current fluorescence-based probes, which can lead to difficulty in interpreting results. A potential solution to these issues is ratiometric imaging, a widely-used imaging modality which relies on a fluorescence ratio rather than intensity where two signals can be used in concert to provide an internal calibration.[38-39] Our laboratory has exploited this strategy for small-molecule and metal detection.[40-42] Only one example of a ratiometric FA probe has been reported, but this dye relies on UV excitation (318 nm), which can have potential limitations due to spectral overlap with absorption and autofluorescence of native biological chromophores like NADH.[26]

We now present the design, synthesis, and biological applications of a Ratiometric Formaldehyde Probe (RFAP) platform of indicators that feature selective and sensitive FA detection in living systems with visible excitation and emission profiles. These probes act as chemodosimeters, where the total signal can be accumulated over time and measured at various times as endpoint assays. As such, these reagents can increase signal-to-noise responses to transient molecules like FA even with the relatively high efficiency of FA metabolism in biological systems, thus allowing one to utilize relatively slow reactivity triggers that do not perturb and buffer endogenous FA pools. Such irreversible probes complement reversible chemosensors, such as employed by Lin and colleagues,[27, 28, 31] where higher real-time resolution may be obtained. RFAP-0, RFAP-1, and RFAP-2 utilize aminocoumarin as the excitation-ratiometric fluorophore with an appended homoallylamine as the FA-responsive trigger. Condensation with FA triggers a 2-aza-Cope rearrangement with subsequent hydrolysis to release an aldehyde product with a red-shifted excitation wavelength, giving rise to a ratiometric readout (Scheme 3.1). Iterative synthetic designs to improve FA reactivity via a *gem*-dimethyl substitution as well as cellular localization provide a first-generation ratiometric FA probe with visible excitation and emission profiles, RFAP-2, that enables detection of differences in resting levels of FA between wildtype and knockout models lacking ADH5, a major FA-metabolizing enzyme that regulates endogenous FA pools in the cell.

3.2. Methods

3.2.1. General methods

All reactions utilizing air- or moisture-sensitive reagents were performed in dried glassware under an atmosphere of dry N_2. When dry solvent was used, the solvent was passed over activated alumina. Other reagents were used without further purification. Silica gel P60 (SiliCycle) was used for column chromatography and SiliCycle 60 F254 silica gel (precoated sheets, 0.25 mm thick) was used for analytical thin layer chromatography and visualized by fluorescence quenching under UV light. Coumarins **1**, **2**, and RFAP-1-Ald were synthesized according to literature procedures.[43] 2-(2-((6-chlorohexyl)oxy)ethoxy)ethan-1-amine was synthesized according to literature procedures.[44] Prenylboronic acid solution was prepared using a slightly modified literature procedure.[45] 3-methyl-2-buten-1-ol and tetrahydroxydiboron were purchased from AK Scientific (Union City, CA); ethyl 4-pentenoate was purchased from TCI America (Portland, OR); 2-(7-Aza-1H-benzotriazole-1-yl)-1,1,3,3-tetramethyluronium hexafluorophosphate was purchased from ChemPep Inc. (Wellington, FL); 4-hydroxynonenal solution was purchased from

Cayman Chemical (Ann Arbor, MI); glucosone was purchased from Santa Cruz Biotech (Dallas, TX); and all other reagents were purchased from Sigma-Aldrich (St. Louis, MO). ^{1}H NMR and ^{13}C NMR spectra were collected in $CDCl_3$ or C_6D_6 (Cambridge Isotope Laboratories, Cambridge, MA) at 25 °C on Bruker AVB-400, AVQ-400, AV-500, and AV-600 with ^{13}C operating frequencies of 101 MHz, 126 MHz, and 150 MHz, respectively, at the College of Chemistry NMR Facility at the University of California, Berkeley. All chemical shifts are reported in the standard δ notation of parts per million relative to residual solvent peak at 7.26 ($CDCl_3$) or 7.16 (C_6D_6) for ^{1}H and 77.16 ($CDCl_3$) or 128.06 (C_6D_6) for ^{13}C as an internal reference. Splitting patterns are indicated as follows: br, broad; s, singlet; d, doublet; t, triplet; m, multiplet; dd, doublet of doublets. Low-resolution electrospray mass spectral analyses were carried out using a LC-MS (Agilent Technology 6130, Quadrupole LC/MS). High resolution mass spectral analyses (ESI-MS) were carried out at the College of Chemistry Mass Spectrometry Facility at the University of California, Berkeley.

3.2.2. Probe synthesis and new compound characterization

Preparation of RFAP-0.

*Synthesis of compound **2***. Compound **2** was prepared through alkyl cuprate addition into compound **1** according to published procedures.[43]

*Synthesis of compound **3***. To a solution of compound **2** (100 mg, 0.23 mmol) in 5 mL of 4:1 MeOH:DCM at 0 °C was added 0.33 mL of NH_3 solution (7 N in MeOH, 2.3 mmol). The reaction mixture was stirred at 0 °C for 30 min, then allylboronic acid pinacol ester (51 μL, 0.27 mmol) was added, and the reaction mixture was warmed to ambient temperature and stirred for 10 h. The solvent was removed under reduced pressure, and purification by silica column chromatography (0→3% MeOH /DCM) afforded compound **3** as a pale yellow solid (105 mg, 96%). ^{1}H NMR (500 MHz, $CDCl_3$) δ 7.09 (s, 1H), 5.74 (ddt, *J* = 17.1, 10.0, 7.2 Hz, 1H), 5.08 (dd, *J* = 17.1, 2.0 Hz, 1H), 4.99 (dd, *J* = 10.0, 2.1 Hz, 1H), 4.04 (br s, 1H), 3.72 (t, *J* = 5.6 Hz, 2H), 3.23 (dt, *J* = 10.9, 6.0 Hz, 4H), 2.87 (t, *J* = 6.5 Hz, 2H), 2.84 – 2.72 (m, 4H), 2.72 – 2.59 (m, 2H), 2.34 (br s, 2H), 2.08 – 1.85 (m, 4H), 1.80 – 1.70 (m, 2H), 0.94 (s, 9H), 0.09 (s, 6H). LRMS calcd. for $C_{28}H_{43}N_2O_3Si$ (M+H) 483.3, found 483.5.

Synthesis of RFAP-0. Compound **3** (20 mg, 40 μmol) was dissolved in 1.5 mL of 3:1 AcOH:H_2O, and the reaction mixture was stirred for 10 hours. The reaction mixture was carefully basified with 10% K_2CO_3/H_2O to pH >11, then extracted with DCM (4 x 25 mL). The combined organic layers were washed with brine (1 x 100 mL). The organic layer was dried over anhydrous Na_2SO_4, and the solvent was removed under reduced pressure. Purification by silica column chromatography (gradient from DCM to 10% MeOH/DCM) afforded RFAP-0 as a yellow powder (11 mg, 72% yield). ^{1}H NMR (600 MHz, $CDCl_3$) δ 7.06 (s, 1H), 5.69 (dt, *J* = 17.0, 8.1 Hz, 1H), 5.12 (d, *J* = 17.0 Hz, 1H), 5.05 (d, *J* = 9.9 Hz, 1H), 4.60 (br s, 1H), 3.66 – 3.35 (m, 7H), 3.26 (dt, *J* = 11.6, 5.5 Hz, 4H), 3.08 – 2.98 (m, 1H), 2.90 – 2.82 (m, 2H), 2.81 – 2.71 (m, 3H), 2.03 – 1.92 (m, 4H), 1.82 (br s, 1H). HRMS calcd. for $C_{22}H_{29}N_2O_3$ (M+H) 369.2173, found 369.2175.

Preparation of prenylboronic acid solution. A 0.3 M solution of H_2PdCl_4 was prepared by dissolving $PdCl_2$ (54 mg, 0.3 mmol) in 1 mL 0.9 M aqueous HCl and stirring for 8 h. Prenol (0.61 mL, 6 mmol) was dissolved in 12 mL of 4:1 DMSO:H_2O, followed by addition of 0.3 M H_2PdCl_4 (0.98 mL, 0.3 mmol) and $B_2(OH)_4$ (0.65 g, 7.2 mmol). The reaction mixture was stirred under N_2

for 10 h, then diluted with 22 mL $CHCl_3$ and stirred for an additional 10 minutes. The reaction mixture was filtered through a cotton plug, then 20 mL brine was added. The biphasic mixture was vigorously agitated and the layers were allowed to separate. The organic layer was collected, followed by additional brine washes (2 x 20 mL). The organic layer was dried over Na_2SO_4, the volume was measured, and the solution was used directly in further reactions. The yield was assumed to be 50%,[45] resulting in ca. 0.13 M prenylboronic acid solution.

Preparation of RFAP-1.

*Synthesis of compound **5***. Commercial 7N NH_3 solution (0.33 mL, 2.3 mmol) was added to coumarin aldehyde **2** (100 mg, 230 μmol) dissolved in 5 mL of 4:1 MeOH:DCM and stirred under N_2 for 30 minutes. Freshly prepared (see preparation above) 0.13 M prenylboronic acid solution (2.3 mL, 300 μmol) was added, and a white precipitate immediately formed. After stirring for 1 hour, the reaction mixture became homogeneous. The reaction mixture was stirred for an additional 9 h, and TLC (5% MeOH/DCM) showed complete consumption of starting material. The solvent was removed under reduced pressure. Purification by silica column chromatography (gradient from 1% MeOH/DCM with 0.2% NH_4OH to 3% MeOH/DCM with 0.2% NH_4OH) afforded **5** as a yellow powder (110 mg, 95% yield). ^{1}H NMR (400 MHz, $CDCl_3$) δ 7.08 (s, 1H), 5.93 (dd, J = 17.3, 10.8 Hz, 1H), 5.01 – 4.91 (m, 2H), 3.87 (s, 1H), 3.75 – 3.64 (m, 2H), 3.26 – 3.15 (m, 4H), 2.95 – 2.76 (m, 4H), 2.75 (t, J = 6.4 Hz, 2H), 2.33 (br s, 2H), 2.01 – 1.88 (m, 4H), 1.80 – 1.65 (m, 2H), 1.08 (d, J = 12.5 Hz, 6H), 0.93 (s, 9H), 0.08 (s, 6H); ^{13}C NMR (101 MHz, $CDCl_3$) δ 161.9, 153.3, 150.4, 147.0, 145.1, 122.4, 118.3, 118.1, 111.6, 108.2, 106.4, 62.5, 58.5, 49.9, 49.5, 43.5, 32.7, 27.9, 26.1, 25.5, 25.3, 24.0, 21.8, 20.8, 20.4, 18.4, -5.2; LRMS calcd. for $C_{30}H_{47}N_2O_3Si$ (M+H) 511.34, found 511.5.

Synthesis of RFAP-1. Compound **5** (53 mg, 100 μmol) was dissolved in 4 mL of 3:1 AcOH:H_2O, and the reaction mixture was stirred for 10 hours. The reaction mixture was carefully basified with 10% K_2CO_3/H_2O to pH >11, then extracted with DCM (4 x 25 mL). The combined organic layers were washed with brine (1 x 100 mL). The organic layer was dried over anhydrous Na_2SO_4, and the solvent was removed under reduced pressure. Purification by silica column chromatography (gradient from 4% MeOH/DCM to 10% MeOH/DCM) afforded RFAP-1 as a yellow powder (28 mg, 68% yield). ^{1}H NMR (400 MHz, $CDCl_3$) δ 7.06 (s, 1H), 5.97 – 5.84 (m, 1H), 5.05 – 4.95 (m, 2H), 4.09 (s, 1H), 3.63 – 3.56 (m, 1H), 3.52 – 3.43 (m, 1H), 3.40 – 3.19 (m, 7H), 3.17 – 3.06 (m, 1H), 2.95 – 2.81 (m, 3H), 2.81 – 2.71 (m, 2H), 2.03 – 1.90 (m, 5H), 1.79 – 1.68 (m, 1H), 1.08 (s, 3H), 1.04 (s, 3H); ^{13}C NMR (101 MHz, $CDCl_3$) δ 162.2, 154.7, 150.6, 146.1, 145.6, 122.7, 118.5, 115.5, 113.1, 108.0, 106.5, 60.1, 58.2, 50.0, 49.6, 43.5, 32.2, 28.0, 25.7, 25.0, 23.4, 21.8, 20.8, 20.5. HRMS calcd. for $C_{24}H_{33}N_2O_3$ (M+H) 397.2486, found 397.2484.

Preparation of RFAP-2.

Synthesis of compound 7. To prepare a solution of the alkylborane coupling partner **6**, a round-bottom flask was charged with ethyl 4-pentenoate (0.56 mL, 3.9 mmol) and commercial 0.5 M 9-BBN solution (8.6 mL, 4.3 mmol). The reaction mixture was stirred overnight and used directly for Suzuki coupling. A 2-neck round-bottom flask was charged with Compound **1** (0.66 g, 2.2 mmol), potassium phosphate tribasic monohydrate (0.81 g, 3.5 mmol), and PEPPSI-IPr catalyst (60 mg, 90 μmol). The atmosphere was replaced with N_2 by 5 evacuation/refill cycles, then a freshly-prepared 0.4 M solution of compound **6** (8.8 mL, 3.5 mmol) was added. The reaction mixture was stirred for 10 h, and TLC (EtOAc) showed complete consumption of starting material.

The reaction mixture was diluted with 50 mL EtOAc, run through a plug of silica gel (with EtOAc washes), and concentrated under reduced pressure. Purification by silica column chromatography (gradient from 25% EtOAc/hexanes to 35% EtOAc/hexanes) afforded **7** as an orange oil (0.5 g, 58% yield). ^{1}H NMR (400 MHz, C_6D_6) δ 10.85 (s, 1H), 7.02 (s, 1H), 3.97 (q, J = 7.1 Hz, 2H), 3.22 – 3.11 (m, 2H), 2.61 (t, J = 6.5 Hz, 2H), 2.57 – 2.47 (m, 4H), 2.35 (t, J = 6.1 Hz, 2H), 2.21 (t, J = 7.2 Hz, 2H), 1.81 (p, J = 7.3 Hz, 2H), 1.64 – 1.51 (m, 2H), 1.41 – 1.34 (m, 4H), 0.97 (t, J = 7.1 Hz, 3H); ^{13}C NMR (101 MHz, $CDCl_3$) δ 190.9, 173.6, 163.6, 163.1, 152.6, 148.6, 124.3, 119.6, 110.4, 108.2, 106.1, 60.3, 50.3, 49.8, 34.0, 29.9, 27.8, 27.3, 25.3, 21.2, 20.2, 20.2, 14.3. LRMS calcd. for $C_{23}H_{28}NO_5$ (M+H) 398.20, found 398.4.

*Synthesis of compound **8***. Commercial 7N NH_3 solution (3.2 mL, 23 mmol) was added to coumarin aldehyde **7** (0.9 g, 2.3 mmol) dissolved in 25 mL of 3:2 MeOH:DCM and stirred under N_2 for 30 minutes. Freshly prepared (see preparation above) 0.13 M prenylboronic acid solution (35 mL, 4.6 mmol) was added, and the reaction mixture was stirred for 10 h. The solvent was removed under reduced pressure. The residue was dissolved in 100 mL DCM and washed sequentially with 1% K_2CO_3 (2 x 100 mL) and brine (1 x 100 mL). The organic layer was dried over anhydrous Na_2SO_4, and the solvent was removed under reduced pressure. Purification by silica column chromatography (gradient from DCM to 3% MeOH/DCM) afforded **8** as a yellow oil (0.66 g, 62% yield). ^{1}H NMR (400 MHz, $CDCl_3$) δ 6.98 (s, 1H), 5.93 (dd, J = 17.3, 10.8 Hz, 1H), 5.03 – 4.93 (m, 2H), 4.12 (q, J = 7.2 Hz, 2H), 3.82 (s, 1H), 3.28 – 3.17 (m, 4H), 2.89 – 2.65 (m, 6H), 2.56 – 2.26 (m, 4H), 2.02 – 1.90 (m, 4H), 1.83 – 1.73 (m, 2H), 1.68 –1.50 (m, 2H), 1.24 (t, J = 7.1 Hz, 3H), 1.10 (s, 3H), 1.07 (s, 3H); ^{13}C NMR (101 MHz, C_6D_6) δ 172.7, 161.4, 151.6, 151.1, 147.9, 145.0, 122.6, 120.3, 117.9, 111.2, 108.7, 107.0, 60.2, 59.5, 49.8, 49.4, 43.8, 33.9, 29.2, 28.6, 28.1, 25.4, 25.2, 25.1, 22.1, 21.0, 20.8, 14.4. LRMS calcd. for $C_{28}H_{39}N_2O_4$ (M+H) 467.29, found 467.4.

*Synthesis of compound **9***. Compound **8** (0.28 g, 0.6 mmol) was dissolved in 10 mL of 3:1:1 MeOH:THF:H_2O and LiOH•H_2O (33 mg, 0.78 mmol) was added. The reaction was stirred for 10 h, and TLC (20% MeOH/DCM) showed complete consumption of starting material. The solvent was removed under reduced pressure. Purification by silica column chromatography (gradient from 5% MeOH/DCM to 20% MeOH/DCM) afforded **9** as a yellow powder (0.25 g, 90% yield). ^{1}H NMR (400 MHz, $CDCl_3$) δ 8.19 (br s, 3H), 7.01 (s, 1H), 5.91 (dd, J = 17.4, 10.7 Hz, 1H), 5.11 – 5.01 (m, 2H), 4.43 (s, 1H), 3.27 – 3.12 (m, 4H), 2.86 – 2.68 (m, 5H), 2.62 (br s, 1H), 2.20 (br s, 2H), 2.02 – 1.83 (m, 4H), 1.83 – 1.69 (br s, 1H), 1.68 – 1.50 (br s, 3H), 1.16 (s, 3H), 1.13 (s, 3H); ^{13}C NMR (101 MHz, $CDCl_3$) δ 179.3, 162.5, 156.8, 150.6, 145.8, 144.6, 122.6, 118.7, 113.8, 111.5, 107.9, 106.2, 56.3, 49.9, 49.5, 42.6, 35.6, 28.4, 28.0, 27.9, 25.8, 25.0, 24.1, 21.6, 20.6, 20.3. LRMS calcd. for $C_{26}H_{35}N_2O_4$ (M+H) 439.26, found 439.4.

Synthesis of RFAP-2. A flame-dried round bottom flask was charged with compound **9** (5 mg, 11.4 μmol), 2-(2-((6-chlorohexyl)oxy)ethoxy)ethan-1-amine (8 mg, 34.2 μmol), and HATU (13 mg, 34.2 μmol), followed by addition of 1 mL dry DMF and triethylamine (10 μL, 57 μmol). The reaction mixture as stirred under N_2 for 8 h. The solvent was removed under reduced pressure. Purification by silica column chromatography (gradient from 6% MeOH/DCM to 8% MeOH/DCM) afforded RFAP-2 as a yellow powder (1.6 mg, 22% yield). ^{1}H NMR (400 MHz, C_6D_6) δ 7.80 (br s, 2H), 7.29 (s, 1H), 6.84 (s, 1H), 6.15 (dd, J = 17.3, 10.8 Hz, 1H), 5.26 (d, J = 10.8 Hz, 1H), 5.15 (d, J = 17.3 Hz, 1H), 4.77 (s, 1H), 3.52 – 3.39 (m, 6H), 3.38 – 3.29 (m, 3H), 3.22 (t, J = 6.7 Hz, 2H), 2.96 – 2.84 (m, 2H), 2.84 – 2.54 (m, 8H), 2.40 – 2.29 (m, 2H), 2.01 – 1.89 (m, 2), 1.88 – 1.76 (m, 2H), 1.70 – 1.40 (m, 9H), 1.29 – 1.11 (m, 10H); ^{13}C NMR (101 MHz, C_6D_6) δ 174.7, 163.4, 159.6, 151.2, 146.9, 143.0, 123.7, 120.1, 116.4, 108.0, 107.1, 106.1, 71.2, 70.3,

70.2, 69.9, 57.5, 49.9, 49.3, 45.2, 43.0, 39.7, 36.3, 32.9, 29.8, 29.7, 28.9, 27.9, 27.0, 26.1, 25.7, 25.0, 22.4, 21.6, 20.6, 20.5. HRMS calcd. for $C_{36}H_{55}ClN_3O_5$ (M+H) 644.3825, found 644.3823.

Preparation of RFAP-2-Ald.

Synthesis of RFAP-2-Ald. RFAP-2 (1 mg, 1.5 μmol) was dissolved in 1 mL 2:1 MeOH:H_2O and 15 μL of a 1 M solution of formaldehyde (15 μmol) were added. The reaction mixture was stirred for 10 h, then the solvent was removed under reduced pressure. Purification by silica column chromatography (gradient from DCM to 2.5% MeOH/DCM) afforded RFAP-2-Ald as an orange film (0.4 mg, 44% yield). ^{1}H NMR (400 MHz, $CDCl_3$) δ 10.34 (s, 1H), 7.21 (s, 1H), 6.21 (s, 1H), 3.61 – 3.51 (m, 5H), 3.48 – 3.43 (m, 3H), 3.35 (dt, *J* = 9.3, 5.8 Hz, 2H), 3.23 (t, *J* = 8.2 Hz, 2H), 2.88 (t, *J* = 6.4 Hz, 2H), 2.80 (t, *J* = 6.2 Hz, 2H), 2.31 (t, *J* = 7.4 Hz, 2H), 2.03 – 1.93 (m, 3H), 1.86 (p, *J* = 7.3 Hz, 2H), 1.77 (p, *J* = 6.8 Hz, 2H), 1.64 – 1.51 (m, 15H*), 1.47 – 1.33 (m, 4H). *Note: multiplet at 1.64 – 1.51 overlaps with H_2O peak. HRMS calcd. For $C_{31}H_{43}ClN_2O_6Na$ (M+Na) 597.2702, found 597.2707.

3.2.3. Spectroscopic materials and methods

Milli-Q water was used to prepare all aqueous solutions. All spectroscopic measurements were performed in 20 mM PBS, pH 7.4. Absorption spectra were recorded using a Varian Cary 50 spectrophotometer, and fluorescence spectra were recorded using a Photon Technology International Quanta Master 4 L-format scan spectrofluorometer equipped with an LPS-220B 75-W xenon lamp and power supply, A-1010B lamp housing with integrated igniter, switchable 814 photocounting/analog photomultiplier detection unit, and MD5020 motor driver. Samples for absorption and emission measurements were contained in 1-cm × 1-cm quartz cuvettes (1.4-mL volume, Starna). All excitation spectra were corrected for the emission profile of the xenon lamp.

3.2.4. Quantum yield determinations

Quantum yield was determined using coumarin 153 (λ_{ex} = 420 nm) and fluorescein (λ_{ex} = 470 nm) as standards according to a published method.[46] For RFAP-1-Ald, RFAP-1, RFAP-2, coumarin 153, and fluorescein, the absorbance spectra were measured within an absorbance range below 0.1. The quantum yield was calculated according to the equation:

$$\phi_{sample} = \phi_{standard} (Grad_{sample}/Grad_{standard})(\eta_{sample}^2/\eta_{standard}^2)$$

where ϕ is the quantum yield, $\phi_{coumarin\ 153}$ = 0.38 in EtOH,[46] $\phi_{fluorescein}$ = 0.91 in 0.1 M aqueous NaOH,[46] Grad is the slope of the plot of absorbance versus integrated emission intensity, and η is the refractive index of the solvent.

3.2.5. RFAP-0, RFAP-1, and RFAP-2 fluorescence response to FA

995 μL of a 10.05 μM solution of RFAP-0, RFAP-1, or RFAP-2 in 20 mM PBS (pH 7.4) was prepared by diluting a 5 mM DMSO stock solution of RFAP-0, RFAP-1, or RFAP-2 into pre-warmed PBS (37 °C) in a 1-cm × 1-cm quartz cuvette, followed by a 15-minute incubation. 5 μL of 20 mM stock solution of FA (freshly prepared by diluting commercial 37 wt. % in H_2O FA solution) was added (for a final concentration of 100 μM), and the mixture was mixed by vigorous pipetting for 5 s, followed by acquisition of the t = 0 spectrum. Excitation spectra (λ_{ex} = 400–500 nm, λ_{em} = 510 nm) were collected at 0, 30, 60, 90, and 120 min. Temperature was maintained at 37 °C throughout the experiment by immersing the cuvette in a heated water bath between measurements.

3.2.6. RFAP-0 and RFAP-1 bimolecular rate constant determination

995 μL of a 10.05 μM solution of RFAP-0 or RFAP-1 in 20 mM PBS (pH 7.4) was prepared by diluting a 5 mM DMSO stock solution of RFAP-0 or RFAP-1 into pre-warmed PBS (37 °C) in a 1-cm × 1-cm quartz cuvette, followed by a 15 minute incubation. 5 μL of 20 mM stock solution of FA (freshly prepared by diluting commercial 37 wt. % in H_2O FA solution) was added (for a final concentration of 100 μM), and the mixture was mixed by vigorous pipetting for 5 s, followed by acquisition of the t = 0 spectrum. Excitation spectra (λ_{ex} = 400–500 nm, λ_{em} = 510 nm) were collected at timepoints until saturation was observed. Temperature was maintained at 37 °C throughout the experiment by immersing the cuvette in a heated water bath between measurements. The reaction was assumed to be pseudo-first order under these conditions, and the slope of a best-fit line to the plot of $\ln((R_{max}-R)/(R_{max}-R_0))$ vs time (where R_{max} indicates saturated excitation ratio, R_0 indicates initial excitation ratio, and R indicates excitation ratio at the current timepoint) was divided by the concentration of FA (100 μM) to give the bimolecular rate constant.

3.2.7. Selectivity tests

995 μL of a 10.05 μM solution of RFAP-1 or RFAP-2 (unless otherwise specified) in 20 mM PBS (pH 7.4) was prepared by diluting a 5 mM DMSO stock solution of RFAP-1 or RFAP-2 into pre-warmed PBS (37 °C) in a 1-cm × 1-cm quartz cuvette, followed by a 15-minute incubation. The analyte of interest was added to the cuvette to bring the concentration of analyte to 100 μM (unless otherwise specified) and the concentration of RFAP-1 or RFAP-2 to 10 μM, followed by mixing by vigorous pipetting for 5 seconds, and a t = 0 spectrum was acquired. The cuvette was placed in a 37 °C water bath. Excitation spectra were recorded by quickly removing the cuvette from the water bath, obtaining the spectrum, and returning the cuvette to the bath. Spectra were taken at t = 0, 30, 60, 90, and 120 min. Stock solutions and addition volumes were as follows (see Appendix 3 for detailed protocols).

FA: 5 μL of a 20 mM stock solution of FA in Milli-Q water (freshly prepared by diluting commercial 37 wt. % FA solution with Milli-Q water).

Acetaldehyde: 5 μL of a 20 mM stock solution of acetaldehyde in Milli-Q water (freshly prepared by diluting neat acetaldehyde with Milli-Q water).

Glucose: 5 μL of a 200 mM stock solution of glucose in Milli-Q water (freshly prepared by dissolving glucose in Milli-Q water); final concentration 1 mM glucose.

4-hydroxynonenal (4-HNE): 5 μL of 20 mM stock solution of 4-HNE in 7:1 EtOH:Milli-Q water (diluted from commercial 64 mM EtOH stock with Milli-Q water).

Dehydroascorbate: 5 μL of a 20 mM stock solution of dehydroascorbic acid in 1:1 DMSO:Milli-Q water (freshly prepared by dissolving dehydroascorbic acid in 1:1 DMSO:Milli-Q water).

Glucosone: 5 μL of a 20 mM stock solution of glucosone in Milli-Q water (freshly prepared by dissolving gluocosone in Milli-Q water).

Sodium pyruvate: 5 μL of a 20 mM stock solution of sodium pyruvate in Milli-Q water (freshly prepared by dissolving sodium pyruvate in Milli-Q water).

Oxaloacetate: 5 μL of a 20 mM stock solution of oxaloacetate in Milli-Q water (freshly prepared by dissolving oxaloacetic acid in Milli-Q water).

H_2O_2: 5 μL of a 20 mM stock solution of H_2O_2 in Milli-Q water (freshly prepared by diluting commercial 9.8 M H_2O_2 with Milli-Q water).

Glutathione: All buffers and stocks were deoxygenated by bubbling a stream of nitrogen gas for 30 minutes. 25 μL of a 200 mM stock solution of glutathione in PBS (freshly prepared by dissolving glutathione in deoxygenated PBS; pH was brought to 7.4 with deoxygenated 1 M NaOH) was added to 975 □L of a 10.25 μM solution of RFAP-2 in deoxygenated PBS. The screw-top cuvette was capped for the duration of the timecourse. Final concentration 5 mM glutathione.

Methylglyoxal: 5 μL of a 20 mM stock solution of methylglyoxal in Milli-Q water or 5 μL of 2 mM stock solution of methylglyoxal in Milli-Q water (freshly prepared by diluting neat methylglyoxal with Milli-Q water); final concentration 100 μM or 10 μM methylglyoxal.

Sodium Bisulfite: 5 μL of a 40 mM stock solution of sodium bisulfite in Milli-Q water (freshly prepared by dissolving sodium bisulfite in Milli-Q water); final concentration 200 μM.

3.2.8. RFAP-2 in vitro *detection limit*

995 μL of a 10.05 μM solution of RFAP-2 in 20 mM PBS (pH 7.4) was prepared by diluting a 5 mM DMSO stock solution of RFAP-2 into pre-warmed PBS (37 °C) in a 1-cm × 1-cm quartz cuvette, followed by a 15-minute incubation. 5 μL of a FA stock solution (8 mM, 6 mM, 4 mM, 2 mM, or 1 mM, freshly prepared by diluting commercial 37 wt. % FA solution with Milli-Q water) or 5 μL of PBS was added (for a final concentration of 40 μM, 30 μM, 20 μM, 10 μM, 5 μM, or 0 μM FA), and the mixture was mixed by vigorous pipetting for 5 s and placed in a 37 °C water bath. Excitation spectra were obtained after 120 min. The standard deviation (σ) of three replicates of blank (0 μM FA) samples as well as the slope of the linear regression curve fitted to the 470/420 nm excitation ratio in the range of [FA] from 0 to 40 μM were used to determine the detection limit (3σ/slope) of 0.3 μM according to published methods.[47]

3.2.9. Cell culture procedures

Cells were maintained by the UC Berkeley Tissue Culture Facility. HEK293T cells were maintained as a monolayer in exponential growth at 37 °C in a 5% CO_2 atmosphere in Dulbecco's Modified Eagle Medium (DMEM, Gibco) supplemented with 10% fetal bovine serum (FBS, Seradigm), 1% glutamax (Gibco), and 1% non-essential amino acids (NEAA, Gibco). HeLa, RKO, and U-2OS were maintained as a monolayer in exponential growth at 37 °C in a 5% CO_2 atmosphere in DMEM supplemented with 10% FBS and 1% glutamax. MCF-7 and SH-SY5Y cells were maintained as a monolayer in exponential growth at 37 °C in a 5% CO_2 atmosphere in DMEM supplemented with 10% FBS, 1% glutamax, 1% NEAA, and sodium pyruvate. MCF-10A were maintained as a monolayer in exponential growth at 37 °C in a 5% CO_2 atmosphere in DMEM/F-12 supplemented with 5% horse serum (Hyclone), 10 mM HEPES, 0.5 mg/mL hydrocortizone, 100 ng/mL cholera toxin, 20 ng/mL EGF, 10 μg/ml insulin. ADH5 -/- and genetically matched WT HAP1 cells were maintained in exponential growth at 37 °C in a 5% CO_2 atmosphere as a monolayer in Iscove's Modified Dulbecco's Medium, high glucose, (IMDM, Invitrogen) supplemented with 10% FBS. One day before imaging, HEK293T, MCF-7, SH-SY5Y, HAP1 ADH5 -/-, and HAP1 WT cells were passaged and plated on poly-L-lysine-coated 4-well Lab Tek borosilicate chambered coverglass slides (Nunc) at 1.8 × 105 per well and allowed to grow to between 70 and 80% confluence before imaging. One day before imaging, HeLa, MCF-10A, RKO, and U- 2OS cells were passaged and plated on 4-well Lab Tek borosilicate chambered coverglass slides and allowed to grow to between 70 and 80% confluence before imaging.

3.2.10. Confocal fluorescence imaging experiments

Confocal fluorescence imaging studies were performed with a Zeiss laser scanning microscope 710 with a 20x or 63x oil immersion objective lens using Zen 2009 software (Carl Zeiss). RFAP-1 and RFAP-2 were excited using 405 nm diode laser and 488 nm argon laser, and emission was collected using a META detector between 410 to 550 nm (405 nm excitation) and 493 to 550 nm (488 nm excitation). BSS (136.9 mM NaCl, 5.37 mM KCl, 1.26 mM $CaCl_2$, 0.81 mM $MgSO_4$, 0.44 mM KH_2PO_4, 0.335 mM Na_2HPO_4, 10 mM PIPES; pH to 7.2 with NaOH) was used as the imaging buffer for all confocal experiments. The cells were imaged at 37 °C throughout the course of the experiment. Image analysis and quantification was performed using ImageJ (National Institutes of Health). For quantification of excitation ratio, three fields of cells within the same well were imaged. A region of interest (ROI) was created around each cell in each image. The mean fluorescence intensity of each cell was measured (using "Measure" function) for each excitation wavelength and averaged across the three fields imaged. For each condition, multiple wells were analyzed using this process, and the 488/405 excitation ratios were averaged across independent experiments for statistical analysis. Statistical analyses for multiple comparisons were performed using one-way ANOVA with the Bonferroni correction in the statistical analysis software, R.

3.2.11. Exogenous FA addition experiments in various cell types

One day before imaging, HEK293T, MCF-7, and SH-SY5Y cells were passaged and plated on poly-L-lysine-coated 4-well Lab Tek borosilicate chambered coverglass slides and allowed to grow to between 70 and 80% confluence before imaging. One day before imaging, HeLa, MCF-10A, RKO, and U- 2OS cells were passaged and plated on 4-well Lab Tek borosilicate chambered coverglass slides and allowed to grow to between 70 and 80% confluence before imaging. The DMEM media was aspirated from the chambers containing cells and replaced with 500 μL DMEM (supplemented with 10% FBS and glutamax) containing 10 μM RFAP-1 or RFAP-2 (diluted from 5 mM stock in DMSO) and incubated at 37 °C for 30 minutes. The buffer was then replaced with 500 μL fresh DMEM (supplemented with 10% FBS and glutamax) containing no probe, and the cells were incubated at 37 °C for 10 minutes to remove any excess probe. The buffer was then replaced with 500 μL BSS, and cells were imaged to provide the t = 0 timepoint. 200 μL of the buffer was removed from each well and mixed with vehicle control (5 μL H_2O) or FA (5 μL of 20.2 mM FA for 200 μM final concentration upon re-addition to well, 5 μL of 10.1 mM FA for 100 μM final concentration upon re-addition to well, 5 μL of 5.05 mM FA for 50 μM final concentration upon re-addition to well; 5 μL of 25.025 mM FA for 25 μM final concentration upon re-addition to well; all FA stocks freshly prepared by diluting 37 wt. % commercial FA). The cells were then incubated at 37 °C for 30 or 60 min prior to imaging for the t = 30 or t = 60 timepoint.

3.2.12. HAP1 ADH5 -/- and WT confocal imaging and flow cytometry experiments

Confocal Imaging Experiments. One day before imaging, ADH5-/- and WT HAP1 cells were passaged and plated on poly-L-lysine-coated 4-well Lab Tek borosilicate chambered coverglass slides and allowed to grow to between 70 and 80% confluence before imaging. The media was aspirated from the chambers containing cells and replaced with 500 μL BSS containing 500 nM RFAP-2 (diluted from 500 μM stock in DMSO) and incubated at 37 °C for 30 minutes. The buffer was then replaced with 500 μL BSS supplemented with either vehicle control (5 μL H_2O) or 100 μM FA (5 μL of a 10.1 mM FA stock). The cells were then incubated at 37 °C for 60 min prior to imaging for the t = 60 timepoint.

Flow Cytometry Experiments. One day before imaging, ADH5 -/- and WT HAP1 cells were passaged and plated on 12-well polystyrene culture plates (Corning) and allowed to grow to 80% confluence. The media was aspirated from the wells containing cells and replaced with 500 μL BSS containing 500 nM RFAP-2 (diluted from 500 μM stock in DMSO) and incubated at 37 °C for 30 minutes. The buffer was then replaced with 500 μL BSS supplemented with either vehicle control (5 μL H_2O) or 100 μM FA (5 μL of a 10.1 mM FA stock). The cells were then incubated at 37 °C for 60 min, then exchanged into PBS containing 5 nM Sytox Red (Invitrogen) and incubated for 5 min. Cells were dislodged from wells by gentle agitation and filtered through 35 μm nylon mesh cap into a 12 x 75 mm polystyrene tube (Corning) for flow cytometry. Cells were analyzed using a BD LSRFortessa X-20 cell analyzer equipped with 405 nm, 488 nm, and 640 nm lasers; fluorescence emission was collected using standard AmCyan filter (525/50 nm bandpass filter with 475 nm longpass filter) for 405 nm excitation, standard FITC filter (530/30 nm bandpass filter with 505 nm longpass filter) for 488 nm excitation, and standard APC filter (670/14 nm bandpass filter) for 640 nm excitation. Quantification was performed using FlowJo software (FlowJo, LLC); live cells were selected and median 488/405 nm excitation ratios were averaged across 3 technical replicates per biological replicate. Median 488/405 nm excitation ratios were then averaged across independent biological replicates for statistical analysis. Statistical analyses for multiple comparisons were performed using one-way ANOVA with the Bonferroni correction in the statistical analysis software, R.

3.3. Results

3.3.1. Synthesis and characterization of RFAP-0

To develop a ratiometric FA indicator, we set out to incorporate the parent unsubstituted homoallylamine trigger that was independently developed by our lab and Chan's[23-24] onto a julolidine-based coumarin indicator and synthesized RFAP-0 in three steps from known compound 1.[43] In this design, we envisioned that the push-pull nature of the product fluorophore bearing an electron-withdrawing aldehyde group would be electronically distinct from the masked probe bearing a more electron-rich homoallylamine functionality. Reaction with FA would enable conversion of this electron-rich group into an electron-poor one via an aza-Cope rearrangement.

The homoallylamine trigger was installed by a allylboronic acid pinacol ester-mediated aminoallylation (Scheme 3.2). We evaluated the reactivity of RFAP-0 toward 100 μM FA in aqueous solution at physiological pH (PBS, pH 7.4) and found that it displays the predicted 50-nm shift in excitation wavelength from 420 nm to 470 nm upon reaction with FA (Figure 3.1a) as it forms aldehyde product RFAP-1-Ald. However, the reaction rate was found to be sluggish, with a bimolecular rate constant of 0.017 $M^{-1}s^{-1}$ (Figure 3.2), limiting its application to detection of FA in biological systems. Indeed, after a 2-hour incubation of 10 μM RFAP-0 with 100 μM FA, only a 1.6-fold excitation ratio change was observed (Figure 3.1b).

To accelerate the kinetics of the FA detection reaction, we redesigned the RFAP platform to include a geminal dimethyl group in the homoallylamine trigger (Scheme 3.3). It is well-established that such geminal dialkyl substituents accelerate reactions with cyclic transition states via the Thorpe-Ingold effect,[48] so we reasoned that this substitution may significantly increase the rate of the aza-Cope rearrangement. In particular, we hypothesized that the increased thermodynamic stabilization on going from a monosubstituted alkene to a trisubstituted alkene during the course of the reaction could further bias the aza-Cope rearrangement toward the desired product.

3.3.2. Synthesis and characterization of RFAP-1

With these design considerations in mind, RFAP-1 was synthesized in two steps from compound **2**. The key functionalization step involved a prenylboronic acid-mediated aminoallylation (Scheme 3.4).[45, 49] With RFAP-1 in hand, we evaluated its properties in aqueous solution buffered to physiological pH (PBS, pH 7.4). Similar to RFAP-0, the probe shows a 50 nm shift in excitation wavelength upon incubation with 100 μM FA *in vitro* (Figure 3.3a). Gratifyingly, this occurs with a bimolecular rate constant of 0.12 $M^{-1}s^{-1}$, showing a ca. 7-fold rate increase relative to RFAP-0 (Figure 3.2). Accordingly, RFAP-1 displays an improved 3.2-fold excitation ratio change after incubation with 100 μM FA for 2 hours (Figure 3.3b). This ratiometric shift is also observed in the UV/visible absorbance spectra (Figure 3.4), and matches the excitation profile of independently prepared RFAP-1-Ald (Figure 3.5). Based on the excitation spectra of RFAP-1 and RFAP-1-Ald, the minimum *in vitro* 470/420 nm excitation ratio R_{min} is 0.1 and the maximum excitation ratio R_{max} is 3.1. Additionally, the emission profiles of RFAP-1 and RFAP-1-Ald suggest that RFAP-1 could be used in an emission ratiometric mode (Figure 3.5). To verify that the observed ratiometric FA response was the result of the proposed 2-aza-Cope reaction, the reaction between RFAP-1 and FA was monitored by LC-MS, which shows clean conversion from RFAP-1 to a product with the expected mass of RFAP-1-Ald (Figure 3.6).

The high optical brightness of both RFAP-1 (ϕ_{fl} = 0.61, $\varepsilon_{420} = 2\times10^3$ $M^{-1}cm^{-1}$) and its aldehyde product RFAP-1-Ald (ϕ_{fl} = 0.45, $\varepsilon_{470} = 4\times10^4$ $M^{-1}cm^{-1}$) results in a large change in absolute intensity upon conversion of an electron-donating amine pendant to a more electron-withdrawing aldehyde functionality. Moreover, RFAP-1 also displays no pH-dependent variations within the physiological range, showing a consistent excitation ratio from pH 4–8 (Figure 3.7). Owing to its aza-Cope trigger, RFAP-1 exhibits high selectivity for FA over an array of potentially competing RCS and carbonyl-containing molecules (Figure 3.3c). Only methylglyoxal added at superphysiological concentrations (100 μM) gives a slight ratio response, but no background reactivity is observed with 10 μM methylglyoxal, which is patently above its single-digit micromolar physiological range.[50]

3.3.3. Application of RFAP-1 to imaging FA in living cells

We next evaluated the ability of RFAP-1 to detect changes in FA levels in living cells using confocal microscopy to monitor FA-dependent fluorescence signals in ratiometric mode (Figure 3.8). HEK293T cells were loaded with 10 μM RFAP-1 for 30 minutes and then washed to remove excess probe. Then, varying concentrations of FA were added. The data show a significant, dose-dependent excitation ratio change in cells treated with FA compared to control cells (Figure 3.8). We verified that neither RFAP-1 nor the aldehyde product RFAP-1-Ald of the 2-aza-Cope reaction have a significant impact on cell viability by a Sytox Red exclusion assay (Figure 3.9). Additionally, HEK293T cells incubated in buffer alone show negligible autofluorescence under our imaging conditions, verifying that the observed signal is from RFAP-1 (Figure 3.10). Importantly, the fluorescence ratio change was statistically significant for levels of exogenously added FA down to 50 μM (Figure 3.8k), which represents a ca. 10-fold improvement in FA sensitivity in cells for this ratiometric indicator over the previously-reported turn-on fluorescent probe FAP-1 that also relies on a 2-aza-Cope reaction trigger.[23] We determined the maximum possible in cellulo ratio change ΔR_{max} as 470 ± 10 by comparing HEK293T cells loaded with RFAP-1 to cells loaded with RFAP-1-Ald (Figure 3.11). However, more detailed analyses showed the subcellular localization of RFAP-1 to be uneven and adopt a punctate staining pattern (Figure 3.12), which may pose a potential limitation for its use in other cell types.

3.3.4. Design, synthesis, and in vitro *characterization of RFAP-2, a second-generation ratiometric FA indicator*

To provide a fluorescent FA probe that exhibits more homogeneous staining and subcellular localization over diverse cell types while maintaining high FA selectivity and responsiveness in a ratiometric mode, we focused our attention on retaining the same *gem*-dimethyl homoallylamine coumarin core with modification of the pendant hydroxypropyl sidechain. In particular, we decided to install a carboxylic acid moiety as a general and hydrophilic synthetic handle to provide access to a variety of modified RFAPs through standard amide coupling approaches. To this end, an ester side chain was installed on the coumarin core through an sp^2-sp^3 Suzuki coupling reaction,[51] followed by aminoallylation and saponification, furnishing the carboxylic acid-functionalized coumarin intermediate **9** (Scheme 3.5). We then surveyed a variety of amines to couple to this RFAP building block; one representative example is RFAP-2, which contains an amide with an ethylene glycol-hexyl chloride moiety reminiscent of the HaloTag substrate.[52] This sidechain was initially installed to facilitate labelling of the HaloTag protein, but it was found to display substantially improved staining in cells and was carried forward as a second-generation ratiometric FA probe.

RFAP-2 shows similar photophysical properties (ϕ_{fl} = 0.69, $\varepsilon_{420} = 1.1\times10^4$ $M^{-1}cm^{-1}$) and *in vitro* reactivity to FA compared to RFAP-1, with a 6-fold excitation ratio change to 100 μM FA observed in 2 hours (Figure 3.13a, 3.13b). This ratiometric change is also reflected in the corresponding UV/visible absorbance spectra upon conversion of the homoallylamine probe to aldehyde product RFAP-2-Ald (Figure 3.4), and matches the excitation profile of independently-prepared RFAP-2-Ald (Figure 3.5). RFAP-2 also displays no pH-dependent variations within the physiological range, showing a consistent excitation ratio from pH 4–8 (Figure 3.7). Similar to RFAP-1 and RFAP-1-Ald, RFAP-2 and RFAP-2-Ald also display emission profiles that suggesting RFAP-2 could be used in an emission ratiometric mode (Figure 3.5). Based on the excitation spectra of RFAP-2 and RFAP-2-Ald, the minimum *in vitro* 470/420 nm excitation ratio R_{min} is 0.1 and the maximum excitation ratio R_{max} is 3.1. At a 10 μM RFAP-2 concentration and a 2-hour cutoff, the *in vitro* detection limit for FA was found to be 0.3 μM (Figure 3.14). Owing to its 2-aza-Cope reactivity switch, RFAP-2 retains the high selectivity of RFAP-1 for FA (Figure 3.13c) over a variety of potential biologically relevant RCS competitors (4-hydroxynonenal, dehydroascorbate, glucosone, oxaloacetate, acrolein, and methylglyoxal), various carbonyl-containing molecules (acetaldehyde, pyruvate, and glucose), as well as oxidizing and reducing reagents/conditions that could be encountered in the cell (H_2O_2 and glutathione). Similar to RFAP-1, superphysiological levels of methylglyoxal (100 μM) can provide a minor background response, but addition of methylglyoxal at physiological concentrations (10 μM) gives no significant fluorescence ratio change.

3.3.5. Application of RFAP-2 to ratiometric fluorescence imaging changes in FA levels in living cells

With data establishing that RFAP-2 can selectively detect FA in aqueous solution with high sensitivity, we next evaluated its ability to detect changes in FA levels *in cellulo* by ratiometric fluorescence imaging using confocal microscopy. HEK293T cells were treated with 10 μM RFAP-2 for 30 min, followed by washing to remove excess probe and addition of FA at various doses (50 to 200 μM). The cells show a significant and FA dose-dependent excitation ratio change similar to what is observed for RFAP-1 (Figure 3.15). Moreover, RFAP-2 displayed an even staining pattern in HEK293T cells, in contrast to the punctate localization of RFAP-1 (Figure 3.12), presaging its broader utility for probing FA biology. We determined the maximum possible in

cellulo ratio change ΔR_{max} as 770 ± 20 by comparing HEK293T cells loaded with RFAP-2 to cells loaded with RFAP-2-Ald (Figure 3.11). We additionally found that incubation with 10 μM RFAP-2 had no significant impact on cell viability using a Sytox Red exclusion assay (Figure 3.9). To validate the use of RFAP-2 for FA detection in a wider range of biological models, we evaluated its performance in a variety of commonly-used cell lines, including HeLa, MCF-7, MCF-10A, RKO, SH-SY5Y, and U-2OS cells. In the cell lines tested, RFAP-2 displayed excellent FA responsiveness (Figure 3.16), as well as generally diffuse cell staining (Figure 3.17), in all cell types tested with the exception of U-2OS cells, where the dye is FA-responsive but localizes with a punctate staining pattern.

It is worth noting that cells incubated with RFAP-2 alone show relatively small changes in excitation ratio over time, indicating that resting levels of intracellular FA may potentially be lower than estimated based on bulk measurements on tissue and animal samples in the literature that place FA levels on the order of 100-200 μM or more.[3, 14-16] From the RFAP-2 data collected, the predicted endogenous intracellular FA concentration estimated from a calibration curve under these conditions is in the range of ca. 25 μM (Figure 3.18). However, because FA can rapidly diffuse across cellular membranes,[50] differences observed between the present measurements in dissociated culture versus tissue and animal samples may be markedly influenced by the various media exchanges used in dissociated cell culture procedures that could wash out endogenously-produced FA.

3.3.6. Ratiometric fluorescence imaging identifies elevated FA levels in an ADH5 genetic knockout model

To demonstrate the use of RFAP-2 as a chemical tool beyond exogenous FA detection, we decided to investigate its potential for detecting changes in endogenous FA metabolism and turned our attention to an ADH5 genetic knockout model.[531] Since ADH5 is the predominant FA-metabolizing enzyme in the cell and is central to regulating the resting levels of this one-carbon metabolite, we predicted that cells lacking ADH5 would have elevated levels of FA. Additionally, challenging these cells with exogenous FA should lead to increased levels of FA in ADH5 -/- cells relative to wild-type (WT) cells due to impaired FA metabolism.

Accordingly, we treated genetically matched HAP1 ADH5 -/- and WT cells with 500 nM RFAP-2 for 30 min, followed by washing to remove excess probe and incubation with either vehicle or 100 μM FA for 60 minutes. As predicted, ADH5 -/- cells showed a statistically significant increase in RFAP-2 excitation ratio relative to WT cells under both vehicle and 100 μM FA treatment by confocal microscopy (Figure 3.19a, 3.19b). The observed increase in RFAP-2 excitation ratio observed in ADH5 -/- cells treated with vehicle confirms our hypothesis that ADH5 is involved in regulating resting levels of FA in cells and that ADH5 -/- cells have higher endogenous, basal levels of FA relative to WT cells. Moreover, the data verify that RFAP-2 is capable of detecting changes in endogenous levels of FA. Along the same lines, the statistically significant difference in RFAP-2 excitation ratio between ADH5 -/- and WT cells challenged with 100 μM FA confirms the impaired ability of ADH5 -/- cells to metabolize FA. Additionally, we found that incubation of ADH5 -/- or WT HAP1 cells with 10 μM RFAP-2 in the presence or absence of 100 μM FA showed no significant differences in cell viability by a Sytox Red exclusion assay (Figure 3.20).

To further validate the ability of RFAP-2 to detect these changes in endogenous FA concentration and metabolism in ADH5 -/- vs WT HAP1 cells, we turned to flow cytometry, a high-throughput analytical technique that allows analysis of far greater numbers of cells. We treated ADH5 -/- and WT HAP1 cells with the same conditions as above and observed a

statistically significant increase in RFAP-2 excitation ratio for vehicle-treated ADH5 -/- cells relative to WT cells, as well as a statistically significant increase in RFAP-2 excitation ratio for 100 μM FA-treated ADH5-/- cells relative to WT cells (Figure 3.19c, 3.19d). The flow cytometry results corroborate our confocal imaging results, establishing that RFAP-2 is capable of detecting changes in endogenous levels and metabolism of FA, and presage the potential utility of RFAP-2 in FACS-mediated screens for changes in FA levels.

3.4. Conclusions

To summarize, we have presented the design, synthesis, and biological evaluation of the RFAP series of excitation-ratiometric FA probes. These reagents feature visible excitation and emission profiles and show high selectivity and sensitivity to changes in FA levels *in vitro* and *in cellulo*. The RFAP platform utilizes an aminocoumarin core with an appended FA-responsive homoallylamine, where upon condensation with FA and subsequent 2-aza-Cope rearrangement and hydrolysis, generates a resultant electron-withdrawing aldehyde moiety that causes an excitation wavelength shift of ca. 50 nm from 420 nm to 470 nm. Importantly, the introduction of a geminal dimethyl substituent increases FA-dependent probe reactivity by ca. one order of magnitude. Utilizing dual excitation wavelengths, RFAP-1 and RFAP-2 enable ratiometric imaging of FA fluxes in living cells, and the latter probe is amenable to flow cytometry as well. RFAP-1 and RFAP-2 possess a variety of attractive photophysical characteristics, including visible excitation and emission profiles, high optical brightness for both dye and product to enable high-sensitivity FA detection, as well as a marked insensitivity to changes in pH within physiological ranges spanning acidic to basic conditions.

While sensitive and selective to FA, RFAP-1 displays uneven staining patterns that can limit its utility in certain applications. Development of a next-generation RFAP-2 reagent alleviates this issue and allows for more even staining in a wider variety of cell types. Indeed, the data showcase the broad applicability of RFAP-2 to image changes in FA levels in a variety of common cell lines. We further utilized this reagent to identify changes in endogenous levels of FA in cells lacking the FA-metabolizing enzyme ADH5, as well as impairments in FA metabolism in these cells. Current efforts are focused on applying RFAP-2 to discover and study new sources in FA fluxes in biological systems, as well as on using this platform as a general starting point to develop probes for molecular imaging of FA within specific subcellular locales, including mitochondrial and nuclear systems that are likely to utilize this one-carbon unit in various pathways spanning signalling to metabolism.

3.5. Acknowledgements

We thank the NIH (GM 79465) for financial support for synthetic aspects of the work. C.J.C. is an Investigator of the Howard Hughes Medical Institute. T.F.B. was partially supported by a Chemical Biology Training Grant from the NIH (T32 GM066698). We thank Alison Killilea and Carissa Tasto (UC Berkeley Tissue Culture Facility) as well as Hector Nolla (UC Berkeley Flow Cytometry Facility) for expert technical assistance.

Figures

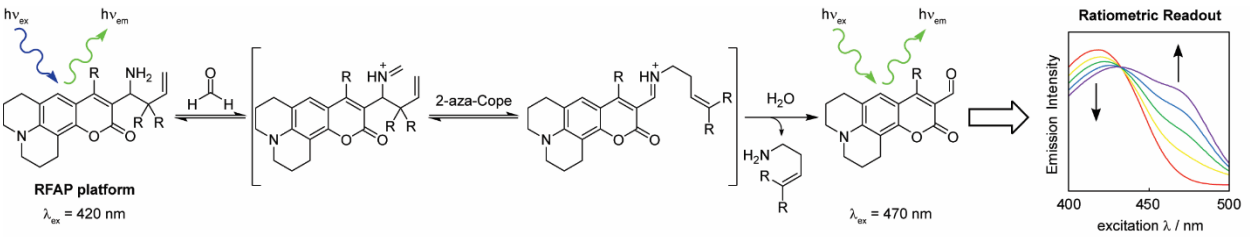

Scheme 3.1. Design of a Ratiometric Formaldehyde Probe (RFAP) platform.

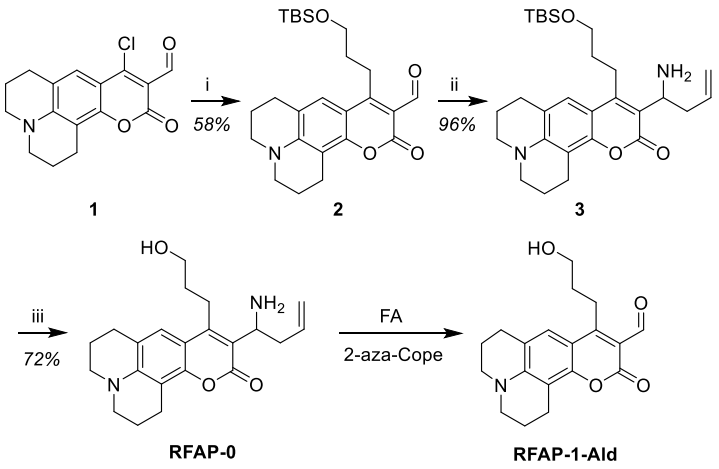

Scheme 3.2. Synthesis of RFAP-0. Reagents and conditions: (i) lithium bis(3-((tert-butyldimethylsilyl)oxy)propyl)copper, Et_2O, THF, -20 °C, 3 h; (ii) NH_3, MeOH, 0 °C, then allylboronic acid pinacol ester, rt, 10 h; (iii) AcOH, H_2O, rt, 14 h.

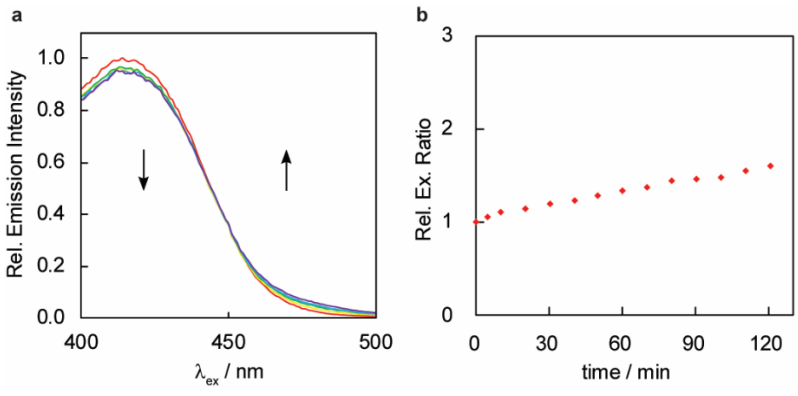

Figure 3.1. FA response of RFAP-0. Data were acquired at 37 °C in 20 mM PBS (pH 7.4). Excitation spectra were collected between 400 and 500 nm with emission monitored at λ_{em} = 510 nm. (a) Excitation ratiometric response of 10 μM RFAP-0 to 100 μM FA. Excitation spectra are shown at 0, 30, 60, 90, and 120 min (red, yellow, green, blue, and purple traces, respectively) after addition of FA. (b) Quantification of 470/420 nm excitation ratio over time.

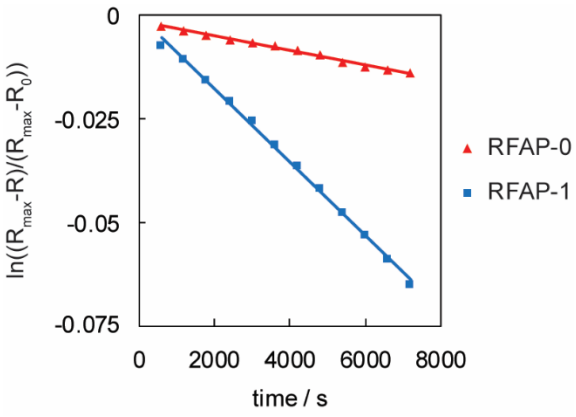

Figure 3.2. Linearized integrated rate law of reaction between 100 μM FA and 10 μM RFAP-0 (red triangles) or RFAP-1 (blue squares) assuming pseudo-first order kinetics.

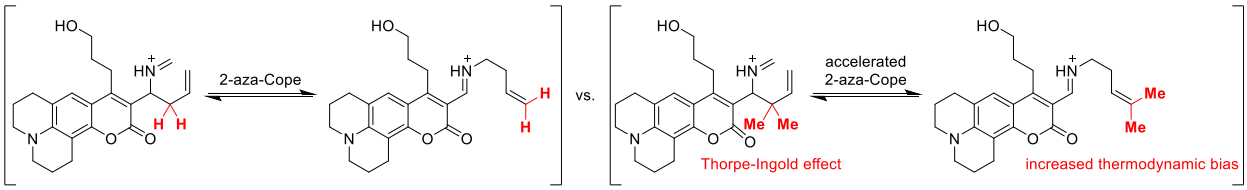

Scheme 3.3. Installation of a geminal dimethyl group is designed to accelerate the 2-aza-Cope rearrangement and thermodynamically bias the reaction toward product.

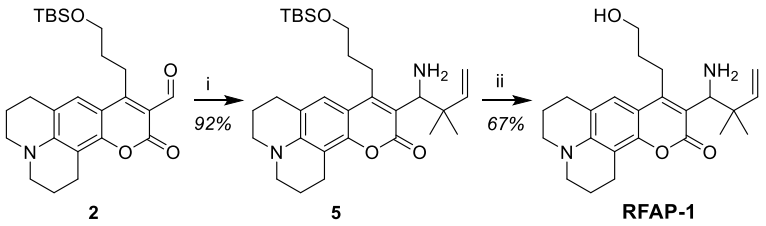

Scheme 3.4. Synthesis of RFAP-1. Reagents and conditions: (i) NH_3, MeOH, 0 °C, then prenylboronic acid, rt, 10 h; (ii) AcOH, H_2O, rt, 14 h.

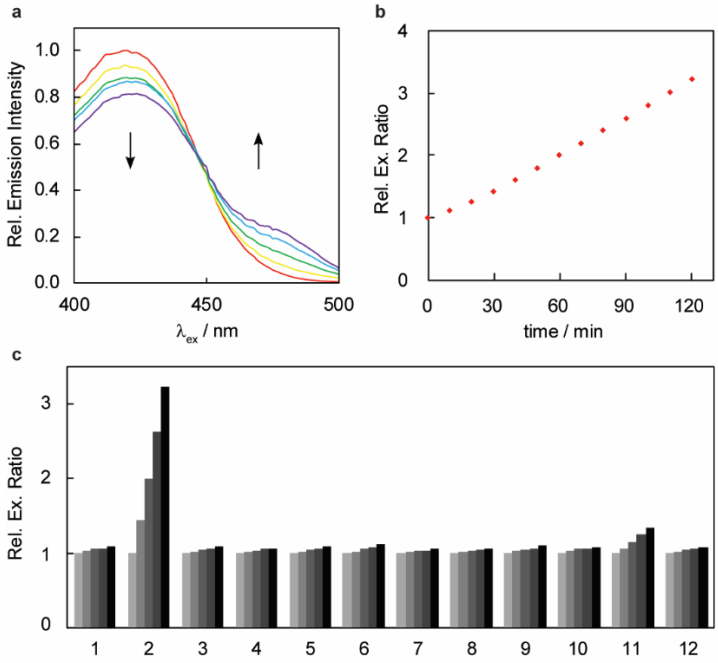

Figure 3.3. FA response and selectivity of RFAP-1. Data were acquired at 37 °C in 20 mM PBS (pH 7.4). Excitation spectra were collected between 400 and 500 nm with emission monitored at λ_{em} = 510 nm. (a) Excitation ratiometric response of 10 μM RFAP-1 to 100 μM FA. Excitation spectra are shown at 0, 30, 60, 90, and 120 min (red, yellow, green, blue, and purple traces, respectively) after addition of FA. (b) Quantification of 470/420 nm excitation ratio over time. (c) Excitation ratiometric response of 10 μM RFAP-1 to biologically relevant RCS and related molecules. Bars represent relative 470/420 nm excitation ratio responses at 0, 30, 60, 90, and 120 (black) min after addition of a given analyte. Data shown are for 100 μM of all species unless otherwise denoted. Legend: (1) PBS; (2) FA; (3) acetaldehyde; (4) pyruvate; (5) glucose, 1 mM; (6) 4-HNE; (7) dehydroascorbate; (8) oxaloacetate; (9) glucosone; (10) acrolein; (11) methylglyoxal; (12) methylglyoxal, 10 μM.

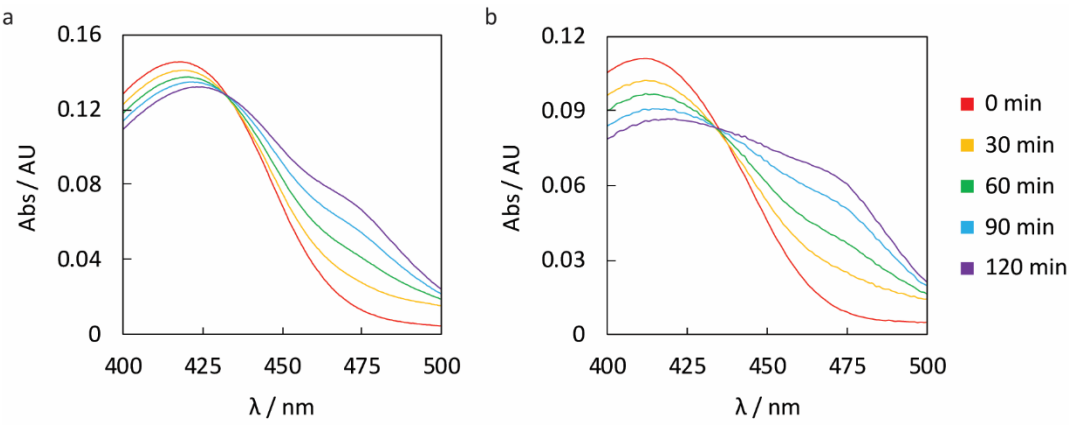

Figure 3.4. UV-visible FA response for RFAP-1 and RFAP-2. Data were acquired in 20 mM PBS (pH 7.4). (a) UV-visible response of 10 µM RFAP-1 to 100 µM FA. (b) UV-visible response of 10 µM RFAP-2 to 100 µM FA. Time points represent 0, 30, 60, 90, and 120 minutes after addition of 100 µM FA; saturation was not reached during this time.

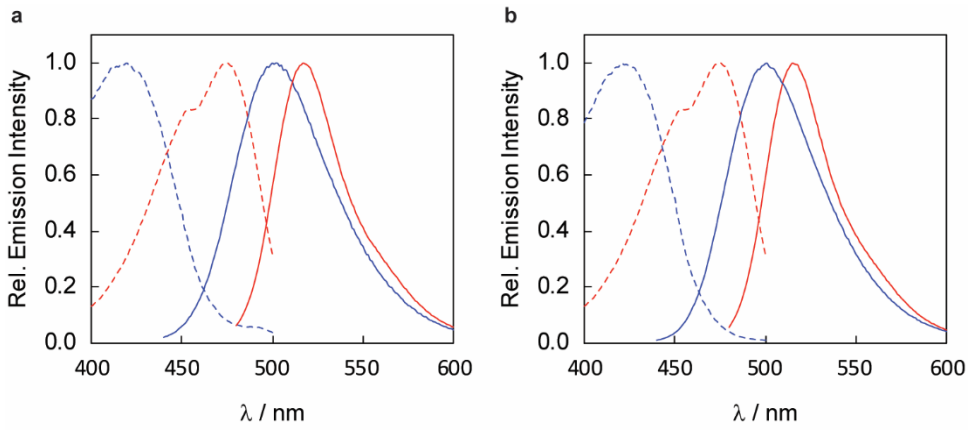

Figure 3.5. Normalized excitation and emission spectra for RFAP-1, RFAP-1-Ald, RFAP-2, and RFAP-2-Ald (all at 10 µM). Data were acquired in 20 mM PBS (pH 7.4) at 37 °C. (a) Spectra for RFAP-1 (blue traces) and RFAP-1-Ald (red traces). RFAP-1 excitation spectrum (blue, dashed trace) acquired with λ_{em} = 510 nm and emission spectrum (blue, solid trace) with λ_{ex} = 420 nm; RFAP-1-Ald excitation spectrum (red, dashed trace) acquired with λ_{em} = 510 nm and emission spectrum (red, solid trace) with λ_{ex} = 470 nm. (b) Spectra for RFAP-2 (blue traces) and RFAP-2-Ald (red traces). RFAP-2 excitation spectrum (blue, dashed trace) acquired with λ_{em} = 510 nm and emission spectrum (blue, solid trace) with λ_{ex} = 420 nm; RFAP-2-Ald excitation spectrum (red, dashed trace) acquired with λ_{em} = 510 nm and emission spectrum (red, solid trace) with λ_{ex} = 470 nm.

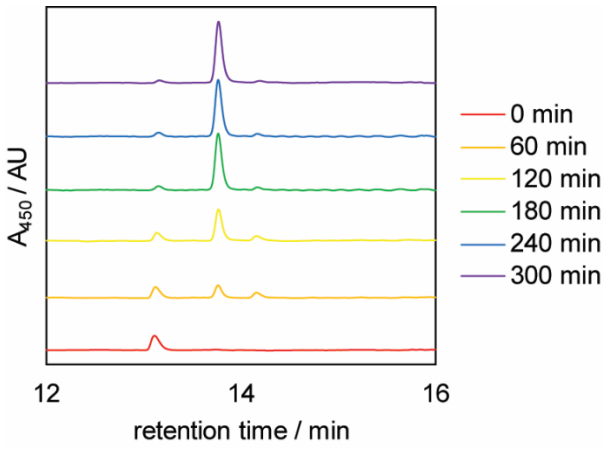

Figure 3.6. LC-MS timecourse of reaction between 100 μM RFAP-1 and 1 mM FA at 25 °C in 20 mM PBS (pH 7.4). HPLC runs used a linear gradient from 5 % MeCN / 95 % H_2O / 0.05 % formic acid to 95 % MeCN / 5 % H_2O / 0.05 % formic acid over 16 min using an Agilent 300extend-C18, 3.5 μm, 4.6 × 100mm column. Traces represent reverse-phase HPLC profile at 450 nm at different timepoints during reaction.

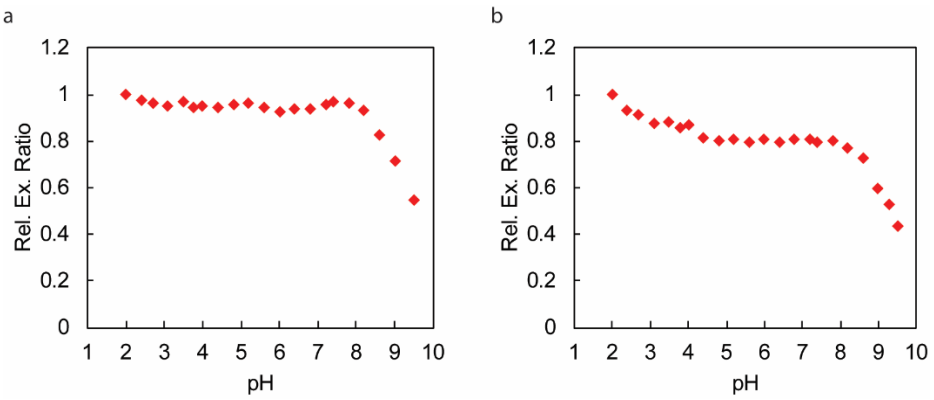

Figure 3.7. Excitation ratio pH profiles for (a) RFAP-1 and (b) RFAP-2. Data were acquired at 37 °C with 10 μM probe in 50 mM glycine (pH 2–3.8), 50 mM NaOAc (pH 4–5.6), 50 mM MOPS (pH 6–6.8), 50 mM HEPES (pH 7.2–8.2), and 50 mM bicine (pH 8.6–9.5).

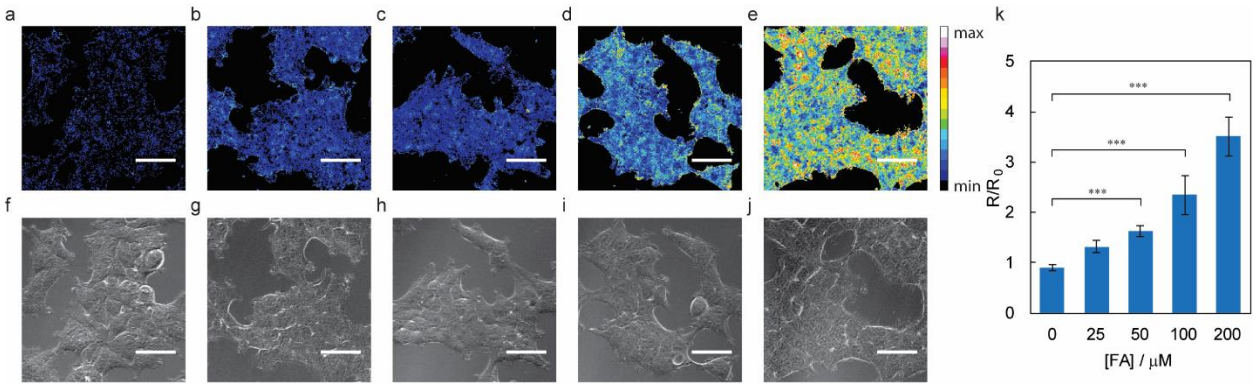

Figure 3.8. Representative ratiometric confocal microscopy images of FA detection in live HEK293T cells loaded with 10 μM RFAP-1. Images are taken 60 min after addition of (a) vehicle, (b) 25 μM FA, (c) 50 μM FA, (d) 100 μM, and (e) 200 μM FA. (f)–(j) Bright-field images of cells in (a)–(e). Scale bar represents 40 μm in all images. (k) Mean 488/405 excitation ratios of HEK293T cells treated with varying concentrations of FA for 60 min relative to mean 488/405 excitation ratios before FA addition; error bars denote SEM, n = 5. *** $P < 0.001$.

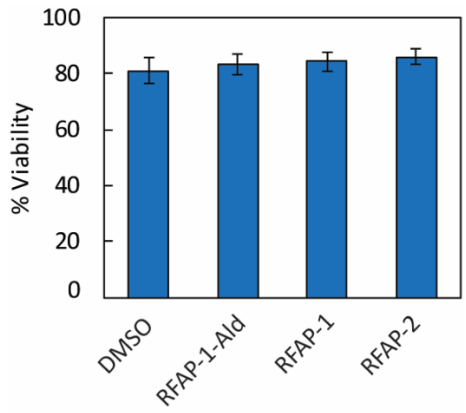

Figure 3.9. Flow cytometric analysis of HEK293T cell viability using Sytox Red staining. Cells were plated in 12-well polystyrene culture plates (Corning). After the designated treatments below, cells were dislodged from wells by gentle agitation and filtered through 35 μm nylon mesh cap into a 12 x 75 mm polystyrene tube (Corning) for flow cytometry. Cell viability was calculated as the percentage of Sytox Red-negative cells. HEK293T cells were incubated with vehicle (DMSO), 10 μM RFAP-1, 10 μM RFAP-2, or 10 μM RFAP-1-Ald in BSS at 37 °C for 60 min, then exchanged into PBS containing 5 nM Sytox Red and incubated for 10 min before flow cytometry. Error bars denote SEM, n=3.

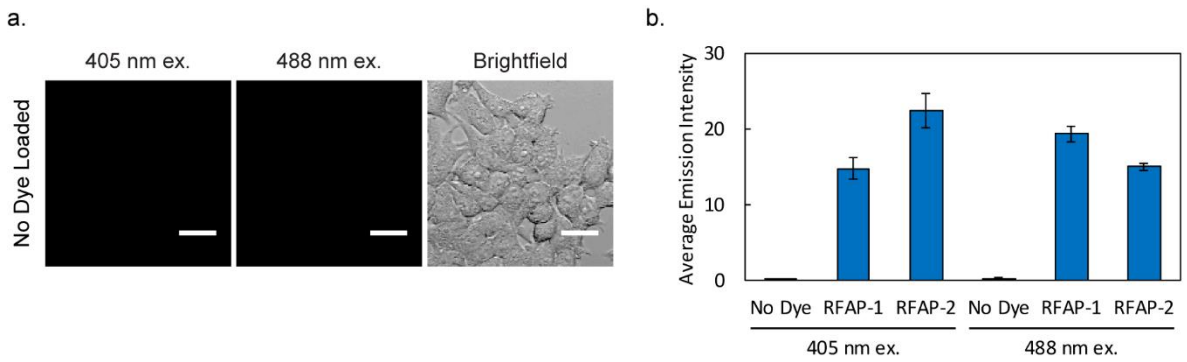

Figure 3.10. No-dye control has negligible fluorescence background using the same laser settings used for imaging RFAP-1 and RFAP-2. (a) Images of HEK293T cells treated with BSS for 30 min at 37 °C, washed with fresh BSS, then imaged. Scale bar represents 25 μm. (b) Quantification of fluorescence intensity in no-dye control compared to average fluorescence intensities of HEK93T cells loaded with 10 μM RFAP-1 or RFAP-2 under the same laser settings. Error bars represent SEM, n = 3 replicates with 3 fields of cells per replicate.

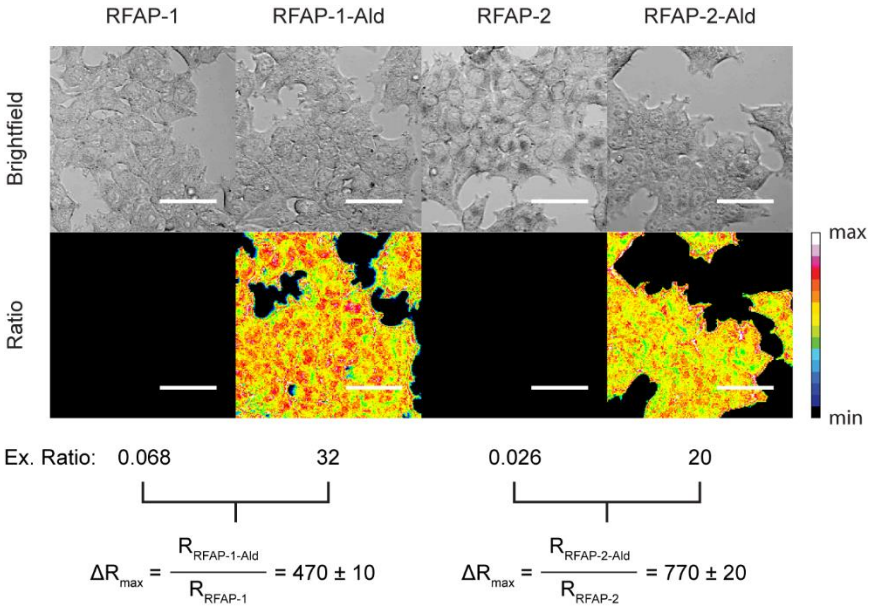

Figure 3.11. Maximum ratio change *in cellulo*. HEK293T cells were treated with 10 μM RFAP-1, RFAP-1-Ald, RFAP-2, or RFAP-2-Ald in BSS for 30 min at 37 °C, washed with fresh BSS, then imaged. Note that laser settings were altered so that RFAP-1-Ald and RFAP-2-Ald would not have saturated pixels for this analysis. Excitation ratios are an average across 2 replicates with 3 fields of cells per replicate; error represents SEM. Scale bar represents 50 μm.

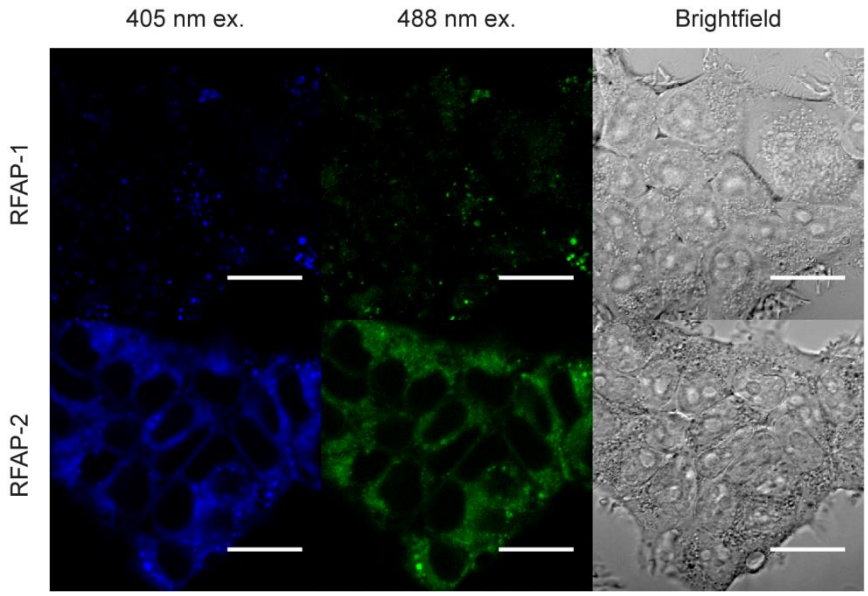

Figure 3.12. RFAP-1 displays punctate staining in HEK293T cells. HEK293T cells were treated with 10 μM RFAP-1 or RFAP-2 in BSS for 30 min at 37 °C, washed with fresh BSS, then imaged. Scale bar represents 20 μm.

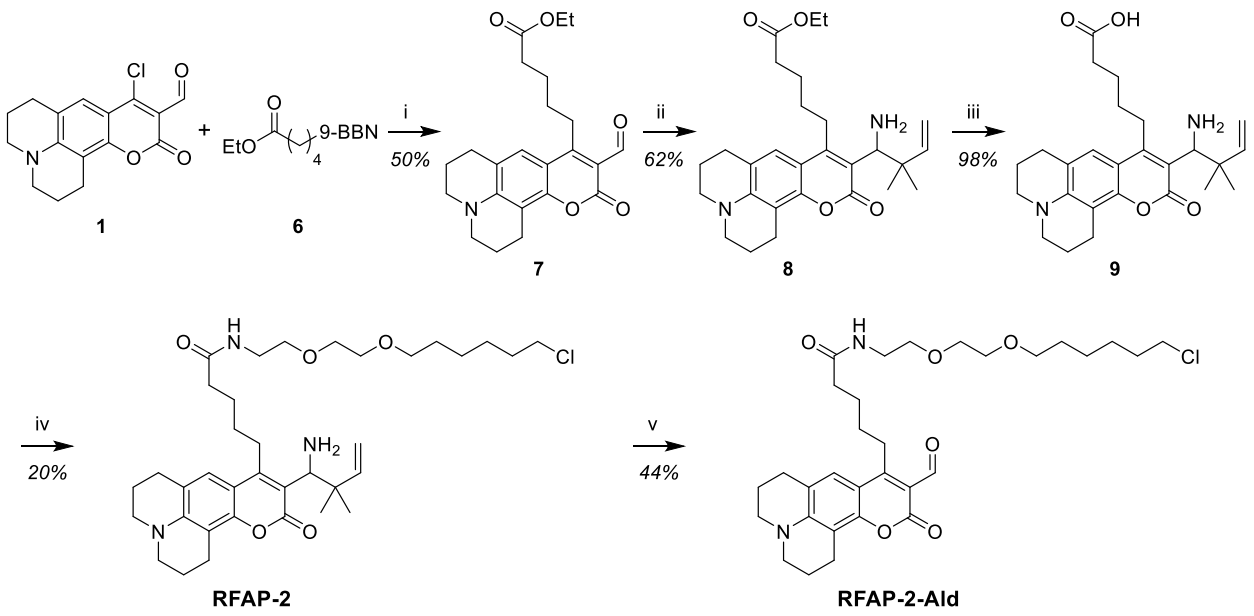

Scheme 3.5. Synthesis of RFAP-2. Reagents and conditions: (i) Pd-PEPPSI-IPr, $K_3PO_4 \cdot H_2O$ THF, rt, 10 h; (ii) NH_3, MeOH, 0 °C, then prenylboronic acid, rt, 10 h; (iii) LiOH, THF/MeOH/H_2O, rt, 6 h; (iv) 2-(2-((6-chlorohexyl)oxy)ethoxy)ethan-1-amine, HATU, DIPEA, DMF, rt, 12 h; (v) formaldehyde, MeOH:H_2O 2:1.

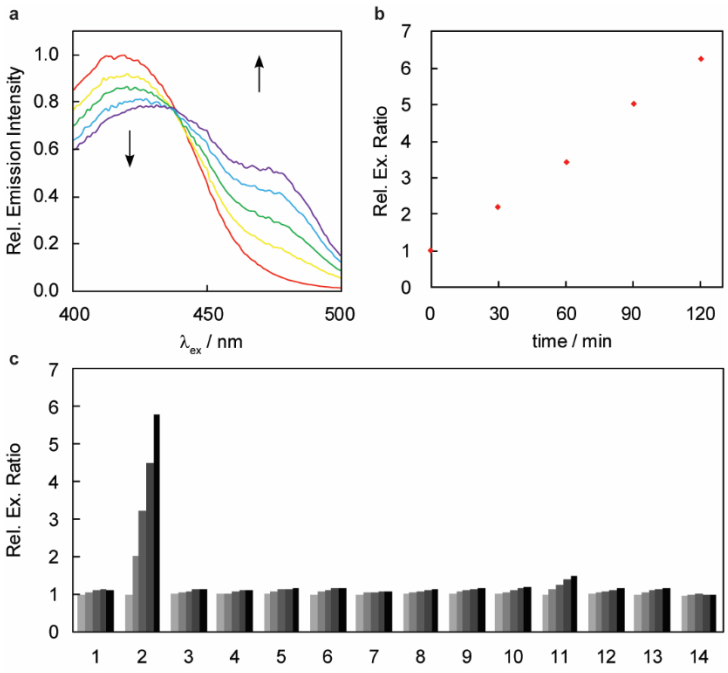

Figure 3.13. FA response and selectivity of RFAP-2. Data were acquired at 37 °C in 20 mM PBS (pH 7.4). Excitation spectra were collected between 400 and 500 nm with emission monitored at λ_{em} = 510 nm. (a) Excitation ratiometric response of 10 μM RFAP-2 to 100 μM FA. Excitation spectra are shown at 0, 30, 60, 90, and 120 min (red, yellow, green, blue, and purple traces, respectively) after addition of FA. (b) Quantification of 470/420 nm excitation ratio over time. (c) Excitation ratiometric response of 10 μM RFAP-2 to biologically relevant RCS and related molecules. Bars represent relative 470/420 nm excitation ratio at 0, 30, 60, 90, and 120 (black) min after addition. Data shown are for 100 μM of all species unless otherwise denoted. Legend: (1) PBS; (2) FA; (3) acetaldehyde; (4) pyruvate; (5) 1 mM glucose; (6) 4-HNE; (7) dehydroascorbate; (8) oxaloacetate; (9) glucosone; (10) acrolein; (11) methylglyoxal; (12) 10 μM methylglyoxal; (13) H_2O_2; (14) 5 mM glutathione.

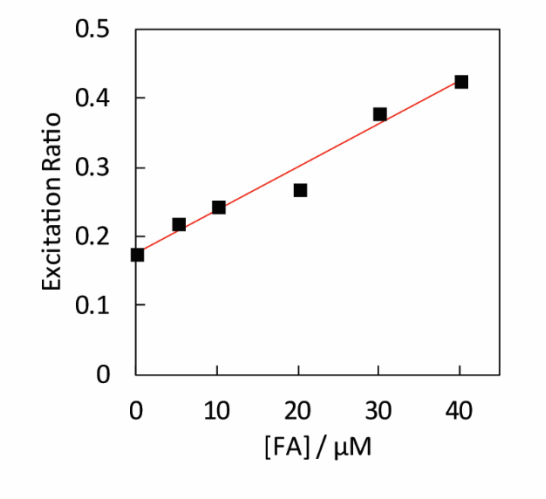

Figure 3.14. *In vitro* detection limit determination for RFAP-2. Excitation spectra were acquired in 20 mM PBS (pH 7.4) at 37 °C with emission at λ_{em} = 510 nm. Bars represent 470/420 nm excitation ratio 2 hours after FA addition. The standard deviation (σ) of three replicates of blank (0 μM FA) samples as well as the slope of the linear regression curve fitted to the 470/420 nm excitation ratio in the range of [FA] from 0 to 40 μM were used to determine the detection limit (3σ/slope) of 0.3 μM.

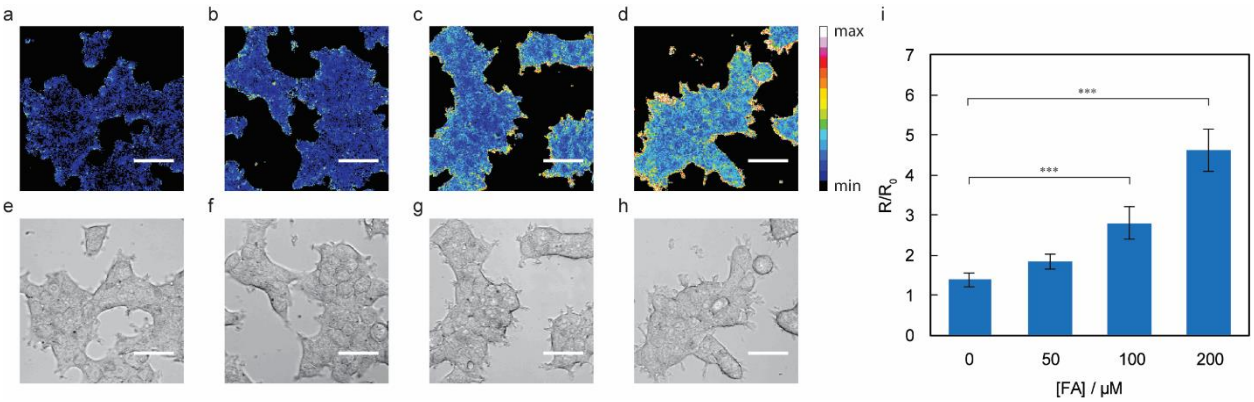

Figure 3.15. Representative ratiometric confocal microscopy images of FA detection in live HEK293T loaded with 10 μM RFAP-2. Images are taken 60 min after addition of (a) vehicle, (b) 50 μM FA, (c) 100 μM, and (d) 200 μM FA. (e)–(h) Bright-field images of cells in (a)–(d). Scale bar represents 40 μm in all images. (k) Mean 488/405 excitation ratios of HEK293T cells treated with varying concentrations of FA for 60 min relative to mean 488/405 excitation ratios before FA addition; error bars denote SEM, n = 4. *** $P < 0.001$.

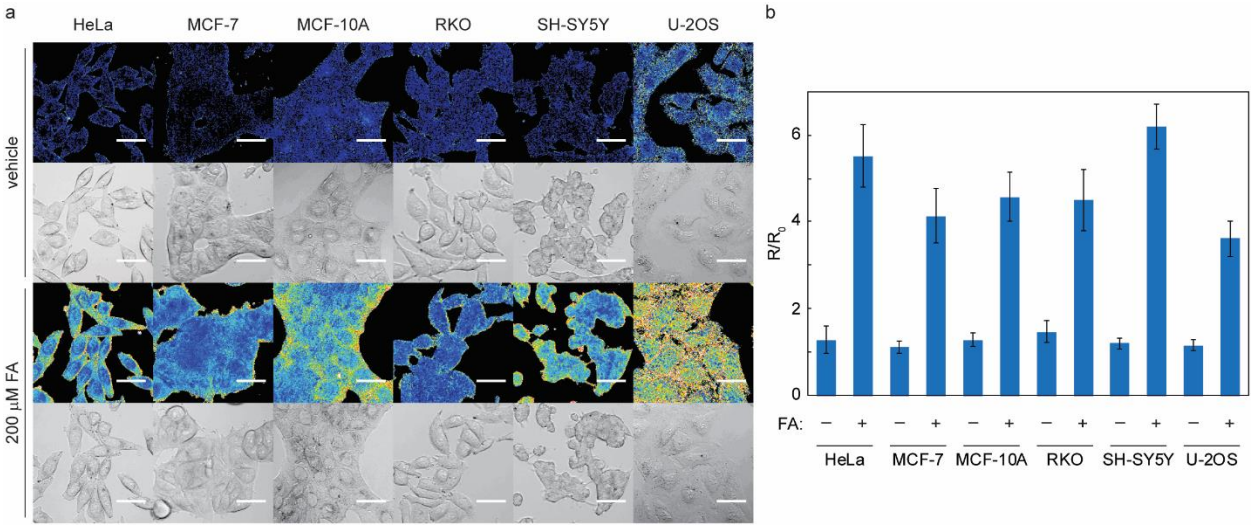

Figure 3.16. Representative ratiometric confocal microscopy images of FA detection in various cell lines using RFAP-2. Images are taken 30 min after addition of either vehicle or 200 μM FA. Scale bar represents 40 μm in all images. (a) ratio and bright-field images; (b) Mean 488/405 excitation ratios of cells treated with vehicle or 200 μM FA for 30 min relative to mean 488/405 excitation ratios before vehicle or FA addition; error bars denote SEM, n = 2 (3 fields per condition).

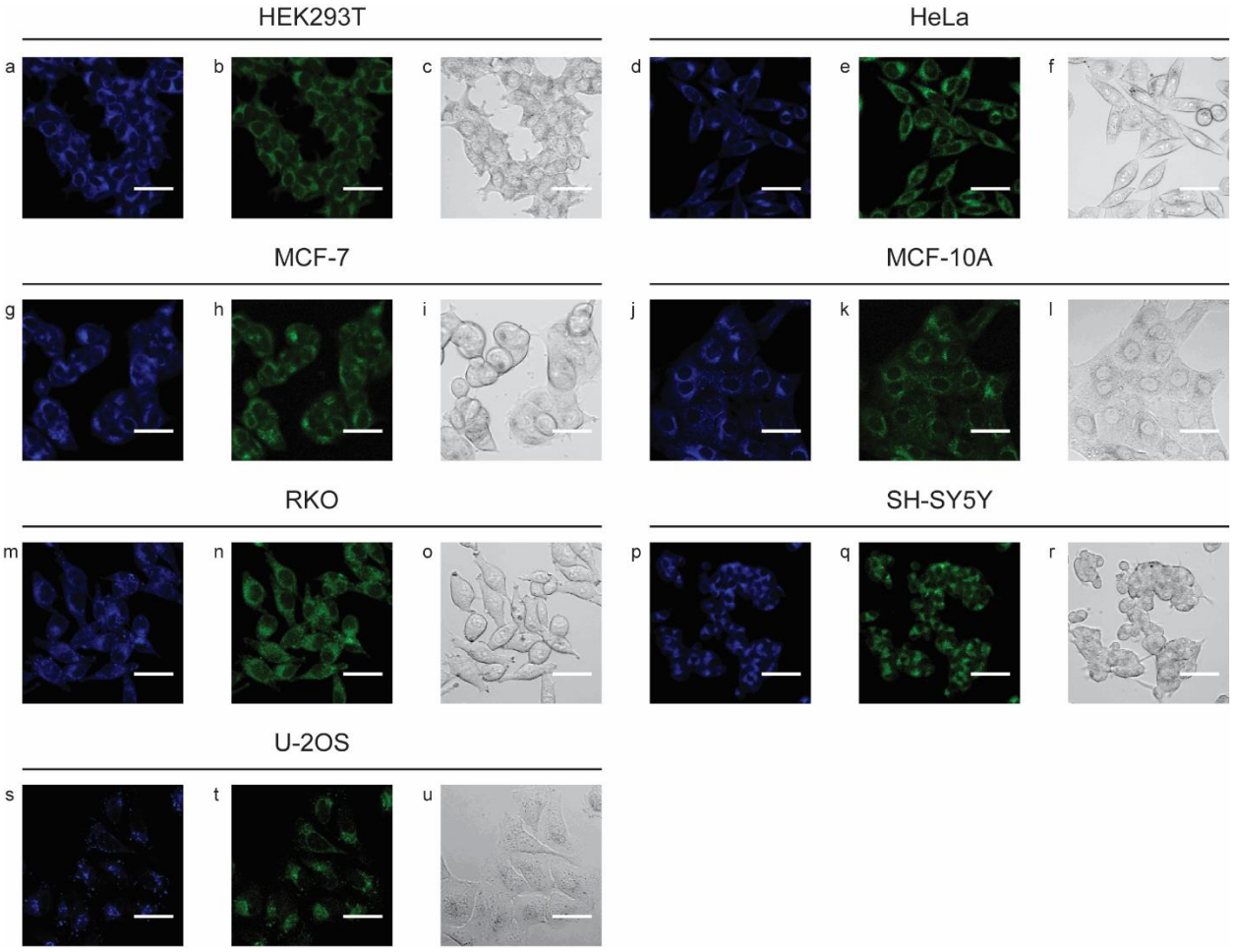

Figure 3.17. RFAP-2 staining patterns in various cell lines. Cells were treated with 10 μM RFAP-2 in BSS for 30 min at 37 °C, washed with fresh BSS, then imaged. Scale bar represents 40 μm in all images. HEK293T cells: (a) 405 nm excitation, (b) 488 nm excitation, (c) bright-field; HeLa cells: (d) 405 nm excitation, (e) 488 nm excitation, (f) bright-field; MCF-7 cells: (g) 405 nm excitation, (h) 488 nm excitation, (i) bright-field; MCF-10A cells: (j) 405 nm excitation, (k) 488 nm excitation, (l) bright-field; RKO cells: (m) 405 nm excitation, (n) 488 nm excitation, (o) bright-field; SH-SY5Y cells: (p) 405 nm excitation, (q) 488 nm excitation, (r) bright-field; U-2OS cells: (s) 405 nm excitation, (t) 488 nm excitation, (u) bright-field.

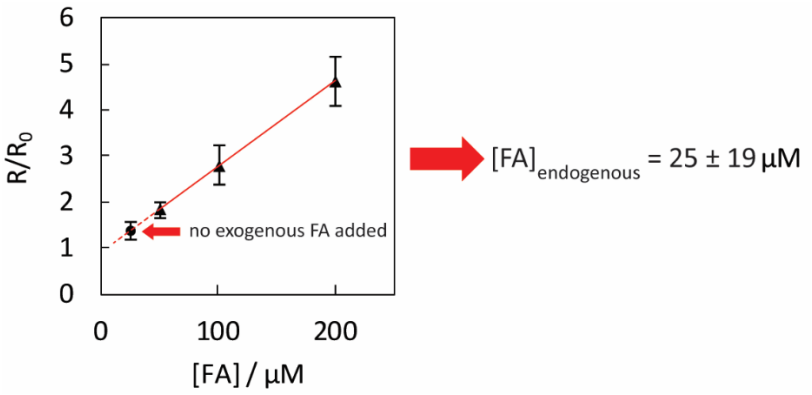

Figure 3.18. Calibration curve for [FA] in HEK293T cells using RFAP-2. Intracellular [FA] was assumed to be equivalent to exogenous [FA] (except in case of no exogenous FA) to construct calibration curve. Least-squares fit was extrapolated to observed R/R_0 for $[FA]_{exogenous}$ = 0 μM to give predicted $[FA]_{endogenous}$ = 25 ± 19 μM, where ± 19 μM is the 95% confidence interval.

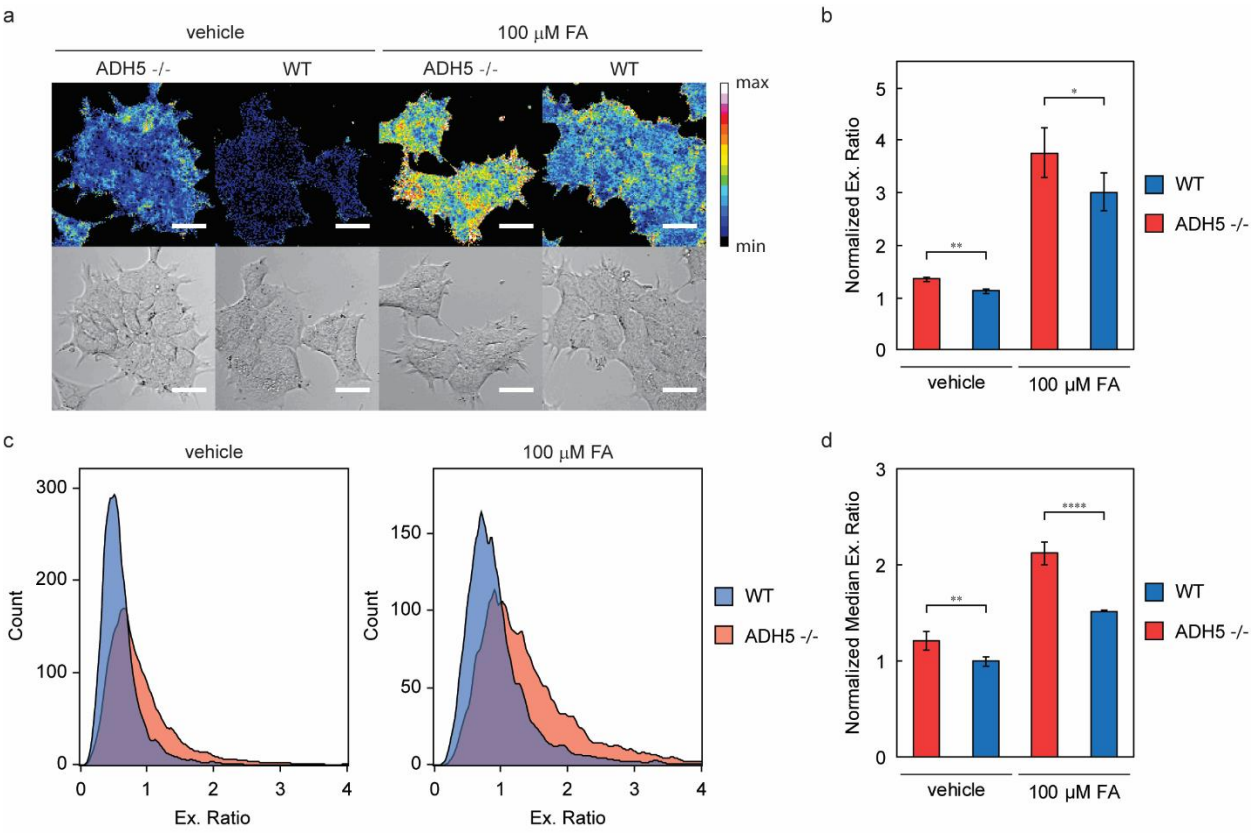

Figure 3.19. FA detection in ADH5 -/- vs. WT HAP1 cells with 500 nM RFAP-2. (a) Representative ratiometric confocal microscopy images taken 60 min after treatment with vehicle or 100 μM FA. Scale bare represents 25 μm in all images. (b) Normalized mean 488/405 excitation ratios of ADH5 -/- and WT HAP1 cells treated with vehicle or 100 μM FA for 60 min by confocal microscopy; error bars denote SEM, n =5. (c) Representative histograms obtained via flow cytometric analysis of ADH5 -/- and WT HAP1 cells treated with either vehicle or 100 μM FA for 60 min. (d) Normalized median 488/405 excitation ratios of ADH5 -/- and WT HAP1 cells treated with vehicle or 100 mM FA for 60 min by flow cytometry; error bars denote SEM, n=5. * $P < 0.05$, ** $P < 0.01$, **** $P < 0.0001$.

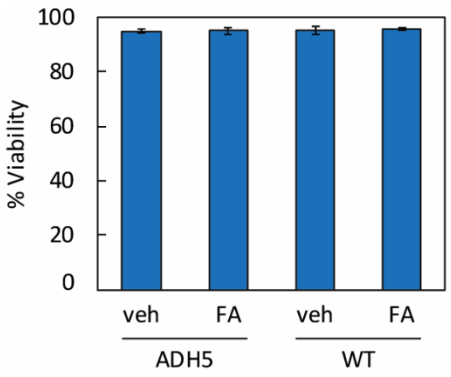

Figure 3.20. Flow cytometric analysis of ADH5 -/- and WT cell viability using Sytox Red exclusion. Cells were plated in 12-well polystyrene culture plates (Corning). After the designated treatments below, cells were dislodged from wells by gentle agitation and filtered through 35 μm nylon mesh cap into a 12 x 75 mm polystyrene tube (Corning) for flow cytometry. Cell viability was calculated as the percentage of Sytox Red-negative cells. ADH5 -/- and WT HAP1 cells were incubated with 500 nM RFAP-1 in BSS at 37 °C for 30 min, then exchanged into BSS containing either vehicle control or 100 μM FA and incubated at 37 °C for a further 60 min. Cells were then exchanged into PBS containing 5 nM Sytox Red and incubated for 10 min before flow cytometry. Error bars denote SEM, n=3.

3.6. References

1. Liteplo, R. G.; Beauchamp, R.; Meek, M. E.; Chénier, R., In *Formaldehyde (Concise International Chemical Assessment Documents)*, World Health Organization: Geneva, 2002.
2. Baan, R.; Grosse, Y.; Straif, K.; Secretan, B.; El Ghissassi, F.; Bouvard, V.; Benbrahim-Tallaa, L.; Guha, N.; Freeman, C.; Galichet, L.; Cogliano, V. *Lancet Oncol.* **2009,** *10*, 1143-1144.
3. Tong, Z.; Han, C.; Luo, W.; Wang, X.; Li, H.; Luo , H.; Zhou, J.; Qi, J.; He, R. *Age* **2013,** *35*, 583-596.
4. Miao, J.; He, R., *Chronic Formaldehyde-Mediated Impairments and Age-Related Dementia*. InTech: Shanghai, 2012.
5. Tulpule, K.; Dringen, R. *J. Neurochem.* **2013,** *127*, 7-21.
6. Porter, D. H.; Cook, R. J.; Wagner, C. *Arch. Biochem. Biophys.* **1985,** *243*, 396-407.
7. Leys, D.; Basran, J.; Scrutton, N. S. *EMBO J.* **2003,** *22*, 4038-4048.
8. Wu, T. P.; Wang, T.; Seetin, M. G.; Yongquan, L.; Zhu, S.; Kaixuan, L.; Liu, Y.; Byrum, S. D.; Mackintosh, S. G.; Zhong, M.; Tackett, A.; Wang, G.; Hon, L. S.; Fang, G.; Swenberg, J. A.; Xiao, A. Z. *Nature* **2016,** *532*, 329-333.
9. Fu, Y.; Dominissini, D.; Rechavi, G.; He, C. *Nat. Rev. Genet.* **2014,** *15*, 293-306.
10. Shi, Y.; Whetsine, J. R. *Mol. Cell* **2007,** *25*, 1-14.
11. O'Sullivan, J.; Unzeta, M.; Healy, J.; O'Sullivan, M. I.; Davey, G.; Tipton, K. F. *NeuroToxicology* **2004,** *25*, 303-315.
12. Dhareshwar, S. S.; Stella, V. J. *J. Pharm. Sci.* **2007,** *97*, 4184-4193.
13. Teng, S.; Beard, K.; Pourahmad, J.; Moridani, M.; Easson, E.; Poon, R.; O'Brien, P. J. *Chem.-Biol. Interact.* **2001,** *130-132*, 285-296.
14. Heck, H. d. A.; Casanova-Schmitz, M.; Dodd, P. B.; Schachter, E. N.; Witek, T. J.; Tosun, T. *AIHA J.* **1985,** *46*, 1-3.
15. Andersen, M. E.; Clewell, H. J.; Bermudez, E.; Dodd, D. E.; Willson, G. A.; Campbell, J. L.; Thomas, R. S. *Toxicol. Sci.* **2010,** *118*, 716-731.
16. Tong, Z.; Luo, W.; Wang, Y.; Yang, F.; Han, Y.; Li, H.; Luo, H.; Duan, B.; Xu, T.; Maoying, Q.; Tan, H.; Wang, J.; Zhao, H.; Liu, F.; Wan, Y. *PLoS One* **2010,** *5*, e10234.
17. Szarvas, T.; Szatloczky, E.; Volford, J.; Trezl, L.; Tyihak, E.; Rusznak, I. *J. Radioanal. Nucl. Chem.* **1986,** *106*, 357-367.
18. Ebeler, S. E.; Clifford, A. J.; Shibamoto, T. *J. Chromatogr., Biomed. Appl.* **1997,** *702*, 211-215.
19. Spanel, P.; Smith, D.; Holland, T. A.; Al Singary, W.; Elder, J. B. *Rapid Commun. Mass Spectrom.* **1999,** *13*, 1354-1359.
20. Kato, S.; Burke, P. J.; Koch, T. H.; Bierbaum, V. M. *Anal. Chem.* **2001,** *73*, 2992-2997.
21. Yu, P. H.; Cauglin, C.; Wempe, K. L.; Gubisne-Harberle, D. *Anal. Biochem.* **2003,** *318*, 285-290.
22. Luo, W. H.; Li, H.; Zhang, Y.; Ang, C. Y. W. *J. Chromatogr., Biomed. Appl.* **2001,** *753*, 253-257.
23. Brewer, T. F.; Chang, C. J. *J. Am. Chem. Soc.* **2015,** *137*, 10886-10889.
24. Roth, A.; Li, H.; Anorma, C.; Chan, J. *J. Am. Chem. Soc.* **2015,** *137*, 10890-10893.
25. Xu, J.; Zhang, Y.; Zeng, L.; Liu, J.; Kinsella, J. M.; Sheng, R. *Talanta* **2016,** *160*, 645-652.
26. He, L.; Yang, X.; Liu, Y.; Kong, X.; Lin, W. *Chem. Commun.* **2016,** *52*, 4029-4032.

27. Tang, Y.; Kong, X.; Liu, Z.; Xu, A.; Lin, W. *Anal. Chem.* **2016,** *88*, 9359-9363.
28. Tang, Y.; Kong, X.; Xu, A.; Dong, B.; Lin, W. *Angew. Chem. Int. Ed.* **2016,** *55*, 3356-3359.
29. Xie, Z.; Ge, J.; Zhang, H.; Bai, T.; He, S.; Ling, J.; Sun, H.; Zhu, Q. *Sens. Actuators B Chem.* **2016**, In Press.
30. He, L.; Yang, X.; Ren, M.; Kong, X.; Liu, Y.; Lin, W. *Chem. Commun.* **2016,** *52*, 9582-9585.
31. Lee, Y. H.; Tang, Y.; Verwilst, P.; Lin, W.; Kim, J. S. *Chem. Commun.* **2016,** *52*, 11247-11250.
32. He, L.; Yang, X.; Ren, M.; Kong, X.; Liu, Y.; Lin, W. *Chem. Commun.* **2016,** *52*, 9582-9585.
33. Liu, C.; Jiao, X.; He, S.; Zhao, L.; Zeng, X. *Dyes Pigm.* **2017,** *138*, 23-29.
34. Chan, J.; Dodani, S. C.; Chang, C. J. *Nat. Chem.* **2012,** *4*, 973-984.
35. Chen, X.; Tian, X.; Shin, I.; Yoon, J. *Chem. Soc. Rev.* **2011,** *40*, 4783-4804.
36. Cho, D.-G.; Sessler, J. L. *Chem. Soc. Rev.* **2009,** *38*, 1647-1662.
37. Yang, Y.; Zhao, Q.; Feng, W.; Li, F. *Chem. Rev.* **2013,** *113*, 192-270.
38. Tsien, R. Y. *TINS* **1988,** *11*, 419-424.
39. Lee, M. H.; Kim, J. S.; Sessler, J. L. *Chem. Soc. Rev.* **2015,** *44*, 4185-4191.
40. Srikun, D.; Miller, E. W.; Domaille, D. W.; Chang, C. J. *J. Am. Chem. Soc.* **2008,** *130*, 4596-4597.
41. Albers, A. E.; Okreglak, V. S.; Chang, C. J. *J. Am. Chem. Soc.* **2006,** *128*, 9640-9641.
42. Aron, A. T.; Loehr, M. O.; Bogena, J.; Chang, C. J. *J. Am. Chem. Soc.* **2016,** *138*, 14338-14346.
43. Rooker, D. R.; Buccella, D. *Chem. Sci.* **2015,** *6*, 6456-6461.
44. Neklesa, T. K.; Tae, H. S.; Schneekloth, A. R.; Stulberg, M. J.; Corson, T. W.; Sundberg, T. B.; Raina, K.; Holley, S. A.; Crews, C. M. *Nat. Chem. Biol.* **2011,** *7*, 538-543.
45. Raducan, M.; Alam, R.; Szabó, K. J. *Angew. Chem. Int. Ed.* **2012,** *51*.
46. Brouwer, A. M. *Pure Appl. Chem.* **2011,** *83*, 2213-2228.
47. Chen, Y.; Zhu, C.; Yang, Z.; Chen, J.; He, Y.; Jiao, Y.; He, W.; Qiu, L.; Cen, J.; Guo, Z. *Angew. Chem.* **2013,** *125*, 1732-1735.
48. Jung, M. E.; Piizzi, G. *Chem. Rev.* **2005,** *105*, 1735-1766.
49. Sugiura, M.; Hirano, K.; Kobayashi, S. *J. Am. Chem. Soc.* **2004,** *126*, 7182-7183.
50. Kalapos, M. P. *Diabetes Res. Clin. Pract.* **2013,** *99*, 260-271.
51. Valente, C.; Baglione, S.; Candito, D.; O'Brien, C. J.; Organ, M. G. *Chem. Commun.* **2008**, 735-737.
52. Los, G. V.; Encell, L. P.; McDougall, M. G.; Hartzell, D. D.; Karassina, N.; Zimprich, C.; Wood, M. G.; Learish, R.; Ohana, R. F.; Urh, M.; Simpson, D.; Mendez, J.; Zimmerman, K.; Otto, P.; Vidugiris, G.; Zhu, J.; Darzins, A.; Klauber, D. H.; Bulleit, R. F.; Wood, K. V. *ACS Chem. Biol.* **2008,** *3*, 373-382.
53. Pontel, L. B.; Rosado, I. V.; Burgos-Barragan, G.; Garaycoechea, J. I.; Yu, R.; Arends, M. J.; Chandrasekaran, G.; Broecker, V.; Wei, W.; Liu, L.; Swenberg, J. A.; Crossan, G. P.; Patel, K. J. *Mol. Cell* **2015,** *60*, 177-188.

Chapter 4

Toward *in vivo* FA detection methods: immunohistochemistry- and bioluminescence-based probes for formaldehyde

Portions of this work were performed in collaboration with the following persons:

In vitro luminescence assays were performed by Marie C. Heffern.

4.1. Introduction

The previous chapters have demonstrated the utility of the 2-aza-Cope strategy for the generation of fluorescence-based probes which can detect FA in living cells. However, to move to *in vivo* model systems such as whole animals, imaging modalities other than fluorescence are more desirable, as there can be significant issues with background autofluorescence and lack of transmittance through tissue in the fluorescence mode. Accordingly, this chapter focuses on the development of two new 2-aza-Cope-based FA probes whose readouts are compatible with whole-animal studies, namely immunohistochemistry and bioluminescence.

4.2. Materials and methods

4.2.1 General synthetic methods

All reactions utilizing air- or moisture-sensitive reagents were performed in dried glassware under an atmosphere of dry N_2. When dry solvent was used, the solvent was passed over activated alumina. Other reagents were used without further purification. Silica gel P60 (SiliCycle) was used for column chromatography and SiliCycle 60 F254 silica gel (precoated sheets, 0.25 mm thick) was used for analytical thin layer chromatography and visualized by fluorescence quenching under UV light. Prenylboronic acid solution was prepared using a slightly modified literature procedure.[1] 3-methyl-2-buten-1-ol and tetrahydroxydiboron were purchased from AK Scientific (Union City, CA); thiophenol was purchased from Oakwood Chemical (Estill, SC); 6-amino-2-cyanobenzothiazole was purchased from Abblis Chemicals LLC (Houston, TX); puromycin dihydrochloride was purchased from Cayman Chemical (Ann Arbor, MI); and all other reagents were purchased from Sigma-Aldrich (St. Louis, MO). ^{1}H NMR and ^{13}C NMR spectra were collected in $CDCl_3$, CD_3OD, or D_2O (Cambridge Isotope Laboratories, Cambridge, MA) at 25 °C on Bruker AVB-400, AVQ-400, and AV-600 with ^{13}C operating frequencies of 101 MHz and 150 MHz, respectively, at the College of Chemistry NMR Facility at the University of California, Berkeley. All chemical shifts are reported in the standard δ notation of parts per million relative to residual solvent peak at 7.26 ($CDCl_3$), 3.31 (CD_3OD), or 4.79 (D_2O) for ^{1}H and 77.16 ($CDCl_3$) or 3.31 (CD_3OD) for ^{13}C as an internal reference. Splitting patterns are indicated as follows: br, broad; s, singlet; d, doublet; t, triplet; q, quartet; m, multiplet; dd, doublet of doublets; dt, doublet of triplets; td, triplet of doublets; qd, quartet of doublets; ddd, doublet of doublet of doublets; dtd, doublet of triplet of doublets. Low-resolution electrospray mass spectral analyses were carried out using a LC-MS (Agilent Technology 6130, Quadrupole LC/MS). High resolution mass spectral analyses (ESI-MS) were carried out at the College of Chemistry Mass Spectrometry Facility at the University of California, Berkeley.

4.2.2. Probe synthesis and new compound characterization

Synthesis of azo transfer reagent imidazole-1-sulfonyl azide hydrochloride.

Imidazole-1-sulfonyl azide hydrochloride was prepared according to a reported procedure.[2] NaN_3 (6 g, 92 mmol) was suspended in MeCN (100 mL) and cooled to 0 °C with an ice bath. Sulfuryl chloride (7.46 mL, 92 mmol) was added dropwise, and the reaction mixture was allowed to warm to room temperature and stirred overnight. The reaction mixture was cooled to 0 °C with an ice bath, and imidazole (11.94 g, 175 mmol) was added portion-wise. The resultant slurry was allowed to warm to room temperature and stirred for a further 3 h. The reaction mixture was diluted with EtOAc (200 mL) and washed with H_2O (2 x 200 mL) and sat. aq. $NaHCO_3$ (2 x 200 mL), then dried over $MgSO_4$ and filtered. To isolate the hydrochloride salt, a solution of HCl in

EtOH [freshly made via dropwise addition of acetyl chloride (9.9 mL, 138 mmol) to ice-cold EtOH (40 mL)] was added dropwise to the EtOAc solution of imidazole-1-sulfonyl azide obtained above (cooled in an ice-water bath). The formed precipitate was filtered with a sintered funnel and washed with EtOAc (3 x 200 mL), giving imidazole-1-sulfonyl azide hydrochloride as white powder (13.9 g, 72% yield). ^{1}H NMR (400 MHz, D_2O) δ 9.42 (t, J = 1.5 Hz, 1H), 8.02 (t, J = 1.91 Hz, 1H), 7.61 (dd, J = 2.2, 1.3 Hz, 1H). ^{13}C NMR (101 MHz, D_2O) δ 137.7, 123.3, 120.1.

Preparation of prenylboronic acid solution.

A 0.3 M solution of H_2PdCl_4 was prepared by dissolving $PdCl_2$ (540 mg, 3 mmol) in 10 mL 0.9 M aqueous HCl and stirring for 8 h. Prenol (6.1 mL, 60 mmol) was dissolved in 120 mL of 4:1 DMSO:H_2O, followed by addition of 0.3 M H_2PdCl_4 (10 mL, 3 mmol) and $B_2(OH)_4$ (6.5 g, 72 mmol). The reaction mixture was stirred under N_2 for 10 h, then diluted with 220 mL $CHCl_3$ and stirred for an additional 10 minutes. The reaction mixture was filtered through a cotton plug, then 200 mL brine was added. The biphasic mixture was vigorously agitated and the layers were allowed to separate. The organic layer was collected, followed by additional brine washes (2 x 200 mL). The organic layer was dried over Na_2SO_4, the volume was measured, and the solution was used directly in further reactions. The yield was assumed to be 50%,[1] resulting in ca. 0.13 M prenylboronic acid solution.

Synthesis of 3-azido-3,4,4-trimethylhex-5-en-1-ol (3).

*Synthesis of 3-amino-3,4,4-trimethylhex-5-en-1-ol (**1**).* Commercial 7N NH_3 solution (24 mL, 170 mmol) was added to 4-hydroxy-2-butanone (1.5 mL, 17 mmol) dissolved in 5 mL of MeOH and stirred under N_2 for 30 minutes. Freshly prepared (see preparation above) 0.13 M prenylboronic acid solution (170 mL, 22 mmol) was added, and the reaction mixture was allowed to stir for 12 h, during which time the reaction mixture became pearlescent, milky white. The solvent was removed under reduced pressure. The resultant crude material was partitioned between EtOAc (100 mL) and 5% citric acid (100 mL) and the organic layer was further extracted with 5% citric acid (2 x 100 mL). The aqueous layer was basified to pH 12 with solid NaOH, then extracted with $CHCl_3$ (3 x 100 mL). The combined organic layers were dried over Na_2SO_4, and the solvent was removed under reduced pressure to afford **1** as a clear oil (0.56 g, 21%). ^{1}H NMR (400 MHz, $CDCl_3$) δ 5.92 (dd, J = 17.5, 10.9 Hz, 1H), 5.10 (dd, J = 10.8, 1.4 Hz, 1H), 5.00 (dd, J = 17.5, 1.4 Hz, 1H), 3.96 (td, J = 11.5, 2.3 Hz, 1H), 3.72 (ddd, J = 11.1, 4.6, 2.9 Hz, 1H), 2.88 (br s, 2H), 1.47 (t, J = 2.7 Hz, 1H), 1.43 (t, J = 2.7 Hz, 1H), 1.14 (s, 3H), 1.00 (s, 6H). ^{13}C NMR (101 MHz, $CDCl_3$) δ 144.29, 113.24, 59.62, 43.79, 40.51, 35.12, 21.64, 20.86, 19.60. LRMS calcd. for $C_9H_{19}NO$ (M + H) 158.15, found 158.3.

*Synthesis of 3-azido-3,4,4-trimethylhex-5-en-1-ol (**2**).* Imidazole-1-sulfonyl azide hydrochloride (0.9 g, 4.3 mmol) was added to a solution of 3-amino-3,4,4-trimethylhex-5-en-1-ol **1** (0.56 g, 3.6 mmol), $CuSO_4$•$5H_2O$ (9 mg, 40 µmol), and K_2CO_3 (0.84 g, 6 mmol) in 15 mL MeOH and stirred for 12 h under N_2. The reaction mixture was partitioned between EtOAc (100 mL) and 1 M HCl (100 mL), then the aqueous layer was further extracted with EtOAc (1 x 100 mL). The combined organic layers were washed sequentially with 1 M HCl (1 x 100 mL), sat. $NaHCO_3$ (1 x 100 mL), and brine (1 x 100 mL), then dried over anhydrous Na_2SO_4. The solvent was removed under reduced pressure. Purification by silica column chromatography (5 → 20% EtOAc in hexanes) afforded **2** as a clear oil (0.44 g, 67%). ^{1}H NMR (400 MHz, $CDCl_3$) δ 5.93 (dd, J = 17.4, 10.9 Hz, 1H), 5.10 – 4.99 (m, 2H), 3.82 – 3.67 (m, 2H), 2.38 (s, 1H), 1.86 (dt, J = 14.0, 7.0 Hz,

1H), 1.66 (ddd, J = 14.0, 7.0, 6.0 Hz, 1H), 1.31 (s, 3H), 1.05 (d, J = 2.7 Hz, 6H). 13C NMR (101 MHz, $CDCl_3$) δ 143.8, 113.9, 67.8, 59.4, 45.6, 38.0, 22.4, 22.3, 17.9. LRMS calcd. for $C_9H_{17}N_3O$ (M + H) 184.14, found 184.3.

Synthesis of Puromycin-FA-1 (Puro-FA-1).

*Synthesis of 3-azido-3,4,4-trimethylhex-5-en-1-yl (4-nitrophenyl) carbonate (**3**)*. 4-nitrophenyl chloroformate (180 mg, 0.9 mmol) was added to a solution of compound **2** (150 mg, 0.8 mmol) and triethylamine (0.17 mL, 1.2 mmol) in 7.5 mL DCM, and the resultant mixture was stirred for 12 hours under N_2. The reaction mixture was diluted was Et_2O (100 mL) and filtered through celite. The solvent was removed under reduced pressure. Purification by silica column chromatography (5% EtOAc in hexanes) afforded **3** as a clear oil (245 mg, 86%). ^{1}H NMR (400 MHz, $CDCl_3$) δ 8.35 – 8.22 (m, 2H), 7.42 – 7.34 (m, 2H), 5.95 (dd, J = 17.4, 10.9 Hz, 1H), 5.17 – 5.01 (m, 2H), 4.42 (t, J = 7.1 Hz, 2H), 2.12 – 1.99 (m, 1H), 1.94 – 1.82 (m, 1H), 1.38 (s, 3H), 1.09 (s, 6H). ^{13}C NMR (101 MHz, $CDCl_3$) δ 155.6, 152.5, 145.5, 143.5, 125.4, 121.9, 114.3, 67.0, 66.5, 45.7, 34.3, 22.4, 22.3, 17.9.

*Synthesis of compound **4***. Puromycin dihydrochloride (68 mg, 120 µmol), compound **3** (40 mg, 110 µmol), 4-dimethylaminopyridine (2 mg, 20 µmol), and *N*,*N*-diisopropylethylamine (100 µL, 600 µmol) were dissolved in 2 mL DMF, and the resultant mixture was stirred for 12 h under N_2. The reaction mixture was partitioned between EtOAc (50 mL) and sat. $NaHCO_3$ (50 mL), and the aqueous layer was further extracted with EtOAc (3 x 50 mL). The combined organic layers were washed sequentially with sat $NaHCO_3$ (1 x 100 mL) and brine (2 x 100 mL), then dried over anhydrous Na_2SO_4 and filtered. The solvent was removed under reduced pressure, and purification by silica column chromatography (100% DCM → 3% MeOH in DCM) afforded **4** as a white solid (66 mg, 84%). ^{1}H NMR (400 MHz, $CDCl_3$) δ 7.93 (d, J = 1.8 Hz, 1H), 7.90 (s, 1H), 7.13 (d, J = 8.1 Hz, 2H), 6.98 (br s, 1H), 6.84 (d, J = 8.2 Hz, 2H), 6.01 – 5.77 (m, 2H), 5.62 (br s, 1H), 5.47 (d, J = 4.8 Hz, 1H), 5.10 – 4.93 (m, 2H), 4.77 (s, 1H), 4.54 (q, J = 7.7 Hz, 1H), 4.47 – 4.39 (m, 1H), 4.23 – 4.03 (m, 2H), 4.01 (s, 1H), 3.86 (d, J = 12.7 Hz, 1H), 3.75 (s, 3H), 3.66 (d, J = 12.8 Hz, 1H), 3.35 (br s, 6H), 2.99 (qd, J = 13.7, 7.5 Hz, 2H), 1.85 (dtd, J = 14.1, 7.1, 4.8 Hz, 1H), 1.68 (dt, J = 15.9, 7.1 Hz, 1H), 1.31 – 1.17 (m, 3H), 1.01 (s, 6H). ^{13}C NMR (101 MHz, $CDCl_3$) δ 172.4, 158.7, 156.4, 154.6, 151.3, 148.4, 143.7, 137.9, 130.4, 128.6, 120.8, 114.3, 114.0, 90.9, 85.0, 72.7, 67.3, 67.2, 62.5, 62.3, 56.6, 55.4, 51.8, 45.5, 38.6, 34.5, 22.3, 22.3, 17.7, 17.7, 14.3.

Synthesis of Puro-FA-1. Compound **4** (66 mg, 97 µmol) and tris(2-carboxyethyl)phosphine hydrochloride (280 mg, 970 µmol) were dissolved in 5 mL of degassed 3:2:1 MeOH:H_2O:Et_3N, then stirred for 12 h under N_2. The reaction mixture was partitioned between DCM (20 mL) and 0.3 M NaOH (20 mL). The aqueous layer was further extracted with DCM (3 x 20 mL), then the combined organic layers were washed sequentially with 0.3 M NaOH (1 x 50 mL) and brine (1 x 50 mL) and dried over anhydrous Na_2SO_4. The solvent was removed under reduced pressure, and purification by reverse-phase HPLC (5→100% CH_3CN in H_2O with 0.05% formic acid) afforded Puro-FA-1 as a white solid (13 mg, 20% yield). ^{1}H NMR (400 MHz, $CDCl_3$) δ 8.14 (d, J = 6.5 Hz, 1H), 8.01 (d, J = 2.7 H, 1H), 7.32 – 7.18 (m, 1H), 7.10 (d, J = 8.2 Hz, 2H), 6.80 (d, J = 8.1 Hz, 2H), 6.31 (d, J = 30.9 Hz, 1H), 5.88 (ddd, J = 17.5, 10.8, 2.8 Hz, 1H), 5.65 (s, 1H), 5.17 – 4.93 (m, 2H), 4.73 – 4.56 (m, 2H), 4.44 – 4.35 (m, 1H), 4.35 – 4.22 (m, 1H), 4.17 – 3.95 (m, 2H), 3.88 (d, J = 13.0 Hz, 1H), 3.73 (s, 3H), 3.63 (d, J = 12.9 Hz, 1H), 3.45 (br s, 6H), 3.05 – 2.89 (m, 2H), 1.85 – 1.60 (m, 2H), 1.01 (s, 6H). ^{13}C NMR (101 MHz, $CDCl_3$) δ 172.8, 172.7, 158.7, 156.3, 154.9, 151.8, 149.0, 143.6, 137.7, 130.5, 128.7, 121.2, 114.9, 114.1, 91.2, 85.0, 73.0, 62.3, 57.0, 56.2,

55.4, 51.4, 43.8, 34.5, 22.0, 21.9, 21.0, 20.7. HRMS calcd. for $C_{32}H_{47}N_8O_7$ (M+H) 655.3562, found 655.3572.

Synthesis of FA-Luciferin-1 (FA-Luc-1).

*Synthesis of compound **5***. 6-Amino-2-cyanobenzothiazole (25 mg, 140 µmol) was suspended in 10 mL dry toluene, then triphosgene (42 mg, 140 µmol) and 4-dimethylaminopyridine (18 mg, 140 µmol) were added and the reaction mixture was heated at reflux for 3 h. The reaction mixture was cooled to 50 °C, and compound **2** (30.9 mg, 170 µmol) and 4-dimethylaminopyridine (18 mg, 140 µmol) were added. The reaction mixture was stirred for 12 h at ambient temperature. The reaction mixture was partitioned between EtOAc (30 mL) and H_2O (30 mL), then the aqueous layer was further extracted with EtOAc (2 x 30 mL). The combined organic layers were washed with brine (100 mL) and dried over anhydrous Na_2SO_4. The solvent was removed under reduced pressure, and purification by silica column chromatography (5→10% EtOAc in hexanes) afforded compound **5** as a yellow solid (40 mg, 73%). ^{1}H NMR (600 MHz, $CDCl_3$) δ 8.40 (s, 1H), 8.08 (d, J = 8.9 Hz, 1H), 7.36 (d, J = 9.0 Hz, 1H), 7.15 (s, 1H), 5.94 (dd, J = 17.4, 11.0 Hz, 1H), 5.15 – 5.01 (m, 2H), 4.46 – 4.35 (m, 1H), 4.35 – 4.25 (m, 1H), 2.01 (dt, J = 14.5, 7.2 Hz, 1H), 1.84 (dt, J = 14.1, 6.7 Hz, 1H), 1.36 (s, 3H), 1.08 (s, 6H). ^{13}C NMR (151 MHz, $CDCl_3$) δ 153.2, 148.3, 143.6, 138.8, 137.2, 134.9, 125.5, 119.9, 114.2, 113.2, 109.8, 67.3, 62.7, 45.5, 34.6, 22.4, 17.7.

*Synthesis of compound **6***. A round-bottom flask was charged with compound **5** (40 mg, 100 µmol), D-cysteine hydrochloride monohydrate (28 mg, 160 µmol), and K_2CO_3 (26 mg, 190 µmol), and the atmosphere was replaced with N_2 by three evacuation/refill cycles. 1.65 mL of deoxygenated 5:5:2 DCM:MeOH:H_2O were added, and the reaction mixture was stirred overnight under N_2. The reaction was quenched with 420 µL of 1 M HCl, then diluted with H_2O (10 mL) and extracted with DCM (4 x 15 mL). The combined organic layers were washed with brine and dried over Na_2SO_4, and the solvent was removed under reduced pressure to yield compound **6** as a light-yellow powder (57 mg, 100%); mixture of diastereomers. ^{1}H NMR (600 MHz, $CDCl_3$) δ 8.17 (s, 1H), 7.96 (d, J = 8.9 Hz, 1H), 7.75 (br s, 1H), 7.31 (dd, J = 8.9, 2.2 Hz, 1H), 5.92 (dd, J = 17.5, 10.8 Hz, 1H), 5.43 (t, J = 9.4 Hz, 1H), 5.15 – 4.96 (m, 2H), 4.44 – 4.18 (m, 2H), 3.76 (dt, J = 27.9, 11.1 Hz, 2H), 1.97 (dt, J = 14.4, 7.2 Hz, 1H), 1.81 (dt, J = 14.0, 6.8 Hz, 1H), 1.33 (s, 3H), 1.06 (d, J = 2.5 Hz, 6H). ^{13}C NMR (600 MHz, $CDCl_3$) δ 173.4, 167.4, 159.0 149.3, 143.8, 143.6, 137.5, 124.9, 119.1, 114.2, 114.0, 110.6, 78.0, 67.3, 59.6, 45.5, 35.2, 34.6, 22.5, 22.4, 22.3, 22.3, 17.9, 17.7.

Synthesis of FA-Luc-1. A stock solution of thiophenol and triethylamine in acetonitrile was prepared by adding 0.48 mL thiophenol and 0.8 mL triethylamine to a 10 mL volumetric flask and diluting to 10 mL with acetonitrile. $SnCl_2$ (36 mg, 190 µmol) was added to a 20-dram vial, then 1.25 mL of the thiophenol/triethylamine stock were added and the reaction mixture was stirred for 5 min. Compound **6** (25 mg, 52 µmol) was dissolved in 1 mL MeCN and added to the $SnCl_2$/thiophenol/triethylamine reaction mixture, and the reaction mixture was stirred for 2 h at which point the solvent was removed under reduced pressure. Purification by reverse-phase silica column (10→80% MeOH in H_2O) afforded FA-Luc-1 as a light-yellow powder (3.2 mg, 13%); mixture of diastereomers. ^{1}H NMR (400 MHz, CD_3OD) δ 8.29 (d, *J* = 2.2 Hz, 1H), 7.97 (d, *J* = 9.0 Hz, 1H), 7.54 (dd, *J* = 9.0, 2.2 Hz, 1H), 6.09 – 5.97 (m, 1H), 5.49 (s, 1H), 5.34 (t, *J* = 9.0 Hz, 1H), 5.15 – 5.06 (m, 2H), 4.40 – 4.25 (m, 2H), 3.76 (d, *J* = 9.9 Hz, 2H), 2.06 – 1.86 (m, 2H), 1.42 (s, 3H), 1.11 (d, *J* = 2.2 Hz, 6H). LRMS calcd. for $C_{21}H_{27}N_4O_4S_2$ (M+H) 463.15, found 463.1.

4.2.3. Cell culture

HEK293T cells were maintained in exponential growth as a monolayer in Dulbecco's Modified Eagle Medium, high glucose, (DMEM, Invitrogen) supplemented with glutamax (Gibco), 10% fetal bovine serum (FBS, Hyclone) and 1% non-essential amino acids (NEAA, Gibco), and incubated at 37 °C in 5% CO_2. One day before FA addition experiments, the cells were passaged and plated in DMEM with glutamax (phenol red-free) supplemented with 10% FBS on poly-d-lysine-coated 4-well Lab Tek borosilicate chambered coverglass slides (Nunc) at 1.8×10^5 per well and allowed to grow to 65% confluence before FA addition experiments.

4.2.4. FA addition in HEK293T cells

One day before FA addition experiments, HEK293T cells were passaged and plated on poly-L-lysine-coated 8-well Lab Tek borosilicate chambered coverglass slides and allowed to grow to between 70 and 80% confluence. The DMEM media was aspirated from the chambers and replaced with 300 µL BSS (136.9 mM NaCl, 5.37 mM KCl, 1.26 mM $CaCl_2$, 0.81 mM $MgSO_4$, 0.44 mM KH_2PO_4, 0.335 mM Na_2HPO_4, 10 mM PIPES; pH to 7.2 with NaOH) containing 0 or 1000 µM FA and incubated at 37 °C for 30 minutes. The buffer was then replaced with 500 µL fresh DMEM (supplemented with 10% FBS and glutamax) containing no probe, 1 µM puromycin, or 1 µM Puro-FA-1, and the cells were incubated at 37 °C for 3 h. The media was aspirated from the chambers and replaced with fresh PBS, then incubated for 5 min at 37 °C. This wash step was repeated another time, then the cells were fixed by treating with MeOH at -20 °C for 10 min. The chambers were washed twice with PBS, then permeabilized with PBS containing 0.1% Triton X-100 for 10 min. Cells were blocked with 5% donkey serum in PBS containing 0.1% Triton X-100 for 1 h at 37 °C, then washed with PBS and PBS containing 0.1% Triton X-100. Cells were stained with Kerafast anti-puromycin antibody (3RH11; 1:500 in PBS containing 0.1% Triton X-100 and 10% FBS) for 1 h at 37 °C, then washed with PBS and PBS containing 0.1% Triton X-100. Cells were stained with ThermoFisher donkey anti-mouse secondary antibody AlexaFluor 488 (R37114; 1:100 in PBS containing 0.1% Triton X-100 and 10% FBS) for 1 h at 37 °C, then washed with PBS containing 0.1% Triton X-100 and PBS and stored in PBS at 4 °C until the time of imaging (< 24 hours).

Confocal fluorescence imaging studies were performed with a Zeiss laser scanning microscope 710 with a 20x objective lens using Zen 2009 software (Carl Zeiss). Donkey anti-Mouse IgG Secondary Antibody, Alexa Fluor 488 was excited using 488 nm argon laser, and emission was collected using a META detector between 493 to 600 nm. PBS was used as the imaging buffer. Image analysis and quantification was performed using ImageJ (National Institutes of Health). For quantification of fluorescence intensity, four fields of cells within the same well were imaged. A region of interest (ROI) was created around each cell in each image. The mean fluorescence intensity of each cell was measured (using "Measure" function) and averaged across the four fields imaged. For each condition, multiple wells were analyzed using this process, and the fluorescence intensities were averaged across independent experiments. Statistical analysis was performed using two-tailed student's t-test.

4.2.5. In vitro *luminescence assays*

Millipore water was used to prepare concentrated aqueous stock solutions (20x) of FA. Incubation of FA at varying concentrations (20x dilution of the concentrated aqueous stock, final concentrations of 0 – 100 µM and 1 mM) was performed in PBS with 5 µM of FA-Luc-1 (100x dilution of a 500 µM stock in DMSO). Similar experiments were performed with 1 µM of the parent aminoluciferin (100x dilution of a 100 µM stock in DMSO) to determine any effects of the

FA treatments on luciferase activity. At the end of the incubation period, 50 μL each of the solution was transferred to a well of a white, opaque 96-well plate (Corning). An equal volume (50 μL) of a solution of luciferase (100 μg/mL, Promega) in 50 mM Tris buffer at pH 7.4, with 10 mM Mg^{2+} ($MgCl_2$), 0.1 mM Zn^{2+} ($ZnCl_2$) and 2 mM ATP was added and mixed well. Bioluminescent signals were measured using a Synergy Mx plate reader at 37°C for 30 min. The integrated photon flux was determined by taking the area under the curve of a plot of relative photon flux versus time of the bioluminescent signal acquisition.

4.3. Results and Discussion

4.3.1. Design and synthesis of Puro-FA-1

To design a FA probe whose readout would be compatible with whole-animal studies, one possible approach is to render an immunogenic compound FA responsive. To do so, we decided to cage puromycin, an aminonucleoside that becomes incorporated into nascent polypeptide chains[3] and can be detected with puromycin-specific antibodies,[4] using a modified version of our recently-developed generalizable 2-aza-Cope-based FA trigger.[5] A similar approach has been used previously by the Renslo lab for Fe^{2+} detection.[6] In our strategy, the α-amino group of puromycin, which is required for incorporation into peptides, is caged as a carbamate and thus rendered unreactive toward ribosomal peptide synthesis. Condensation with FA and subsequent 2-aza-Cope rearrangement and hydrolysis reveals a β-(carbamoyloxy)ketone which can undergo β-elimination and CO_2 extrusion to reveal free puromycin (Figure 4.1). FA-caged puromycin (Puro-FA-1) was synthesized in 5 steps from 4-hydroxybutan-2-one and puromycin (Scheme 4.1). Briefly, aminoallylation of 4-hydroxybutan-2-one provides homoallylamine **1**, which is protected as the azide **2** via diazotransfer from the Goddard-Borger reagent.[2] Preactivation as 4-nitrophenyl carbonate **3** followed by reaction with puromycin affords the azide-protected probe **4**, which can be reduced to the free amine by tris(2-carboxyethyl)phosphine (TCEP) to afford Puro-FA-1.

4.3.2. Detection of exogenous FA in cellulo *with Puro-FA-1*

To evaluate the ability of Puro-FA-1 to respond to FA in mammalian cells, we used immunofluorescence to compare the extent of puromycin incorporation from Puro-FA-1 in HEK293T cells pretreated with either FA or vehicle control. In these experiments, we compared puromycin incorporation from Puro-FA-1 to incorporation from free puromycin to normalize for changes in protein synthesis rates that may result from changes in FA levels. Gratifyingly, we observed a significant increase in puromycin incorporation from Puro-FA-1 in HEK293T cells pretreated with 1 mM FA relative to those pretreated with vehicle (Figure 4.2). Importantly, there was no increase in puromycin incorporation for HEK293T cells pretreated with 1 mM FA relative to those pretreated with vehicle when cells are treated with free puromycin, indicating that the increase in puromycin incorporation from Puro-FA-1 in FA-treated cells is indeed from 2-aza-Cope-induced uncaging. These results demonstrate the utility of the immunohistochemical readout for FA detection in living samples, and the flexibility of the antibody-based detection system will allow for facile tuning of the imaging modality since the secondary antibody can be conjugated to a variety of reporters (e.g. radiolabels, enzymes, nanoparticles). The irreversible nature of puromycin incorporation into biological samples also prevents time-dependent losses in signal, allowing for less-stringent imaging conditions than traditional real-time reporters.

4.3.3. Design and synthesis of FA-Luc-1

An alternative approach to *in vivo* imaging is through the use of bioluminescence produced by the firefly enzyme luciferase. Bioluminescence is an attractive modality for *in vivo* imaging because it allows for greater tissue penetration than traditional fluorescence-based methods which require incident light to generate a signal.[7-9] Since luciferase isn't a native enzyme in mammalian systems and requires no excitation light, there is essentially no background signal. Moreover, because luciferase is genetically encodable, it allows for an additional layer of spatial resolution within biological samples since expression can be targeted to certain populations of cells.[10-11] In addition to these technical benefits, bioluminescence imaging experiments don't require animals to be sacrificed, which enables real-time imaging and allows the tracking of analytes of interest throughout the lifespan of a single animal, allowing each animal to be its own control and greatly enhancing signal-to-noise.

To render the luciferin-luciferase system responsive to an analyte of interest, a common approach is to cage the luciferin substrate with a chemical trigger which releases free luciferin upon reaction with the analyte of interest.[12-18] We decided to take a similar approach, caging aminoluciferin with a modified version of our newly-developed generalizable 2-aza-Cope-based FA trigger (Figure 4.3).[5] As for Puro-FA-1, FA-Luc-1 undergoes condensation with FA and subsequent 2-aza-Cope rearrangement and hydrolysis reveals a β-(carbamoyloxy)ketone which can undergo β-elimination and CO_2 extrusion to reveal free aminoluciferin. Free aminoluciferin can then be recognized as a substrate by luciferase and undergo oxidation to generate photons via bioluminescence that can be detected to read out FA levels. FA-Luc-1 was synthesized in 3 steps from 6-amino-2-cyanobenzothiazole and compound **2** (Scheme 4.2). Briefly, 6-amino-2-cyanobenzothiazole was activated as the isocyanate by reaction with triphosgene, followed by nucleophilic trapping with compound **2** to give carbamate **5**. Condensation with D-cysteine forms the dihydrothiazole of the aminoluciferin core, and reduction by a nucleophilic $SnCl_2$ complex furnishes FA-Luc-1.

4.3.4. In vitro *evaluation of FA-Luc-1*

With FA-Luc-1 in-hand, we tested its FA responsiveness *in vitro* using a luciferase luminescence assay. As a control for potential effects of FA on luciferase activity, we performed the same assay using the parent aminoluciferin. The luminescent response of FA-Luc-1 to varied FA concentrations (0 to 100 μM), as well as for aminoluciferin, is depicted in Figure 4.4. Gratifyingly, FA-Luc-1 shows good responsiveness to FA, with ca. 2.7-fold turn-on to 100 μM FA after 2 h. Importantly, incubation with 0 to 100 μM FA does not appreciably interfere with luciferase luminescent signal for the aminoluciferin control. We did observe a decrease in luminescence intensity at high concentrations of FA (1 mM; data not shown), so caution should be taken in interpreting results when similar concentrations of FA are expected (e.g. intratumorally).[19-20] Overall, these results presage the utility of FA-Luc-1 for monitoring FA fluxes in living animals.

4.4. Conclusion

This work showcases the versatility of the 2-aza-Cope platform for investigating the roles of biological FA by extending it to two new modalities: immunohistochemistry and bioluminescence. Future efforts will focus on applying Puro-FA-1 and FA-Luc-1 to whole-animal studies; in particular, we are interested in investigating a diabetes disease model. Semicarbazide-sensitive amine oxidase (SSAO), as well as its substrate methylamine, are known to be elevated in diabetes and contribute to the formation of FA.[21] We will apply these *in vivo* probes to study FA

in transgenic mice with diabetes, hopefully affording insights into this understudied component of diabetes pathology. Both Puro-FA-1 and FA-Luc-1 operate through a 2-aza-Cope/hydrolysis/β-elimination sequence, releasing an amine-tethered payload through CO_2 extrusion from an unmasked carbamic acid. Beyond these two probes, this work demonstrates the feasibility of caging virtually any amino group with a FA-responsive trigger, opening up many possible avenues for future development of FA imaging probes.

Figures

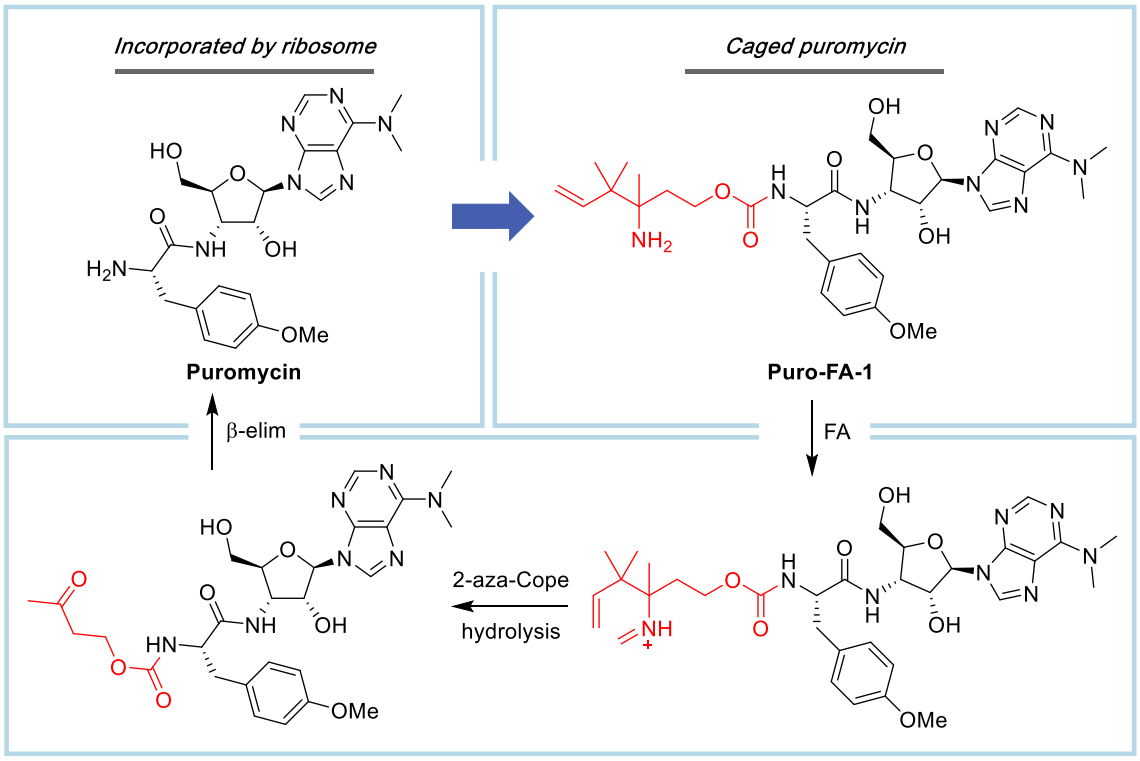

Figure 4.1. Design strategy for a FA-caged puromycin (Puro-FA-1).

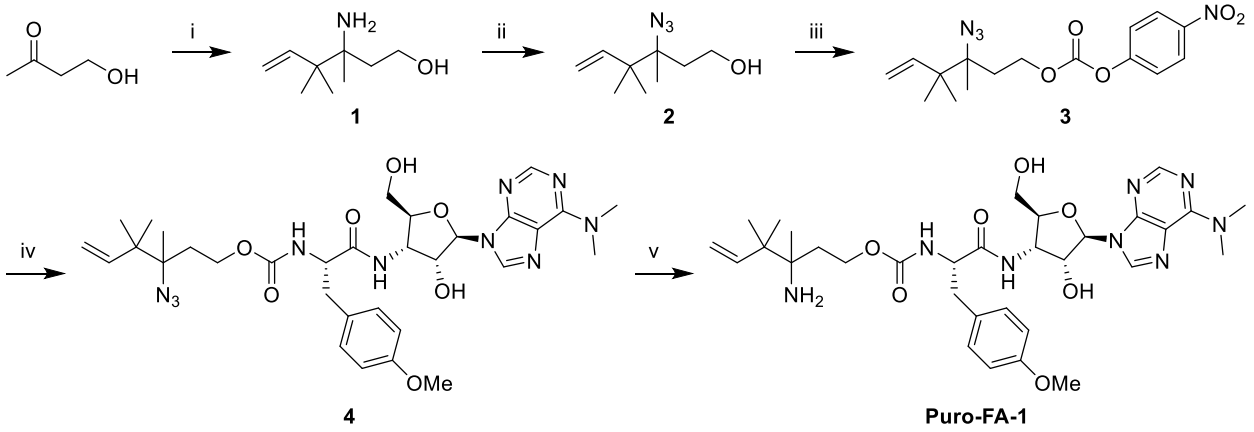

Scheme 4.1. Synthesis of Puro-FA-1. Reagents and conditions: (i) NH_3, MeOH, 0 °C, then prenylboronic acid, rt, 12 h; (ii) imidazole-1-sulfonyl azide hydrochloride, $CuSO_4 \cdot 5H_2O$, K_2CO_3, rt, 12 h; (iii) 4-nitrophenyl chloroformate, triethylamine DCM, rt, 12 h; (iv) puromycin dihydrochloride, 4-dimethylaminopyridine, *N*,*N*-diisopropylethylamine, DMF, rt, 12 h; (v) tris(2-carboxyethyl)phosphine hydrochloride, 3:2:1 MeOH:H_2O:triethylamine, rt, 12 h.

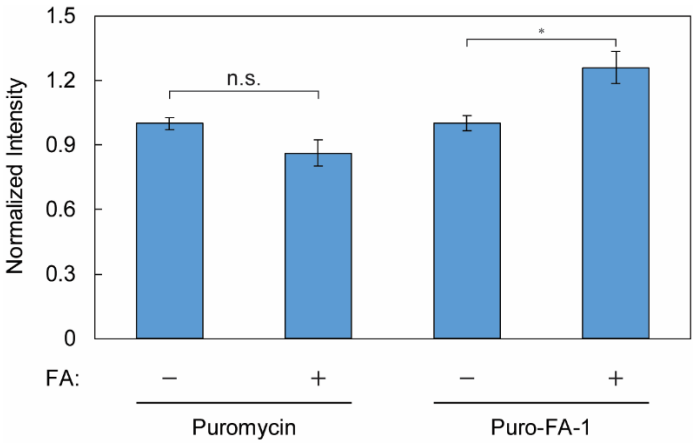

Figure 4.2. Puromycin incorporation in HEK293T cells treated with 1000 µM FA or vehicle control. Intensities are normalized to vehicle control for each probe. * $P < 0.05$; n =3. Error bars represent ± SEM.

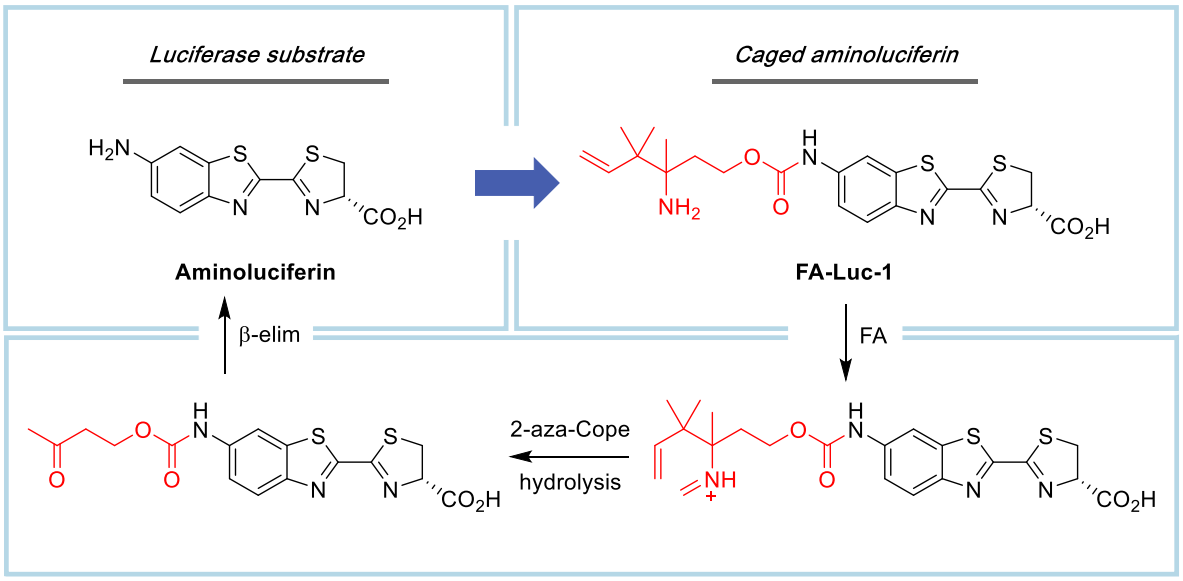

Figure 4.3. Design of FA-responsive caged aminoluciferin FA-Luc-1.

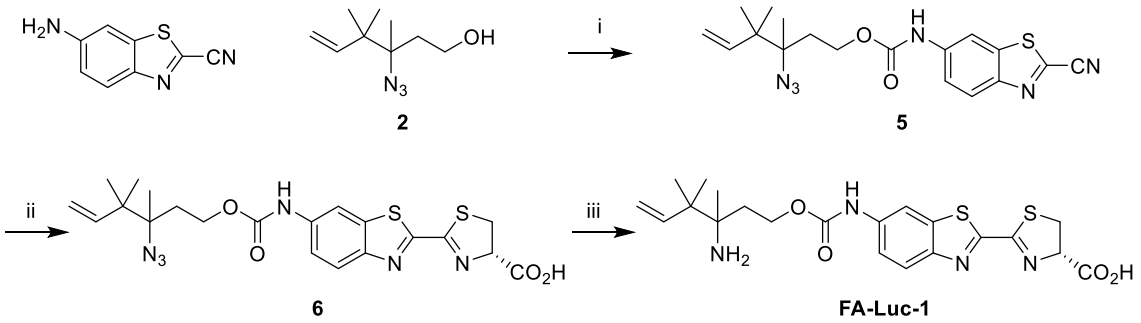

Scheme 4.2. Synthesis of FA-Luc-1. Reagents and conditions: (i) triphosgene, 4-dimethylaminopyridine, toluene, reflux, 3 h, then compound **2** and 4-dimethylaminopyridine, rt, 12 h; (ii) D-cysteine hydrochloride monohydrate, K_2CO_3, 5:5:2 DCM:MeOH:H_2O, rt, overnight; (iii) $SnCl_2$, thiophenol, triethylamine, MeCN, rt, 2 h.

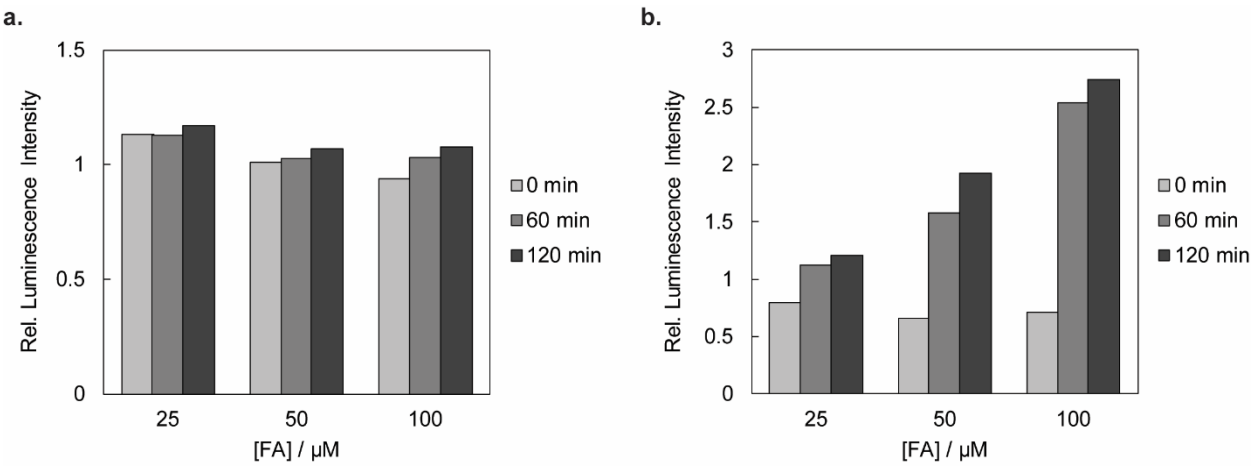

Figure 4.4. Luminescent response of (a) aminoluciferin and (b) FA-Luc-1 to FA *in vitro*. Relative luminescence intensity is reported as the total photon flux at a particular concentration of FA and time divided by the total photon flux of 0 µM FA at the same timepoint; n = 1.

4.5. References

1. Raducan, M.; Alam, R.; Szabó, K. J. *Angew. Chem. Int. Ed.* **2012,** *51*.
2. Goddard-Borger, E. D.; Stick, R. V. *Org. Lett.* **2007,** *9*, 3797-3800.
3. Nathans, D. *Proc. Natl. Acad. Sci. USA* **1964,** *51*, 585-592.
4. Eggers, D. K.; Welch, W. J.; Hansen, W. J. *Mol. Biol. Cell* **1997,** *8*, 1559-1573.
5. Bruemmer, K. J.; Walvoord, R. R.; Brewer, T. F.; Burgos-Barragan, G.; Wit, N.; Pontel, L. B.; Patel, K. J.; Chang, C. J. *J. Am. Chem. Soc.* **2017**, DOI: 10.1021/jacs.6b12460.
6. Spangler, B.; Morgan, C. W.; Fontaine, S. D.; Vander Wal, M. N.; Chang, C. J.; Wells, J. A.; Renslo, A. R. *Nat. Chem. Biol.* **2016,** *12*, 680-685.
7. Baker, M. *Nature* **2010,** *463*, 977-980.
8. Paley, M. A.; Prescher, J. A. *Med. Chem. Commun.* **2014,** *5*, 255-267.
9. Prescher, J. A.; Contag, C. H. *Curr. Opin. Chem. Biol.* **2010,** *14*, 80-89.
10. Kircher, M. F.; Gambhir, S. S.; Grimm, J. *Nat. Rev. Clin. Oncol.* **2011,** *8*, 677-688.
11. O'Neill, K.; Lyons, S. K.; Gallagher, W. M.; Curran, K. M.; Byrne, A. T. *J. Pathol.* **2009,** *220*, 317-327.
12. Van de Bittner, G. C.; Bertozzi, C. R.; Chang, C. J. *J. Am. Chem. Soc.* **2013,** *135*, 1783-1795.
13. Van de Bittner, G. C.; Dubikovskaya, E. A.; Bertozzi, C. R.; Chang, C. J. *Proc. Natl. Acad. Sci. USA* **2010,** *107*, 21316-21321.
14. Godina, A.; Park, H. M.; Miller, S. C.; Cheng, K.; Hanahan, D.; Sanman, L. E.; Bogyo, M.; Yu, A.; Nikitin, G. F.; Stahl, A.; Dubikovskaya, E. A. *ACS Chem. Biol.* **2013,** *8*, 987-999.
15. Sellmyer, M. A.; Bronsart, L.; Imoto, H.; Contag, C. H.; Wandless, T. J.; Prescher, J. A. *Proc. Natl. Acad. Sci. USA* **2013,** *110*, 8567-8572.
16. Porterfield, W. B.; Jones, K. A.; McCutcheon, D. C.; Prescher, J. A. *J. Am. Chem. Soc.* **2015,** *137*, 8656-8659.
17. Mofford, D. M.; Adams, S. T.; Reddy, G. S.; Reddy, G. R.; Miller, S. C. *J. Am. Chem. Soc.* **2015,** *137*, 8684-8687.
18. Heffern, M. C.; Park, H. M.; Au-Yeung, H. Y.; Van de Bittner, G. C.; Ackerman, C. M.; Stahl, A.; Chang, C. J. *Proc. Natl. Acad. Sci. USA* **2016,** *113*, 14219-14224.
19. Matsunami, H.; Tong, Z.; Luo, W.; Wang, Y.; Yang, F.; Han, Y.; Li, H.; Luo, H.; Duan, B.; Xu, T.; Maoying, Q.; Tan, H.; Wang, J.; Zhao, H.; Liu, F.; Wan, Y. *PLoS ONE* **2010,** *5*, e10234.
20. Mei, L.; Liu, J.; Liu, F.-Y.; Tong, Z.-Q.; Li, Z.-H.; Chen, W.; Luo, W.-H.; Li, H.; Luo, H.-J.; Tang, Y.; Tang, J.-M.; Cai, J.; Liao, F.-F.; Wan, Y. *PLoS ONE* **2013,** *8*, e58957.
21. Obata, T. *Life Sci.* **2006,** *79*, 417-422.

Appendix 1

Preparation and evaluation of cell-trappable superoxide probes

Portions of this work were performed in collaboration with the following persons:

Compounds **27a**, **27b**, **27c**, **28a**, **28b**, and **28c** were synthesized by Jaeho Paek. Portions of some imaging experiments were done in collaboration with Mark N. Vander Wal.

A1.1. Synopsis

Superoxide ($O_2^{\bullet -}$) has been implicated as a biological signaling molecule in diverse cellular processes such as mitogenic growth, apoptosis, and cardiovascular homeostasis, among many others.[1-4] One widely-used method for detecting superoxide in live systems relies on the fluorescent probe dihydroethidium (DHE) and its derivatives, which undergo a superoxide-specific reaction to produce a highly fluorescent product detectable by conventional fluorescence microscopy or other analytical methods such as HPLC.[5-8] Despite its widespread use, there are significant technical challenges that limit the utility of DHE.[4, 9] We have developed a new, efficient synthetic route to access and functionalize DHE to rapidly screen new derivatives for desired properties. This appendix presents the development of DHE derivatives with altered subcellular localization and cellular trappability, important parameters in developing useful fluorescent probes.

A1.2. Methods

A1.2.1. General synthetic methods

All reactions utilizing air- or moisture-sensitive reagents were performed in dried glassware under an atmosphere of dry N_2. When dry solvent was used, the solvent was passed over activated alumina. Other reagents were used without further purification. Silica gel P60 (SiliCycle) was used for column chromatography and SiliCycle 60 F254 silica gel (precoated sheets, 0.25 mm thick) was used for analytical thin layer chromatography and visualized by fluorescence quenching under UV light. 2-bromo-5-nitroaniline was purchased from AK Scientific (Union City, CA); all other reagents were purchased from Sigma-Aldrich (St. Louis, MO). ^{1}H NMR and ^{13}C NMR spectra were collected in $CDCl_3$, $(CD_3)_2CO$, or $(CD_3)_2SO$ (Cambridge Isotope Laboratories, Cambridge, MA) at 25 °C on Bruker AV-300, AVB-400, AVQ-400, AV-500 and AV-600 with ^{13}C operating frequencies of 75 Mhz, 101 MHz, 126 Mhz and 150 MHz, respectively, at the College of Chemistry NMR Facility at the University of California, Berkeley. All chemical shifts are reported in the standard δ notation of parts per million relative to residual solvent peak at 7.26 ($CDCl_3$), 2.05 ($(CD_3)_2CO$), or 2.50 ($(CD_3)_2SO$) for ^{1}H and 77.16 ($CDCl_3$), 29.84 ($(CD_3)_2CO$), or 39.52 ($(CD_3)_2SO$) for ^{13}C as an internal reference. Splitting patterns are indicated as follows: br, broad; s, singlet; d, doublet; t, triplet; q, quartet; m, multiplet; dd, doublet of doublets; dt, doublet of triplets; td, triplet of doublets; qd, quartet of doublets; ddd, doublet of doublet of doublets; dtd, doublet of triplet of doublets. Low-resolution electrospray mass spectral analyses were carried out using a LC-MS (Agilent Technology 6130, Quadrupole LC/MS). High resolution mass spectral analyses (ESI-MS) were carried out at the College of Chemistry Mass Spectrometry Facility at the University of California, Berkeley.

A1.2.2. Synthesis

General method I for nitro group reduction.

A round-bottom flask is charged with nitro compound (1 equiv.) and Pd/C (1 equiv.), then dry EtOAc is added. The flask is sparged with H_2 (balloon) for 5 min, then placed under H_2 (balloon) overnight. The reaction mixture is filtered through celite, evaporated to dryness, and purified by silica column chromatography or preparatory TLC to afford desired amino compound.

General method II for nitro group reduction.

A 20-dram vial was charged with nitro compound (1 equiv.), Zn powder (20 equiv.), and NH_4Cl (20 equiv.), then 1:1 MeOH:THF was added and the vial was capped. The reaction mixture was stirred overnight then filtered through celite and evaporated to dryness. Purification by silica column chromatography or preparatory TLC afforded desired amino compound.

General method III for amide coupling.

A round-bottom flask was charged with carboxylic acid compound (1 equiv.) and HATU (2.2 equiv.), then dry DMF, DIPEA (5 equiv.), and amine compound (2 equiv.) were added. The reaction mixture was stirred overnight then diluted with EtOAc and washed sequentially with sat. NH_4Cl, sat. $NaHCO_3$, and brine. The organic layer was dried over anhydrous $MgSO_4$ then evaporated to dryness under reduced pressure. Purification by silica column chromatography afforded desired amide compound.

Synthesis of *N*-(2-bromo-5-nitrophenyl)benzamide (1)

To a solution of 2-bromo-5-nitroaniline (20 g, 92 mmol) and K_2CO_3 (25.5 g, 184 mmol) in 240 mL THF was added benzoyl chloride (14.8 mL, 128 mmol). The reaction mixture was stirred overnight, then poured into 1.4 L H_2O and stirred for 30 min to hydrolyze excess benzoyl chloride. The aqueous solution was extracted with DCM (3 x 500 mL), and the combined organic layers were washed sequentially with 1 M HCl (1 x 1 L) and brine (1 x 1 L), then dried over anhydrous $MgSO_4$ and concentrated under reduced pressure. Purification by recrystallization from toluene (320 mL) afforded **1** as a yellow solid (22.2 g, 100% yield). ^{1}H NMR (300 MHz, $CDCl_3$) δ 9.51 (d, J = 2.7 Hz, 1H), 8.59 (s, 1H), 8.00 – 7.93 (m, 2H), 7.90 (dd, J = 8.8, 2.7 Hz, 1H), 7.78 (d, J = 8.8 Hz, 1H), 7.69 – 7.52 (m, 3H).

Synthesis of *N*-(4,4'-dinitro-[1,1'-biphenyl]-2-yl)benzamide (2)

A round-bottom flask was charged with compound **1** (5 g, 21 mmol), 4-nitrophenylboronic acid pinacol ester (5.2 g, 21 mmol), KOAc (41 g, 42 mmol), and Pd(dppf) (0.86 g, 1 mmol), then the atmosphere was replaced with N_2 by 5 evacuation/refill cycles. Deoxygenated 4:1 dioxane:H_2O (110 mL) was added, and the reaction mixture was heated at reflux overnight. The reaction mixture was partitioned between H_2O (500 mL) and DCM (500 mL), then the aqueous layer was further extracted with DCM (5 x 200 mL). The combined organic layers were washed with brine (1 x 1 L), dried over anhydrous $MgSO_4$, filtered, and concentrated under reduced pressure. The residue was run through a short plug of silica gel (eluent 100% EtOAc) with copious amounts of washing, the filtrate was evaporated to dryness, then recrystallization from glacial acetic acid afforded **2** as a yellow solid (4.5 g, 58% yield). ^{1}H NMR (400 MHz, $CDCl_3$) δ 9.35 (d, *J* = 2.3 Hz, 1H), 8.43 (d, *J* = 8.7 Hz, 2H), 8.14 (dd, *J* = 8.5, 2.3 Hz, 1H), 7.82 (s, 1H), 7.68 (d, *J* = 8.7 Hz, 2H), 7.63 (d, *J* = 7.3 Hz, 2H), 7.57 (t, *J* = 7.3 Hz, 1H), 7.51 – 7.43 (m, 3H).

Synthesis of 3,8-dinitro-6-phenylphenanthridine (3)

A round-bottom flask was charged with compound **2** (6.2 g, 17 mmol), then nitrobenzene (26 mL) and $POCl_3$ (3 mL, 32 mmol) were added and the reaction mixture was heated at reflux for 24 hours. Excess $POCl_3$ was carefully quenched by slow addition of the reaction mixture to ice-cold 2M NaOH (200 mL) followed by vigorous stirring for 1 hour. The aqueous layer was extracted with DCM (3 x 150 mL), then the combined organic layers were washed with brine (1 x 400 mL), dried over anhydrous $MgSO_4$, filtered, and concentrated under reduced pressure until all

DCM was removed. The remaining nitrobenzene solution of the crude material was allowed to sit overnight, whereupon **3** crystallized out of solution. Crystals of **3** were collected by filtration and washed once with DCM affording **3** as a goldenrod solid (3.7 g, 63% yield). ^{1}H NMR (500 MHz, $CDCl_3$) δ 9.17 (d, *J* = 2.4 Hz, 1H), 9.13 (d, *J* = 2.3 Hz, 1H), 8.92 (d, *J* = 9.0 Hz, 1H), 8.81 (d, *J* = 9.0 Hz, 1H), 8.75 (dd, *J* = 9.0, 2.3 Hz, 1H), 8.56 (dd, *J* = 9.0, 2.4 Hz, 1H), 7.82 – 7.76 (m, 2H), 7.70 – 7.64 (m, 3H).

Synthesis of 3,8-dinitro-6-phenyl-5,6-dihydrophenanthridine (4)

An Erlenmeyer flask was charged with compound **3** (150 mg, 0.43 mmol), then glacial acetic acid (5.2 mL) was added and the reaction mixture was cooled to 17 °C (just above the freezing point of AcOH). $NaBH_4$ was added portion-wise with vigorous stirring until complete consumption of compound **3** was observed by TLC (25% EtOAc/hexanes mobile phase). The reaction mixture was carefully poured into 75 mL H_2O, extracted with DCM (3 x 50 mL), then the combined organic layers were washed with brine (1 x 150 mL), dried over anhydrous $MgSO_4$, filtered, and concentrated under reduced pressure. The crude material was run through a plug of silica gel (100% DCM eluent) to afford **4** as a red solid (150 mg, 99% yield). ^{1}H NMR (300 MHz, $CDCl_3$) δ 8.19 (dd, *J* = 8.6, 2.4 Hz, 1H), 7.92 (d, *J* = 8.7 Hz, 1H), 7.86 (d, *J* = 8.6 Hz, 1H), 7.72 (d, *J* = 2.3 Hz, 1H), 7.67 (dd, *J* = 8.5, 2.2 Hz, 1H), 7.50 (d, *J* = 2.3 Hz, 1H), 7.40 – 7.31 (m, 5H), 5.71 (s, 1H).

Synthesis of methyl 3-(3,8-dinitro-6-phenylphenanthridin-5(6H)-yl)propanoate (5)

Compound **4** (0.145 g, 0.42 mmol) was suspended in methyl acrylate (1 mL), and conc. H_2SO_4 (0.5 mL) was carefully added. The reaction mixture was heated at 80 °C for 15 min, then poured into 60 mL ice-cold H_2O and the resulting precipitate was collected by filtration. Purification by silica column chromatography (50→90% DCM in hexanes) afforded **5** as a red solid (40 mg, 22% yield). ^{1}H NMR (300 MHz, $CDCl_3$) δ 8.16 (dd, J = 8.8, 2.3 Hz, 1H), 8.03 (d, J = 2.3 Hz, 1H), 7.95 – 7.85 (m, 2H), 7.68 (dd, J = 8.6, 2.1 Hz, 1H), 7.52 (d, J = 2.1 Hz, 1H), 7.28 – 7.19 (m, 3H), 7.20 – 7.13 (m, 2H), 5.80 (s, 1H), 3.74 (dd, J = 7.4, 5.6 Hz, 2H), 3.62 (s, 3H), 2.74 (dt, J = 16.4, 7.3 Hz, 1H), 2.57 (dt, J = 16.8, 5.5 Hz, 1H).

Synthesis of methyl 3-(3,8-diamino-6-phenylphenanthridin-5(6H)-yl)propanoate (6)

Compound **5** (40 mg, 92 µmol) was reduced following general method II and purified by preparatory TLC (10% MeOH in DCM) to afford compound **6** (18 mg, 46% yield). ^{1}H NMR (300 MHz, $CDCl_3$) δ 7.52 – 7.42 (m, 2H), 7.18 (qd, J = 4.9, 2.5 Hz, 5H), 6.65 – 6.52 (m, 1H), 6.38 (t, J = 1.6 Hz, 1H), 6.18 (dd, J = 8.2, 1.8 Hz, 1H), 6.00 (d, J = 1.8 Hz, 1H), 5.35 (s, 1H), 3.62 (d, J = 1.2 Hz, 3H), 3.56 (t, J = 7.1 Hz, 2H), 2.66 (dt, J = 15.5, 7.6 Hz, 1H), 2.57 – 2.40 (m, 1H).

Synthesis of 3-(3,8-dinitro-6-phenylphenanthridin-5(6H)-yl)propanoic acid (7)

Compound **4** (1.26 g, 3.6 mmol) was suspended in acrylic acid (10 mL), and conc. H_2SO_4 (5 mL) was carefully added while maintaining the temperature at 25 °C. The reaction mixture was stirred for 90 min under N_2, then diluted into 500 mL ice-cooled H_2O with the immediate formation of a red precipitate. The precipitate was filtered and washed with H_2O, then purified by silica column chromatography (100% DCM until first two UV-active compounds elute, then 0→40% EtOAc/DCM) to afford compound **7** as a bright red solid (1.14 g, 75% yield). ^{1}H NMR (400 MHz, $(CD_3)_2CO$) δ 8.24 (s, 1H), 8.18 (d, *J* = 1.4 Hz, 2H), 8.15 (d, *J* = 8.6 Hz, 1H), 7.73 (d, *J* = 2.2 Hz,

1H), 7.64 (dd, *J* = 8.6, 2.3 Hz, 1H), 7.37 (dd, *J* = 7.8, 1.8 Hz, 2H), 7.31 – 7.22 (m, 3H), 6.17 (s, 1H), 4.06 – 3.95 (m, 1H), 3.82 (dt, *J* = 14.9, 7.4 Hz, 1H), 2.91 – 2.79 (m, 1H), 2.79 – 2.68 (m, 1H).

Synthesis of compound 8a.

Compound **7** (250 mg, 0.6 mmol) was coupled with di-*tert*-butyl iminodiacetate following general method III to afford compound **8a** (385 mg, 100% yield), which was used without further purification. ^{1}H NMR (600 MHz, $CDCl_3$) δ 8.07 (dd, J = 8.7, 2.4 Hz, 1H), 8.00 (d, J = 2.3 Hz, 1H), 7.85 (d, J = 1.8 Hz, 1H), 7.83 (d, J = 1.6 Hz, 1H), 7.58 (dd, J = 8.6, 2.2 Hz, 1H), 7.46 (d, J = 2.2 Hz, 1H), 7.20 – 7.14 (m, 5H), 5.96 (s, 1H), 3.98 (s, 2H), 3.88 – 3.79 (m, 3H), 3.67 (dt, J = 15.1, 5.0 Hz, 1H), 2.69 (ddd, J = 16.3, 8.9, 5.2 Hz, 1H), 2.51 (dt, J = 16.4, 4.9 Hz, 1H), 1.36 (s, 9H), 1.30 (s, 9H).

Synthesis of compound 8b.

Compound **8a** (385 mg, 0.6 mmol) was dissolved in 1:1 TFA:DCM (60 mL), and the reaction mixture was stirred for 3 h. The solvent was removed under reduced pressure, then the residue was dissolved in DCM (12 mL) and 1/6 of the solution was transferred to a round-bottom flask and evaporated to dryness under reduced pressure. The residue was dissolved in DMF (5 mL), and TEA (0.33 mL, 2.4 mmol) and bromomethyl acetate (0.2 mL, 2 mmol) were added. The reaction mixture was stirred overnight then was diluted with 60 mL EtOAc and washed sequentially with sat. $NaHCO_3$ (2 x 60 mL), sat. NH_4Cl (2 x 60 mL), and brine (2 x 60 mL). The organic layer was dried over anhydrous $MgSO_4$ and evaporated to dryness under reduced pressure to afford compound **8b** (318 mg, 100% yield), which was used without further purification. ^{1}H NMR (300 MHz, $CDCl_3$) δ 8.11 (dd, J = 8.8, 2.5 Hz, 1H), 8.04 – 8.00 (m, 1H), 7.88 (dd, J = 8.7, 3.1 Hz, 2H), 7.62 (dd, J = 8.5, 2.3 Hz, 1H), 7.47 (d, J = 2.3 Hz, 1H), 7.23 – 7.12 (m, 5H), 5.89 (s, 1H), 5.78 – 5.72 (m, 2H), 5.69 – 5.65 (m, 2H), 4.19 – 4.12 (m, 2H), 4.10 – 4.00 (m, 2H), 3.90 – 3.66 (m, 2H), 2.78 – 2.62 (m, 1H), 2.54 (dt, J = 16.5, 5.5 Hz, 1H), 1.99 (s, 6H).

Synthesis of compound 8c.

Compound **7** (30 mg, 70 µmol) was coupled with methyl 6-aminohexanoate hydrochloride following general method III to afford compound **8c** (39 mg, 100% yield), which was used without further purification. ^{1}H NMR (400 MHz, $CDCl_3$) δ 8.14 (dd, J = 8.7, 2.4 Hz, 1H), 8.03 (d, J = 2.3 Hz, 1H), 7.93 – 7.85 (m, 2H), 7.63 (dd, J = 8.6, 2.2 Hz, 1H), 7.52 (d, J = 2.2 Hz, 1H), 7.25 – 7.15 (m, 5H), 5.85 (s, 1H), 5.66 (t, J = 5.8 Hz, 1H), 3.88 (ddd, J = 14.9, 9.3, 5.4 Hz, 1H), 3.71 (dt, J = 15.0, 5.0 Hz, 1H), 3.62 (s, 3H), 3.23 – 3.05 (m, 2H), 2.57 (ddd, J = 14.9, 9.3, 5.4 Hz, 1H), 2.45 (dt, J = 15.2, 5.0 Hz, 1H), 2.19 (t, J = 7.4 Hz, 2H), 1.54 – 1.43 (m, 2H), 1.36 – 1.26 (m, 2H), 1.23 – 1.11 (m, 2H).

Synthesis of compound 9a.

Compound **8b** (34 mg, 50 µmol) was reduced following general method I and purified by silica column chromatography (0→75% EtOAc in DCM) to afford compound **9a** (12 mg, 40% yield). ^{1}H NMR (500 MHz, $CDCl_3$) δ 7.45 (t, J = 8.0 Hz, 2H), 7.22 – 7.13 (m, 5H), 6.58 (dd, J = 8.4, 2.4 Hz, 1H), 6.36 (d, J = 2.4 Hz, 1H), 6.16 (dd, J = 8.1, 2.1 Hz, 1H), 5.96 (d, J = 2.2 Hz, 1H), 5.75 – 5.67 (m, 4H), 5.31 (s, 1H), 4.16 (d, J = 5.2 Hz, 2H), 4.08 – 3.93 (m, 2H), 3.69 – 3.52 (m, 2H), 2.55 (ddd, J = 15.5, 8.6, 6.5 Hz, 1H), 2.45 (ddd, J = 16.2, 8.9, 5.3 Hz, 1H), 2.12 (s, 3H), 2.08 (s, 3H).

Synthesis of compound 9b.

Compound **8c** (39 mg, 70 µmol) was reduced following general method I and purified by silica column chromatography (1→2.5% MeOH in DCM) to afford compound **9b** (10 mg, 29% yield). ^{1}H NMR (400 MHz, $CDCl_3$) δ 7.45 (dd, J = 8.3, 3.2 Hz, 2H), 7.20 – 7.08 (m, 5H), 6.58 (dd, J = 8.4, 2.4 Hz, 1H), 6.37 (d, J = 2.5 Hz, 1H), 6.19 (dd, J = 8.2, 2.2 Hz, 1H), 6.02 (d, J = 2.2 Hz, 1H), 5.71 (t, J = 5.7 Hz, 1H), 5.24 (s, 1H), 3.66 (s, 3H), 3.61 – 3.53 (m, 2H), 3.17 – 3.07 (m, 1H), 3.04 – 2.94 (m, 1H), 2.51 (ddd, J = 14.7, 8.8, 6.0 Hz, 1H), 2.31 (dt, J = 14.5, 5.0 Hz, 1H), 2.21 (t, J = 7.6 Hz, 2H), 1.55 – 1.44 (m, 2H), 1.28 – 1.07 (m, 4H).

Synthesis of compound 10.

Compound **7** (30 mg, 70 µmol) was dissolved in 5 mL dry DMF, then DIPEA (90 µL, 500 µmol) and bromomethyl acetate (28 µL, 290 µmol) were added. The reaction mixture was stirred overnight under N_2, then diluted with 30 mL EtOAc and washed sequentially with sat. $NaHCO_3$ (2 x 30 mL), sat. NH_4Cl (1 x 30 mL), and brine (1 x 30 mL). The organic layer was dried over anhydrous $MgSO_4$ and evaporated to dryness under reduced pressure to afford compound **10** (35 mg, 100% yield) which was used without further purification. ^{1}H NMR (400 MHz, $CDCl_3$) δ 8.21 (dd, J = 8.8, 2.4 Hz, 1H), 8.09 (d, J = 2.4 Hz, 1H), 7.96 (dd, J = 8.7, 5.9 Hz, 2H), 7.74 (dd, J = 8.6, 2.2 Hz, 1H), 7.55 (d, J = 2.2 Hz, 1H), 7.30 – 7.26 (m, 3H), 7.25 – 7.19 (m, 2H), 5.85 (s, 1H), 5.75 (d, J = 5.7 Hz, 1H), 5.70 (d, J = 5.7 Hz, 1H), 3.81 (dd, J = 8.2, 5.7 Hz, 2H), 2.93 – 2.79 (m, 1H), 2.69 (dt, J = 17.2, 5.3 Hz, 1H), 2.09 (s, 3H).

Synthesis of compound 11.

Compound **10** (35 mg, 70 µmol) was reduced following general method I and purified by preparatory TLC (60% EtOAc/hexanes) to afford compound **11** (10 mg, 35% yield). ^{1}H NMR (400 MHz, $CDCl_3$) δ 7.44 (dd, J = 8.3, 3.9 Hz, 2H), 7.22 – 7.12 (m, 5H), 6.57 (dd, J = 8.4, 2.5 Hz, 1H), 6.36 (d, J = 2.4 Hz, 1H), 6.17 (dd, J = 8.2, 2.1 Hz, 1H), 5.97 (d, J = 2.2 Hz, 1H), 5.68 (q, J = 5.7 Hz, 2H), 5.33 (s, 1H), 3.55 (dd, J = 7.5, 6.3 Hz, 2H), 2.71 (dt, J = 16.4, 7.4 Hz, 1H), 2.52 (dt, J = 16.5, 6.3 Hz, 1H), 2.04 (s, 3H).

Synthesis of methyl 4-((2-bromo-5-nitrophenyl)carbamoyl)benzoate (12).

To a solution of 2-bromo-5-nitroaniline (10 g, 46 mmol) and K_2CO_3 (12.8 g, 92 mmol) in 250 mL THF was added methyl 4-(chlorocarbonyl)benzoate (12.8 g, 64 mmol). The reaction mixture was stirred overnight, then poured into 1.5 L H_2O and stirred for 30 min to hydrolyze excess benzoyl chloride, during which time a large amount of precipitate formed. The precipitate was collected by filtration, and purification by recrystallization from EtOAc/toluene afforded compound **12** as a yellow solid (14.8 g, 85% yield). ^{1}H NMR (400 MHz, $CDCl_3$) δ 9.49 (d, J = 2.7 Hz, 1H), 8.59 (s, 1H), 8.29 – 8.19 (m, 2H), 8.08 – 7.97 (m, 2H), 7.92 (dd, J = 8.8, 2.7 Hz, 1H), 7.79 (d, J = 8.8 Hz, 1H), 3.98 (s, 3H).

Synthesis of methyl 4-((4',4-dinitro-[1,1'-biphenyl]-2-yl)carbamoyl)benzoate (13).

A round-bottom flask was charged with compound **12** (3 g, 8 mmol), 4-nitrophenylboronic acid pinacol ester (2 g, 8 mmol), KOAc (1.6 g, 16 mmol), and Pd(dppf) (0.33 g, 0.4 mmol), then the atmosphere was replaced with N_2 by 5 evacuation/refill cycles. Deoxygenated 4:1 dioxane:H_2O (75 mL) was added, and the reaction mixture was heated at reflux overnight. The reaction mixture was partitioned between H_2O (400 mL) and DCM (400 mL), then the aqueous layer was further extracted with DCM (3 x 200 mL). The combined organic layers were washed

with brine (1 x 1 L), dried over anhydrous $MgSO_4$, filtered, and concentrated under reduced pressure. The residue was triturated with EtOAc and the solid was collected by filtration to afford compound **13** as a yellow solid (2.2 g, 65% yield). ^{1}H NMR (400 MHz, $CDCl_3$) δ 9.33 (d, J = 2.3 Hz, 1H), 8.47 – 8.37 (m, 2H), 8.17 (dd, J = 8.4, 2.3 Hz, 1H), 8.14 – 8.09 (m, 2H), 7.81 (s, 1H), 7.71 – 7.65 (m, 4H), 7.53 – 7.47 (m, 1H), 3.94 (s, 3H).

Synthesis of 4-(3,8-dinitrophenanthridin-6-yl)benzoic acid (14).

A round-bottom flask was charged with compound **13** (1.8 g, 4.4 mmol), then nitrobenzene (20 mL) and $POCl_3$ (1.36 mL, 14.6 mmol) were added and the reaction mixture was heated at reflux for 24 hours. Excess $POCl_3$ was carefully quenched by slow addition of the reaction mixture to ice-cold 2M NaOH (200 mL) followed by vigorous stirring for 1 hour, during which time a precipitate formed. The precipitate was collected by filtration, washed with hexanes, and dried to afford compound **14** (1.0 g, 58% yield). ^{1}H NMR (400 MHz, $CDCl_3$) δ 9.18 (d, J = 2.3 Hz, 1H), 9.01 (d, J = 2.2 Hz, 1H), 8.96 (d, J = 9.2 Hz, 1H), 8.84 (d, J = 9.1 Hz, 1H), 8.82 – 8.78 (m, 1H), 8.62 (dd, J = 9.1, 2.4 Hz, 1H), 8.43 (d, J = 8.4 Hz, 2H), 7.96 (d, J = 8.4 Hz, 2H).

Synthesis of 4-(5-methyl-3,8-dinitro-5,6-dihydrophenanthridin-6-yl)benzoic acid (15).

Compound **14** (450 mg, 1.16 mmol) and K_2CO_3 (0.48 g, 3.47 mmol) were suspended in DMF (10 mL), and Me_2SO_4 (1 mL, 10.5 mmol) was added. The reaction mixture was heated to 165 °C for 2 h, then diluted into 100 mL H_2O and filtered. $NaCNBH_3$ (750 mg, 12 mmol) was added to the filtrate, and the reaction mixture was stirred for 1 h. The aqueous solution was extracted with DCM (3 x 100 mL), and the combined organic layers were evaporated to dryness under reduced pressure. Purification by silica column chromatography (25→100% EtOAc/hexanes, then 15% MeOH/DCM) afforded compound **15** (55 mg, 11% yield). ^{1}H NMR (400 MHz, $CDCl_3$) δ 8.23 (dd, J = 8.8, 2.4 Hz, 1H), 8.02 (d, J = 1.9 Hz, 3H), 7.96 (d, J = 8.2 Hz, 2H), 7.93 (d, J = 8.6 Hz, 1H), 7.76 – 7.72 (m, 1H), 7.49 (s, 1H), 7.23 (s, 1H), 5.65 (s, 1H), 3.04 (s, 3H).

Synthesis of compound 16.

To a solution of compound **15** (55 mg, 135 µmol) in 5 mL DMF were added TEA (130 µL, 950 µmol) and bromomethyl acetate (80 µL, 810 µmol), and the reaction mixture was stirred overnight under N_2. The reaction mixture was partitioned between sat. NH_4Cl (50 mL) and EtOAc (50 mL), and the organic layer was washed sequentially with sat. $NaHCO_3$ (2 x 50 mL) and brine (2 x 50 mL), dried over anhydrous $MgSO_4$, and evaporated to dryness under reduced pressure to afford compound **16** (64 mg, 99% yield), which was used without further purification. ^{1}H NMR (400 MHz, $CDCl_3$) δ 8.22 (dd, J = 8.8, 2.3 Hz, 1H), 8.03 – 7.98 (m, 2H), 7.97 – 7.94 (m, 2H), 7.92 (d, J = 8.6 Hz, 1H), 7.72 (dd, J = 8.6, 2.2 Hz, 1H), 7.46 (d, J = 2.2 Hz, 1H), 7.25 – 7.21 (m, 2H), 5.92 (d, J = 1.0 Hz, 2H), 5.64 (s, 1H), 3.02 (s, 3H), 2.08 (s, 3H).

Synthesis of compound 17.

Compound **16** (64 mg, 135 µmol) was reduced following general method I and purified by silica column chromatography (50→65% EtOAc/hexanes) to afford compound **17** (30 mg, 53% yield). ^{1}H NMR (600 MHz, $CDCl_3$) δ 7.88 (d, J = 8.3 Hz, 2H), 7.52 (d, J = 8.4 Hz, 1H), 7.45 (d, J = 8.1 Hz, 1H), 7.22 (d, J = 8.3 Hz, 2H), 6.62 (dd, J = 8.4, 2.4 Hz, 1H), 6.34 (d, J = 2.4 Hz, 1H), 6.19 (dd, J = 8.2, 2.2 Hz, 1H), 5.93 – 5.90 (m, 2H), 5.22 (s, 1H), 3.61 (s, 4H), 2.80 (s, 3H), 2.09 (s, 3H).

Synthesis of *N*-(4-nitro-[1,1'-biphenyl]-2-yl)benzamide (18).

A round-bottom flask was charged with compound **1** (0.9 g, 3.8 mmol), phenylboronic acid (0.46 g, 3.8 mmol), KOAc (0.74 g, 7.6 mmol), and Pd(dppf) (0.15 g, 0.19 mmol), then the atmosphere was replaced with N_2 by 5 evacuation/refill cycles. Deoxygenated 4:1 dioxane:H_2O (18 mL) was added, and the reaction mixture was heated at reflux for 4 h. The reaction mixture was partitioned between H_2O (400 mL) and DCM (400 mL), then the aqueous layer was further extracted with DCM (4 x 200 mL). The combined organic layers were washed with brine (1 x 1 L), dried over anhydrous $MgSO_4$, filtered, and concentrated under reduced pressure. Purification by silica column chromatography (100% DCM) afforded **18** as a yellow solid (0.74 g, 66% yield). ^{1}H NMR (300 MHz, $CDCl_3$) δ 9.52 (s, 1H), 8.21 – 8.00 (m, 2H), 7.73 – 7.34 (m, 11H), 5.30 (s, 2H).

Synthesis of 3-nitro-6-phenylphenanthridine (19).

A round-bottom flask was charged with compound **18** (0.74 g, 2.56 mmol), then 1,2-dichlorobenzene (15 mL) and $POCl_3$ (4 mL, 43 mmol) were added and the reaction mixture was heated at reflux for 24 hours. Excess $POCl_3$ was carefully quenched by slow addition of the reaction mixture to ice-cold 2 M NaOH (400 mL) followed by vigorous stirring for 1 hour. The aqueous layer was extracted with DCM (3 x 200 mL), then the combined organic layers were washed with brine (1 x 400 mL), dried over anhydrous $MgSO_4$, filtered, and concentrated under reduced pressure. The residue was run through a plug of silica gel (eluent 100% EtOAc), affording **19** as a goldenrod solid (0.71 g, 94% yield). ^{1}H NMR (300 MHz, $CDCl_3$) δ 9.13 (s, 1H), 8.75 (d, J = 8.1 Hz, 2H), 8.47 (d, J = 9.0 Hz, 1H), 8.22 (d, J = 8.3 Hz, 1H), 7.98 (t, J = 7.8 Hz, 1H), 7.85 – 7.70 (m, 3H), 7.68 – 7.51 (m, 3H).

Synthesis of 3-(3-nitro-6-phenylphenanthridin-5(6H)-yl)propanoic acid (20).

An Erlenmeyer flask was charged with compound **19** (0.71 g, 2.36 mmol), then glacial acetic acid (25 mL) was added and the reaction mixture was cooled to 17 °C (just above the freezing point of AcOH). $NaBH_4$ was added portion-wise with vigorous stirring until complete consumption of compound **19** was observed by TLC. The reaction mixture was carefully poured into 400 mL H_2O, extracted with DCM (3 x 200 mL), then the combined organic layers were washed with brine (1 x 600 mL), dried over anhydrous $MgSO_4$, filtered, and concentrated under reduced pressure.

Without further purification, the residue was dissolved in acrylic acid (3.7 mL), and conc. H_2SO_4 (1.85 mL) was slowly added. The reaction mixture was stirred for 1.5 h, then carefully poured into ice-cold H_2O (400 mL), whereupon an orange precipitate was formed. The precipitate was collected by filtration then purified by recrystallization from toluene/MeCN to afford compound **20** (370 mg, 28% yield). ^{1}H NMR (400 MHz, $CDCl_3$) δ 7.87 (d, J = 8.6 Hz, 1H), 7.81 (dd, J = 7.8, 1.4 Hz, 1H), 7.69 (dd, J = 8.5, 2.2 Hz, 1H), 7.48 (d, J = 2.2 Hz, 1H), 7.34 (td, J = 7.6, 1.6 Hz, 1H), 7.29 (td, J = 7.5, 1.5 Hz, 1H), 7.24 – 7.18 (m, 3H), 7.18 – 7.12 (m, 3H), 5.65 (s, 1H), 3.72 (dd, J = 7.5, 5.8 Hz, 2H), 2.79 (dt, J = 17.0, 7.5 Hz, 1H), 2.61 (dt, J = 16.9, 5.8 Hz, 1H).

Synthesis of compound 21a.

Compound **20** (150 mg, 0.4 mmol) was coupled with di-*tert*-butyl iminodiacetate following general method III to afford compound **21a** (240 mg, 100% yield), which was used without further purification. ^{1}H NMR (500 MHz, $CDCl_3$) δ 7.84 (d, J = 8.6 Hz, 1H), 7.78 (dd, J = 8.0, 1.3 Hz, 1H),

7.63 (dd, J = 8.5, 2.2 Hz, 1H), 7.43 (d, J = 2.3 Hz, 1H), 7.33 – 7.23 (m, 2H), 7.17 (d, J = 5.3 Hz, 6H), 5.79 (s, 1H), 4.03 (d, J = 5.5 Hz, 2H), 3.85 (dd, J = 21.2, 6.2 Hz, 3H), 3.74 – 3.63 (m, 1H), 2.67 (dt, J = 16.3, 7.2 Hz, 1H), 2.53 (ddd, J = 16.4, 6.7, 5.0 Hz, 1H), 1.41 (s, 9H), 1.34 (s, 9H).

Synthesis of compound 21b.

Compound **21a** (240 mg, 0.4 mmol) was dissolved in 1:1 TFA:DCM (40 mL), and the reaction mixture was stirred for 3 h. The solvent was removed under reduced pressure, then the residue was dissolved in 8 mL dry DMF, and TEA (0.96 mL, 6.9 mmol) and bromomethyl acetate (1.1 mL, 11.2 mmol) were added. The reaction mixture was stirred for 48 h under N_2, then diluted with EtOAc (50 mL) and washed sequentially with sat. $NaHCO_3$ (2 x 50 mL), sat. NH_4Cl (1 x 50 mL), and brine (1 x 50 mL). The organic layer was dried over anhydrous $MgSO_4$ and evaporated to dryness to afford compound **21b** (200 mg, 80% yield). ^{1}H NMR (400 MHz, $CDCl_3$) δ 7.83 (dd, J = 22.0, 8.1 Hz, 2H), 7.64 (dd, J = 8.4, 2.2 Hz, 1H), 7.45 (d, J = 2.3 Hz, 1H), 7.36 – 7.25 (m, 2H), 7.19 (s, 6H), 5.78 (s, 1H), 5.75 – 5.69 (m, 4H), 4.20 (s, 2H), 4.08 (d, J = 5.4 Hz, 2H), 3.78 (ddt, J = 39.4, 15.3, 6.6 Hz, 2H), 2.71 (dt, J = 14.9, 7.2 Hz, 1H), 2.63 – 2.49 (m, 1H), 2.12 (s, 3H), 2.06 (s, 3H).

Synthesis of compound 22.

Compound **21b** (20 mg, 30 µmol) was reduced following general method I and purified by silica column chromatography (0→100% EtOAc in DCM) to afford compound **22** (4 mg, 21% yield). ^{1}H NMR (400 MHz, $CDCl_3$) δ 7.63 (d, J = 7.9 Hz, 1H), 7.56 (d, J = 8.3 Hz, 1H), 7.25 – 7.11 (m, 6H), 7.08 – 7.02 (m, 2H), 6.18 (dd, J = 8.2, 2.1 Hz, 1H), 5.99 (d, J = 2.2 Hz, 1H), 5.77 – 5.66 (m, 4H), 5.45 (s, 1H), 4.19 – 4.14 (m, 2H), 4.07 – 3.93 (m, 2H), 3.75 – 3.59 (m, 2H), 2.63 – 2.43 (m, 2H), 2.12 (s, 3H), 2.08 (s, 3H).

Synthesis of compound 23.

Compound **20** (30 mg, 80 µmol) was dissolved in 5 mL dry DMF, and TEA (75 µL, 540 µmol) and bromomethyl acetate (30 µL, 300 µmol) were added. The reaction mixture was stirred for 2.5 h under N_2, then diluted with EtOAc (30 mL) and washed sequentially with sat. $NaHCO_3$ (2 x 30 mL), sat. NH_4Cl (1 x 30 mL), and brine (1 x 30 mL). The organic layer was dried over anhydrous $MgSO_4$ and evaporated to dryness to afford compound **23** (35 mg, 99% yield). ^{1}H NMR (300 MHz, $CDCl_3$) δ 7.86 (d, J = 8.6 Hz, 1H), 7.81 (dd, J = 7.3, 1.8 Hz, 1H), 7.69 (dd, J = 8.5, 2.2 Hz, 1H), 7.46 (d, J = 2.2 Hz, 1H), 7.38 – 7.27 (m, 2H), 7.24 – 7.12 (m, 6H), 5.75 – 5.62 (m, 3H), 3.74 (dd, J = 7.9, 6.0 Hz, 2H), 2.87 – 2.74 (m, 1H), 2.63 (dt, J = 17.0, 5.6 Hz, 1H), 2.03 (s, 3H).

Synthesis of compound 24.

Compound **23** (35 mg, 80 µmol) was reduced following general method II and purified by preparatory TLC (5% MeOH in DCM) to afford compound **24** (5 mg, 15% yield). ^{1}H NMR (400 MHz, $CDCl_3$) δ 7.62 (d, J = 7.9 Hz, 1H), 7.56 (d, J = 8.2 Hz, 1H), 7.24 – 7.14 (m, 6H), 7.11 – 7.03 (m, 2H), 6.20 (dd, J = 8.2, 2.1 Hz, 1H), 6.01 (d, J = 2.1 Hz, 1H), 5.69 (q, J = 5.7 Hz, 2H), 5.48 (s, 1H), 3.61 (t, J = 6.9 Hz, 2H), 2.74 (dt, J = 16.5, 7.5 Hz, 1H), 2.56 (dt, J = 16.5, 6.3 Hz, 1H), 2.04 (s, 3H).

Synthesis of compound 25.

Compound **20** (40 mg, 107 µmol) was reduced following general method II and purified by preparatory TLC (5% MeOH in DCM) to afford compound **25** (25 mg, 67% yield). ^{1}H NMR

(500 MHz, $CDCl_3$) δ 7.63 (d, J = 7.9 Hz, 1H), 7.56 (d, J = 8.2 Hz, 1H), 7.24 – 7.12 (m, 6H), 7.10 – 7.04 (m, 2H), 6.21 (dd, J = 8.2, 2.1 Hz, 1H), 6.05 (d, J = 2.1 Hz, 1H), 5.47 (s, 1H), 3.65 – 3.53 (m, 2H), 2.74 – 2.62 (m, 1H), 2.54 (ddd, J = 16.4, 7.7, 5.5 Hz, 1H).

Synthesis of compound 26.

Compound **25** (3 mg, 8.7 μmol) and Frémy's salt (12 mg, 45 μmol) were dissolved in 2 mL 1:1 MeOH:H_2O, and the reaction mixture was stirred for 10 min. The solvent was removed under reduced pressure, and purification by silica column chromatography (0→10% MeOH/DCM) afforded compound **26** (1 mg, 32% yield). ^{1}H NMR (300 MHz, $(CD_3)_2SO$) δ 8.55 (d, J = 8.6 Hz, 1H), 8.09 (s, 1H), 8.02 (t, J = 7.8 Hz, 1H), 7.72 (s, 5H), 7.54 (dd, J = 15.4, 8.0 Hz, 2H), 7.22 (d, J = 8.5 Hz, 1H), 6.39 (s, 2H), 4.70 – 4.57 (m, 2H), 2.69 – 2.58 (m, 2H).

Synthesis of compound 27a.

Compound **27a** was synthesized by Jaeho Paek.

Synthesis of compound 27b.

Compound **27b** was synthesized by Jaeho Paek.

Synthesis of compound 27c.

Compound **27c** was synthesized by Jaeho Paek.

Synthesis of compound 27d.

Compound **7** (40 mg, 95 μmol) was coupled with n-dodecylamine following general method III and purified by silica column chromatography (1% MeOH in DCM) to afford compound **27d** (46 mg, 82% yield). ^{1}H NMR (500 MHz, $CDCl_3$) δ 8.14 (dd, J = 8.7, 2.4 Hz, 1H), 8.04 (d, J = 2.3 Hz, 1H), 7.89 (dd, J = 8.7, 7.2 Hz, 2H), 7.64 (dd, J = 8.6, 2.2 Hz, 1H), 7.53 (d, J = 2.2 Hz, 1H), 7.25 – 7.21 (m, 3H), 7.21 – 7.15 (m, 2H), 5.85 (s, 1H), 5.46 (t, J = 5.8 Hz, 1H), 3.89 (ddd, J = 14.9, 9.4, 5.3 Hz, 1H), 3.71 (dt, J = 15.1, 4.9 Hz, 1H), 3.20 – 3.05 (m, 2H), 2.56 (ddd, J = 15.0, 9.4, 5.4 Hz, 1H), 2.45 (dt, J = 15.2, 4.9 Hz, 1H), 1.38 – 1.06 (m, 20H), 0.87 (t, J = 6.9 Hz, 3H).

Synthesis of compound 27e.

Compound **7** (40 mg, 95 μmol) was coupled with 7-tridecylamine following general method III and purified by silica column chromatography (50→100% DCM in hexanes) to afford compound **27e** (50 mg, 87% yield). ^{1}H NMR (400 MHz, $CDCl_3$) δ 8.15 (dd, J = 8.8, 2.4 Hz, 1H), 8.03 (d, J = 2.4 Hz, 1H), 7.90 (dd, J = 8.7, 3.8 Hz, 2H), 7.66 (dd, J = 8.6, 2.2 Hz, 1H), 7.52 (d, J = 2.2 Hz, 1H), 7.25 – 7.17 (m, 5H), 5.87 (s, 1H), 5.30 (s, 1H), 5.07 (d, J = 9.1 Hz, 1H), 3.98 – 3.77 (m, 2H), 3.67 (dt, J = 15.1, 4.6 Hz, 1H), 2.64 – 2.40 (m, 2H), 1.32 – 1.04 (m, 13H), 1.02 – 0.92 (m, 6H), 0.89 – 0.77 (m, 6H).

Synthesis of compound 28a.

Compound **28a** was synthesized by Jaeho Paek.

Synthesis of compound 28b.

Compound **28b** was synthesized by Jaeho Paek.

Synthesis of compound 28c.

Compound **28c** was synthesized by Jaeho Paek.

Synthesis of compound 28d.

Compound **27d** (46 mg, 80 µmol) was reduced following general method I and purified by silica column chromatography (2% MeOH in DCM) to afford compound **28d** (14 mg, 34% yield). ^{1}H NMR (600 MHz, $CDCl_3$) δ 7.45 (dd, J = 8.3, 3.9 Hz, 2H), 7.16 (q, J = 6.0, 4.5 Hz, 5H), 6.58 (dd, J = 8.4, 2.5 Hz, 1H), 6.36 (d, J = 2.4 Hz, 1H), 6.19 (dd, J = 8.2, 2.1 Hz, 1H), 6.02 (d, J = 2.1 Hz, 1H), 5.62 (t, J = 5.6 Hz, 1H), 5.26 (s, 1H), 3.71 – 3.50 (m, 6H), 3.05 (ddd, J = 12.9, 7.2, 5.7 Hz, 2H), 2.49 (ddd, J = 14.8, 8.5, 6.4 Hz, 1H), 2.30 (dt, J = 14.7, 5.2 Hz, 1H), 1.33 – 1.08 (m, 16H), 0.88 (t, J = 6.9 Hz, 3H).

Synthesis of compound 28e.

Compound 2**7e** (25 mg, 40 µmol) was reduced following general method I and purified by silica column chromatography (0→2.5% MeOH in DCM) to afford compound **28e** (13 mg, 58% yield). ^{1}H NMR (500 MHz, $CDCl_3$) δ 7.45 (dd, J = 8.3, 5.0 Hz, 2H), 7.16 (s, 5H), 6.59 (dd, J = 8.4, 2.4 Hz, 1H), 6.36 (d, J = 2.4 Hz, 1H), 6.22 (dd, J = 8.2, 2.0 Hz, 1H), 6.06 (d, J = 2.1 Hz, 1H), 5.52 (d, J = 9.1 Hz, 1H), 5.28 (s, 1H), 3.78 (p, J = 5.8 Hz, 1H), 3.55 (dd, J = 8.2, 5.7 Hz, 2H), 2.53 (dt, J = 14.8, 7.4 Hz, 1H), 2.34 (dt, J = 14.7, 5.4 Hz, 1H), 1.34 – 1.06 (m, 18H), 0.90 – 0.83 (m, 6H).

A1.2.3. Spectroscopic materials and methods

Milli-Q water was used to prepare all aqueous solutions. All spectroscopic measurements were performed in 20 mM PBS, pH 7.4, unless otherwise specified. Absorption spectra were recorded using a Varian Cary 50 spectrophotometer, and fluorescence spectra were recorded using a Photon Technology International Quanta Master 4 L-format scan spectrofluorometer equipped with an LPS-220B 75-W xenon lamp and power supply, A-1010B lamp housing with integrated igniter, switchable 814 photocounting/analog photomultiplier detection unit, and MD5020 motor driver. Samples for absorption and emission measurements were contained in 1-cm × 1-cm quartz cuvettes (1.4-mL volume, Starna).

A1.2.4. Cell culture

HEK293T cells were maintained in exponential growth as a monolayer in Dulbecco's Modified Eagle Medium, high glucose, (DMEM, Invitrogen) supplemented with glutamax (Gibco), 10% fetal bovine serum (FBS, Hyclone) and 1% non-essential amino acids (NEAA, Gibco), and incubated at 37 °C in 5% CO_2. One day before imaging experiments, the cells were passaged and plated in DMEM with glutamax (phenol red-free) supplemented with 10% FBS on poly-d-lysine-coated 4-well Lab Tek borosilicate chambered coverglass slides (Nunc) at 1.8 x 10^5 per well and allowed to grow to 65% confluence before imaging experiments.

A1.2.5. Confocal fluorescence imaging experiments

Confocal fluorescence imaging studies were performed with a Zeiss laser scanning microscope 710 with a 20x objective lens using Zen 2009 software (Carl Zeiss). Probes were excited using a 488 nm argon laser, and emission was collected using a META detector between 500 to 700 nm. BSS (136.9 mM NaCl, 5.37 mM KCl, 1.26 mM $CaCl_2$, 0.81 mM $MgSO_4$, 0.44 mM KH_2PO_4, 0.335 mM Na_2HPO_4, 10 mM PIPES; pH to 7.2 with NaOH) was used as the imaging buffer for all confocal experiments. The cells were imaged at 37 °C throughout the course of the

experiment. Image analysis and quantification was performed using ImageJ (National Institutes of Health). For quantification of fluorescence intensity, four fields of cells within the same well were imaged. A region of interest (ROI) was created around each cell in each image. The mean fluorescence intensity of each cell was measured (using "Measure" function) and averaged across the four fields imaged. For each condition, multiple wells were analyzed using this process, and the values were averaged across independent experiments.

A1.2.6. Menadione addition in HEK293T cells

The DMEM media was aspirated from the chambers containing cells and replaced with 500 μL BSS containing 10 μM probe (diluted from 10 mM stock in DMSO) and incubated at 37 °C for 30 minutes. For unwashed experiments, cells were imaged to provide the t = 0 timepoint. For washed experiments, the probe-containing buffer was replaced with 500 μL fresh BSS containing no probe, and the cells were imaged to provide the t = 0 timepoint. For both unwashed and washed experiments, 200 μL of the buffer was removed from each well and mixed with vehicle control (5 μL DMSO) or menadione (5 μL of 1.01 mM menadione stock for 10 μM final concentration upon re-addition to well). The cells were then incubated at 37 °C for 60 min prior to imaging for the t = 60 timepoint.

A1.2.7. ROS selectivity tests

For all oxidants, selectivity reactions were prepared by incubating indicated concentrations of oxidant (described individually below) with 10 μM probe (diluted from 200 μM stock solution in Milli-Q H_2O) for indicated times at 37 °C in 50 mM PBS (diluted from 216 mM stock) containing 100 μM EDTA (diluted form 10.7 mM stock; no EDTA was included for $HO^{\bullet}$ and $^{t}BuO^{\bullet}$ reactions), followed by addition of 0.1 mg/mL salmon sperm DNA (diluted from 5 mg/mL stock in Milli-Q H_2O) and incubation for 1.5 min prior to taking fluorescence spectra. For $HO^{\bullet}$ and $^{t}BuO^{\bullet}$ reactions, all buffers were degassed and experiments were performed in air-tight screw-top cuvettes. Descriptions of individual oxidants:

H_2O_2: A 100 mM stock of H_2O_2 was prepared by diluting commercial 9.79 M H_2O_2 in Milli-Q water. 1 μL of 100 mM H_2O_2 was added to 1 mL of the 10 μM probe solution.

NaOCl: A 100 mM stock of NaOCl was prepared by diluting fresh reagent-grade 1.95 M NaOCl in Milli-Q water. 1 μL of 100 mM NaOCl was added to 1 mL of the 10 μM probe solution.

^{t}BuOOH: A 100 mM stock of ^{t}BuOOH was prepared by diluting fresh reagent-grade 7.3 M ^{t}BuOOH in Milli-Q water. 1 μL of 100 mM ^{t}BuOOH was added to 1 mL of the 10 μM probe solution.

$HO^{\bullet}$: A 100 mM solution of $Fe(NH_4)_2(SO_4)_2 \bullet 6H_2O$ was prepared by dissolving 39.2 mg in 1 mL of 0.1 N degassed aq. HCl. 1 μL of 100 mM H_2O_2 and 10 μL of 5000 U/mL superoxide dismutase were added to 1 mL of the 10 μM probe solution, followed immediately by 10 μL of the iron(II) solution, using a gas-tight microsyringe. The gas-tight cuvette was shaken to mix.

$^{t}BuO^{\bullet}$: A 100 mM solution of $Fe(NH_4)_2(SO_4)_2 \bullet 6H_2O$ was prepared by dissolving 39.2 mg in 1 mL of 0.1 N degassed aq. HCl. 1 μL of 100 mM ^{t}BuOOH and 10 μL of 5000 U/mL superoxide dismutase were added to 1 mL of the 10 μM probe solution, followed immediately by 10 μL of the iron(II) solution, using a gas-tight microsyringe. The gas-tight cuvette was shaken to mix.

$O_2^{\bullet-}$: This assay is described in detail by Sigma-Aldrich in the technical document entitled "Enzymatic Assay of Superoxide Dismutase." Xanthine oxidase activity was determined as previously described via cytochrome c reduction before each experiment. Probe reactions were performed exactly as for cytochrome c reduction, except probe was substituted for cytochrome c.

A1.3. Results and Discussion

A1.3.1. Design of a modular synthetic route for DHE derivatives

The current synthetic route for synthesizing DHE consists of a borohydride reduction of ethidium cation, itself synthesized in 7 steps from biphenyl by iterative nitrations, a Friedel-Crafts acylation, and an alkylation.[10] While efficient for the production of ethidium and DHE, the current synthetic route does not allow for facile derivatization due to the harsh conditions employed. In order to expeditiously access a variety of DHE derivatives and assess their properties, we designed a new, modular synthetic route which uses easily-accessible building blocks (Figure A1.1). A key improvement over previous methods is the introduction of a Suzuki-Miyaura cross-coupling to install the aryl-aryl bond, allowing for mild and convenient introduction of a variety of substituted aryl coupling partners. Indeed, concurrent with our work in this area, the Hartley group pursued a similar strategy for the construction of a palette of phenanthridinium cations, showcasing the generality of the approach.[11] We used our synthetic route to access several classes of DHE derivatives modified at the (I) 5-position, (II) 6-position, and (III) 8-position, as well as combinations thereof (Figure A1.2).

A1.3.2. Synthesis and in cellulo *screening of ester-functionalized DHE derivatives*

We first endeavored to synthesize a variety of DHE derivatives modified at the 5- and 6-positions, as modifications at this position seemed unlikely to have a large impact on the superoxide reactivity and fluorescence properties of DHE. We were specifically interested in installing ester functionality, as esters, and particularly acetoxymethyl (AM) esters, have been widely used to render molecules cell-trappable.[12] Cell-trappability is an important property for small-molecule probes which means that the probes are not washed out of cells during the various media exchanges common during experiments with cultured cells. Probes that are not cell-trappable, like DHE, tend to have variable baseline fluorescence and poor signal due to leakage in experiments where media exchanges are required. To circumvent this, experiments can be conducted with probe present in all media, though this can lead to complications in interpreting experimental data due to possible extracellular reactivity. A more desirable approach is to develop a cell-trappable version of a probe, enabling more controlled studies with a stable baseline, higher signal-to-noise, and lessened risk of extracellular reactivity. Therefore, we synthesized several DHE analogues with ester-containing substituents at the 5- and 6-positions (Scheme A1.1, Scheme A1.2, Scheme A1.3).

We then screened the ester-containing derivatives for trappability in a cell culture model. HEK293T cells were loaded with 10 μM probe for 30 min, then either washed to remove excess probe or left unwashed as a positive control for turn-on. Probe-loaded cells were imaged for a 0 min timepoint, then treated with 10 μM menadione for 60 minutes to stimulate superoxide production.[5] Fluorescence intensity was quantified and compared to the 0 min timepoint to determine turn-on. In these experiments, the unwashed cells served as a positive control to determine whether the modifications of the DHE scaffold diminish superoxide reactivity, and

significant turn-on in the washed cells was interpreted as a probe being cell-trappable. The results for the various ester-containing DHE analogs are tabulated in Figure A1.3. In general, the ester-functionalized DHE derivatives displayed slightly lower turn-on than DHE in unwashed experiments, and most displayed little to no turn-on in washed experiments. However, compound **24** stood out, as it displays good turn-on in both unwashed and washed conditions. Clearly, the presence of an ester moiety does not seem to be the determining factor for trappability of the DHE scaffold, as two other AM-ester-containing probes (compounds **11** and **17**) as well as two probes each containing two AM-esters (compounds **9a** and **22**) show negligible trappability. Instead, compound **24** lacks the amino group at the 8-position of DHE, suggesting that hydrophobicity may play a role in its trappability.

A1.3.3. In vitro *characterization of compound **25***

Given the favorable cell-trappability of compound **24**, we decided to carry it forward and perform *in vitro* characterization. First, the photophysical properties as well as superoxide reactivity of compound **25** (the hydrolyzed version of compound **24** expected to be present intracellularly) were determined, since replacement of the 8-amino group with a hydrogen could have a large impact on these important properties. Compound **25** displays an excitation maximum λ_{ex} = 350 nm (DHE λ_{ex} = 356 nm) and an emission maximum λ_{em} = 416 nm (DHE λ_{em} = 420 nm) (Figure A1.4). When oxidized by Frémy's salt (a surrogate reactant for superoxide),[13] the 2-hydroxy phenanthridinium **26** is formed (Scheme A1.3), just as the oxidation of DHE by Frémy's salt forms 2-hydroxyethidium (2-OH-E^+), suggesting that the mechanism of oxidation is not significantly different between DHE and compound **25**. Compound **26** displays an excitation maximum λ_{ex} = 445 nm (2-OH-E^+ λ_{ex} = 470 nm) and an emission maximum λ_{em} = 595 nm (2-OH-E^+ λ_{em} = 595 nm) (Figure A1.4). We then characterized the selectivity of compound **25** for superoxide against other potentially-competing reactive oxygen species (ROS) including hydrogen peroxide (H_2O_2), hypochlorite (OCl^-), hydroxyl radical ($HO^\bullet$), *tert*-butyl hydroperoxide (^tBuOOH), and *tert*-butoxy radical ($^tBuO^\bullet$). As shown in Figure A1.5, compound **25** shows good selectivity for superoxide over other tested ROS, again demonstrating its similarity in reactivity to DHE.

A1.3.4. Synthesis and in cellulo *screening of hydrophobic DHE derivatives*

Given the favorable trappability of compound **24**, we decided to synthesize several DHE derivatives with hydrophobic tails appended and assess their degree of trappability. To do so, we coupled various alkyl amines to compound **7**, followed by reduction to afford the DHE derivatives depicted in Scheme A1.4. We then screened these derivatives for trappability in HEK293T cells using the same conditions as in section A1.3.2 but instead using flow cytometry as a readout rather than confocal microscopy due to its higher throughput capabilities. The results are depicted in Figure A1.6; all but one alkyl chain-modified DHE (compound **28d**) showed negligible trappability. It is worth noting that, due to a buffer exchange at the last step of the experiment before flow cytometric analysis, unwashed samples may still leak probe before median fluorescence intensities are determined, which may account for the lack of significant turn-on for most of the tested probes even in unwashed experiments. Nevertheless, dodecyl-modified DHE **28d** showed promising trappability, so we carried it forward to confocal imaging studies to confirm trappability through a different readout. Gratifyingly, compound **28d** also showed good trappability and turn-on in HEK293T cells using confocal microscopy, corroborating our flow cytometry results (Figure A1.7). It is worth noting that compound **28d** also displayed a perinuclear-like staining pattern (Figure A1.8), which is distinct from other ethidium derivatives

that typically localize predominantly in the nucleus. The unusual localization of **28d** may be responsible for its cellular trappability.

A1.4. Conclusion

We have developed an expeditious synthetic route to functionalize the DHE scaffold for the generation of diversified libraries of superoxide-responsive probes. Carboxylic acid-functionalized intermediate **7** is a versatile starting point for facile generation of many DHE derivatives via 2-step amide coupling and reduction. This work focused on exploiting this new synthetic route to screen for cell trappability in DHE derivatives, an important property which would expand the utility of this superoxide detection platform. Contrary to the conventional approach of ester-mediated trapping, there is no clear trend for cellular trappability based on the installation of ester functionality, but both mono-amino DHE **24** and dodecyl-modified DHE **28d** serendipitously displayed good cellular retention in washed cells. Further work will focus on the application of these new tools to investigate superoxide signaling in a neuronal setting. We are specifically interested in NOX2-derived superoxide (see discussion in Chapter 1), which is produced extracellularly, and its potential role as an intercellular signaling agent.[14]

Figures

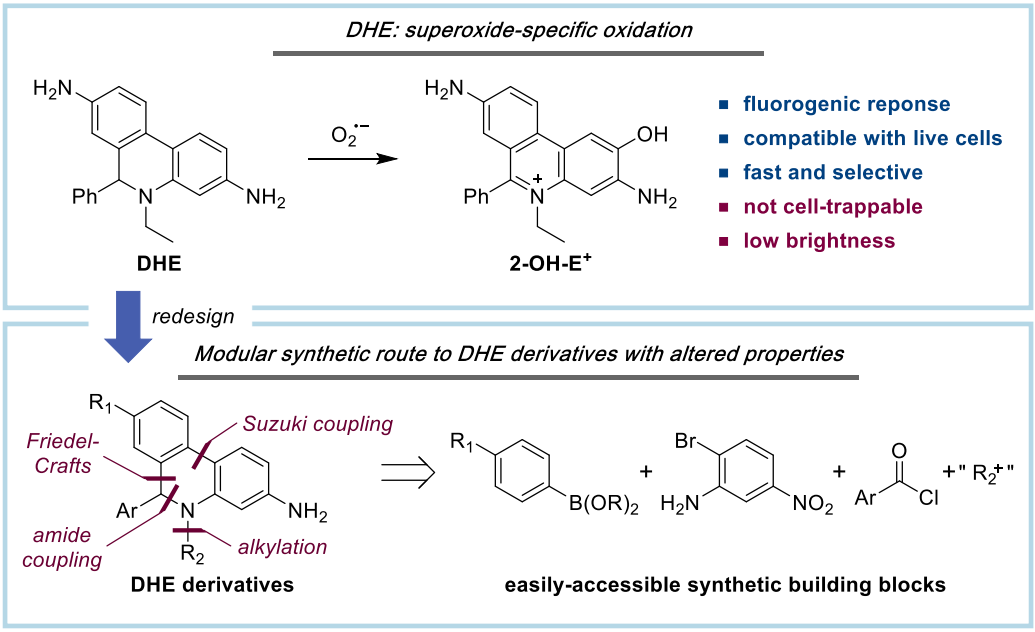

Figure A1.1. Design and retrosynthesis of dihydroethidium (DHE) derivatives.

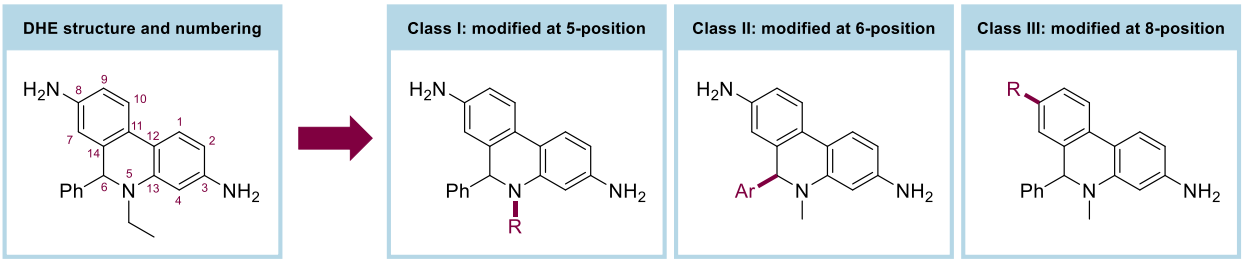

Figure A1.2. Classes of DHE derivatives.

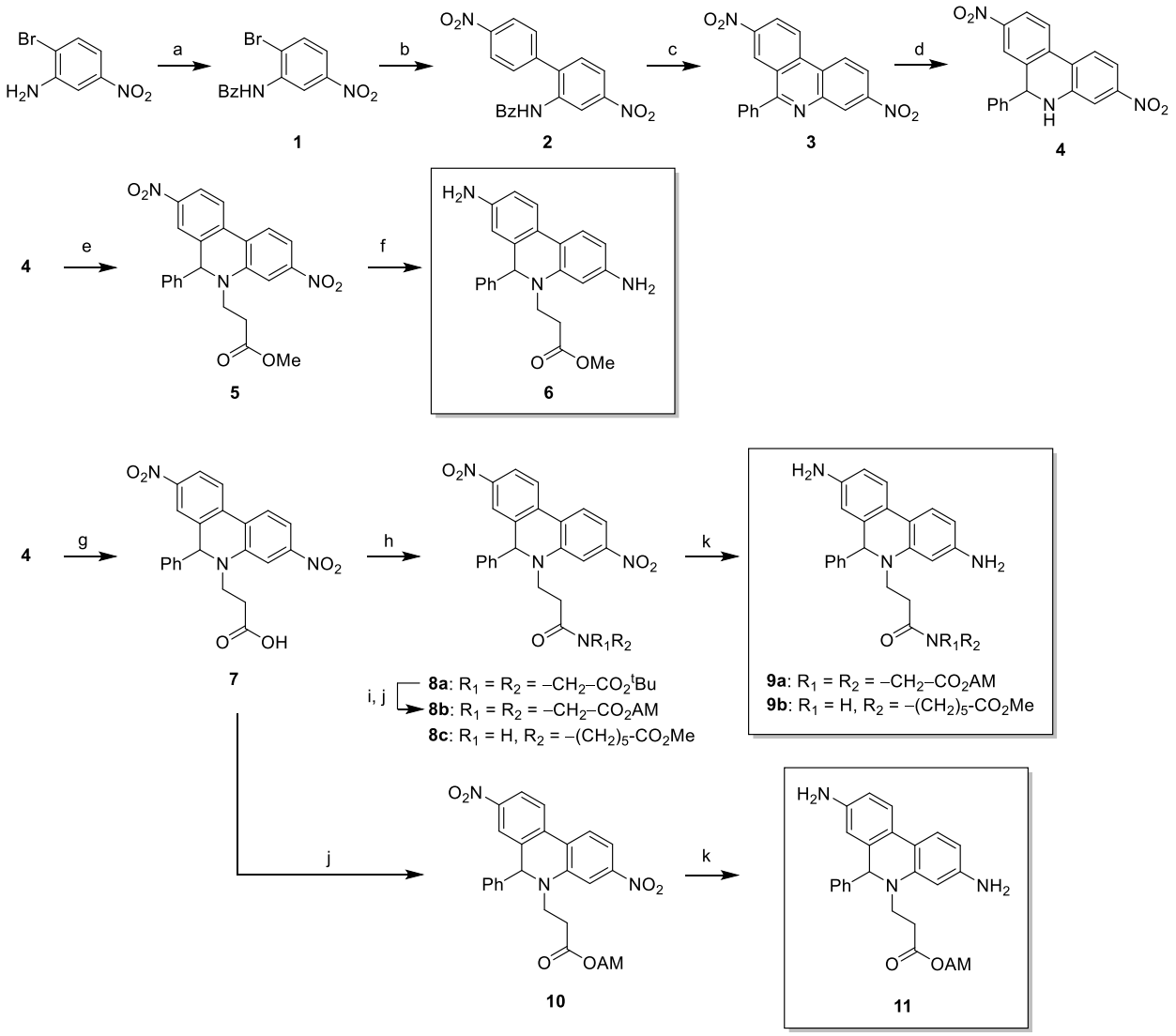

Scheme A1.1. Synthesis of Class I DHE derivatives with ester functionality. Reagents and conditions: (a) BzCl, K_2CO_3, THF, rt, overnight; (b) 4-nitrophenylboronic acid pinacol ester, Pd(dppf), KOAc, dioxane/H_2O, 120 °C, overnight; (c) $POCl_3$, nitrobenzene, 210 °C, 48 h; (d) $NaBH_4$, AcOH, 17 °C, 30 min; (e) methyl acrylate, H_2SO_4, 80 °C, 15 min; (f) Zn, NH_4Cl, MeOH/THF, rt, overnight; (g) acrylic acid, H_2SO_4, rt, 90 min; (h) HNR_1R_2, HATU, DIPEA, DMF, rt, overnight; (i) TFA:DCM, 1:1, rt, 3 h; (j) bromomethyl acetate, TEA, DMF, rt, overnight; (k) H_2 (balloon), Pd/C, EtOAc, rt, overnight.

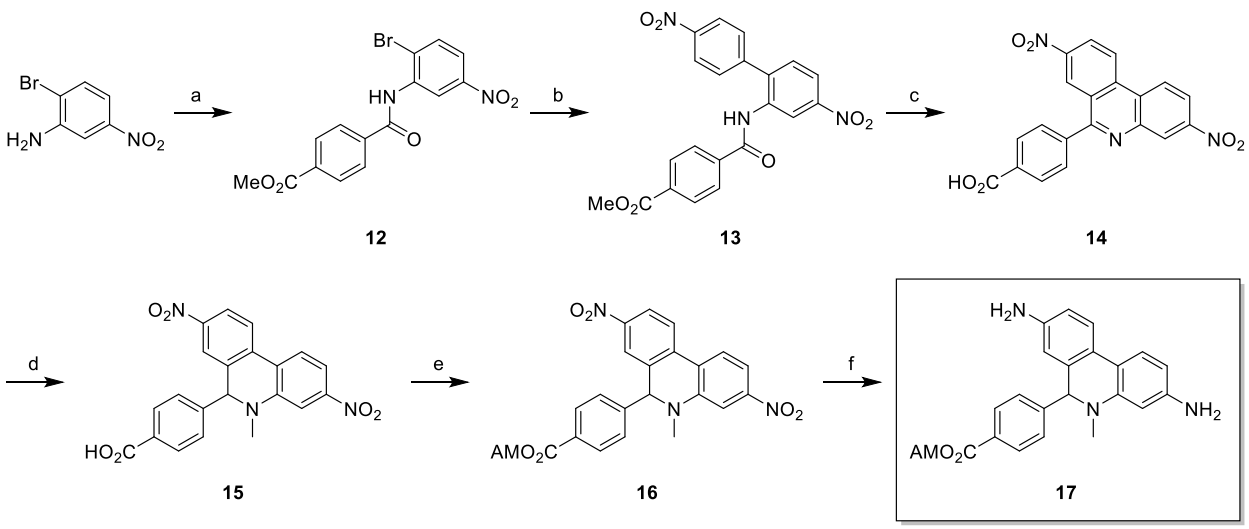

Scheme A1.2. Synthesis of a Class II DHE derivative with ester functionality. Reagents and conditions: (a) methyl 4-(chlorocarbonyl)benzoate, K_2CO_3, THF, rt, overnight; (b) 4-nitrophenylboronic acid pinacol ester, Pd(dppf), KOAc, dioxane/H_2O, 120 °C, overnight; (c) $POCl_3$, nitrobenzene, 210 °C, 48 h; (d) Me_2SO_4, K_2CO_3, DMF, 165 °C, 90 min, then $NaCNBH_3$, DMF, DCM, rt, 10 min; (e) bromomethyl acetate, TEA, DMF, rt, overnight; (f) H_2 (balloon), Pd/C, EtOAc, rt, overnight.

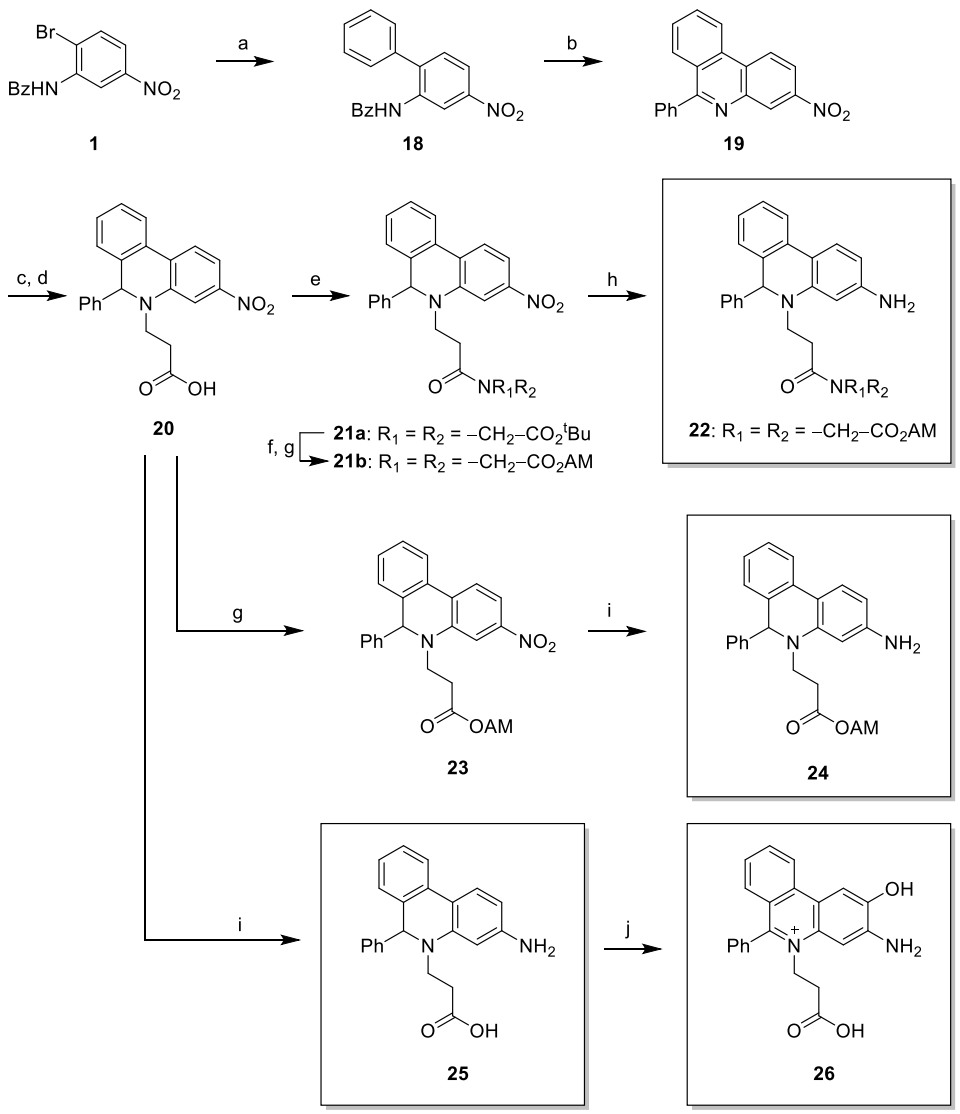

Scheme A1.3. Synthesis of Class I/III DHE derivatives with ester functionality. Reagents and conditions: (a) phenylboronic acid, Pd(dppf), KOAc, dioxane/H_2O, 120 °C, overnight; (b) $POCl_3$, 1,2-dichlorobenzene, 185 °C, overnight; (c) $NaBH_4$, AcOH, 17 °C, 30 min; (d) acrylic acid, H_2SO_4, rt, 90 min; (e) di-*tert*-butyl iminodiacetate, HATU, DIPEA, DMF, rt, overnight; (f) TFA:DCM, 1:1, rt, 3 h; (g) bromomethyl acetate, TEA, DMF, rt, overnight; (h) H_2 (balloon), Pd/C, EtOAc, rt, overnight; (i) Zn, NH_4Cl, THF/H_2O, rt, overnight; (j) Frémy's salt, H_2O/MeOH, rt, 10 min.

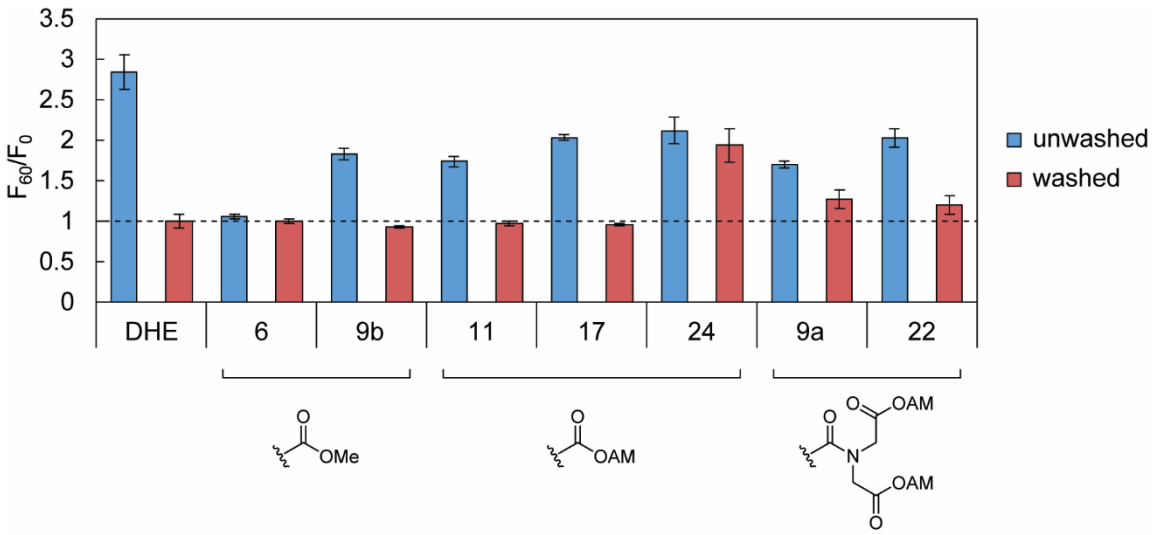

Figure A1.3. Screening for cell trappability in ester-containing DHE derivatives using confocal microscopy. HEK293T cells were treated with 10 µM probe in BSS for 30 min at 37 °C, followed by an exchange into fresh BSS (for 'washed' samples) or no buffer exchange (for 'unwashed' samples). Images were taken for the 0 min timepoint, then 10 µM menadione was added on-stage. Images were then taken after 60 min of menadione treatment. Bars represent fluorescence intensity at 60 min relative to fluorescence intensity at 0 min (F_{60}/F_0). Error bars denote standard deviation between 3 fields of cells per condition.

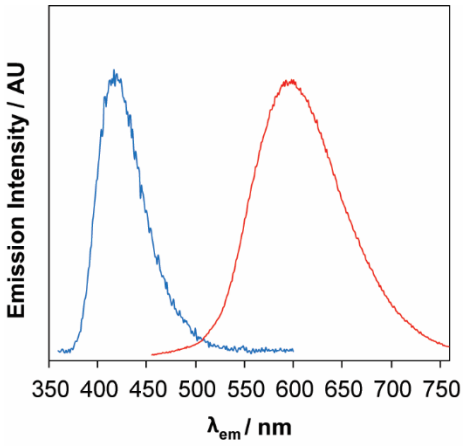

Figure A1.4. Normalized emission spectra for compounds **25** (blue trace, λ_{ex} = 350 nm) and **26** (red trace, λ_{ex} = 445 nm). Spectra were taken with 1 µM probe in 20 mM PBS pH 7.4 at 37 °C.

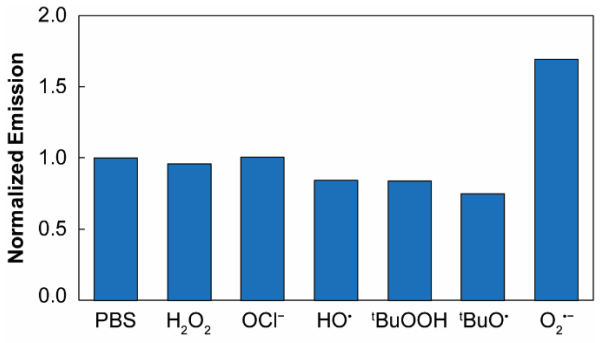

Figure A1.5. Selectivity of compound **25** for superoxide over potentially competing ROS. All experiments were conducted with 10 µM compound **25** in 50 mM phosphate buffer, pH 7.8, at 37 °C. Bars represent normalized emission intensity at 600 nm 30 min after the addition of indicated ROS; spectra were taken after the addition of 0.1 mg/mL salmon sperm DNA to enhance signal. See methods section for details on generation of ROS.

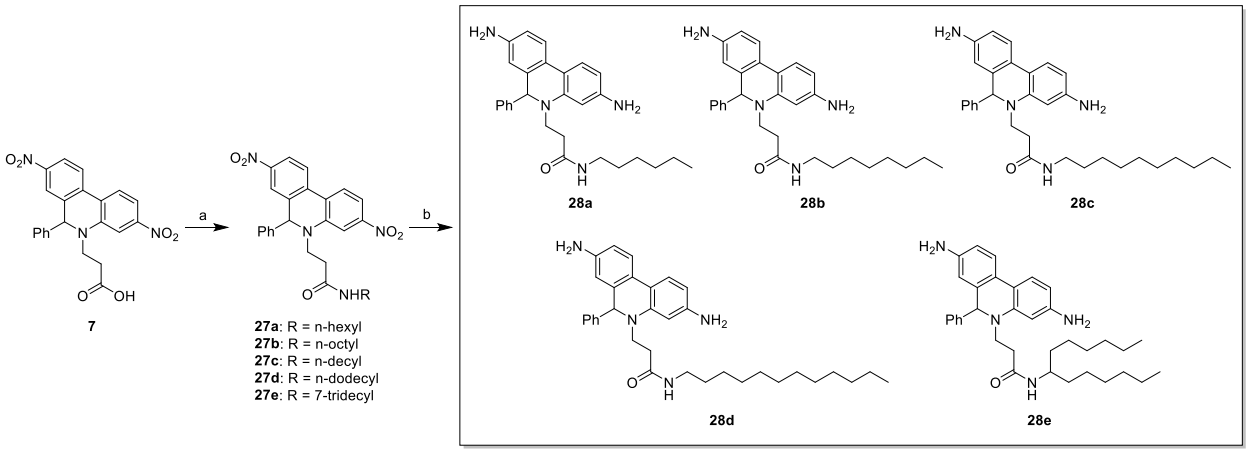

Scheme A1.4. Synthesis of Class I DHE derivatives with various alkyl chains. Reagents and conditions: (a) H_2NR, HATU, DIPEA, DMF, rt, overnight; (b) Zn, NH_4Cl, THF/H_2O, rt, overnight.

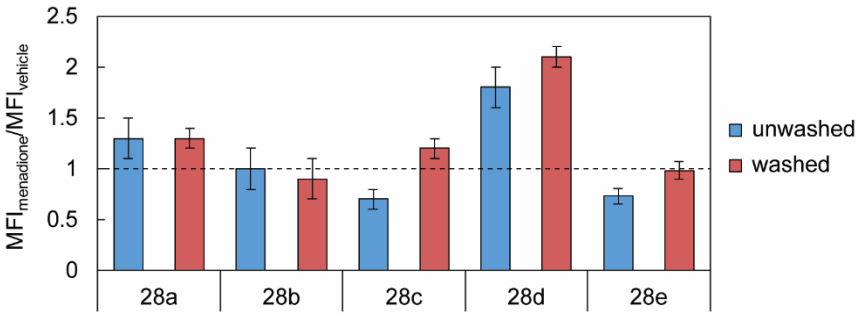

Figure A1.6. Screening for cell trappability in alkyl chain-modified DHE derivatives using flow cytometry. HEK293T cells were treated with 10 µM probe in BSS for 30 min at 37 °C, followed by an exchange into fresh BSS (for 'washed' samples) or no buffer exchange (for 'unwashed' samples). Cells were then treated with 10 µM menadione or vehicle control (DMSO) for 60 min. Cells were then exchanged into PBS, dislodged from wells by gentle agitation, and filtered through 35 µm nylon mesh cap into a 12 x 75 mm polystyrene tube (Corning) for flow cytometric analysis. Excitation was performed with a 488 nm laser, while emission was collected using a standard phycoerythrin filter set (575/26 nm bandpass filter and 550 nm longpass filter). Bars represent median fluorescence intensity (MFI) of menadione-treated samples relative to MFI of vehicle-treated samples. Error bars denote standard deviation between 3 wells of cells per condition.

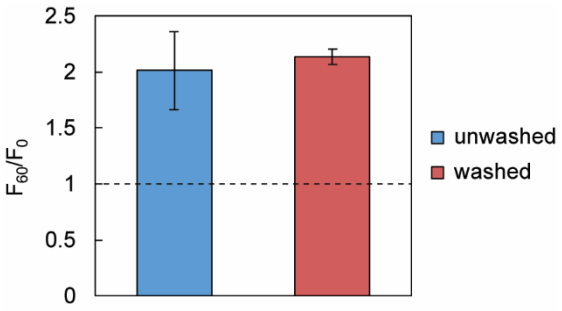

Figure A1.7. Testing cell trappability of compound **29d** using confocal microscopy. HEK293T cells were treated with 10 µM **29d** in BSS for 30 min at 37 °C, followed by an exchange into fresh BSS (for 'washed' samples) or no buffer exchange (for 'unwashed' samples). Images were taken for the 0 min timepoint, then 10 µM menadione was added on-stage. Images were then taken after 60 min of menadione treatment. Bars represent fluorescence intensity at 60 min relative to fluorescence intensity at 0 min (F_{60}/F_0). Error bars denote standard deviation between 3 fields of cells per condition.

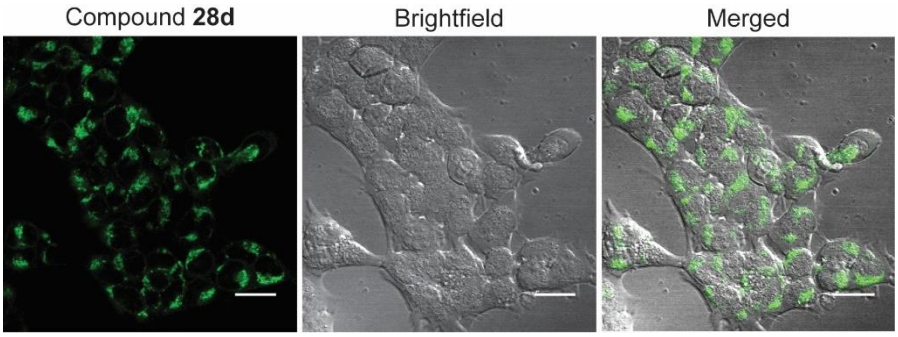

Figure A1.8. Representative image for staining pattern of compound **28d** in HEK293T cells. Scale bar represents 20 μm.

A1.5. References

1. Baas, A. S.; Berk, B. C. *Circ. Res.* **1995,** *77*, 29-36.
2. Kanamori, A.; Catrinescu, M.-M.; Kanamori, N.; Mears, K. A.; Beaubien, R.; Levin, L. A. *Brain* **2010,** *133*, 2612-2625.
3. Zimmerman, M. C.; Lazartigues, E.; Lang, J. A.; Sinnayah, P.; Ahmad, I. M.; Spitz, D. R.; Davisson, R. L. *Circ. Res.* **2002,** *91*, 1038-1045.
4. Nauseef, W. M. *Biochim. Biophys. Acta* **2014,** *1840*, 757-767.
5. Zhao, H.; Joseph, J.; Fales, H. M.; Sokoloski, E. A.; Levine, R. L.; Vasquez-Vivar, J.; Kalyanaraman, B. *Proc. Natl. Acad. Sci. USA* **2005,** *102*, 5727-5732.
6. Robinson, K. M.; Janes, M. S.; Pehar, M.; Monette, J. S.; Ross, M. F.; Hagen, T. M.; Murphy, M. P.; Beckman, J. S. *Proc. Natl. Acad. Sci. USA* **2006,** *103*, 15038-15043.
7. Dikalov, S.; Griendling, K. K.; Harrison, D. G. *Hypertension* **2007,** *49*, 717-727.
8. Zielonka, J.; Kalyanaraman, B. *Free Radic. Biol. Med.* **2010,** *48*, 983-1001.
9. Maghzal, G. J.; Krause, K.-H., Stocker, R.; Jaquet, V. *Free Radic. Biol. Med.* **2012,** *53*, 1903-1918.
10. Osadchii, S. A.; Shubin, V. G.; Kozlova, L. P.; Varlamenko, V. S.; Filipenko, M. L.; Boyarskikh, U. A. *Russ. J. Appl. Chem.* **2011,** *84*, 1541-1548.
11. Cairns, A. G.; Senn, H. M.; Murphy, M. P.; Hartley, R. C. *Chem. Eur. J.* **2014,** *20*, 3742-3751.
12. Tsien, R. Y. *Nature* **1981,** *290*, 527-528.
13. Zielonka, J.; Zhao, H.; Xu, Y.; Kalyanaraman, B. *Free Radic. Biol. Med.* **2005,** *39*, 853-863.
14. Reyes, R. C.; Brennan, A. M.; Shen, Y.; Baldwin, Y.; Swanson, R. A. *J. Neurosci.* **2012,** *32*, 12973-12978.

Appendix 2

Preparation and evaluation of dihydroethidium derivatives with altered photophysical properties

Portions of this work were performed in collaboration with the following persons:

Compounds **1** and **3** were synthesized by Mark N. Vander Wal, and compound **2** was synthesized by Jaeho Paek.

A2.1 Synopsis

As described in Appendix 1, dihydroethidium (DHE) is a commonly-used probe for the detection of superoxide. However, its oxidation product 2-hydroxy ethidium (2-OH-E^+) has a rather poor quantum yield in the absence of DNA,[1-2] which limits its application in the detection of low fluxes of superoxide. Additionally, 2-OH-E^+ has a broad excitation that limits its utility in dual-analyte imaging experiments or in combination with fluorescent protein-based assays. Appendix 2 describes efforts to improve upon the brightness of 2-OH-E^+, as well as to alter its excitation and emission profiles. We take a computational approach using time-dependent density functional theory (TDDFT) to predict the excitation and emission properties of 2-OH-E^+ derivatives. To increase brightness, we designed and synthesized ethidium derivatives whose 6-substituents had varied electron-withdrawing capacity and/or hindered rotation.

A2.2. Methods

A2.2.1. General synthetic methods

All reactions utilizing air- or moisture-sensitive reagents were performed in dried glassware under an atmosphere of dry N_2. When dry solvent was used, the solvent was passed over activated alumina. Other reagents were used without further purification. Silica gel P60 (SiliCycle) was used for column chromatography; SiliCycle 60 F254 silica gel (precoated sheets, 1 mm thick) was used for preparatory thin layer chromatography; and SiliCycle 60 F254 silica gel (precoated sheets, 0.25 mm thick) was used for analytical thin layer chromatography and visualized by fluorescence quenching under UV light. 2-bromo-5-nitroaniline was purchased from AK Scientific (Union City, CA); all other reagents were purchased from Sigma-Aldrich (St. Louis, MO). ^{1}H NMR and ^{13}C NMR spectra were collected in $CDCl_3$, CD_3OD, or $(CD_3)_2SO$ (Cambridge Isotope Laboratories, Cambridge, MA) at 25 °C on Bruker AV-300, AVB-400, AVQ-400, DRX-500, AV-500 and AV-600 at the College of Chemistry NMR Facility at the University of California, Berkeley. All chemical shifts are reported in the standard δ notation of parts per million relative to residual solvent peak at 7.26 ($CDCl_3$), 3,31 (CD_3OD), or 2.50 ($(CD_3)_2SO$) for ^{1}H as an internal reference. Splitting patterns are indicated as follows: br, broad; s, singlet; d, doublet; t, triplet; q, quartet; m, multiplet; dd, doublet of doublets; dt, doublet of triplets; td, triplet of doublets; qd, quartet of doublets; ddd, doublet of doublet of doublets; dtd, doublet of triplet of doublets. Low-resolution electrospray mass spectral analyses were carried out using a LC-MS (Agilent Technology 6130, Quadrupole LC/MS).

A2.2.2. Synthesis

Compounds **1** and **3** were made by Mark N. Vander Wal, and compound **2** was made by Jaeho Paek.

General method I for amide formation.

To a solution of 2-bromo-5-nitroaniline (1 equiv.) and K_2CO_3 (2 equiv.) in THF was added aroyl chloride (1.4 equiv.). The reaction mixture was stirred overnight, then poured into H_2O and stirred for 30 min to hydrolyze excess aroyl chloride. The aqueous solution was extracted with DCM (3x), and the combined organic layers were washed sequentially with 1 M HCl (1x) and brine (1x), then dried over anhydrous $MgSO_4$ and concentrated under reduced pressure. Purification by various methods afforded amide-coupled product.

General method II for Suzuki coupling.

A round-bottom flask was charged with aryl bromide (1 equiv.), 4-nitrophenylboronic acid pinacol ester (1 equiv.), KOAc (2 equiv.), and Pd(dppf) (0.05 equiv.), then the atmosphere was replaced with N_2 by 5 evacuation/refill cycles. Deoxygenated 4:1 dioxane:H_2O was added, and the reaction mixture was heated at reflux overnight. The reaction mixture was partitioned between H_2O and DCM, then the aqueous layer was further extracted with DCM (3x). The combined organic layers were washed with brine (1x), dried over anhydrous $MgSO_4$, filtered, and concentrated under reduced pressure. Purification by various methods afforded cross-coupled product.

General method III for Friedel-Crafts-type cyclization.

A round-bottom flask was charged with *N*-([1,1'-biphenyl]-2-yl)benzamide compound (1 equiv.), then nitrobenzene and $POCl_3$ (1.9 equiv.) were added and the reaction mixture was heated at reflux for 24 hours. Excess $POCl_3$ was carefully quenched by slow addition of the reaction mixture to ice-cold 2M NaOH followed by vigorous stirring for 1 hour. The aqueous layer was extracted with DCM (3x), then the combined organic layers were washed with brine (1x), dried over anhydrous $MgSO_4$, filtered, and concentrated under reduced pressure. Purification by various methods afforded cyclized product.

General method IV for alkylation/reduction of phenanthridines.

Phenanthridine compound was suspended in 10:1 DMF:Me_2SO_4 (75 mM in starting material). The reaction mixture was heated to 165 °C for 3 h, then diluted into H_2O and filtered. Excess $NaCNBH_3$ was added to the filtrate, and the reaction mixture was stirred for 1 h. The aqueous solution was extracted with DCM (3x), and the combined organic layers were evaporated to dryness under reduced pressure. Purification by various methods afforded reduced product.

General method V for nitro group reduction.

A 20-dram vial was charged with nitro compound (1 equiv.), Zn powder (20 equiv.), and NH_4Cl (20 equiv.), then 1:1 MeOH:THF was added and the vial was capped. The reaction mixture was stirred overnight then filtered through celite and evaporated to dryness. Purification by silica column chromatography or preparatory TLC afforded desired amino product.

General method VI for nitro group reduction.

A round-bottom flask was charged with nitro compound (1 equiv.) and Pd/C (1 equiv.), then dry EtOAc was added. The flask was sparged with H_2 (balloon) for 5 min, then placed under H_2 (balloon) overnight. The reaction mixture was filtered through celite, evaporated to dryness, and purification by various methods afforded desired amino product.

General method VII for phenanthridine oxidation.

Phenanthridine compound (1 equiv.) and Frémy's salt (5 equiv.) were dissolved in 1:1 MeOH:H_2O, and the reaction mixture was stirred for 10 min. The solvent was removed under reduced pressure, and purification by silica column chromatography or preparatory TLC afforded desired phenanthridinium product.

Synthesis of compound 4a.

2-Bromo-5-nitroaniline was coupled with 2-tolyl chloride (1.44 mL, 11 mmol) following general method I, and purification by recrystallization from toluene afforded compound **4a** (2.75 g, 89% yield). ^{1}H NMR (500 MHz, $CDCl_3$) δ 9.48 (d, J = 2.7 Hz, 1H), 8.16 (s, 1H), 7.89 (dd, J = 8.8, 2.7 Hz, 1H), 7.77 (d, J = 8.8 Hz, 1H), 7.59 (dd, J = 7.8, 1.5 Hz, 1H), 7.49 – 7.42 (m, 1H), 7.37 – 7.30 (m, 2H), 2.58 (s, 3H).

Synthesis of compound 4b.

2-Bromo-5-nitroaniline was coupled with 2-(trifluoromethyl)benzoyl chloride (2.72 mL, 18.4 mmol) following general method I, and purification by sequential trituration with H_2O and hexanes afforded compound **4b** (3.44 g, 96% yield). ^{1}H NMR (400 MHz, $CDCl_3$) δ 9.43 (d, J = 2.7 Hz, 1H), 8.05 (s, 1H), 7.93 (dd, J = 8.8, 2.7 Hz, 1H), 7.82 (d, J = 7.4 Hz, 1H), 7.78 (d, J = 8.8 Hz, 1H), 7.75 – 7.65 (m, 3H).

Synthesis of compound 4c.

2-Bromo-5-nitroaniline was coupled with 2,3,4,5,6-pentafluorobenzoyl chloride (10.6 mL, 74 mmol) following general method I, and purification by trituration with H_2O afforded compound **4c** (14.9 g, 98% yield). ^{1}H NMR (400 MHz, $CDCl_3$) δ 9.39 (d, J = 2.6 Hz, 1H), 8.29 (s, 1H), 7.97 (dd, J = 8.8, 2.7 Hz, 1H), 7.81 (d, J = 8.8 Hz, 1H).

Synthesis of compound 4d.

2-Bromo-5-nitroaniline was coupled with 4-cyanobenzoyl chloride (4.6 g, 28 mmol) following general method I, and purification by recrystallization from toluene afforded compound **4d** (3.85 g, 80% yield). ^{1}H NMR (600 MHz, $CDCl_3$) δ 9.46 (d, J = 2.6 Hz, 1H), 8.55 (s, 1H), 8.06 (d, J = 8.3 Hz, 2H), 7.94 (dd, J = 8.8, 2.7 Hz, 1H), 7.87 (d, J = 8.3 Hz, 2H), 7.81 (d, J = 8.7 Hz, 1H).

Synthesis of compound 5a.

Compound **4a** (1 g, 3 mmol) was coupled with 4-nitrophenylboronic acid pinacol ester following general method II, and purification by recrystallization from AcOH afforded compound **5a** (0.49 g, 43% yield). ^{1}H NMR (400 MHz, $CDCl_3$) δ 9.28 (d, J = 2.3 Hz, 1H), 8.42 – 8.35 (m, 2H), 8.14 (dd, J = 8.4, 2.3 Hz, 1H), 7.67 – 7.58 (m, 2H), 7.49 – 7.41 (m, 2H), 7.36 (td, J = 7.4, 1.6 Hz, 1H), 7.25 – 7.17 (m, 3H), 2.43 (s, 3H).

Synthesis of compound 5b.

Compound **4b** (1.5 g, 3.8 mmol) was coupled with 4-nitrophenylboronic acid pinacol ester following general method II, and purification by sequential trituration with H_2O and hexanes afforded compound **5b** (1.0 g, 61% yield). ^{1}H NMR (400 MHz, $CDCl_3$) δ 9.28 (s, 1H), 8.35 (d, J = 8.6 Hz, 2H), 8.17 (dd, J = 8.5, 2.3 Hz, 1H), 7.72 (d, J = 7.4 Hz, 1H), 7.68 – 7.57 (m, 4H), 7.49 (dd, J = 14.4, 8.0 Hz, 2H).

Synthesis of compound 5c.

Compound **4c** (1.5 g, 3.6 mmol) was coupled with 4-nitrophenylboronic acid pinacol ester following general method II, and purification by trituration with H_2O afforded compound **5c** (1.2 g, 72% yield). ^{1}H NMR (500 MHz, $(CD_3)_2SO$) δ 11.01 (s, 1H), 8.48 (d, J = 2.5 Hz, 1H), 8.34 (d, J = 8.3 Hz, 2H), 8.28 (dd, J = 8.5, 2.4 Hz, 1H), 7.76 (dd, J = 13.9, 8.4 Hz, 3H).

Synthesis of compound 5d.

Compound **4d** (1.0 g, 2.9 mmol) was coupled with 4-nitrophenylboronic acid pinacol ester following general method II, and purification by trituration with EtOAc afforded compound **5d** (0.85 g, 76% yield). ^{1}H NMR (600 MHz, $CDCl_3$) δ 9.28 (d, J = 2.3 Hz, 1H), 8.43 (d, J = 8.2 Hz, 2H), 8.19 (dd, J = 8.7, 2.2 Hz, 1H), 7.81 – 7.70 (m, 5H), 7.66 (d, J = 8.2 Hz, 2H), 7.51 (d, J = 8.4 Hz, 1H).

Synthesis of compound 6a.

Compound **5a** (200 mg, 0.53 mmol) was cyclized following general method III, and purification by silica column chromatography (10% EtOAc in hexanes) afforded compound **6a** (152 mg, 80% yield). ^{1}H NMR (400 MHz, $CDCl_3$) δ 9.15 (t, J = 2.0 Hz, 1H), 8.92 (dd, J = 9.1, 1.6 Hz, 1H), 8.83 (dd, J = 9.1, 1.6 Hz, 1H), 8.73 (dt, J = 9.0, 2.0 Hz, 1H), 8.68 (t, J = 2.0 Hz, 1H), 8.57 (dt, J = 9.0, 2.0 Hz, 1H), 7.57 – 7.49 (m, 1H), 7.49 – 7.36 (m, 3H), 2.16 (s, 3H).

Synthesis of compound 6b.

Compound **5b** (0.83 g, 1.9 mmol) was cyclized following general method III and purification by silica column chromatography (0→0.5% MeOH in DCM) afforded compound **6b** (0.64 g, 80% yield). ^{1}H NMR (300 MHz, $CDCl_3$) δ 9.05 (d, J = 2.4 Hz, 1H), 8.93 (d, J = 9.1 Hz, 1H), 8.83 (d, J = 9.1 Hz, 1H), 8.70 (dd, J = 9.1, 2.3 Hz, 1H), 8.58 – 8.46 (m, 2H), 7.94 (dd, J = 7.1, 2.1 Hz, 1H), 7.86 – 7.73 (m, 2H), 7.58 (dd, J = 6.9, 2.0 Hz, 1H).

Synthesis of compound 6c.

Compound **5c** (1.0 g, 2.2 mmol) was cyclized following general method III and purification by silica column chromatography (50% hexanes in DCM) afforded compound **6c** (0.46 g, 48% yield). ^{1}H NMR (400 MHz, $CDCl_3$) δ 9.16 (d, J = 2.3 Hz, 1H), 8.98 (d, J = 9.1 Hz, 1H), 8.88 (d, J = 9.0 Hz, 1H), 8.82 (dd, J = 9.1, 2.3 Hz, 1H), 8.72 – 8.64 (m, 2H).

Synthesis of compound 6d.

Compound **5d** (0.4 g, 1 mmol) was cyclized following general method III and purification by recrystallization from nitrobenzene afforded compound **6d** (0.15 g, 40% yield). ^{1}H NMR (400 MHz, $CDCl_3$) δ 9.16 (d, J = 2.4 Hz, 1H), 9.02 – 8.92 (m, 2H), 8.81 (dd, J = 19.3, 9.0 Hz, 2H), 8.61 (dd, J = 9.2, 2.3 Hz, 1H), 7.98 (d, J = 7.9 Hz, 2H), 7.93 (d, J = 7.9 Hz, 2H).

Synthesis of compound 7a.

Compound **6a** (50 mg, 140 µmol) was alkylated and reduced following general method IV and purified by preparatory TLC (15% EtOAc in hexanes) to afford compound **7a** (50 mg, 96% yield). ^{1}H NMR (400 MHz, $CDCl_3$) δ 8.14 (dd, J = 8.8, 2.4 Hz, 1H), 7.96 (d, J = 8.8 Hz, 1H), 7.88 (d, J = 8.6 Hz, 1H), 7.75 (d, J = 2.4 Hz, 1H), 7.65 (dd, J = 8.6, 2.2 Hz, 1H), 7.43 (d, J = 2.3 Hz, 1H), 7.23 – 7.16 (m, 2H), 7.11 – 7.00 (m, 2H), 6.01 (s, 1H), 2.85 (s, 3H), 2.52 (s, 3H).

Synthesis of compound 7b.

Compound **6b** (100 mg, 242 µmol) was alkylated and reduced following general method IV to afford compound **7b** (42 mg, 40% yield) without further purification. ^{1}H NMR (400 MHz, $CDCl_3$) δ 8.18 (dd, J = 8.8, 2.4 Hz, 1H), 8.02 (d, J = 8.7 Hz, 1H), 7.96 – 7.91 (m, 2H), 7.78 – 7.67 (m, 2H), 7.46 (d, J = 2.2 Hz, 1H), 7.44 – 7.31 (m, 3H), 6.17 (s, 1H), 2.90 (s, 3H).

Synthesis of compound 7c.

Compound **6c** (50 mg, 110 µmol) and trimethyloxonium tetrafluoroborate (325 mg, 2.2 mmol) were dissolved in 8 mL nitrobenzene and heated at reflux overnight. The reaction mixture was cooled to ambient temperature and diluted with 20 mL DCM. $NaBH_4$ (excess) was added, and the reaction mixture was stirred for 1 h then carefully poured into 200 mL H_2O. The mixture was extracted with DCM (3 x 100 mL), then the combined organic layers were washed with brine (1 x 300 mL) and dried over anhydrous $MgSO_4$. The solvent was removed under reduced pressure, and the residue was purified by silica column chromatography (0→50% DCM in hexanes) to afford compound **7c** (20 mg, 40% yield). ^{1}H NMR (400 MHz, $CDCl_3$) δ 8.25 (dd, J = 8.8, 2.3 Hz, 1H), 8.03 (d, J = 8.8 Hz, 1H), 8.01 – 7.93 (m, 2H), 7.75 (dd, J = 8.6, 2.2 Hz, 1H), 7.47 (d, J = 2.2 Hz, 1H), 6.39 (s, 1H), 3.01 (s, 3H).

Synthesis of compound 7d.

Compound **6d** (150 mg, 400 µmol) was alkylated and reduced following general method IV, and purification by silica column chromatography (65→80% DCM in hexanes) afforded compound **7d** (20 mg, 13% yield). ^{1}H NMR (500 MHz, $CDCl_3$) δ 8.25 (dd, J = 8.8, 2.2 Hz, 1H), 8.02 (dd, J = 5.5, 3.1 Hz, 2H), 7.94 (d, J = 8.6 Hz, 1H), 7.75 (dd, J = 8.6, 2.1 Hz, 1H), 7.56 (d, J = 8.3 Hz, 2H), 7.50 (d, J = 2.2 Hz, 1H), 7.25 (d, J = 8.2 Hz, 2H), 5.64 (s, 1H), 3.05 (s, 3H).

Synthesis of compound 8a.

Compound **7a** (50 mg, 130 µmol) was reduced following general method VI, and purification by preparatory TLC (40% EtOAc in hexanes) afforded compound **8a** (21 mg, 50% yield). ^{1}H NMR (400 MHz, $CDCl_3$) δ 7.51 (d, J = 8.4 Hz, 1H), 7.45 (d, J = 8.1 Hz, 1H), 7.19 – 7.07 (m, 3H), 7.01 (td, J = 7.4, 1.9 Hz, 1H), 6.58 (dd, J = 8.4, 2.5 Hz, 1H), 6.19 – 6.13 (m, 2H), 5.95 (d, J = 2.2 Hz, 1H), 5.66 (s, 1H), 3.54 (br s, 4H), 2.68 (s, 3H), 2.48 (s, 3H).

Synthesis of compound 8b.

Compound **7b** (42 mg, 98 µmol) was reduced following general method VI, and purification by silica column chromatography (25→100% DCM in hexanes, then 0→1% MeOH in DCM) afforded compound **8b** (23 mg, 63% yield). ^{1}H NMR (400 MHz, $CDCl_3$) δ 7.66 – 7.60 (m, 1H), 7.56 (d, J = 8.4 Hz, 1H), 7.51 – 7.43 (m, 2H), 7.31 – 7.22 (m, 2H), 6.60 (dd, J = 8.4, 2.5 Hz, 1H), 6.37 (d, J = 2.4 Hz, 1H), 6.20 (dd, J = 8.1, 2.2 Hz, 1H), 5.95 (d, J = 2.2 Hz, 1H), 5.80 (s, 1H), 3.60 (s, 4H), 2.74 (s, 3H).

Synthesis of compound 8c.

Compound **7c** (20 mg, 44 µmol) was reduced following general method V, and purification by silica column chromatography (1% MeOH in DCM) afforded compound **8c** (7 mg, 40% yield). ^{1}H NMR (400 MHz, $CDCl_3$) δ 7.53 (d, *J* = 8.5 Hz, 1H), 7.48 (d, *J* = 8.2 Hz, 1H), 6.65 (dd, *J* = 8.5, 2.5 Hz, 1H), 6.31 (d, *J* = 2.5 Hz, 1H), 6.20 (dd, *J* = 8.2, 2.2 Hz, 1H), 6.09 (s, 1H), 5.93 (d, *J* = 2.2 Hz, 1H), 3.63 (br s, 4H), 2.81 (s, 3H).

Synthesis of compound 8d.

Compound **7d** (20 mg, 50 µmol) was reduced following general method V, and purification by silica column chromatography (1% MeOH in DCM) afforded compound **8d** (2.5 mg, 15% yield). ^{1}H NMR (600 MHz, $CDCl_3$) δ 7.53 (d, *J* = 8.6 Hz, 1H), 7.49 – 7.43 (m, 3H), 7.24 (d, *J* =

8.3 Hz, 2H), 6.64 (d, *J* = 8.5 Hz, 1H), 6.35 (s, 1H), 6.21 (d, *J* = 8.1 Hz, 1H), 5.94 (s, 1H), 5.21 (s, 1H), 3.64 (br s, 4H), 2.83 (s, 3H).

Synthesis of compound 9a.

Compound **8a** (2 mg, 6.3 µmol) was oxidized following general method VII and purified by preparatory TLC (20% MeOH in DCM) to afford compound **9a** (0.5 mg, 20% yield). ^{1}H NMR (400 MHz, CD_3OD) δ 8.61 (dd, J = 14.9, 9.1 Hz, 1H), 8.43 (d, J = 9.2 Hz, 1H), 7.62 – 7.54 (m, 3H), 7.44 – 7.39 (m, 1H), 7.39 – 7.34 (m, 1H), 7.27 (s, 1H), 6.38 (d, J = 2.4 Hz, 1H), 4.06 (s, 3H), 2.01 (s, 3H). LRMS calcd. for $C_{21}H_{20}N_3O$ (M^+) 330.2, observed 330.2.

Synthesis of compound 9b.

Compound **8b** (3 mg, 8.1 µmol) was oxidized following general method VII and purified by silica column chromatography (0→20% MeOH in DCM) to afford compound **9b** (0.6 mg, 18% yield). ^{1}H NMR (600 MHz, $(CD_3)_2SO$) δ 8.29 (d, *J* = 9.2 Hz, 1H), 8.14 (d, *J* = 8.0 Hz, 1H), 8.04 (t, *J* = 7.6 Hz, 1H), 7.98 (d, *J* = 7.8 Hz, 1H), 7.78 (d, *J* = 7.6 Hz, 1H), 7.73 – 7.65 (m, 1H), 7.53 (s, 1H), 7.35 (dd, *J* = 9.1, 2.5 Hz, 1H), 7.17 (s, 1H), 6.09 (s, 2H), 6.02 (d, *J* = 2.3 Hz, 1H), 5.77 (s, 2H), 3.90 (s, 3H). LRMS calcd. for $C_{21}H_{17}F_3N_3O$ (M^+) 384.1, observed 384.2.

Synthesis of compound 9c.

Compound **8c** (2 mg, 5.1 µmol) was oxidized following general method VII and purified by silica column chromatography (20% MeOH in DCM) to afford compound **9c** (0.7 mg, 31% yield). ^{1}H NMR (400 MHz, $(CD_3)_2SO$) δ 8.37 (d, J = 9.2 Hz, 1H), 7.80 (s, 1H), 7.53 (d, J = 9.1 Hz, 1H), 7.33 (s, 1H), 6.53 (s, 1H), 6.38 (s, 2H), 5.93 (s, 2H), 4.27 (s, 3H). LRMS calcd. for $C_{20}H_{13}F_5N_3O$ (M^+) 406.1, observed 406.1.

Synthesis of compound 9d.

Compound **8d** (1.5 mg, 4.6 µmol) was oxidized following general method VII and purified by silica column chromatography (35% MeOH in DCM) to afford compound **9d** (0.3 mg, 17% yield). ^{1}H NMR (400 MHz, $(CD_3)_2SO$) δ 8.32 (d, J = 9.2 Hz, 1H), 8.27 (d, J = 8.2 Hz, 2H), 7.96 (s, 1H), 7.89 (d, J = 8.3 Hz, 2H), 7.55 – 7.47 (m, 1H), 7.36 (s, 1H), 6.23 (d, J = 2.3 Hz, 1H), 6.15 (s, 2H), 5.95 (s, 2H), 3.96 (s, 3H). LRMS calcd. for $C_{21}H_{17}N_4O$ (M^+) 341.1, observed 341.2.

A2.2.3. TDDFT calculations

Gaussian 09, revision C.01,[3] was used for all TDDFT calculations. Calculations were performed at the UC Berkeley Molecular Graphics and Computational Facility. TDDFT calculations for fluorescence excitation and emission wavelengths were performed as previously reported.[4] A detailed protocol for similar calculations is available on the Gaussian website on the SCRF keyword page (http://gaussian.com/scrf/) under the examples tab. An example of inputs for each of the 6 steps required is provided for 2-OH-E^+ (note that only the first 2 steps are required to calculate excitation wavelength).

Step 1: Ground state geometry optimization and frequencies (equilibrium solvation)

```
%nprocshared=6
%mem=22200MB
%chk=2-OH-E_step1.chk
# opt freq rb3lyp/6-31+g(d,p) scrf=(iefpcm,solvent=water) geom=connectivity
```

2-OH-E step 1

1 1

C	1.71798900	3.32674300	0.12111400
C	1.86567000	1.94769400	0.03685900
C	0.73441900	1.09116900	-0.00661300
C	-0.58765700	1.63217100	0.02708000
C	-0.70922600	3.04327800	0.11217600
C	0.39508300	3.85907700	0.15975100
C	0.90274700	-0.32124200	-0.08319600
C	-1.70776900	0.73928400	-0.02804800
C	-1.48774000	-0.66455100	-0.10151300
C	-2.58206100	-1.55389300	-0.15736800
H	-2.43581900	-2.62332500	-0.19991600
C	-3.89452300	-1.09097900	-0.14589100
C	-4.11207900	0.32229500	-0.07335300
C	-3.05296000	1.19334800	-0.01676500
H	2.85897400	1.51646800	0.01269200
H	-1.68751200	3.50668600	0.14449900
H	0.26102500	4.93503000	0.23235900
H	-3.26037700	2.25607100	0.03377000
C	2.28033400	-0.90250500	-0.12497900
C	2.92684100	-1.08679700	-1.35778600
C	2.95495500	-1.21441700	1.06483900
C	4.22529600	-1.59938700	-1.39721100
H	2.41662500	-0.82848200	-2.28162900
C	4.25468400	-1.72498300	1.01914900
H	2.47147200	-1.04876900	2.02336200
C	4.88939700	-1.92169200	-0.21003900
H	4.71696600	-1.74280800	-2.35433800
H	4.77002900	-1.96444500	1.94407800
H	5.89921200	-2.31848800	-0.24279000
N	-0.16603100	-1.14479300	-0.12226700
C	0.04741500	-2.62400300	-0.16730700
H	-0.64989100	-3.02800500	-0.90161200
H	1.04747600	-2.79193900	-0.55638500
N	2.79589500	4.17474700	0.21366200
H	3.71887600	3.82504200	0.00611700
H	2.66291600	5.16163100	0.05450200
N	-4.97937700	-1.91311100	-0.18402500
H	-4.87932400	-2.90625100	-0.31507800
H	-5.90468800	-1.51684900	-0.23760300
O	-5.42159400	0.69311500	-0.06913800
H	-5.52224200	1.65355900	-0.01994700
C	-0.10496000	-3.28984000	1.20110400

H	0.66447300	-2.93730000	1.89250800
H	-1.08301200	-3.10457300	1.65105800
H	0.01902800	-4.37069200	1.08384600

1 2 1.5 6 1.5 34 1.5
2 3 1.5 15 1.0
3 4 1.5 7 1.5
4 5 1.5 8 1.5
5 6 2.0 16 1.0
6 17 1.0
7 19 1.0 30 1.5
8 9 1.5 14 1.5
9 10 1.5 30 1.0
10 11 1.0 12 1.5
11
12 13 1.5 37 1.5
13 14 2.0 40 1.0
14 18 1.0
15
16
17
18
19 20 1.5 21 1.5
20 22 1.5 23 1.0
21 24 1.5 25 1.0
22 26 1.5 27 1.0
23
24 26 1.5 28 1.0
25
26 29 1.0
27
28
29
30 31 1.0
31 32 1.0 33 1.0 42 1.0
32
33
34 35 1.0 36 1.0
35
36
37 38 1.0 39 1.0
38
39
40 41 1.0
41
42 43 1.0 44 1.0 45 1.0

43
44
45

Step 2: Vertical excitation with state-specific solvation

```
%nprocshared=6
%mem=44400MB
%chk=2-OH-E_step2.chk
# rb3lyp/6-31+g(d,p) scrf=(iefpcm,solvent=water,read) geom=check

2-OH-E step 2

1 1

NonEq=write

--link1--
%chk=2-OH-E_step2.chk
%nprocshared=12
%mem=44400MB
# B3LYP/6-31+G(d,p) TD(NStates=6,Root=1)
  SCRF=(iefpcm,Solvent=water,ExternalIteration,Read)
  Geom=Check Guess=Read

2-OH-E step 2 part 2

1 1

NonEq=read
```

NOTE: in the output file, excitation wavelength may be found in this text string:

“
Excitation energies and oscillator strengths:

Excited State 1: Singlet-A 2.4870 eV **498.54 nm** f=0.2375 <S**2>=0.000
”

Step 3: Relaxation of the excited-state geometry

```
%chk=2-OH-E_step3.chk
%nprocshared=12
%mem=44400MB
# td=(nstates=6,root=1) b3lyp/6-31+g(d,p) scrf=(iefpcm,solvent=water)
```

guess=read geom=modify opt

2-OH-E step 3

1 1

Step 4: Vibrational frequencies of the excited-state structure

%chk=2-OH-E_step4.chk
%nprocshared=12
%mem=50000MB
# freq td=(nstates=6,root=1) b3lyp/6-31+g(d,p) scrf=(iefpcm,solvent=water)
guess=read geom=check

2-OH-E step 4

1 1

Step 5: Emission state-specific solvation (part 1)

%chk=2-OH-E_step5.chk
%nprocshared=6
%mem=22200MB
# td=(nstates=6,root=1,read) b3lyp/6-31+g(d,p)
scrf=(iefpcm,solvent=water,read,externaliteration) guess=read geom=check

2-OH-E step5

1 1

NonEq=write

NOTE: the energy (in Hartree) of the first excited state in its optimized geometry may be found in this text string in the output file:

“
After PCM corrections, the energy is **-1051.64681134** a.u.
”

Step 6: Emission to final ground state (part 2)

%chk=2-OH-E_step6.chk
%nprocshared=6
%mem=44400MB
b3lyp/6-31+g(d,p) scrf=(iefpcm,solvent=water,read) guess=read geom=check

2-OH-E step6

1 1

NonEq=read

NOTE: the energy (in Hartree) of the ground state from a non-equilibrium solvation calculation in solution using the optimized geometry of the first excited state may be found in this text string in the output file:

“
SCF Done: E(RB3LYP) = **-1051.71067965** A.U. after 13 cycles
”

Determining excitation and emission wavelengths from Gaussian output files

With the calculations finished, it is straightforward to determine excitation and emission wavelengths from the output files.

The excitation wavelength can be directly read out from the output file for Step 2 (see note in Step 2 input file description for where this information is located).

To determine the emission wavelength, the energy difference between the first excited state in its optimized geometry (Step 5) and the ground state in a non-equilibrium geometry (i.e., the optimized geometry of the first excited state, Step 6) must be calculated (see notes in Step 5 and Step 6 input file descriptions for where this information is located). For 2-OH-E+, this value is:

$$E_{em} = -1051.64681134\ A.U. + 1051.71067964\ A.U. = \ 0.06386831\ A.U.$$

An energy conversion calculation converts this energy to wavelength (where *c* is the speed of light and *h* is Planck’s constant; E_{em} is converted to eV for this calculation):

$$\lambda_{em} = \frac{ch}{E_{em}}$$

A2.2.3. Spectroscopic materials and methods

Milli-Q water was used to prepare all aqueous solutions. All spectroscopic measurements were performed in 20 mM PBS, pH 7.4, unless otherwise specified. Absorption spectra were recorded using a Varian Cary 50 spectrophotometer, and fluorescence spectra were recorded using a Photon Technology International Quanta Master 4 L-format scan spectrofluorometer equipped with an LPS-220B 75-W xenon lamp and power supply, A-1010B lamp housing with integrated igniter, switchable 814 photocounting/analog photomultiplier detection unit, and MD5020 motor driver. Samples for absorption and emission measurements were contained in 1-cm × 1-cm quartz cuvettes (1.4-mL volume, Starna).

A2.2.4. Cell culture

HEK293T cells were maintained in exponential growth as a monolayer in Dulbecco's Modified Eagle Medium, high glucose, (DMEM, Invitrogen) supplemented with glutamax (Gibco), 10% fetal bovine serum (FBS, Hyclone) and 1% non-essential amino acids (NEAA, Gibco), and incubated at 37 °C in 5% CO_2. One day before imaging experiments, the cells were passaged and plated in DMEM with glutamax (phenol red-free) supplemented with 10% FBS on poly-d-lysine-coated 4-well Lab Tek borosilicate chambered coverglass slides (Nunc) at 1.8 x 10^5 per well and allowed to grow to 65% confluence before imaging experiments.

A2.2.5. Confocal fluorescence imaging experiments

Confocal fluorescence imaging studies were performed with a Zeiss laser scanning microscope 710 with a 20x objective lens using Zen 2009 software (Carl Zeiss). Probes were excited using a 488 nm argon laser, and emission was collected using a META detector between 500 to 700 nm. BSS (136.9 mM NaCl, 5.37 mM KCl, 1.26 mM $CaCl_2$, 0.81 mM $MgSO_4$, 0.44 mM KH_2PO_4, 0.335 mM Na_2HPO_4, 10 mM PIPES; pH to 7.2 with NaOH) was used as the imaging buffer for all confocal experiments. The cells were imaged at 37 °C throughout the course of the experiment. Image analysis and quantification was performed using ImageJ (National Institutes of Health). For quantification of fluorescence intensity, four fields of cells within the same well were imaged. A region of interest (ROI) was created around each cell in each image. The mean fluorescence intensity of each cell was measured (using "Measure" function) and averaged across the four fields imaged. For each condition, multiple wells were analyzed using this process, and the values were averaged across independent experiments.

A2.2.6. Menadione addition in HEK293T cells

The DMEM media was aspirated from the chambers containing cells and replaced with 500 μL BSS containing 10 μM probe (diluted from 10 mM stock in DMSO) and incubated at 37 °C for 30 minutes. 200 μL of the buffer was removed from each well and mixed with vehicle control (5 μL DMSO) or menadione (5 μL of 1.01 mM menadione stock for 10 μM final concentration upon re-addition to well). The cells were then incubated at 37 °C for 60 min prior to imaging for the t = 60 timepoint.

A2.3. Results and Discussion

A2.3.1. Computational screening of excitation wavelengths for ethidium derivatives

To design ethidium derivatives with shifted excitation/emission profiles, we decided to use a computational approach to speed up the screening process. To assess the feasibility of predicting the spectral profiles of ethidium derivatives, we first used Gaussian 09 to perform time-dependent density functional theory (TDDFT) calculations using a state-specific (SS) polarizable continuum model (PCM), as previously described,[4] predicting the excitation and emission profiles of several ethidium derivatives we had already prepared (Figure A2.1). Though the experimental excitation and emission wavelengths differ numerically from the calculated wavelengths, they follow the same trends and are well-correlated. With this small set of initial data, we were hopeful that TDDFT calculations would be a useful predictive tool for designing ethidium derivatives whose excitation and emission profiles differed significantly from the parent ethidium structure.

We designed a library of theoretical probe ("TP") ethidium-like molecules (Figure A2.2) and submitted them to the excitation wavelength calculations as above. We chose to only perform excitation wavelength calculations for two reasons; first, they don't require an optimization and

frequency calculation of the excited-state geometry, which can be a time-intensive calculation; and second, ethidium derivatives with adequately-resolved excitation wavelengths can be used in multicolor experiments based on differential excitation wavelengths. The results from these calculations are summarized in Figure A2.3. A full tabulation of the results is shown in Table A2.1. One major trend that emerged was that excitation wavelength tended to redshift as the donor ability of the 3- and 8-amino substituents increased (e.g. **TP5**, **TP6**) and/or as the 5- and 6-positions became more electron-deficient (e.g. **TP1**, **TP41**). Future efforts will focus on the synthesis of these redshifted ethidium probes, both to verify the results of this computational screen and to assess their reduced congeners' utility as redshifted superoxide-responsive probes.

A2.3.2. Design and synthesis of ethidium derivatives with increased quantum yield

To design ethidium derivatives with increased brightness, we were inspired by the work of Nagano and coworkers who showed that the electron density of the pendant aryl ring of fluorescein derivatives has a large impact on their quantum yield.[5] Additionally, the Nagano group determined that the *ortho* substituent on the pendant aryl substituent inhibits fluorescence quenching by keeping the two aryl rings orthogonal. We hypothesized that, though their structures differ significantly, similar factors could influence the quantum yield of ethidium derivatives as for fluorescein derivatives (Figure A2.4). Thus, we designed and synthesized a small library of ethidium derivatives altered at the 6-position to include pendant aryl rings with decreased electron density and/or *ortho* substituents to inhibit rotation (Scheme A2.1). We took advantage of our synthetic route for DHE derivatives from Appendix 1 to synthesize these molecules with no significant hurdles, again showcasing the generality of this synthetic approach. Compounds **8a**, **8b**, **8c**, and **8d** all formed predominantly OH-incorporated products **9a**, **9b**, **9c**, and **9d** upon reaction with Frémy's salt, suggesting they may undergo superoxide-specific oxidation similar to the parent DHE compound.

We next characterized the photophysical properties of compounds **9a**, **9b**, **9c**, and **9d**, and the results are tabulated in Table 2.2. Gratifyingly, compounds **9a**, **9b**, and **9c** all have quantum yields higher than the parent 2-OH-E^+ molecule, with the 2-(trifluoromethyl)phenyl derivative **9b** having the highest quantum yield (ca. 2.5-fold higher than 2-OH-E^+). Encouraged by these results, we tested the superoxide responsiveness and brightness of compound **8b** (the unoxidized congener of **9b**) in HEK293T cells, and the results are shown in Figure A2.5. Compound **8b** showed similar superoxide responsiveness to DHE, but, to our surprise, displayed *decreased* brightness *in cellulo*. Closer inspection of the staining pattern of **8b** revealed a possible reason for this unexpected decrease in brightness despite higher quantum yield—it no longer localizes primarily in the nucleus and therefore cannot intercalate in DNA. Since DNA intercalation greatly increases the quantum yield of ethidium derivatives,[1-2] and 2-OH-E^+ localizes primarily in the nucleus, the actual *in cellulo* quantum yield of 2-OH-E^+ is likely higher than that of **9b**.

A2.4. Conclusion

DHE is a useful tool for investigating superoxide fluxes in living samples, but its utility could be expanded by increasing its brightness and diversifying its excitation and emission profiles for use in multi-analyte, multi-color experiments. To develop a variety of DHE derivatives with altered photophysical properties, we have taken a predictive computational approach to screen a library of ethidium-like molecules for changes in excitation wavelength with a particular focus on redshifted excitations. Our TDDFT predictions correlated well with experimental values for a small training set of already-synthesized ethidium derivatives. Several of the screened ethidium-like structures show promising redshifts in their predicted excitation wavelengths, and future

efforts will focus on their synthesis and validation of their experimental properties. In complementary work, we also endeavored to increase the quantum yield of ethidium through substitutions on the pendant aryl ring at the 6-position. Phenanthridiniums with an *ortho* substituent on the pendant aryl ring (compounds **9a**, **9b**) showed significant increases in quantum yield relative to 2-OH-E^+, and electron-deficient perfluorophenyl derivative **9c** also showed an appreciable increase in quantum yield relative to 2-OH-E^+. We further characterized the most promising *ortho*-CF_3 probe **8b** *in cellulo* and found it to display similar superoxide responsiveness to DHE; however, it displayed non-nuclear staining lowering its effective *in cellulo* quantum yield below that of 2-OH-E^+. Future efforts will focus on incorporating the insights from these initial studies onto ethidium derivatives which retain nuclear localization.

Figures

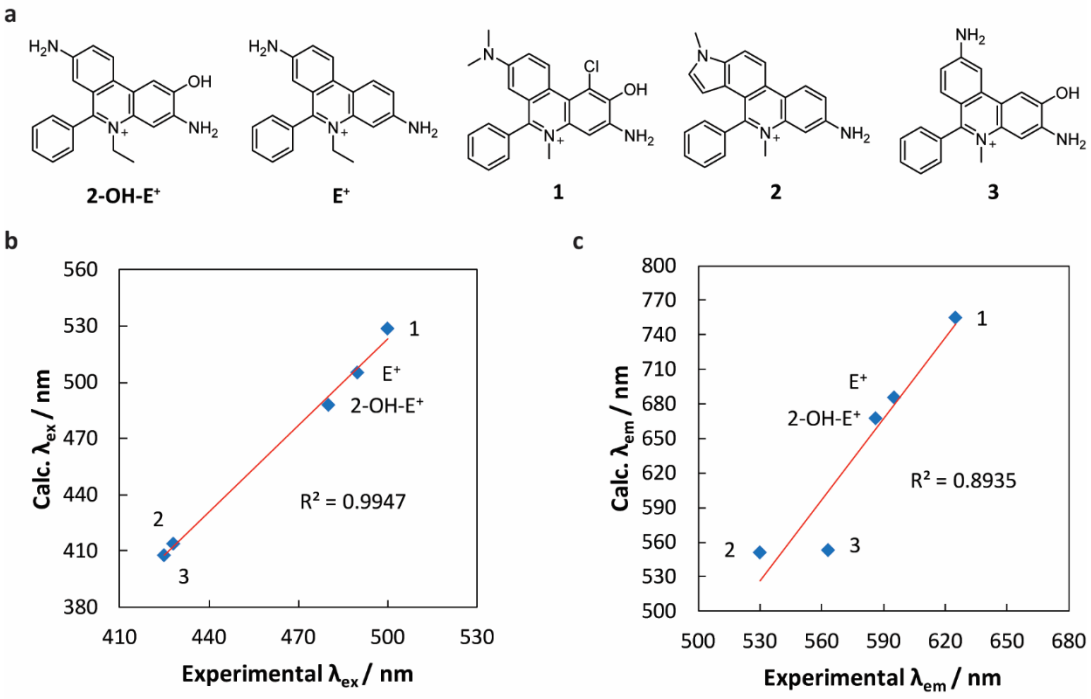

Figure A2.1. Training set for computational prediction of excitation and emission wavelengths of ethidium derivatives. (a) structures of ethidium derivatives used for training set; (b) calculated and experimental excitation wavelengths; (c) calculated and experimental emission wavelengths.

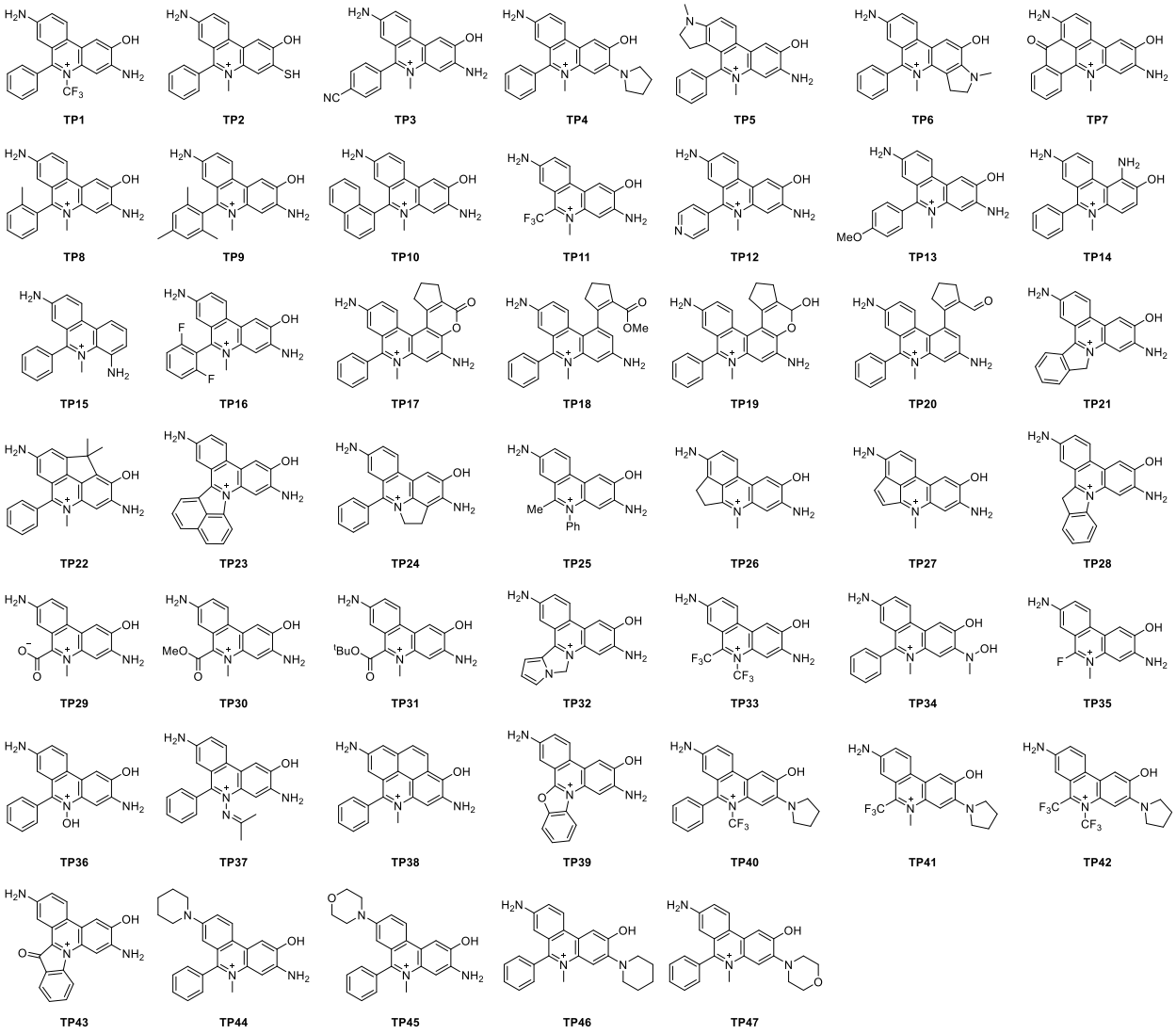

Figure A2.2. Ethidium-like molecules whose excitation and emission profiles were calculated using TDDFT.

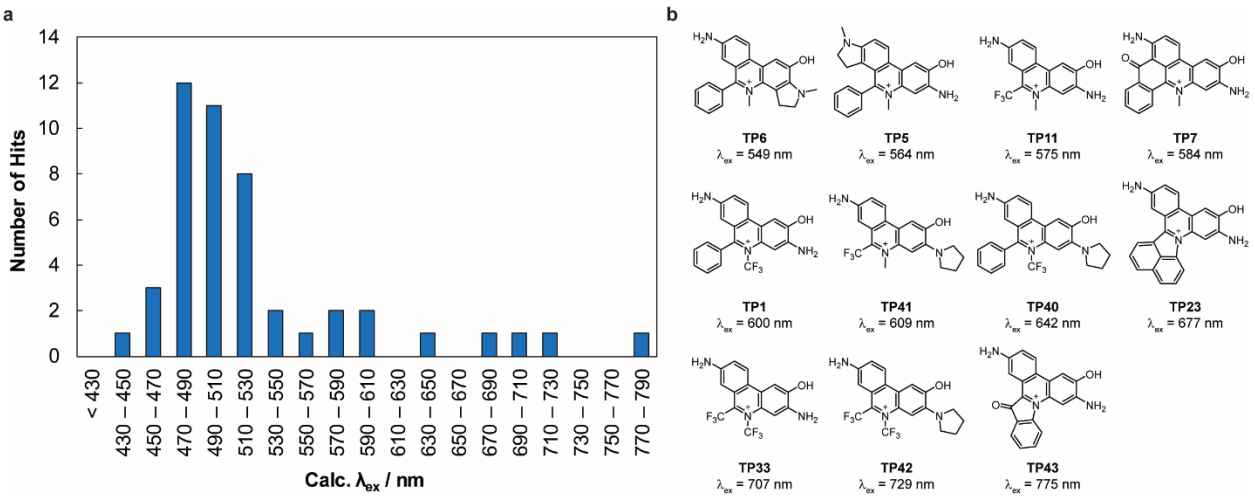

Figure A2.3. Summary of results from TDDFT calculations on the TP library. (a) Histogram of calculated excitation wavelengths for TP library. (b) TP structures whose excitation wavelength is greater than 540 nm.

Sorted by λ_{ex}		Sorted by Molecule #	
Molecule	**λ_{ex}, nm**	**Molecule**	**λ_{ex}, nm**
TP29	437	TP1	600
TP34	451	TP2	454
TP2	454	TP3	495
TP26	463	TP4	525
TP35	475	TP5	564
TP39	476	TP6	549
TP24	481	TP7	584
TP25	481	TP8	486
TP36	484	TP9	485
TP9	485	TP10	490
TP31	485	TP11	575
TP8	486	TP12	494
TP13	486	TP13	486
TP37	486	TP14	511
TP22	488	TP15	504
TP10	490	TP16	504
TP30	491	TP17	514
TP12	494	TP18	509
TP3	495	TP19	509
TP45	496	TP20	512
TP38	500	TP21	527
TP15	504	TP22	488
TP16	504	TP23	677
TP47	507	TP24	481
TP18	509	TP25	481
TP19	509	TP26	463
TP28	509	TP27	537
TP14	511	TP28	509
TP20	512	TP29	437
TP17	514	TP30	491
TP46	520	TP31	485
TP4	525	TP32	525
TP32	525	TP33	707
TP21	527	TP34	451
TP44	529	TP35	475
TP27	537	TP36	484
TP6	549	TP37	486
TP5	564	TP38	500
TP11	575	TP39	476
TP7	584	TP40	642
TP1	600	TP41	609
TP41	609	TP42	729

TP40	642	TP43	775
TP23	677	TP44	529
TP33	707	TP45	496
TP42	729	TP46	520
TP43	775	TP47	507

Table A2.1. Tabulated excitation wavelengths for all TP molecules.

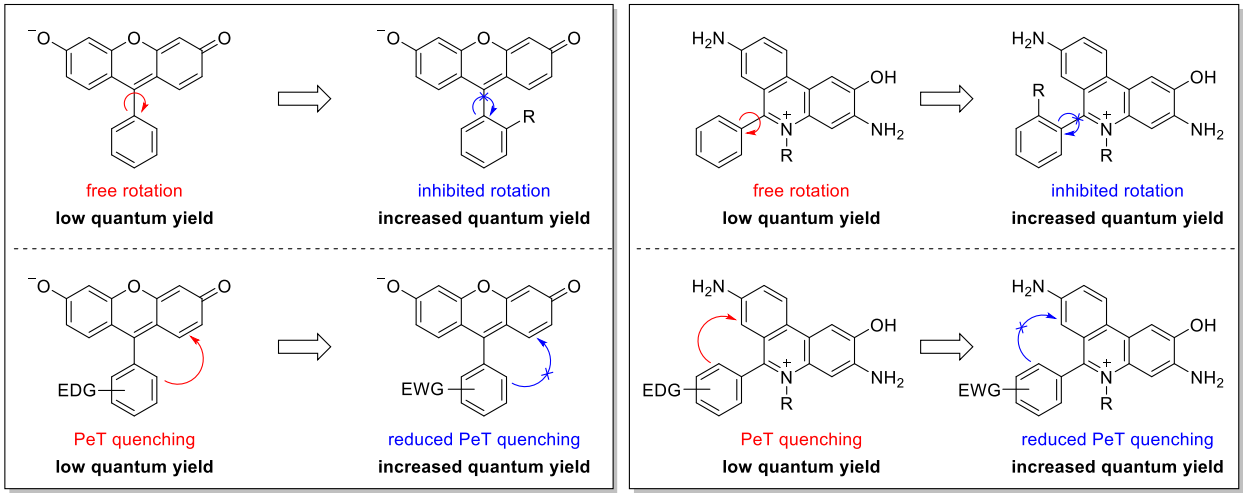

Figure A2.4. Comparison of potential similarities between fluorescein and ethidium scaffolds.

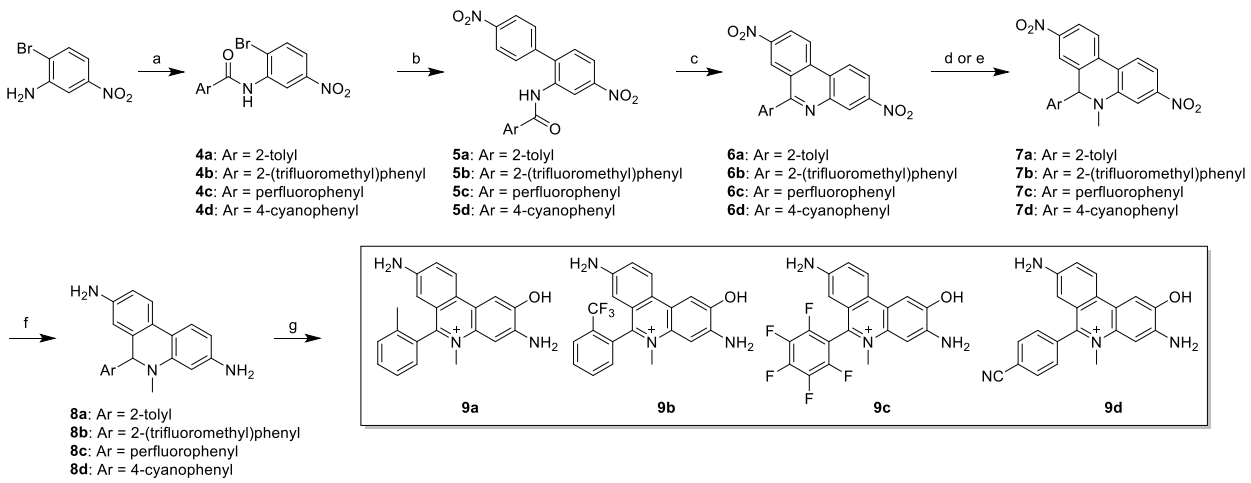

Scheme A2.1. Synthesis of a library of ethidium-like structures with varied aryl substituents at the 6-position. Reagents and conditions: (a) ArCOCl, K_2CO_3, THF, rt, overnight; (b) 4-nitrophenylboronic acid pinacol ester, Pd(dppf), KOAc, dioxane/H_2O, 120 °C, overnight; (c) $POCl_3$, nitrobenzene, 210 °C, 48 h; (d) Me_2SO_4, K_2CO_3, DMF, 165 °C, 90 min, then $NaCNBH_3$, DMF, DCM, rt, 10 min; (e) Me_3OBF_4, nitrobenzene, reflux, overnight, then $NaBH_4$, DCM, rt, 1 h; (f) Zn, NH_4Cl, THF/H_2O, rt, overnight; (g) Frémy's salt, H_2O/MeOH, rt, 10 min.

Compound	λ_{ex}, nm	λ_{em}, nm	ϕ_{fl}
2-OH-E^+	480	586	0.035
9a	470	595	0.045
9b	480	600	0.088
9c	493	615	0.055
9d	480	625	0.019

Table A2.2. Tabulated photophysical properties for compounds **9a**, **9b**, **9c**, and **9d**.

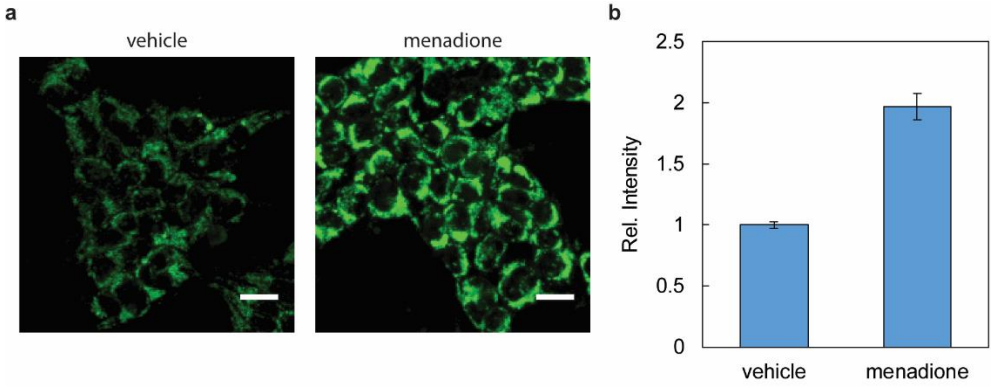

Figure A2.5. Superoxide response of compound **8b** *in cellulo*. HEK293T cells were treated with 10 µM 8b in BSS for 30 min at 37 °C, followed by addition of 10 µM menadione. Images were then taken after 60 min of menadione treatment. (a) representative image; (b) quantification of fluorescence intensity after 60 min treatment with vehicle or 10 µM menadione. Error bars denote standard deviation between 3 fields of cells per condition. Scale bar represents 20 µm.

A2.5. References

1. Luedtke, N. W.; Liu, Q.; Tor, Y. *Bioorg. Med. Chem.* **2003,** *11*, 5235-5247.
2. Prunkl, C.; Pichlmaier, M.; Winter, R.; Kharlanov, V.; Rettig, W.; Wagenknecht, H.-A. *Chem. Eur. J.* **2010,** *16*, 3392-3402.
3. Frisch, M. J.; Trucks, G. W.; Schlegel, H. B.; Scuseria, G. E.; Robb, M. A.; Cheeseman, J. R.; Scalmani, G.; Barone, V.; Mennucci, B.; Petersson, G. A.; Nakatsuji, H.; Caricato, M.; Li, X.; Hratchian, H. P.; Izmaylov, A. F.; Bloino, J.; Zheng, G.; Sonnenberg, J. L.; Hada, M.; Ehara, M.; Toyota, K.; Fukuda, R.; Hasegawa, J.; Ishida, M.; Nakajima, T.; Honda, Y.; Kitao, O.; Nakai, H.; Vreven, T.; J. A. Montgomery, J.; Peralta, J. E.; Ogliaro, F.; Bearpark, M.; Heyd, J. J.; Brothers, E.; Kudin, K. N.; Staroverov, V. N.; Keith, T.; Kobayashi, R.; Normand, J.; Raghavachari, K.; Rendell, A.; Burant, J. C.; Iyengar, S. S.; Tomasi, J.; Cossi, M.; Rega, N.; Millam, J. M.; Klene, M.; Knox, J. E.; Cross, J. B.; Bakken, V.; Adamo, C.; Jaramillo, J.; Gomperts, R.; Stratmann, R. E.; Yazyev, O.; Austin, A. J.; Cammi, R.; Pomelli, C.; Ochterski, J. W.; Martin, R. L.; Morokuma, K.; Zakrzewski, V. G.; Voth, G. A.; Salvador, P.; Dannenberg, J. J.; Dapprich, S.; Daniels, A. D.; Farkas, O.; Foresman, J. B.; Ortiz, J. V.; Cioslowski, J.; Fox, D. J. *Gaussian 09, Revision C.01*, Gaussian, Inc.: Wallingford, CT, 2010.
4. Improta, R.; Scalmani, G.; Frisch, M. J.; Barone, V. *J. Chem. Phys.* **2007,** *127*, 074504.
5. Urano, Y.; Kamiya, M.; Kanda, K.; Ueno, T.; Hirose, K.; Nagano, T. *J. Am. Chem. Soc.* **2005,** *127*, 4888-4894.

Appendix 3

Selectivity tests for reactive carbonyl species

A3.1. Synopsis

This appendix describes the preparation of stock solutions and a protocol for conducting *in vitro* selectivity tests using reactive carbonyl species (RCS) and related molecules. General notes and comments on precision and reproducibility are adapted and expanded from Appendix 5 of Vivian S. Lin's thesis (Fall 2014).

A3.2. General notes

- Generally, RCS are tested at a final concentration of 100 μM.
- All stock solutions should be kept on ice throughout experiments.
- Any highly-abundant species should be tested at their most biologically-relevant concentration, e.g. 1–5 mM for glucose.
- The concentration of dye or probe being tested typically ranges from 1–10 μM. Dye concentration and/or fluorometer settings may need adjustment if the dye fluorescence reads outside of the linear range or is saturating during selectivity tests.
- Readings are typically taken at 15–30 min intervals. Fluorescence response is typically represented as integrated emission intensity over a given range.
- A blank run and a positive control should be performed on each day of data collection.

A3.3. Precision and Reproducibility

- Reagents used to generate reactive species should be dated upon delivery and/or first use. Reagents that appear discolored or otherwise expired should be quenched and discarded. Titrating a reagent, when possible, is useful for ensuring that the commercially-reported concentration corresponds with the effective concentration.
- The measurements and volumes provided below are based on specific products from commercial sources. All reagents should be inspected and any measurements recalculated if the composition (e.g. concentration, density) of a new reagent differs from the values listed here. Special attention should be paid to the units used for concentration.
- Any milligram quantities of solid reagents should be weighed using a microbalance for accuracy. Weighing inaccuracies when preparing stock solutions can affect experimental reproducibility.
- Fluorometer settings (e.g. slit widths) should be recorded and kept the same between runs for consistency.
- The buffer used for each RCS should be noted. Common buffers include HEPES, MOPS, and PBS or DPBS (NOTE: buffers containing secondary or primary amines, such as Tris, TES, ACES, TAPSO, tricine, TAPS, CHES, and CAPS should **not** be used as the amines can have cross-reactivity with RCS). Selectivity tests should be conducted in the same buffer for all species whenever possible.
- Be aware of the accuracy ratings for the micropipettors that you are using, especially when measuring low microliter volumes. If accuracy with very low volumes is suspect, prepare diluted stocks, e.g. 10 mM, and deliver larger quantities to achieve the desired final concentration. As a general rule of thumb, pipetting < 1 μL should be avoided.

A3.4. Preparation of stock solutions

A3.4.1. Formaldehyde

Commercial 37 wt % formaldehyde (ca. 13.3 M) can be purchased from chemical suppliers such as Sigma-Aldrich. This concentrated solution is relatively bench-stable, but should be replaced after 2 years of initial receipt. Working stock solutions should be made fresh by dilution with Milli-Q water on each day of experimentation. A typical stock concentration is 50 – 100 mM for *in vitro* experiments.

For 100 mM stock: dilute 15 µL of 13.3 M FA solution to 2 mL with Milli-Q H_2O

A3.4.2. Methylglyoxal

Commercial 40 wt % methylglyoxal (a.k.a. pyruvaldehyde; 6.54 M) can be purchased from chemical suppliers such as Sigma-Aldrich. This concentrated solution is relatively stable when stored at 4 °C, but should be replaced after 3 years of initial receipt. Working stock solutions should be made fresh by dilution with Milli-Q water on each day of experimentation. A typical stock concentration is 50 – 100 mM for *in vitro* experiments.

For 100 mM stock: dilute 30.6 µL of 6.54 M methylglyoxal solution to 2 mL with Milli-Q H_2O

A3.4.3. Dehydroascorbic acid

(L)-dehydroascorbic acid is available as a solid from chemical suppliers such as Sigma-Aldrich. The solid should be stored at −20 °C. Working stock solutions should be made fresh by dissolution in 1:1 DMSO:Milli-Q water on each day of experimentation. A typical stock concentration is 50 – 100 mM for *in vitro* experiments.

For 100 mM stock: dissolve 10 mg of dehydroascorbic acid in 5.74 mL of 1:1 DMSO:Milli-Q H_2O

A3.4.4. Glucosone

(D)-glucosone (a.k.a. 2-keto-D-glucose) is available as a solid from chemical suppliers such as Sigma-Aldrich. The solid should be stored at −20 °C. Working stock solutions should be made fresh by dissolution in Milli-Q water on each day of experimentation. Since glucosone is relatively expensive, it can be pre-aliquoted and aliquots can be reconstituted in Milli-Q H_2O as necessary. A typical procedure for aliquoting material is to make a 40 mM stock solution in EtOH, then dispense 50 µL/aliquot (2 µmol/aliquot) using a repeat pipettor into PCR tubes. The tubes can then be placed in a vacuum dessicator (uncapped), allowed to evaporate to dryness, then capped and stored at −20 °C. On the day of an experiment, an aliquot can be reconstituted with 20 µL Milli-Q H_2O to provide a 100 mM working stock solution.

A3.4.5. Acrolein

Neat acrolein is available in a Sure/Seal™ bottle from Sigma-Aldrich. This material is relatively stable when stored at 4 °C. Working stock solutions should be made fresh by dilution with Milli-Q water on each day of experimentation. A typical stock concentration is 50 – 100 mM for *in vitro* experiments.

For 100 mM stock: dilute 200 µL (using syringe instead of micropipettor) of neat acrolein to 30 mL with Milli-Q H_2O

A3.4.6. Acetaldehyde

Neat acetaldehyde can be purchased from chemical suppliers such as Sigma-Aldrich. This material is relatively stable when stored at 4 °C. Working stock solutions should be made fresh by dilution with Milli-Q water on each day of experimentation. A typical stock concentration is 50 – 100 mM for *in vitro* experiments.

For 100 mM stock: dilute 500 µL (using syringe instead of micropipettor; be careful of evaporation from the reduced pressure caused by withdrawing a syringe plunger) of neat acetaldehyde to 89.1 mL with Milli-Q H_2O

A3.4.7. Glucose

(D)-Glucose (a.k.a. dextrose) is available as a solid from chemical suppliers such as Sigma-Aldrich. The solid should be stored at room temperature. Working stock solutions should be made fresh by dissolution in Milli-Q water on each day of experimentation. A typical stock concentration is 1 M for *in vitro* experiments.

For 1 M stock: dissolve 200 mg of glucose in 1.11 mL of Milli-Q H_2O

A3.4.8. Pyruvate

Sodium pyruvate is available as a solid from chemical suppliers such as Sigma-Aldrich. The solid should be stored at 4 °C. Working stock solutions should be made fresh by dissolution in Milli-Q water on each day of experimentation. A typical stock concentration is 100 mM for *in vitro* experiments.

For 100 mM stock: dissolve 20 mg of sodium pyruvate in 1.82 mL of Milli-Q H_2O

A3.4.9. Oxaloacetic acid

Oxaloacetic acid is available as a solid from chemical suppliers such as Sigma-Aldrich. The solid should be stored at −20 °C. Working stock solutions should be made fresh by dissolution in Milli-Q water on each day of experimentation. Since oxaloacetic acid is relatively expensive, it can be pre-aliquoted and aliquots can be reconstituted in Milli-Q H_2O as necessary. A typical procedure for aliquoting material is to make a 20 mM stock solution in EtOH, then dispense 50 µL/aliquot (1 µmol/aliquot) using a repeat pipettor into PCR tubes. The tubes can then be placed in a vacuum dessicator (uncapped), allowed to evaporate to dryness, then capped and stored at −20 °C. On the day of an experiment, an aliquot can be reconstituted with 100 µL Milli-Q H_2O to provide a 10 mM working stock solution.

A3.4.10. 4-Hydroxynonenal

4-Hydroxynonenal is available as a 64 mM solution in EtOH from Cayman Chemical. The solution should be stored at −80 °C. Since 4-hydroxynonenal is relatively expensive, it can be pre-aliquoted and aliquots can be used as necessary to prevent warm/cool cycles for the bulk stock. A typical aliquot volume is 10 µL; care should be taken to minimize evaporation during aliquoting.

Appendix 4

LC-MS usage and maintenance

A4.1. Synopsis

This appendix is meant to provide an overview of use, maintenance, and troubleshooting of the C. Chang lab Advion LC-MS instrument. Portions of the troubleshooting guide in this appendix are adapted and expanded from Appendix 8 of Vivian S. Lin's thesis (Fall 2014).

A4.2. Instrument overview

The Advion Expression-L Compact Mass Spectrometer is rated for low-resolution mass spectrometry detection of both positive and negative ions in the < 2000 m/z range. It is equipped with a single quadrupole analyzer with liquid introduction interface. The ion source is an electrospray ionization (ESI) source; if atmospheric-pressure chemical ionization (APCI) is instead desired at a future time, Advion sells an APCI source which can be easily swapped with the ESI source. The LC portion of the instrument is an Agilent 1220 Infinity series. Liquid samples can also be introduced to the ion source by direct injection from the manual flow injection valve or by the TLC adapter.

A4.3. LC-MS General Use Information

The following general user section can be used as a template for the LC-MS instructions sheet.

Prior to run:

- **Review method conditions, identify corresponding solvent lines, and check solvent levels**
- **Check N_2 tank**

  Pressure should read 60-80 psi. Build pressure in tank (pressure builder) or switch tanks if pressure < 60 psi to avoid shutdown during run. Do not adjust the settings on the regulator.
- **Before turning on any pump, check that your desired source (LC or TLC/Direct) is plumbed to the MS**

  See "Proper Plumbing" section below for detailed instructions for changing source tubing.
- **Equilibrate column (LC) or dead volume (Direct/TLC) with mobile phase prior to running your method (use starting %B for LC runs)**

  LC: Pump pressure should plateau. Flowrate must be ≤ 0.5 mL/min. If pressure exceeds 200 bar, decrease flowrate (very important to monitor pressure). Oscillating pump pressure indicates air bubble(s) in the lines. Turn off pump & ask LC-MS operator for assistance.

  Direct/TLC: Flowrate should be 0.2 mL/min. Do not turn the flowrate higher than 0.3 mL/min, as this may burst the capillaries. To purge dead volume, see "Purging Direct/TLC Dead Volume" section below. Pressure should be ~1100 psi for MeOH + 0.01% FA after purging. Do not open purge valve when there is backpressure on the system, as it may irreversibly damage the pressure dampener.
- **Properly prepare your samples (see 'Sample Preparation' below).**

Use HPLC-grade MeOH, H_2O, or MeCN and filter. If you are unable to use these solvents, ask the LC-MS operator for guidance.

- **Log your LC-MS use in the designated notebook**

Sample Preparation:

1. For solid or oil samples:
    i. Dissolve ~0.5 - 1 mg of sample in 1 mL of HPLC-grade MeOH, H_2O, or MeCN (for direct inject, do not use MeCN if possible)
    ii. Dilute 1 - 10 µL of this solution into 1 mL of HPLC-grade MeOH, H_2O, or MeCN (for direct inject, do not use MeCN if possible)
    iii. FILTER before injection into the LC or MS
        a. for LC, use "syringeless filter" vials
        b. for direct inject, filter using 0.45 micron PTFE syringe filters

2. For liquid samples (e.g. reaction mixtures and flash column fractions):
    i. Dilute 1 - 5 µL into 1 mL of HPLC-grade MeOH, H_2O, or MeCN (for direct inject, do not use MeCN if possible)
    ii. FILTER before injection into the LC or MS
        a. for LC, use "syringeless filter" vials
        b. for direct inject, filter using 0.45 micron PTFE syringe filters

3. If you are unable to use MeOH, H_2O, or MeCN, ask the LC-MS operator about alternative solvents.

Proper Plumbing of the MS:

1. For LC runs, ensure red tubing labeled "LC" is attached to the electrospray chamber before starting pump
2. For direct inject or TLC runs, ensure red tubing labeled "Direct & TLC" is attached to the electrospray chamber before starting pump
3. To change tubing:
    i. Loosen finger-tight fitting around attached tubing. It is not necessary to completely remove; pull out the red tubing once it has come loose.
    ii. Insert end of newly-removed tubing into the designated holster (1-mL plastic pipette taped to MS)
    iii. Insert red tubing from desired source by pushing the end of the tubing into the fitting until it is cannot enter any further.
    iv. Tighten the finger-tight fitting with 2 fingers until it will not easily tighten. Do not overtighten -- this will damage the fittings and the tubing, causing leaks.
    v. Turn on the pump and check for leaks.

Purging Direct/TLC Dead Volume:

1. Check that the Direct/TLC tubing is plumbed into the MS.
2. Turn on the TLC ("SSI") pump to 0.2 mL/min. On the front of the TLC plate adapter, press the ≡ button until PRESS is selected.

3. Wait ~3 minutes; if the pressure does not start to increase (up to ~1100 psi), you may increase the flowrate to 0.3 mL/min. If it still does not start to build pressure, you need to purge the system. If the pressure stabilizes at ~1100 psi, you may skip purging.
4. **Turn off the TLC pump and wait for any backpressure to drop to 0.**
5. To purge the system, first ensure that the backpressure on the system is 0 (from the "PRESS" readout on the front of the TLC adapter). This is very important, as even just one time opening the purge valve with backpressure can irreversibly damage the pressure dampener. If you have any uncertainties about this step, ask the LC-MS operator.
6. Once you are certain that there is no backpressure, insert the plastic syringe at the front of the TLC into the purge valve (black circular valve with ◄ on it) and open the valve by turning counter-clockwise.
7. Withdraw ~5 mL air into the syringe, or until you see some solvent.
8. Turn on purging by pressing the P button on the front of the SSI pump. After a short time, the syringe should begin to fill with solvent. Let the pump purge until there are no visible bubbles in the line from the solvent reservoir.
9. Turn off purging by pressing the P button once more.
10. Close the purge valve by turning clockwise until tight, then remove syringe and expel MeOH into waste.
11. Turn on the TLC ("SSI") pump again at 0.2 mL/min.
12. Let the pump run until the pressure is ~1100 psi. If the pressure does not build after purging, ask the LC-MS operator for assistance.

<u>Setting Up Single LC run</u>:

1. Prepare your sample according to 'Sample Preparation' above.
2. Check that the LC tubing is plumbed into the MS (see 'Proper Plumbing of the MS' above).
3. Go to Control & Status tab in the Mass Express software.
    a. Turn on all LC components by clicking "on" in lower right; wait until all components are green and say "idle"
    b. Set LC pump to the appropriate %B for the start of your method to equilibrate the column
4. Go to Manual Run tab
    a. MS Method tab under Manual Run
        i. Method tab
            1. Check that ion source and tune settings are appropriate for your desired analysis; tune files should be the most recent files.
            2. Check that the selected mass range is appropriate for your desired analysis.
            3. Set the scan time to 500.
        ii. Advanced Method tab
            1. Check that "smooth data" is checked (bottom of page).
    b. Set up your LC gradient on the LC Method tab under Manual Run
        i. Grad Pump tab
            1. Flow should be set to no greater than 0.5 mL/min
            2. Solvent A = H_2O, solvent B = MeOH (make sure that solvent B is checked)
            3. Stoptime: the time the method will stop collecting data

4. Posttime: the time after your method has finished that the program will run solvent at your equilibration %B
5. Timetable: where you set up your gradient

ii. Sampler tab
1. Injection volume should be set to 5 μL for typical sample concentrations

iii. Download your method to the instrument (click 'Download')

5. Turn on the MS (upper right corner); the front of the MS will have a blue light
6. Press the play button (►) and enter the details of your sample
   a. user: your name
   b. sample group: subfolder under your name where your datafile will be
   c. sample ID: filename of your datafile
   d. be sure to set LC settings to "run MS & LC"
   e. click 'OK'
7. After your run, flush the column at 100% MeOH for ~5 min and turn off the LC pump and the UV lamp under the Control & Status tab. Turn the MS to standby.

<u>Setting Up a TLC Run</u>:

1. Check that the Direct/TLC tubing is plumbed into the MS (see 'Proper Plumbing of the MS' above).
2. Follow the 'Purging Direct/TLC Dead Volume' instructions above; leave SSI pump on.
3. Turn on the laser under 'TLC express' in the Control & Status tab
4. Go to Manual Run tab → MS Method tab
   a. Method tab
      i. Check that ion source and tune settings are appropriate for your desired analysis
      ii. Set the run time of the MS method so that it will accommodate extraction of your intended TLC spot(s)
      iii. Check that the selected mass range is appropriate for your desired analysis
      iv. Check that the scan time is 500
   b. Advanced Method tab
      i. Check that "smooth data" is checked (bottom of page)
5. Turn on the MS (upper right corner); the front of the MS will have a blue light
6. Press the play button (►) and enter the details of your sample
   a. User: your name
   b. Sample group: subfolder under your name where your datafile will be
   c. Sample ID: filename of your datafile
   d. Set LC settings to "run MS"
   e. Click 'OK'
7. Sampling a TLC spot:
   a. Position your TLC plate such that the laser pointer is centered on your spot of interest
   b. Use the pull-down menu at the top of the page to select the kind of TLC plate
   c. Click on the icon next to the pull-down to sample your spot
   d. Note: you may sample multiple spots during one sample run

    e. Note: it can be helpful to sample a blank spot on your plate for background subtraction
8. After your run is finished, turn off the TLC laser and double-check that the SSI pump is off and MS is on standby.

Setting Up a Direct Inject Run:

1. Prepare your sample according to 'Sample Preparation' above
2. Check that the Direct/TLC tubing is plumbed into the MS (see 'Proper Plumbing of the MS' above).
3. Follow the 'Purging Direct/TLC Dead Volume' instructions above; leave SSI pump on.
4. Go to Manual Run tab → MS Method tab
    a. Method tab
        i. Check that ion source and tune settings are appropriate for your desired analysis
        ii. Set the run time of the MS method so that it will accommodate extraction of your intended TLC spot(s)
        iii. Check that the selected mass range is appropriate for your desired analysis
        iv. Check that the scan time is 500
    b. Advanced Method tab
        i. Check that "smooth data" is checked (bottom of page)
5. Turn on the MS (upper right corner); the front of the MS will have a blue light
6. Press the play button (►) and enter the details of your sample
    a. User: your name
    b. Sample group: subfolder under your name where your datafile will be
    c. Sample ID: filename of your datafile
    d. Set LC settings to "run MS"
    e. Click 'OK'
7. Check for stable solvent flow (stable TIC trace—may take a couple min)
8. Injecting a sample:
    a. Draw your sample into a 1-mL syringe using the blunt-tipped needle
    b. Wipe the outside of the needle with MeOH, then dry with a clean kimwipe
    c. Ensure the injection port is set to 'load' (to the right)
    d. Insert the blunt-tipped needle into the port and inject 10–20 µL
    e. Turn the injection port to 'inject' (to the left) to inject your sample
9. Note: you may do as many injections as you'd like on a single run; simply wait enough time in between injections for the TIC trace to become stable again.
10. After your run, clean the injection needle and injection port:
    a. Turn the injection port back to 'load' (to the right)
    b. Flush the needle with ~5 mL fresh MeOH
    c. Wipe down the outside of the needle with MeOH
    d. Flush the injection port with ~5 mL fresh MeOH using flushing adapter
11. Ensure that the SSI pump is off and MS is on standby.

Setting up Multiple LC Runs:

1. Ensure that LC tubing is plumbed into the MS (see 'Proper Plumbing of the MS' above)
2. Go to Control & Status tab in the Mass Express software.

a. Turn on all LC components by clicking "on" in lower right; wait until all components are green and say "idle"
b. Set LC pump to the appropriate %B for the start of your method to equilibrate the column

3. Go to Sample List tab → sample list setup tab
    a. In the 'define experiment' box:
        i. Check that the ion source settings & tune settings are appropriate
        ii. Load your MS method under 'method'
        iii. Load your LC method under 'LC method'
    b. In the 'specify data location' box:
        i. User: your name
        ii. Sample group: subfolder under your name where your datafile will be
        iii. Sample ID: filename of your datafile
            1. Note: _X (e.g. _1, _2, _3, ...) will be added to the end of your sample ID when using 'add' or 'add auto samples' functions in 'create samples' box
    c. In the 'create samples' box:
        i. If using 'add':
            1. Enter number of samples in the box
            2. Click 'add' to add samples to the sample list
                a. Note: will not autofill vial #
        ii. If using 'add auto samples':
            1. Click 'add auto samples'
            2. Enter desired start vial
            3. Enter the number of samples in addition to the start vial in the 'increment by row and column' box
                a. Note: will start from the start vial and add 1 to the vial position for each sample in the 'increment by row and column' box
                b. Example: with a start vial of 1 and a 'increment...' # of 2, the program will autofill vials 1, 2, and 3
            4. Click 'add and close' to autofill vials
    d. In the 'other functions' box:
        i. Ensure all boxes are checked ('standby after completion', 'shut down LC after sequence', and 'shut down LC after an error in MS')
        ii. Ensure that 'run MS & LC' is selected
    e. In the 'sample list' table:
        i. If you used the 'add auto samples' function, you may submit your desired samples
        ii. If you used the 'add' function, you need open the 'auto-sample' tab for each sample, enter the vial number, and click save
        iii. On submitting samples:
            1. Queued samples will have a status of 'submitted.' These may be removed from the queue by highlighting and clicking 'unsubmit.'
            2. The sample currently running will say 'acquiring.'
            3. Completed samples will say 'complete.'

4. You may submit new samples at any time during a sequence

Working up data:

- Go to Data Express
- To see progress while sample is running, click the "Refresh" icon
- To look up finished runs, click "Open File"
- There is a separate file for each ion polarity (is1 and is2) — UV traces will only be saved on whichever ion polarity was set to is1.
- Chromatrograms appear in the top pane, while integrated mass spectra appear in the bottom pane. Note that there are two settings above each pane ("replace" and "add") that determine how new chromatograms or integrated spectra will appear.
- Extracted ion chromatograms may be generated by typing m/z values into the text entry field at the bottom of the screen.
- Background subtraction may be performed by clicking "Backgound" and integrating an area of the TIC to set as background (note that this subtraction only applies to spectra integrated after the background spectrum).

A4.4. Maintenance procedures

To maintain the instrument in good working condition, the following tasks should be routinely performed as indicated.

Action	Frequency	Notes
Calibrate mass axis	Weekly	
Check solvent levels in solvent bottles	Weekly	Never top-up bottles; instead, empty and refill with fresh solvent. Use only HPLC-grade solvents and MilliQ water.
Check waste bottle and replace if full	Weekly	
Clean ion source	Biweekly	See procedure below
Autotune (both polarities)	Biweekly	Save new tune files and record in logbook
Clean TLC adapter	Biweekly	See procedure below
Change frits	6 months	
Change foreline pump oil	6 months	Use high-quality pump oil for mass spectrometers (not bulk pump oil from stockroom)
Change nitrogen purifier	Yearly, or upon expiration date	

To clean the ion source (ask LC-MS operator to demo first):

1. Ensure that the MS is on standby.
2. Carefully open the ion source chamber by unclipping from the MS
3. Unscrew the ion source capillary from the MS by turning counter-clockwise; pressing down with 3 fingers of a gloved hand should provide adequate friction to be able to unscrew the capillary.

4. Prepare ~600 mL of a 1:1 solution of HPLC-grade MeOH and MilliQ water supplemented with 0.1% formic acid in an Erlenmeyer flask and submerge the capillary (check that it is fully submerged)
5. Sonicate the capillary in this solution for at least 30 min
6. After sonication, wipe down the capillary with a clean kimwipe and dry the inside with a gentle stream of N_2.
7. Dampen a kimwipe or cotton swab with HPLC-grade methanol or isopropanol and wipe the inside of the ion source (around where the capillary sits in the MS); be careful not to bump the spray-tip of the ESI source.
8. Replace the ion source capillary; use 3 fingers to tighten (do not over-tighten).
9. Close the ion source chamber.

To clean the TLC adapter (ask LC-MS operator to demo first):

1. Open the plastic guard shield of the TLC adapter and unscrew the screw securing the TLC cutter.
2. Release the TLC cutter by pulling down on the two, small handles on the sides of the head of the TLC adapter.
3. Unscrew the cap securing the head of the TLC cutter.
4. Sonicate the TLC cutter head in 1:1 HPLC-grade MeOH and MilliQ water supplemented with 0.1% formic acid for at least 1 hour.
5. After sonication, dry the TLC cutter head with a gentle stream of N_2.
6. Replace the TLC cutter head into the TLC adapter by following the reverse of the steps to release it from the adapter.

A4.5. Replacement Parts & Consumables

Part Number	Description
Sigma-Aldrich 59031 (Supelco)	Column end plugs, for 10-32 coned ports, red Delrin®
IDEX 6000-282RD	Finger-tight PEEK fittings, 1/16”
IDEX 1535	Tubing, PEEK, 1/16” od, 0.005” id, 5 ft
Fisher 03-391-8	Autosampler vials
Fisher 03-391-31	Autosampler vial caps
ThermoFisher F2504-5	0.45 µm, 4 mm diameter PVDF Syringe filters
Fisher 09-923-35	Mini-UniPrep syringeless filters, 0.45 µm, PTFE
Restek 24819	Foreline pump oil, Inland 45, 1 qt
Advion 1011424	TLC adapter removable head (250 µm)

A4.6. Troubleshooting Guide

Software Issues	Troubleshooting Steps
Software is frozen	Reset program (close or force close). Restart computer if needed.

LC Pump Issues	Troubleshooting Steps
Pressure does not exceed 1 bar but pump is running	Check black knob on binary pump. Knob should be closed (turn to the right). If knob is open, pump is flushing directly to waste. Note: Avoid overtightening this knob. Just finger-tight is sufficient.
System overpressurizes (exceeds 250 bar)	Check column. Column should be attached to LC with correct direction for flow. Column may be clogged. Flush gently with MeOH (lower flow rate and flush for a few hours). Can attach column in reverse direction to flush. If backflushing, collect column flowthrough in a separate receptacle (do not let it flow into the UV detector; particulates can be dislodged from column and clog parts downstream). Can remove column from cartridge and wipe surface of particulates. Check PEEK capillary tubing; pieces of dust and debris sometimes clog the tubing if it has come into contact with the dusty benchtop.
Pump displays fluctuating pressure readings	Air bubble in lines. Purge lines by opening purge valve on binary pump. Flush solvent through line containing bubble at 2-5 mL/min when purge valve is open.

SSI Pump Issues	Troubleshooting Steps
Pressure does not build when pump is running	Turn flowrate up to 0.3 mL/min. If pressure does not begin to build, perform a purge of the SSI pump (see directions above).

Nitrogen Tank Issues	Troubleshooting Steps
Nitrogen line has an obvious leak (check with Snoop)	Unscrew regulated and re-attach; check for leaks using Snoop. If several tries to re-attach the regulator are unsuccessful, unscrew outermost brass fitting and replace compression ferrules (one forward, one back) on tubing. Cut Teflon tubing (use new razor blade—cut as straight as possible) and use new ferrules. Screw fitting back into place, carefully (keep tube straight), and do not overtighten to avoid stripping threads; fingertight or slightly more than fingertight ok. Inspect Teflon tubing and consider replacing tubing as needed (1/4 inch outer diameter).

Leak Issues	Troubleshooting Steps
Instrument shuts down and leak indicated, and/or solvent observed pooling on/around instrument	Inspect LC for leaks. Leakage frequently occurs at the bottom UV-Vis module (where flow is directed to the column, UV-vis detector, and then the MSD), particularly after the column has been removed or reattached due to improper reinstallation of the connections. Leaks from the needle seat in the autosampler, or the checkvalve immediately upstream of the needle seat, have also been observed. Leak sensors must be thoroughly dried before instrument will run. A strip of filter paper can be used to

	wick away moisture from the leak sensor in the MSD, which can be hard to reach.
Tubing popping out of place	Frequently, strain due to angle of tubing OR system is overpressurizing. Lower flow rate. Isolate parts that may be contributing to high pressure and inspect sequentially to identify problem. Check PEEK tubing for dust or particulate clogging. Do NOT continuously attempt to run instrument with high pressure if tubing keeps popping out, as this can lead to a severe leak in the system (pressure can exceed capacity of a part, e.g. UV-Vis flow cell, and will destroy the part). Ensure PEEK tubing is threaded all the way through the fitting before tightening.
Clog in PEEK tubing	Cut PEEK capillary with tubing cutter.

MS Issues	**Troubleshooting Steps**
Mass for desired compound not detected, but another mass observed	Besides M+H and M–H, other commonly observed ionic/adduct species include M+23 ($+Na^+$), M+18 ($+NH_4^+$), and M+39 (M+K). Use an alternate analytical method, such as NMR, to clarify. Desired compound might not be detected under method conditions or LC-MS in general. Desired compound might not be present in sample.

Other Issues	**Troubleshooting Steps**
Finger-tight fittings for PEEK tubing are stripped	Replace with new ones
Column caps are stripped	Replace new column end plugs
High contaminant peak. 102 is triethylamine, which should never be used in elution buffers due to suppression of positive ions in the detector. Use of triethylamine in elution buffers will contaminate the entirety of the LC system	To remove contaminants: Sonicate and clean frits Flush lines with warm water Flush lines with warm AcOH in water (5%) Flush lines with flushing solvent (Agilent) Flush lines with IPA Flush lines with MeCN 500 mL minimum, 1 mL/min
UV-Vis lamp ignition fails (lamp not ready error message)	Power cycle UV-Vis module and retry ignition. If ignition continues to fail, lamp may be burned out. Try installing replacement lamp.